

**INNER ELASTICITY**  
**and the**  
**HIGHER-ORDER ELASTICITY**  
**of some**  
**DIAMOND and GRAPHITE**  
**ALLOTROPES**

Submitted by  
Christopher Stanley George Cousins  
to the  
University of Exeter  
as a thesis for the degree of  
Doctor of Philosophy in Physics  
(March 2001)

This thesis is available for Library use on the understanding that it is copyright material and that no quotation from it may be published without proper acknowledgment.

I certify that all material in this thesis which is not my own work has been identified and that no material is included for which a degree has previously been conferred upon me.

## Abstract

Following a brief and selective history of elasticity, the general theory of the rôle of relative **sublattice displacements** on the elasticity of single-crystalline material is elaborated in Chapter 1. This involves the definition of (a) rotationally-invariant **inner displacements** and (b) the **internal strain tensors** that relate those inner displacements to the external strain. The total elastic constants of such materials can then be decomposed into **partial** and **internal** parts, the former free of, and the latter involving, the inner displacement(s). Six families of **inner elastic constants** are needed to characterize the internal parts of the second- and third-order constants. The relation of the second-order inner elastic constants to the longwave coupling constants of lattice dynamics is shown, and a new form of secular equation for the frequencies and eigenvectors of the optic modes at the zone centre is given. In Chapter 2 the **point-group symmetry** implications for the inner elastic constants are explored in detail.

Chapter 3 is an interlude in which the measurement of the internal strain in cubic diamond is described.

In Chapters 4 and 5 the general formalism is applied to **cubic** and **hexagonal diamond** and to **hexagonal** and **rhombohedral graphite**. **Space-group symmetry** implications are described in detail and the formalism is extended to cover **effective constants**, **pressure derivatives**, **elastic compliances** and **compressibilities**. The allotropes are treated individually in terms of the **Keating model** in the following four Chapters. Cubic diamond is treated in Chapter 6 in terms of the original model. A shortcoming of the model—non-transferability of its parameters to alternative descriptions of unit cell geometry—is overcome by redefining both the Keating strain and the Keating parameters. The **modified Keating model** is then extended rigorously and successfully to a non-cubic material, hexagonal graphite, for the first time in Chapter 7. Chapter 8 presents a completely plausible account of the elasticity and zone-centre optic modes in hexagonal diamond by transferring the modified parameters from cubic diamond. The little that is known experimentally, the bulk modulus and three Raman frequencies, is predicted exactly. Chapter 9 extends Keating to the rhombohedral form of graphite using transferred parameters and provides a detailed picture of its transformation to cubic diamond. In Chapter 10 the relation of **bond-order potentials** to the Keating model is explored.

An Appendix contains a **generalised method of homogeneous deformation**, developed to relate the computationally-friendly infinitesimal strain approach to the thermodynamically-rigorous finite strain formalism, and the associated computational protocols needed to determine all elastic and inner elastic constants, and hence all derived quantities, of the allotropes discussed.

# Contents

<b>Abstract</b>	<b>1</b>
<b>List of figures</b>	<b>7</b>
<b>List of tables</b>	<b>10</b>
<b>Foreword</b>	<b>11</b>
<b>1 Elasticity</b>	<b>13</b>
1.1 A little history . . . . .	13
1.2 Inner elasticity . . . . .	16
1.3 Macroscopic strain . . . . .	17
1.4 Microscopic strain . . . . .	18
1.4.1 Occurrence and description of sublattice displacement . . . . .	18
1.4.2 Inner displacement . . . . .	19
1.4.3 Internal strain tensors . . . . .	20
1.5 Energy and elastic constants . . . . .	21
1.5.1 Partial elastic constants . . . . .	21
1.5.2 Inner elastic constants . . . . .	21
1.5.3 External equilibrium of the unstressed crystal . . . . .	22
1.5.4 Internal equilibrium of the stressed crystal . . . . .	22
1.5.5 Composition of the total elastic constants . . . . .	23
1.6 Compliances and compressibilities . . . . .	25
1.7 Computational simplification and sublattice tensors . . . . .	25
1.8 Lattice dynamical connection . . . . .	27
1.8.1 Inner elastic constants and longwave coupling constants . . . . .	27
1.8.2 The secular equation and optic mode frequencies . . . . .	28
1.9 Rationale . . . . .	29
<b>2 Symmetry of inner elastic constants</b>	<b>32</b>
2.1 Point-group symmetry analysis . . . . .	33
2.2 Transformation of sublattice indices . . . . .	39

---

2.3	Transformation of interlattice indices . . . . .	40
2.3.1	Indices connecting sublattices in distinct Wyckoff sets . . . . .	41
2.3.2	Indices connecting sublattices within a single Wyckoff set . . . . .	43
2.4	In conclusion . . . . .	44
<b>3</b>	<b>Experimental interlude: the internal strain parameter of cubic diamond</b>	<b>46</b>
3.1	Introduction . . . . .	46
3.2	Inner displacement due to uniaxial stress . . . . .	47
3.3	Change in structure factor due to inner displacement . . . . .	48
3.4	X-ray methods . . . . .	50
3.5	Experimental details . . . . .	50
3.5.1	Sample . . . . .	51
3.5.2	Uniaxial press . . . . .	51
3.5.3	Working angle . . . . .	51
3.5.4	Beam-tailoring by total external reflection . . . . .	52
3.6	Result . . . . .	52
<b>4</b>	<b>Inner elastic constants, internal strain tensors and zone-centre optic modes</b>	<b>54</b>
4.1	Symmetry . . . . .	55
4.1.1	Cubic diamond and rhombohedral graphite . . . . .	58
4.1.2	Hexagonal diamond and hexagonal graphite . . . . .	58
4.2	Internal strain tensors . . . . .	66
4.2.1	Cubic diamond . . . . .	66
4.2.2	Rhombohedral graphite . . . . .	66
4.2.3	Hexagonal diamond . . . . .	67
4.2.4	Hexagonal graphite . . . . .	67
4.3	The zone-centre optic modes . . . . .	68
4.3.1	Cubic diamond and rhombohedral graphite . . . . .	68
4.3.2	Hexagonal diamond . . . . .	69
4.3.3	Hexagonal graphite . . . . .	71
4.4	Effective inner elastic constants . . . . .	72
4.4.1	Cubic diamond . . . . .	73
4.4.2	Rhombohedral graphite . . . . .	73
4.4.3	Hexagonal diamond . . . . .	73
4.4.4	Hexagonal graphite . . . . .	74
4.5	The pressure dependence of the optic mode frequencies . . . . .	74
4.5.1	Cubic diamond . . . . .	74
4.5.2	Rhombohedral graphite . . . . .	74

---

4.5.3	Hexagonal diamond . . . . .	74
4.5.4	Hexagonal graphite . . . . .	75
4.6	Summary . . . . .	76
<b>5</b>	<b>Total elastic constants, compressibilities etc.</b>	<b>78</b>
5.1	Anatomy of the macroscopic constants . . . . .	78
5.1.1	Cubic diamond . . . . .	80
5.1.2	Rhombohedral graphite . . . . .	80
5.1.3	Hexagonal diamond . . . . .	82
5.1.4	Hexagonal graphite . . . . .	83
5.2	Compliances and compressibilities . . . . .	83
5.2.1	Cubic diamond . . . . .	84
5.2.2	Hexagonal diamond, hexagonal graphite and rhombohedral graphite . . . . .	84
5.3	Effective elastic constants and their pressure derivatives . . . . .	85
5.3.1	Cubic diamond . . . . .	85
5.3.2	Hexagonal diamond and hexagonal graphite . . . . .	85
5.3.3	Rhombohedral graphite . . . . .	86
5.4	Summary . . . . .	86
<b>6</b>	<b>Cubic diamond</b>	<b>88</b>
6.1	Introduction . . . . .	88
6.2	Elastic constants, compliances and pressure derivatives . . . . .	89
6.3	The zone-centre optical modes . . . . .	90
6.3.1	The secular equation under stress . . . . .	90
6.3.2	Phonon deformation potentials . . . . .	92
6.4	The Keating model . . . . .	93
6.4.1	Harmonic interactions . . . . .	93
6.4.2	Anharmonic interactions . . . . .	97
6.5	Summary of results . . . . .	100
6.6	A modified Keating model . . . . .	102
6.6.1	Cubic diamond referred to rhombohedral axes . . . . .	102
6.6.2	Recasting the energy expressions . . . . .	104
6.6.3	Modified Keating parameters . . . . .	104
6.6.4	Modified cubic diamond referred to cubic axes . . . . .	105
6.7	Summary . . . . .	106
<b>7</b>	<b>Hexagonal graphite</b>	<b>108</b>
7.1	Introduction . . . . .	108
7.2	Modelling the elasticity . . . . .	109

7.2.1	Appraisal of input data . . . . .	109
7.2.2	Justification of model . . . . .	111
7.3	The modified Keating model . . . . .	112
7.3.1	The strain variables . . . . .	113
7.3.2	The model parameters . . . . .	113
7.3.3	The energy . . . . .	115
7.3.4	The elastic constants . . . . .	116
7.4	The fitting and the results . . . . .	118
7.5	Commentary . . . . .	125

## **8 Hexagonal diamond: elasticity and zone-centre optic modes *via* transferred Keating parameters** **129**

8.1	Introduction . . . . .	129
8.2	The hexagonal diamond structure . . . . .	130
8.2.1	The quasi- <i>cD</i> case . . . . .	130
8.2.2	The actual <i>hD</i> case . . . . .	130
8.3	Modified Keating model . . . . .	131
8.3.1	The strain variables . . . . .	131
8.3.2	The energy . . . . .	131
8.4	The partial and inner elastic constants . . . . .	132
8.5	The internal strain parameters . . . . .	135
8.6	The total elastic constants and associated pressure derivatives . . . . .	136
8.7	The zone-centre optic modes . . . . .	137
8.8	Summary and sting in the tail . . . . .	139

## **9 Rhombohedral graphite: elasticity, zone-centre optic modes and the *rG-to-cD* transformation *via* transferred Keating parameters** **141**

9.1	Introduction . . . . .	141
9.2	Does the rhombohedral allotrope exist? . . . . .	141
9.3	Cohesive energy . . . . .	143
9.3.1	Equilibrium structure . . . . .	144
9.4	Modified Keating model . . . . .	145
9.4.1	The strain variables . . . . .	146
9.4.2	The energy . . . . .	146
9.5	Elasticity of rhombohedral graphite . . . . .	147
9.5.1	Zone-centre optic modes . . . . .	151
9.6	The <i>rG-to-cD</i> transformation . . . . .	152
9.6.1	Energy minimization calculations . . . . .	153

---

9.6.2	Hydrostatic compression path . . . . .	157
9.7	Summary . . . . .	158
<b>10</b>	<b>Bond-order potentials</b>	<b>160</b>
10.1	Empirical bond-order potentials . . . . .	161
10.1.1	Matched elastic constant predictions . . . . .	165
10.1.2	Matched energy derivatives . . . . .	166
10.2	Analytic bond-order potentials . . . . .	168
<b>11</b>	<b>In conclusion</b>	<b>171</b>
<b>A</b>	<b>Generalised homogeneous deformation</b>	<b>173</b>
A.1	Homogeneous deformation . . . . .	173
A.1.1	Fuchs constants in terms of Brugger constants . . . . .	175
A.2	Computational procedures . . . . .	176
A.2.1	<i>c</i> -Diamond . . . . .	178
A.2.2	<i>h</i> -Graphite, <i>h</i> -Diamond and <i>r</i> -Graphite . . . . .	179
A.2.3	Formal checks . . . . .	182
<b>B</b>	<b>Tensor transformations for non-standard point-group settings</b>	<b>183</b>
<b>C</b>	<b>Keating model parameters from bond-order potential parameters</b>	<b>185</b>
C.1	The Keating model . . . . .	185
C.1.1	Dependencies amongst the variables . . . . .	185
C.2	The bond-order potential . . . . .	187
C.3	Equivalent Keating parameters . . . . .	187

---

## List of Figures

1.1	Sublattice displacement . . . . .	18
3.1	Stress and inner displacement configurations . . . . .	48
3.2	Experiment layout . . . . .	50
4.1	Unit cells of four carbon allotropes . . . . .	56
4.2	Vibration patterns for hexagonal diamond . . . . .	70
4.3	Vibration patterns for hexagonal graphite . . . . .	72
7.1	Structure and unit cell of hexagonal graphite . . . . .	112
7.2	Configurations of bonds in the Keating model . . . . .	114
7.3	Pressure-dependence of the zone-centre optic-mode frequencies . . . . .	124
8.1	Hexagonal cells for $cD$ and $hD$ . . . . .	130
8.2	Pressure-dependence of the zone-centre optic-mode frequencies . . . . .	139
9.1	Force diagram for $hG$ , planar $rG$ and buckled $rG$ . . . . .	144
9.2	Configurations of bonds in the Keating model . . . . .	145
9.3	Pressure dependence of the zone-centre frequencies. . . . .	152
9.4	$rG$ -to- $cD$ transformation path . . . . .	153
9.5	Second-order elastic constants along a transformation path . . . . .	155
9.6	Internal strain parameters along a transformation path . . . . .	156
9.7	Zone-centre frequencies along a transformation path . . . . .	156

## List of Tables

1.1	Tableau of inner displacement assignment . . . . .	19
1.2	The above tableau with introduction of dependencies . . . . .	20
2.1	Non-zero components of $d_i^\alpha$ and $D_i^\lambda$ . . . . .	34
2.2	Non-zero components of $d_{iJ}^\alpha$ , $D_{iJ}^\lambda$ and $A_{iJ}^\lambda$ . . . . .	34
2.3	Non-zero components of $d_{iJK}^\alpha$ , $D_{iJK}^\lambda$ and $A_{iJK}^\lambda$ . . . . .	35
2.4	Non-zero components of $e_{ij}^{\alpha\beta}$ and $E_{ij}^{\lambda\mu}$ . . . . .	36
2.5	Non-zero components of $e_{iJK}^{\alpha\beta}$ and $E_{iJK}^{\lambda\mu}$ . . . . .	36
2.6	Non-zero components of $f_{ijk}^{\alpha\beta\gamma}$ and $F_{ijk}^{\lambda\mu\nu}$ . . . . .	37
2.7	Total numbers of independent elements . . . . .	38
2.8	Assignment of sublattice indices to the atomic sites in the hexagonal allotropes . . . . .	39
2.9	Permutations of sublattice indices corresponding to spacegroup operations . . . . .	39
2.10	Allocation of interlattice indices . . . . .	40
3.1	Effect of stress on structure factor . . . . .	49
4.1	Essential geometry and the assignment of sublattice indices to the atomic sites . . . . .	55
4.2	The symmetry of the individual sublattice tensors in $cD$ . . . . .	56
4.3	The symmetry of the individual sublattice tensors in $rG$ , $hD$ and $hG$ . . . . .	57
4.4	Independent components of the inner elastic constants . . . . .	59
4.5	Permutations of sublattice indices corresponding to spacegroup symmetry operations . . . . .	60
4.6	Interrelation of components of the inner elastic constants of hexagonal diamond . . . . .	63
4.7	Interrelation of components of the inner elastic constants of hexagonal graphite . . . . .	65
5.1	The symmetry of the elastic constants of hexagonal diamond and hexagonal graphite . . . . .	78
5.2	The symmetry of the elastic constants of cubic diamond and rhombohedral graphite . . . . .	79
6.1	Parametrization of the harmonic part of the Keating model . . . . .	94
6.2	Phonon frequencies at the $\Gamma$ , $X$ and $L$ points . . . . .	96
6.3	Parametrization of the anharmonic part of the Keating model . . . . .	99
6.4	The inner elastic constants and internal strain parameters . . . . .	100
6.5	The second-order elastic constants . . . . .	101
6.6	The third-order elastic constants . . . . .	101

---

6.7	Calculated second-order partial and inner elastic constants of cubic diamond with respect to both cubic and rhombohedral axes . . . . .	103
6.8	Calculated third-order partial and inner elastic constants of cubic diamond with respect to both cubic and rhombohedral axes . . . . .	103
6.9	Modified Keating parameters . . . . .	104
7.1	SWMcC model parameters $\gamma_i$ and the bond interactions selected for the Keating model . . . . .	113
7.2	Coefficients of the modified Keating parameters in the second-order elastic constants	116
7.3	Coefficients of the modified Keating parameters at the third order (1) . . . . .	117
7.4	Coefficients of the modified Keating parameters at the third order (2) . . . . .	118
7.5	Target data for the harmonic part of the modified Keating model . . . . .	119
7.6	Target data for the anharmonic part of the modified Keating model . . . . .	120
7.7	The modified Keating parameters . . . . .	121
7.8	The internal strain tensors . . . . .	121
7.9	The inner elastic constants . . . . .	122
7.10	The composition of the calculated elastic stiffnesses and the corresponding compliances and compressibilities . . . . .	123
7.11	The zone-centre optic modes . . . . .	124
8.1	Modified Keating parameters . . . . .	132
8.2	Coefficients of the modified Keating parameters in the second-order elastic constants	133
8.3	Coefficients of the modified Keating parameters at the third order (1) . . . . .	134
8.4	Coefficients of the modified Keating parameters at the third order (2) . . . . .	135
8.5	The internal strain parameters . . . . .	136
8.6	The second- and third-order elastic constants . . . . .	136
8.7	The composition of the calculated elastic stiffnesses and the corresponding compliances and compressibilities . . . . .	137
8.8	The zone-centre optical modes . . . . .	138
8.9	Pressure-derivatives of optic-mode frequencies . . . . .	138
9.1	The modified Keating parameters . . . . .	147
9.2	Coefficients of the modified Keating parameters in the second-order elastic constants	148
9.3	Coefficients of the modified Keating parameters at the third order . . . . .	149
9.4	Calculated second- and third-order partial and inner elastic constants . . . . .	150
9.5	The internal strain tensors . . . . .	150
9.6	The composition of the calculated elastic stiffnesses and the corresponding compliances and compressibilities . . . . .	151
9.7	End-points and transition-state parameters . . . . .	152

- 9.8 Hydrostatic compression path . . . . . 157
  
- 10.1 Empirical bond-order potential parameters . . . . . 163
- 10.2 SOECs of *c*D predicted by bond-order potentials . . . . . 165
- 10.3 TOECs of *c*D predicted by bond-order potentials . . . . . 166
- 10.4 Keating parameters of *c*D from derivatives of the bond-order potential . . . . . 167
- 10.5 Keating parameters of graphene from derivatives of the bond-order potential . . . . . 167
  
- A.1 Specification of the shape-changing matrices *P* and the scaling functions . . . . . 177
- A.2 Linear combinations of Brugger constants for cubic crystals . . . . . 178
- A.3 Linear combinations of Brugger constants for hexagonal and rhombohedral crystals 179
  
- B.1 Transformations from standard to variant point-group settings:1 . . . . . 183
- B.2 Transformations from standard to variant point-group settings:2 . . . . . 184

## Foreword

Most doctoral theses in science are submitted by young men and women in their twenties. They encapsulate the positive aspects of the novel quests that were undertaken as *rites de passage* between the student world and the professional world.

This one is quite different. Its author is sixty-six years old and, following ten years of early retirement, has come to the end of thirty-six years as a member of staff of the Department, now School, of Physics. It was triggered by the realization that his very recent work (on the elasticity of diamond and graphite) together with some that was twenty years old (on inner elasticity) formed a coherent and original whole. This thesis thus serves no professional purpose and has been submitted for purely personal reasons: to celebrate a life-long interest in number and symmetry and to provide a satisfyingly-academic closure to an academic career.

There are important tributes to be paid. Firstly to my parents Stan and Amy who, deprived of secondary education themselves, made sure that I took full advantage of mine. Then to N. B. C. Lucas (Luke), the inspiring Headmaster of Midhurst Grammar School, whose Jungian sympathies ensured that all his pupils were treated as individuals and encouraged to achieve their full potential. At Oxford my Tutor was Roy Meads, the first scientist that I had ever met. His tutorials were held in his research room amidst racks of electronics and flashing displays. The ambience and his enthusiasm ensured that my interest in physics was sustained. Some years later, after Roy had come to Exeter, he was indirectly responsible for my joining the Department when I became disenchanted with my short career in schoolteaching. Not only that—in the few years before his retirement, after his own research projects had come to an end, he became a valued member of my own research group. Other colleagues to whom I am grateful are Ray Drabble, who first interested me in higher-order elasticity and Brian Sheldon who was a supportive and enterprising right-hand man in experimental work at Exeter, at the Synchrotron Radiation Source at Daresbury and at the Technical University and Ørsted Institute in Denmark. Particular thanks go to Malcolm Heggie, currently Reader in Theoretical Chemistry at the University of Sussex, whose graphite project, on which I began to work six years ago, has burgeoned into this thesis. I also thank my supervisor, Bob Jones, for his pertinent comments on the rough draft which have led to significant improvements.

Finally to Claire, my loyal and loving wife of forty-two years, and our dynasty: our daughter Kate and her children Lucy and Sophie; our son Adam and his children Danny, Katie and Jack. Without the pleasure and happiness that they have given me I would have achieved very little.

---

The writing-up has had to compete with my parallel pursuit of an MA in Creative Writing, during which I wrote the following poem <sup>1</sup> about my dawning awareness of symmetry:

*My Tray*

*When I was six a student came  
to take Miss Steeds's class  
and turned her room  
into the Pedlar's Caravan.  
We'd all to bring from home  
card, paper, crayons, glue or string  
to make the different sorts of thing  
the pedlar'd sell.*

*For me*

*some cardboard from a pad of forms  
(my father's time-sheets) and coloured,  
gummy squares.*

*I snip*

*into the corners of the card  
and bend the edges up to make a frame.  
I cut some pieces, pink and chocolate,  
red, green and blue, squares, diamonds,  
and stick them on. Each piece to left  
is balanced on the right, in colour  
and in shape. And pieces up by pieces down.  
Turn it right round and it still looks the same.  
It is my tray!*

*Others made plates and cups*

*and knives and forks, yet those I don't  
recall.*

*But bright as yesterday*

*I see my desk, the texture of the tray,  
and, above all, its awesome symmetry.*

---

<sup>1</sup>*The Pedlar's Caravan*, in line 4, was a popular children's poem by the writer William Brighty Rands

# Chapter 1

## Elasticity

### 1.1 A little history

This thesis inhabits the region where elasticity and crystallography overlap. These two grand schemes began, almost simultaneously, in the second half of the 17th century, in a magnificent era that saw the birth of modern science.

Elasticity has grown from the very first law to be formulated in what is now called solid-state physics. Robert Hooke, who has been described as ‘Europe’s last Renaissance man and England’s Leonardo’ [9], originally published his law as a Latin anagram

c e d i i n n o o p s s t t u u

in *A description of Helioscopes and some other Instruments* [22, p.32] in 1676. This playful 17th century conceit was a popular way of simultaneously announcing a discovery, establishing priority and intellectually challenging one’s peers. The solution was published two years later in *De potentia Restitutiva, or of Spring Explaining the Power of Springing Bodies* [23, p.5]:

Ut Pondus sic Tensio

As the weight, so the (ex)tension.

A few years later, when there was a better appreciation of the nature of weight and the significance of the force within the spring, the more familiar form of the law appeared:

Ut Tensio sic Vis

As the (ex)tension, so the force.

In 1669 Niels Steensen, a Dane known as Nicolaus Steno, published a dissertation which included a detailed study of sections cut from various samples of quartz. This laid the groundwork for what, nearly a century later, came to be called the Law of Constancy of Angle and is now seen as a fundamental law of crystallography. Another such, the Law of Rational Indices, was given by Haüy in 1784. We owe to Haüy the idea that minute, identical building blocks, *molécules intégrantes*, underlie the macroscopic forms of crystals. Yet some credit is surely due to Hooke

also: in his hugely influential study of the microscopic world *Micrographia*, published in 1665, he clearly intimates the close-packing of spheres when he writes

There was not any regular Figure, which I have hitherto met withall, of [Metals, Minerals, Precious Stones, Salts and Earths] that I could not with the composition of bullets or globules, and one or two other bodies, imitate, even almost by shaking them together.

The painstaking observation of the morphology of countless specimens by mineralogists and chemists led to the realization that all crystals could be divided between seven distinct crystal systems on the basis of the shape of their *molécules intégrantés*, or unit cells. Then Bravais, amongst others, showed in 1848 that there were just 14 space lattices into which the unit cells could be packed. The development of the theory of finite groups confirmed earlier speculation that crystals could be assigned to just 32 classes, each of which possessed a distinctive point group formed from the identity and some of the symmetry elements of inversion, rotation and reflection.

The first half of the 19th century saw important conceptual advances in elasticity: the notions of stress and strain replaced force and extension; and different elastic moduli were associated with linear, torsional and bulk strains. Three of the French giants of mathematical physics—Navier [32], Cauchy [8] and Poisson [34]—each derived, independently, general equations governing the equilibrium and motion of elastic bodies. The resulting classical theory of elasticity was based on the assumption that bodies were homogeneous and isotropic, the movements of particles within them were very small, and the relation between stress and strain was linear.

The initial development of the theory was driven by the desire to understand the properties of the æther, the medium proposed by Fresnel to support the propagation of light. It was the practical aspect, however, that was seized on by the developers of machines and the designers of buildings: the understanding of the effects of load and vibration on material bodies, the bending and twisting of rods, the flexure of plates and the stability of beams. Already the notions of the elastic limit and of the yield point were showing up the limitations of the linear theory. St. Venant [37] and Kirchhoff [25] began to study the implications of large strains and laid the foundations of the non-linear theory of elasticity.

In the same period both Mayer and Joule presented their results on the mechanical equivalent of heat and Helmholtz asserted that the principle of the conservation of energy had universal validity and was applicable to all natural phenomena. Thermodynamics was thereby born and elastic behaviour fell clearly within its scope. Whilst crystallographers were developing a deep understanding of symmetry through their studies of crystals with exotic optical properties, engineers and physicists were focused on isotropic material, metals and alloys, and hardly needed anything more sophisticated than the simple moduli and Poisson's ratio. Wood was an exception: it was an important material and clearly had different elastic properties in different directions. It was termed *æolotropic* and different moduli were assigned along the grain and across the grain in an idealized

model, anticipating the correct description of uniaxial material.

The last five years of the 19th century and the first five of the 20th were a miraculous decade in which X-rays, radioactivity and the electron were discovered, and the foundations of quantum mechanics and special relativity were laid. The subsequent application of X-ray diffraction, the establishment of the nuclear atom and the development of wave mechanics brought about a revolution in understanding the structure of solids. Max Born was a prime mover in this area. As early as 1915 he had produced a study entitled *Dynamik der Kristallgitter* followed in 1923 by the influential *Atomtheorie des festen Zustandes*. Techniques of summation were developed to compute the contribution of Coulomb interactions to the cohesive energy of ionic crystals (Madelung 1918). For non-ionic crystals, where there was no clear-cut potential function, an inductive method was employed by Lennard-Jones (1924). Initially seeking the form of the molecular force field of argon atoms to account for the observed viscosity and isotherms of the gaseous phase he was able to propose a number of models that fitted the data but was unable to discriminate between them. He then appealed to lattice parameter and compressibility measurements on solid argon and used functions of the form  $F(r) = \lambda_n/r^n - \lambda_m/r^m$  to achieve discrimination. This occurred when  $n$  and  $m$  were 15 and 5, i.e. the exponents in what is now called the Lennard-Jones potential were 14 and 4. Much later, in a tribute to the memory of van der Waals (Lennard-Jones 1937), he settled on 6 for the attractive term, consonant with the theory of the van der Waals interaction, and a range from 9 to 12 for the repulsive term, dependent on the molecule involved.

Such potentials, with their simple analytical forms, and similar ones involving terms like  $A \exp(-r/\rho)$ , became the functions of choice in a wide variety of studies of both perfect crystals and crystals with defects. In particular Born, with various co-workers, published numerous papers on the stability of crystals over a period that extended to 1954 when, with Kun Huang, he published his masterpiece on the thermodynamics of lattices: the *Dynamical Theory of Crystal Lattices*.

In his Preface Born rebukes crystallographers for their profligate use of the letters of the alphabet: the Miller indices  $h, k, l$  for example use three where a single subscripted letter would suffice. The antidote of course is to use tensor notation wherever possible. The great scope for this was almost immediately illustrated in Nye's *Physical Properties of Crystals: their Representation by Tensors and Matrices* which appeared first in 1957 and then in 1985 with corrections and updated material.

Neither Born and Huang nor Nye however venture into the realm of higher-order elasticity, an area opened up experimentally by Bridgman's work on the compressibility of media up to high pressure ( $10^5$  atmospheres) and theoretically by Murnaghan in his 1951 book *Finite Deformation of an Elastic Solid*. Slightly flawed definitions in the latter were made thermodynamically consistent by Brugger (1964). For many years second-order elastic constants (SOECs) had been deduced from the speeds of longitudinal and transverse elastic waves in different crystal directions. In 1965 Brugger published [6] an exhaustive account of how the third-order elastic constants (TOECs) determine the (small) changes of such speeds under stress for all crystal classes and [7] protocols

for experiments to determine full sets of TOECs for all crystal classes. Around this time there was a burst of activity to measure TOECs. The time was ripe for several reasons: high-quality single crystals of many materials were becoming available; advances in electronics allowed small changes in the speeds of elastic waves through crystals to be measured accurately; and techniques for applying uniaxial stresses to crystal samples could be added to those for applying hydrostatic pressure, thereby generating the number of distinct elastic wave modes needed.

It was at this point that I entered the field, choosing first to work on the theory of the TOECs of noble metals [10]. Later, after involvement with metals that crystallized in the close-packed hexagonal structure and which therefore involved internal strain [11, 12, 13, 14, 15, 16], I became more interested in the formal theory [17, 18]. Now read on.

## 1.2 Inner elasticity

I introduced the term inner elasticity as the title of [17] to emphasize that the paper concerned the specific area of elasticity that dealt with the response to deformation of crystals whose structures contained atoms at sites lacking inversion symmetry. This approach features the specification of **sublattice displacement, inner displacement, internal strain tensors, partial elastic constants and inner elastic constants**. Certain of the inner elastic constants define the frequencies of optic modes at the zone centre. These may be combined with components of the internal strain tensor to give the specific contributions to the **total elastic constants** that are due to the inner displacements.

The earliest works in this area were published between 1954 and 1972 by Born and Huang [3], Srinivasan [36], Keating [24], Barron, Gibbons and Munn [1] and Fuller and Naimon [20]. A massive review of developments in lattice theory was presented in 1967 by Ludwig [28]. Because these different works lacked an agreed nomenclature, and sometimes suffered from an extremely opaque notation, their most important ideas were frequently ignored in situations where they should have been invoked: Ludwig, in particular, writes in his Introduction that he has used a different notation from Anglo-American papers because ‘there is no uniformity in different languages, and we think [our notation] is the most consistent and unique one’. This curious logic has resulted in pages where the equations feature symbols bearing two columns of four labels! I addressed this problem in [17] by proposing nomenclature<sup>1</sup> that was close to that of macroscopic elasticity, by introducing a rational notation and by treating the subject with complete generality. The remainder of this chapter gives a condensed summary of that paper with some improvements in presentation that have arisen as a result of applying the formalism in subsequent years. I eschew thermodynamic intricacies, ignore external electric and magnetic fields and concentrate on non-

---

<sup>1</sup>The nomenclature and notation were first proposed in a post-graduate lecture course on Higher-order Elasticity that I gave in 1972/3 in the Department of the Structural Properties of Materials at the Technical University of Denmark. Amongst those present was my colleague John Martin who first exposed the formalism publicly in his study of many-body forces in non-primitive crystals [30], published in 1975.

piezoelectric crystals. Strains are assumed to be applied isothermally so that the relevant energy function is the Helmholtz free energy.

As I was, at that time (1976/7), unaware of any treatment of symmetry relevant to the tensors with which I was concerned I covered the topic myself in [18], which is summarized in Chapter 2. Subsequently I learnt of Thurston's article on waves in solids [38] where the effect of symmetry on a host of material coefficients (elastic, dielectric, piezoelectric, electro-optic etc.) is considered and the results of a number of authors are collated. These results can be related to mine and are, with one or two exceptions, completely equivalent to them. The differences are indicated later in the appropriate place.

### 1.3 Macroscopic strain

There are two approaches to the definition of macroscopic elastic strain, both involving the notion of homogeneous deformation. The latter is specified by a deformation gradient matrix  $H$  whose effect is to transform any vector  $\vec{r}_0$  in the material into  $\vec{r}$  where

$$\vec{r} = H\vec{r}_0. \quad (1.1)$$

The first approach, historically, is through the infinitesimal strain matrix  $\epsilon = H - I$ , where  $I$  is the unit  $3 \times 3$  matrix, and the second, exploited first by Born in works referred to earlier, is via the finite, or Lagrangian, strain matrix  $\eta$ , given by  $2\eta + I = \tilde{H}H$ , where the tilde denotes transposition. The two forms continue to coexist because strains in the first case are more computationally-friendly when contributions to the energy are not simple analytical functions of interatomic distances or atomic volume whilst strains in the second case are rotationally-invariant and therefore rigorous thermodynamically.

Complex treatments of elasticity, *via* total energy calculations for example, or models in which many-body terms are introduced to represent bond order, are not easily handled analytically and usually require the energy to be calculated for a sufficiently large set of deformations and the results processed by numerical differentiation. Such calculations are most readily handled through infinitesimal approach and the resulting Fuchs constants [19] converted subsequently to Brugger constants [5], their finite strain counterparts. This procedure, which is particularly intricate for the inner elastic constants, has been completely generalized and underlies all the calculations in the thesis. It is detailed extensively in Appendix A and augmented by a full exposition of computational procedures of sufficient scope to enable all constants to be computed.

It is the finite strain approach, however, that is followed from a formal point of view. As  $\eta$  is symmetric the usual Voigt contraction of suffixes has been implemented: the strain represented by  $\eta_I$  where  $I$  runs from 1 to 6.

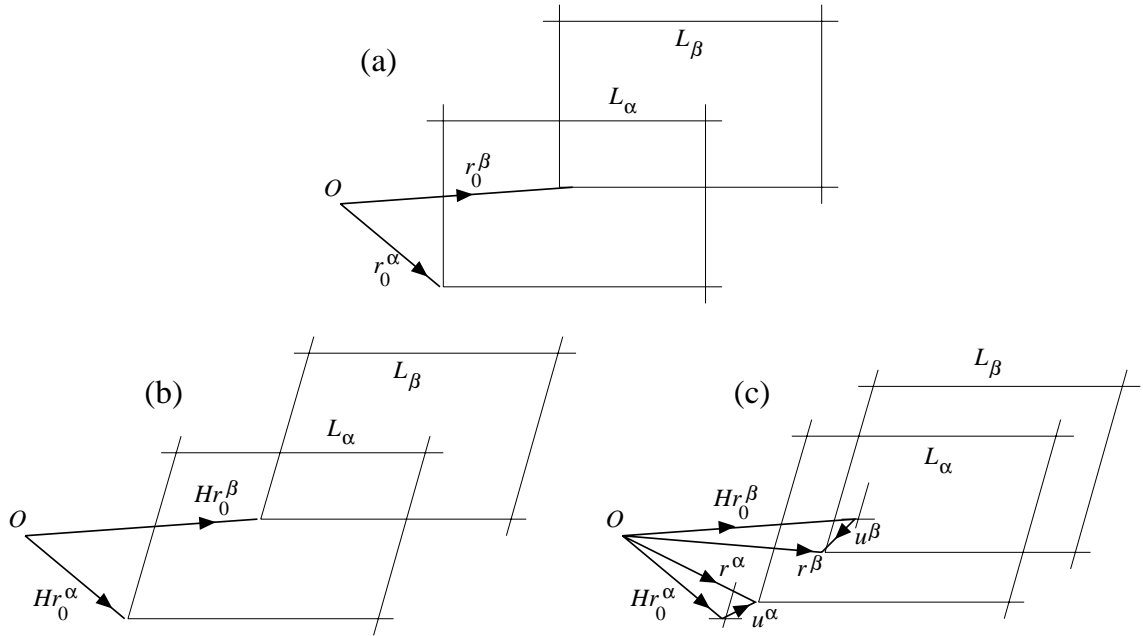


Figure 1.1: Schematic of occurrence of sublattice displacement

## 1.4 Microscopic strain

### 1.4.1 Occurrence and description of sublattice displacement

If each lattice point in a crystal structure is associated with a basis of  $n$  distinguishable material units (atoms, ions, etc.) then the crystal can be considered as  $n$  interpenetrating identical sublattices  $L_1, L_2, \dots, L_n$ . All sites on a given sublattice have the same symmetry but different sublattices may have different symmetries. The group of point operations that embodies the symmetry of the environment of sites on  $L_\alpha$  will be denoted by  $G_\alpha$ . Compatibility with translational periodicity constrains  $G_\alpha$  to be one of the 32 point groups normally encountered in crystal classification. The occurrence of sublattice displacement is illustrated in Fig. 1.1. This shows schematically the effect of a homogeneous deformation, represented by the matrix  $H$ , on two sublattices  $L_\alpha$  and  $L_\beta$ . Fig. 1.1(a) is the situation before deformation. Fig. 1.1(b) shows the effect of  $H$  when both  $G_\alpha$  and  $G_\beta$  contain the inversion. The crucial rôle of the inversion is easily appreciated: if it is present in  $G_\alpha$  then the equivalence of the vectors  $\vec{r}$  and  $-\vec{r}$  with respect to any site on  $L_\alpha$  prevents the atom at such a site from being preferentially displaced asymmetrically with respect to the environment. The same argument applies to the atoms on  $L_\beta$ . Since the atoms on  $L_\alpha$  are part of the environment of those on  $L_\beta$  and conversely, it is a necessary condition for the occurrence of sublattice displacement that at least one of  $G_\alpha$  and  $G_\beta$  should lack the inversion. Fig. 1.1(c) shows the situation when both  $L_\alpha$  and  $L_\beta$  suffer sublattice displacements.

In the infinitesimal approach atomic positions are given by

$$\vec{r}^{\alpha} = H\vec{r}_0^{\alpha} + \vec{u}^{\alpha} \quad (1.2)$$

where  $\alpha$  runs from 1 to  $n$ , with  $\vec{u}^{\alpha} \equiv 0$  when  $G_{\alpha}$  contains the inversion. In the finite strain approach rotational invariance is obtained by redefining the sublattice displacement as  $\vec{w}^{\alpha} = \tilde{H}\vec{u}^{\alpha}$  whence

$$\vec{r}^{\alpha} = H\vec{r}_0^{\alpha} + \tilde{H}^{-1}\vec{w}^{\alpha}. \quad (1.3)$$

The  $\vec{w}^{\alpha}$  are not all independent because homogeneous deformation does not shift the centre of mass. Thus  $\sum_1^n m^{\alpha}\vec{w}^{\alpha} / \sum_1^n m^{\alpha} = 0$ , where  $m^{\alpha}$  is the mass of the atoms on sublattice  $\alpha$ .

### 1.4.2 Inner displacement

Interatomic vectors, rather than individual atomic position vectors, are the entities most intimately involved in elasticity calculations:

$$\vec{r}^{\beta} - \vec{r}^{\alpha} = H(\vec{r}_0^{\beta} - \vec{r}_0^{\alpha}) + \tilde{H}^{-1}(\vec{w}^{\beta} - \vec{w}^{\alpha}). \quad (1.4)$$

The relative sublattice displacements implied are then used to define rotationally-invariant inner displacement through

$$\vec{\zeta}^{\lambda} = \vec{w}^{\beta} - \vec{w}^{\alpha} = \tilde{H}(\vec{u}^{\beta} - \vec{u}^{\alpha}), \quad (1.5)$$

where  $\lambda$ , the interlattice index, is methodically related to the ordered pair  $\alpha, \beta$ , where  $\beta > \alpha$ , by

$$\lambda = \alpha + \frac{1}{2}(\beta - \alpha - 1)(2n - \beta + \alpha). \quad (1.6)$$

This prescription can be visualized in the following tableau which illustrates the case when  $n = 6$  and locates  $\vec{\zeta}^{\lambda}$  at the intersection of the sloping lines that run from a particular  $\vec{w}^{\alpha}$  and  $\vec{w}^{\beta}$ .

Table 1.1:

Sublattice displacement					
$\vec{w}^1$	$\vec{w}^2$	$\vec{w}^3$	$\vec{w}^4$	$\vec{w}^5$	$\vec{w}^6$
$\vec{\zeta}^1$		$\vec{\zeta}^2$		$\vec{\zeta}^3$	
	$\vec{\zeta}^6$		$\vec{\zeta}^7$		$\vec{\zeta}^8$
		$\vec{\zeta}^{10}$		$\vec{\zeta}^{11}$	
			$\vec{\zeta}^{13}$		$\vec{\zeta}^{14}$
				$\vec{\zeta}^{15}$	
					$\vec{\zeta}^5$
					$\vec{\zeta}^9$
					$\vec{\zeta}^{12}$
					$\vec{\zeta}^4$
					$\vec{\zeta}^2$
					$\vec{\zeta}^1$
					$\vec{\zeta}^3$
					$\vec{\zeta}^7$
					$\vec{\zeta}^{11}$
					$\vec{\zeta}^{15}$
					$\vec{\zeta}^5$
					$\vec{\zeta}^9$
					$\vec{\zeta}^{13}$
					$\vec{\zeta}^{17}$
					$\vec{\zeta}^{21}$
					$\vec{\zeta}^{25}$
					$\vec{\zeta}^{29}$
					$\vec{\zeta}^{33}$
					$\vec{\zeta}^{37}$
					$\vec{\zeta}^{41}$
					$\vec{\zeta}^{45}$
					$\vec{\zeta}^{49}$
					$\vec{\zeta}^{53}$
					$\vec{\zeta}^{57}$
					$\vec{\zeta}^{61}$
					$\vec{\zeta}^{65}$
					$\vec{\zeta}^{69}$
					$\vec{\zeta}^{73}$
					$\vec{\zeta}^{77}$
					$\vec{\zeta}^{81}$
					$\vec{\zeta}^{85}$
					$\vec{\zeta}^{89}$
					$\vec{\zeta}^{93}$
					$\vec{\zeta}^{97}$
					$\vec{\zeta}^{101}$
					$\vec{\zeta}^{105}$
					$\vec{\zeta}^{109}$
					$\vec{\zeta}^{113}$
					$\vec{\zeta}^{117}$
					$\vec{\zeta}^{121}$
					$\vec{\zeta}^{125}$
					$\vec{\zeta}^{129}$
					$\vec{\zeta}^{133}$
					$\vec{\zeta}^{137}$
					$\vec{\zeta}^{141}$
					$\vec{\zeta}^{145}$
					$\vec{\zeta}^{149}$
					$\vec{\zeta}^{153}$
					$\vec{\zeta}^{157}$
					$\vec{\zeta}^{161}$
					$\vec{\zeta}^{165}$
					$\vec{\zeta}^{169}$
					$\vec{\zeta}^{173}$
					$\vec{\zeta}^{177}$
					$\vec{\zeta}^{181}$
					$\vec{\zeta}^{185}$
					$\vec{\zeta}^{189}$
					$\vec{\zeta}^{193}$
					$\vec{\zeta}^{197}$
					$\vec{\zeta}^{201}$
					$\vec{\zeta}^{205}$
					$\vec{\zeta}^{209}$
					$\vec{\zeta}^{213}$
					$\vec{\zeta}^{217}$
					$\vec{\zeta}^{221}$
					$\vec{\zeta}^{225}$
					$\vec{\zeta}^{229}$
					$\vec{\zeta}^{233}$
					$\vec{\zeta}^{237}$
					$\vec{\zeta}^{241}$
					$\vec{\zeta}^{245}$
					$\vec{\zeta}^{249}$
					$\vec{\zeta}^{253}$
					$\vec{\zeta}^{257}$
					$\vec{\zeta}^{261}$
					$\vec{\zeta}^{265}$
					$\vec{\zeta}^{269}$
					$\vec{\zeta}^{273}$
					$\vec{\zeta}^{277}$
					$\vec{\zeta}^{281}$
					$\vec{\zeta}^{285}$
					$\vec{\zeta}^{289}$
					$\vec{\zeta}^{293}$
					$\vec{\zeta}^{297}$
					$\vec{\zeta}^{301}$
					$\vec{\zeta}^{305}$
					$\vec{\zeta}^{309}$
					$\vec{\zeta}^{313}$
					$\vec{\zeta}^{317}$
					$\vec{\zeta}^{321}$
					$\vec{\zeta}^{325}$
					$\vec{\zeta}^{329}$
					$\vec{\zeta}^{333}$
					$\vec{\zeta}^{337}$
					$\vec{\zeta}^{341}$
					$\vec{\zeta}^{345}$
					$\vec{\zeta}^{349}$
					$\vec{\zeta}^{353}$
					$\vec{\zeta}^{357}$
					$\vec{\zeta}^{361}$
					$\vec{\zeta}^{365}$
					$\vec{\zeta}^{369}$
					$\vec{\zeta}^{373}$
					$\vec{\zeta}^{377}$
					$\vec{\zeta}^{381}$
					$\vec{\zeta}^{385}$
					$\vec{\zeta}^{389}$
					$\vec{\zeta}^{393}$
					$\vec{\zeta}^{397}$
					$\vec{\zeta}^{401}$
					$\vec{\zeta}^{405}$
					$\vec{\zeta}^{409}$
					$\vec{\zeta}^{413}$
					$\vec{\zeta}^{417}$
					$\vec{\zeta}^{421}$
					$\vec{\zeta}^{425}$
					$\vec{\zeta}^{429}$
					$\vec{\zeta}^{433}$
					$\vec{\zeta}^{437}$
					$\vec{\zeta}^{441}$
					$\vec{\zeta}^{445}$
					$\vec{\zeta}^{449}$
					$\vec{\zeta}^{453}$
					$\vec{\zeta}^{457}$
					$\vec{\zeta}^{461}$
					$\vec{\zeta}^{465}$
					$\vec{\zeta}^{469}$
					$\vec{\zeta}^{473}$
					$\vec{\zeta}^{477}$
					$\vec{\zeta}^{481}$
					$\vec{\zeta}^{485}$
					$\vec{\zeta}^{489}$
					$\vec{\zeta}^{493}$
					$\vec{\zeta}^{497}$
					$\vec{\zeta}^{501}$
					$\vec{\zeta}^{505}$
					$\vec{\zeta}^{509}$
					$\vec{\zeta}^{513}$
					$\vec{\zeta}^{517}$
					$\vec{\zeta}^{521}$
					$\vec{\zeta}^{525}$
					$\vec{\zeta}^{529}$
					$\vec{\zeta}^{533}$
					$\vec{\zeta}^{537}$
					$\vec{\zeta}^{541}$
					$\vec{\zeta}^{545}$
					$\vec{\zeta}^{549}$
					$\vec{\zeta}^{553}$
					$\vec{\zeta}^{557}$
					$\vec{\zeta}^{561}$
					$\vec{\zeta}^{565}$
					$\vec{\zeta}^{569}$
					$\vec{\zeta}^{573}$
					$\vec{\zeta}^{577}$
					$\vec{\zeta}^{581}$
					$\vec{\zeta}^{585}$
					$\vec{\zeta}^{589}$
					$\vec{\zeta}^{593}$
					$\vec{\zeta}^{597}$
					$\vec{\zeta}^{601}$
					$\vec{\zeta}^{605}$
					$\vec{\zeta}^{609}$
					$\vec{\zeta}^{613}$
					$\vec{\zeta}^{617}$
					$\vec{\zeta}^{621}$
					$\vec{\zeta}^{625}$
					$\vec{\zeta}^{629}$
					$\vec{\zeta}^{633}$
					$\vec{\zeta}^{637}$
					$\vec{\zeta}^{641}$
					$\vec{\zeta}^{645}$
					$\vec{\zeta}^{649}$
					$\vec{\zeta}^{653}$
					$\vec{\zeta}^{657}$
					$\vec{\zeta}^{661}$
					$\vec{\zeta}^{665}$
					$\vec{\zeta}^{669}$
					$\vec{\zeta}^{673}$
					$\vec{\zeta}^{677}$
					$\vec{\zeta}^{681}$
					$\vec{\zeta}^{685}$
					$\vec{\zeta}^{689}$
					$\vec{\zeta}^{693}$
					$\vec{\zeta}^{697}$
					$\vec{\zeta}^{701}$

It is readily seen that  $n - 1$  of the  $\vec{\zeta}^\lambda$  at most, those with  $\lambda \leq n - 1$ , are independent. All the  $\vec{\zeta}^\lambda$  with  $\lambda \geq n$  can be expressed as sums of consecutive independent ones: for example, in the tableau above,

$$\vec{\zeta}^{11} = \vec{w}^5 - \vec{w}^2 = (\vec{w}^3 - \vec{w}^2) + (\vec{w}^4 - \vec{w}^3) + (\vec{w}^5 - \vec{w}^4) = \vec{\zeta}^2 + \vec{\zeta}^3 + \vec{\zeta}^4. \quad (1.7)$$

It will prove useful later if this independent set is defined via  $\vec{\zeta}^\lambda = \Lambda^{\lambda\alpha} \vec{w}^\alpha$  and the  $(n - 1) \times n$  rectangular matrix

$$\Lambda = \begin{bmatrix} -1 & 1 & \cdot & \cdots & \cdot & \cdot \\ \cdot & -1 & 1 & \cdots & \cdot & \cdot \\ \vdots & \vdots & \vdots & \ddots & \vdots & \vdots \\ \cdot & \cdot & \cdot & \cdots & 1 & \cdot \\ \cdot & \cdot & \cdot & \cdots & -1 & 1 \end{bmatrix}. \quad (1.8)$$

In certain crystal structures some sublattices, say  $n_i$  of them, possess inversion symmetry. Two cases arise: if  $n_i = 1$  then there will still be  $n(n - 1)/2$  non-zero  $\vec{\zeta}^\lambda$  of which  $n - 1$  are independent (essentially it makes no difference to the earlier tableau if  $\vec{w}^6 = 0$ ); if  $n_i \geq 2$  there are  $m(m - 1)/2$  non-zero values of  $\vec{\zeta}^\lambda$ , some repeated, of which  $m - 1 = n - n_i$  are independent. This rather tricky result is illustrated for the  $n = 6$  case with  $n_i = 2$

Table 1.2:

Sublattice displacement					
$\vec{w}^1$	$\vec{w}^2$	$\vec{w}^3$	$\vec{w}^4$	$\vec{w}^5 = 0$	$\vec{w}^6 = 0$
	$\vec{\zeta}^1$	$\vec{\zeta}^2$	$\vec{\zeta}^3$	$\vec{\zeta}^4$	$\vec{\zeta}^5 = 0$
		$\vec{\zeta}^6$	$\vec{\zeta}^7$	$\vec{\zeta}^8$	$\vec{\zeta}^9 = \vec{\zeta}^4$
			$\vec{\zeta}^{10}$	$\vec{\zeta}^{11}$	$\vec{\zeta}^{12} = \vec{\zeta}^8$
				$\vec{\zeta}^{13}$	$\vec{\zeta}^{14} = \vec{\zeta}^{11}$
					$\vec{\zeta}^{15} = \vec{\zeta}^{13}$
					Inner displacement

### 1.4.3 Internal strain tensors

Since the inner displacement is the crystal response to homogeneous deformation, the components of each independent inner displacement vector can be expressed as a Taylor series in the components of the finite strain:

$$\zeta_i^\lambda = A_{iJ}^\lambda \eta_J + \frac{1}{2} A_{iJK}^\lambda \eta_J \eta_K + \cdots \quad \lambda = 1, 2, \dots, m - 1 \quad (1.9)$$

where there is no constant term since  $\zeta_i^\lambda = 0$  when  $\eta = 0$  and  $m - 1 = n - 1$  if  $n_i = 0, 1$  and  $m - 1 = n - n_i$  if  $n_i \geq 2$ . The coefficients  $A_{iJ}^\lambda$  and  $A_{iJK}^\lambda$  are the components of the internal strain tensors.

Further discussion of internal strain tensors is deferred to Sec. 1.5.4 where their relationship to the inner elastic constants is set out.

## 1.5 Energy and elastic constants

An individual contribution to the free energy per unit initial volume of a strained crystal can be expressed as a Taylor series in the components of  $\eta$  and  $\zeta^\lambda$  as follows:

$$\begin{aligned} \rho_0 F(\zeta^\lambda, \eta) = & \rho_0 F(0, 0) + C_I^0 \eta_I + D_i^\lambda \zeta_i^\lambda \\ & + \frac{1}{2} C_{IJ}^0 \eta_I \eta_J + D_{iJ}^\lambda \zeta_i^\lambda \eta_J + \frac{1}{2} E_{ij}^{\lambda\mu} \zeta_i^\lambda \zeta_j^\mu \\ & + \frac{1}{6} C_{IJK}^0 \eta_I \eta_J \eta_K + \frac{1}{2} D_{iJK}^\lambda \zeta_i^\lambda \eta_J \eta_K + \frac{1}{2} E_{ijk}^{\lambda\mu} \zeta_i^\lambda \zeta_j^\mu \eta_K + \frac{1}{6} F_{ijk}^{\lambda\mu\nu} \zeta_i^\lambda \zeta_j^\mu \zeta_k^\nu, \end{aligned} \quad (1.10)$$

where  $F(0, 0)$  is the free energy per unit mass in the unstrained state. Summation over repeated indices is understood, Greek superscripts run from 1 to  $m - 1$  where  $m - 1 = n - 1$  if  $n_i = 0, 1$  or  $m - 1 = n - n_i$  if  $n_i \geq 2$ . If  $m = 2$  the superscripts are all unity and may thus be omitted for clarity. Lower case Roman subscripts run from 1 to 3, upper case from 1 to 6.

### 1.5.1 Partial elastic constants

The coefficients  $C_I^0$ ,  $C_{IJ}^0$  and  $C_{IJK}^0$  are contributions to the *partial* elastic constants which are themselves the contributions to the *total* elastic constants  $C_I$ ,  $C_{IJ}$  and  $C_{IJK}$  that are independent of inner displacement.

### 1.5.2 Inner elastic constants

The tensors characterized by the components  $D_i^\lambda$ ,  $D_{iJ}^\lambda$ ,  $D_{iJK}^\lambda$ ,  $E_{ij}^{\lambda\mu}$ ,  $E_{ijK}^{\lambda\mu}$  and  $F_{ijk}^{\lambda\mu\nu}$  are the *inner* elastic constants. These are all defined in the same way, that is as derivatives of the energy with respect to strain parameters, thus for example

$$D_{iJ}^\lambda = \rho_0 (\partial^2 F / \partial \zeta_i^\lambda \partial \eta_J)_0 \quad (1.11)$$

where the derivative is evaluated at equilibrium. These definitions are analogous to those of Brugger for the total elastic constants [5].

The notation for the inner elastic constants is based on the following considerations: (i) the Cartesian and Voigt subscripts are separated from the interlattice indices as they are different kinds of label; (ii) the subscript sequence is a useful label when the results of symmetry analysis are tabulated, as in the following Chapter; (iii) the sequence  $C$ ,  $D$ ,  $E$  and  $F$  for the tensors with 0, 1, 2 and 3 inner displacement components permits different tensor types to be distinguished when the

subscripts are numerical. Although this is a redundant indication when superscripts are present it comes into its own when they are absent, which commonly happens when  $m = 2$ .

The  $D_{iJ}^\lambda$  elements express the strength of the coupling between internal and external strain and the  $E_{ij}^{\lambda\mu}$ , closely related to lattice-dynamical coupling constants, determine the frequencies, and sometimes the eigenvectors, of the optic modes at the zone centre. The remaining third-order constants,  $D_{iJK}^\lambda$ ,  $E_{ijK}^{\lambda\mu}$  and  $F_{ijk}^{\lambda\mu\nu}$ , are involved in the strain-dependence of various parameters that would be constant in the harmonic approximation.

### 1.5.3 External equilibrium of the unstressed crystal

When all contributions  $\alpha$  to the free energy have been included in Eq. (1.10) equilibrium conditions require that the sums of the first-order terms should be zero:  $C_I = \sum_\alpha (C_I^0)_\alpha \equiv 0$  and  $D_i^\lambda = \sum_\alpha (D_i^\lambda)_\alpha \equiv 0$ . The total free energy is then a minimum with respect to all possible small deformations. If these are homogeneous then all the principal minors of  $C_{IJ}$  are greater than zero [3, ch.3]. These conditions guarantee the vanishing of external stress and a positive definite value for the elastic energy.

The total free energy must also be a minimum with respect to arbitrary spontaneous inner displacements. From (1.10) it can be seen that the term in  $E_{ij}^{\lambda\mu} \zeta_i^\lambda \zeta_j^\mu$  must be positive definite. If this is so there exists a similarity transformation that will diagonalize  $E^{\lambda\mu}$  and render all the diagonal elements positive. The matrix  $E^{\lambda\mu}$  will therefore be non-singular and will possess an inverse  $B^{\lambda\mu}$  given by

$$B^{\lambda\mu} = (\tilde{E}^{\lambda\mu})^\dagger / (\det E^{\lambda\mu}) \quad (1.12)$$

where the tilde denotes transposition, the dagger indicates the formation of the adjugate matrix and det indicates the determinant.

### 1.5.4 Internal equilibrium of the stressed crystal

The application of a stress to a crystal produces a finite strain and a minimization of the free energy by inner displacement. Stability of equilibrium against small changes in the components of inner displacement requires that

$$\rho_0 \left( \frac{\partial F}{\partial \zeta_i^\lambda} \right)_\eta = 0 \quad (1.13)$$

$$\rho_0 \left( \frac{\partial^2 F}{\partial \zeta_i^{\lambda 2}} \right)_\eta > 0 \quad (1.14)$$

and

$$\left[ \rho_0 \left( \frac{\partial^2 F}{\partial \zeta_i^{\lambda 2}} \right)_\eta \right] \left[ \rho_0 \left( \frac{\partial^2 F}{\partial \zeta_j^{\mu 2}} \right)_\eta \right] > \left[ \rho_0 \left( \frac{\partial^2 F}{\partial \zeta_i^\lambda \partial \zeta_j^\mu} \right)_\eta \right]^2. \quad (1.15)$$

The inequalities specialized to the case of vanishing  $\eta$  give

$$E_{ii}^{\lambda\lambda} > 0 \quad (1.16)$$

and

$$E_{ii}^{\lambda\lambda} E_{jj}^{\mu\mu} > (E_{ij}^{\lambda\mu})^2. \quad (1.17)$$

Using (1.9) and (1.10) it is seen that (1.13) becomes

$$\begin{aligned} D_i^\lambda + \eta_I (D_{iI}^\lambda + E_{ij}^{\lambda\mu} A_{jI}^\mu) \\ + \frac{1}{2} \eta_I \eta_J [D_{iIJ}^\lambda + E_{ij}^{\lambda\mu} A_{jIJ}^\mu + (E_{ijI}^{\lambda\mu} A_{jJ}^\mu + E_{ijJ}^{\lambda\mu} A_{jI}^\mu) + F_{ijk}^{\lambda\mu\nu} A_{jI}^\mu A_{kJ}^\nu] \equiv 0. \end{aligned} \quad (1.18)$$

Since this is true for all  $\eta$  the first term and the coefficients of  $\eta_I$  and  $\eta_I \eta_J$  must be separately zero:

$$D_i^\lambda = 0 \quad (1.19)$$

$$D_{iI}^\lambda + E_{ij}^{\lambda\mu} A_{jI}^\mu = 0 \quad (1.20)$$

and

$$D_{iIJ}^\lambda + E_{ij}^{\lambda\mu} A_{jIJ}^\mu + (E_{ijI}^{\lambda\mu} A_{jJ}^\mu + E_{ijJ}^{\lambda\mu} A_{jI}^\mu) + F_{ijk}^{\lambda\mu\nu} A_{jI}^\mu A_{kJ}^\nu = 0. \quad (1.21)$$

Equation (1.20) may be solved for the internal strain tensor by using the inverse defined in (1.12), giving

$$A_{iJ}^\lambda = -B_{ip}^{\lambda\mu} D_{pJ}^\mu. \quad (1.22)$$

Equation (1.21) is formally just as easy to solve despite its apparent complexity. All that is required is the definition of a composite tensor

$$G_{iIJ}^\lambda = D_{iIJ}^\lambda + (E_{ijI}^{\lambda\mu} A_{jJ}^\mu + E_{ijJ}^{\lambda\mu} A_{jI}^\mu) + F_{ijk}^{\lambda\mu\nu} A_{jI}^\mu A_{kJ}^\nu \quad (1.23)$$

from which the solution

$$A_{iJK}^\lambda = -B_{ip}^{\lambda\mu} G_{pJK}^\mu. \quad (1.24)$$

follows.

### 1.5.5 Composition of the total elastic constants

Individual contributions to the total elastic constants are obtained from (1.10) by taking total derivatives with respect to the components of  $\eta$ . The usual Brugger definition of the  $n$ th-order elastic constant may then be generalized to

$$C_{IJ..} = \rho_0 \left( \frac{\mathbf{D}^n F}{\mathbf{D}\eta_I \mathbf{D}\eta_{J..}} \right)_0 \quad (1.25)$$

where

$$\begin{aligned} \frac{D}{D\eta_I} &\equiv \frac{\partial}{\partial \eta_I} + \frac{\partial \zeta_i^\lambda}{\partial \eta_I} \frac{\partial}{\partial \zeta_i^\lambda} && \text{summed over } \lambda = 1, 2, \dots, m-1 \\ &\equiv \frac{\partial}{\partial \eta_I} + (A_{iI}^\lambda + A_{iIP}^\lambda \eta_P + \dots) \frac{\partial}{\partial \zeta_i^\lambda} \end{aligned} \quad (1.26)$$

using (1.9). The contribution to a particular elastic constant is then the sum of terms depending on the different orders of internal strain. Thus to the second order

$$\begin{aligned} C_I &= C_I^0 + C_I^1 \\ C_{IJ} &= C_{IJ}^0 + C_{IJ}^1 + C_{IJ}^2 \\ C_{IJK} &= C_{IJK}^0 + C_{IJK}^1 + C_{IJK}^2 \end{aligned} \quad (1.27)$$

where the first-order internal strain contributions are

$$\begin{aligned} C_I^1 &= A_{iI}^\lambda D_i^\lambda \\ C_{IJ}^1 &= A_{iI}^\lambda (D_{iJ}^\lambda + E_{ij}^{\lambda\mu} A_{jJ}^\mu) + A_{iJ}^\lambda (D_{iI}^\lambda + E_{ij}^{\lambda\mu} A_{jI}^\mu) - A_{iI}^\lambda A_{jJ}^\mu E_{ij}^{\lambda\mu} \\ C_{IJK}^1 &= (A_{iI}^\lambda D_{iJK}^\lambda + A_{iJ}^\lambda D_{iIK}^\lambda + A_{iK}^\lambda D_{iIJ}^\lambda) \\ &\quad + (A_{iI}^\lambda A_{jJ}^\mu E_{ijK}^{\lambda\mu} + A_{iI}^\lambda A_{jK}^\mu E_{ijJ}^{\lambda\mu} + A_{iJ}^\lambda A_{jK}^\mu E_{ijI}^{\lambda\mu}) + A_{iI}^\lambda A_{jJ}^\mu A_{kK}^\nu F_{ijk}^{\lambda\mu\nu} \end{aligned} \quad (1.28)$$

and the second-order contributions are

$$\begin{aligned} C_{IJ}^2 &= A_{iIJ}^\lambda D_i^\lambda \\ C_{IJK}^2 &= A_{iIJ}^\lambda (D_{iK}^\lambda + E_{ij}^{\lambda\mu} A_{jK}^\mu) + A_{iIK}^\lambda (D_{iJ}^\lambda + E_{ij}^{\lambda\mu} A_{jJ}^\mu) + A_{iJK}^\lambda (D_{iI}^\lambda + E_{ij}^{\lambda\mu} A_{jI}^\mu). \end{aligned} \quad (1.29)$$

The symmetrized expressions guarantee the equality of total elastic constants that differ only in the order of their subscripts. Considerable simplification follows the application of the equilibrium conditions, (1.19) and (1.20). First it can be seen that  $C_{IJ}^2 = C_{IJK}^2 = 0$  and that the second-order internal strain has no effect on the elasticity below the fourth order. This conclusion was reached by Srinivasan in [36] using a central force model and a mixture of infinitesimal and finite strain parameters. The derivation here involves no assumptions and holds rigorously. Final results for the composition of the total elastic constants are

$$\begin{aligned} C_I &= C_I^0 = 0 \\ C_{IJ} &= C_{IJ}^0 - A_{iI}^\lambda A_{jJ}^\mu E_{ij}^{\lambda\mu} \\ C_{IJK} &= C_{IJK}^0 + (A_{iI}^\lambda D_{iJK}^\lambda + A_{iJ}^\lambda D_{iIK}^\lambda + A_{iK}^\lambda D_{iIJ}^\lambda) \\ &\quad + (A_{iI}^\lambda A_{jJ}^\mu E_{ijK}^{\lambda\mu} + A_{iI}^\lambda A_{jK}^\mu E_{ijJ}^{\lambda\mu} + A_{iJ}^\lambda A_{jK}^\mu E_{ijI}^{\lambda\mu}) + A_{iI}^\lambda A_{jJ}^\mu A_{kK}^\nu F_{ijk}^{\lambda\mu\nu} \end{aligned} \quad (1.30)$$

## 1.6 Compliances and compressibilities

Measurements of lattice parameter and volume change under pressure by means of X-ray or neutron diffraction may be used to extract elasticity information from crystals too small to subject to more conventional techniques, such as ultrasonics. The primary quantities obtained are compressibilities.

The compatibility of Hooke's law extended to terms quadratic in the strain

$$\sigma_I = C_{IJ}\eta_J + \frac{1}{2}C_{IJK}\eta_J\eta_K \quad (1.31)$$

with its inverse form

$$\eta_I = S_{IJ}\sigma_J + \frac{1}{2}S_{IJK}\sigma_J\sigma_K \quad (1.32)$$

defines implicitly both second- and third-order elastic compliances. The second-order ones are given by standard matrix inversion whilst the third-order ones are given by [2, 21]

$$S_{IJK} = -S_{IP}S_{JQ}S_{KR}C_{PQR}. \quad (1.33)$$

Under hydrostatic pressure  $\sigma_J = -p\delta_J$ , where  $\delta_J = 1$  if  $J = 1, 2$  or  $3$  and zero otherwise, whence

$$\begin{aligned} \eta_I &= -pS_{IJ}\delta_J + \frac{1}{2}p^2S_{IJK}\delta_J\delta_K \\ &= -k_I p + \frac{1}{2}K_I p^2 \end{aligned} \quad (1.34)$$

implicitly defining harmonic and anharmonic linear compressibilities.

## 1.7 Computational simplification and sublattice tensors

In practical computation it is easy to impose a single sublattice displacement and evaluate the consequences. But a single such displacement automatically activates a number of inner displacements, as a glance at the illustrative tableaux presented earlier will show, and there is no way to specify a single inner displacement. It is therefore computationally simpler to introduce sets of **sublattice tensors**  $d$ ,  $e$  and  $f$  that relate to sublattice displacement in the same way that inner elastic constants relate to inner displacement:

$$\begin{aligned} d_i^\alpha &= \rho_0 (\partial F / \partial w_i^\alpha)_0 \\ d_{iJ}^\alpha &= \rho_0 (\partial^2 F / \partial w_i^\alpha \partial \eta_J)_0 \\ d_{iJK}^\alpha &= \rho_0 (\partial^3 F / \partial w_i^\alpha \partial \eta_J \partial \eta_K)_0 \\ e_{ij}^{\alpha\beta} &= \rho_0 (\partial^2 F / \partial w_i^\alpha \partial w_j^\beta)_0 \\ e_{ijK}^{\alpha\beta} &= \rho_0 (\partial^3 F / \partial w_i^\alpha \partial w_j^\beta \partial \eta_K)_0 \\ f_{ijk}^{\alpha\beta\gamma} &= \rho_0 (\partial^3 F / \partial w_i^\alpha \partial w_j^\beta \partial w_k^\gamma)_0 \end{aligned} \quad (1.35)$$

where the Greek superscripts take values from 1 to  $n - n_i$ .

The sublattice tensors are related to the inner elastic constants via chain rule differentiation with the operator

$$\frac{\partial}{\partial w_i^\alpha} = \left( \frac{\partial \zeta_i^\lambda}{\partial w_i^\alpha} \right) \frac{\partial}{\partial \zeta_i^\lambda} = \tilde{\Lambda}^{\alpha\lambda} \frac{\partial}{\partial \zeta_i^\lambda} \quad (1.36)$$

where  $\tilde{\Lambda}$  is the transpose of the matrix defined in (1.8).

The inner elastic constants are then given in terms of sublattice tensors by

$$\begin{aligned} D_{\dots}^\lambda &= - \sum_{p=1}^{\lambda} d_{\dots}^p \\ E_{\dots}^{\lambda\mu} &= \sum_{p=1}^{\lambda} \sum_{q=1}^{\mu} e_{\dots}^{pq} \\ F_{\dots}^{\lambda\mu\nu} &= - \sum_{p=1}^{\lambda} \sum_{q=1}^{\mu} \sum_{r=1}^{\nu} f_{\dots}^{pqr} \end{aligned} \quad (1.37)$$

for all valid subscript sequences  $i, iJ$  or  $iJK$  on  $d$  and  $D$ ; all  $ij$  or  $ijK$  on  $e$  and  $E$ , and all  $ijk$  on  $f$  and  $F$ .

As the  $n - n_i$  sublattice displacements  $\vec{w}^\alpha$  are not independent it follows from application of (1.36) that

$$\begin{aligned} \sum_{p=1}^{n-n_i} d_{\dots}^p &= 0 \\ \sum_{p=1}^{n-n_i} e_{\dots}^{\alpha p} &= \sum_{p=1}^{n-n_i} e_{\dots}^{p\beta} = 0 \\ \sum_{p=1}^{n-n_i} f_{\dots}^{\alpha\beta p} &= \sum_{p=1}^{n-n_i} f_{\dots}^{\alpha p\gamma} = \sum_{p=1}^{n-n_i} f_{\dots}^{p\beta\gamma} = 0 \end{aligned} \quad (1.38)$$

for any values of  $\alpha, \beta$  or  $\gamma$ . The results are true *a fortiori* for double or triple summations.

It is easily seen that as  $\lambda, \mu$  and  $\nu$  increase the number of terms on the right of (1.37) escalates. Smaller numbers can be retrieved by combining (1.37) and (1.38) to give alternative, equivalent, definitions. For example, combining the summations involving  $\lambda$  in corresponding tensors gives

$$\begin{aligned} D_{\dots}^\lambda &= + \sum_{p=\lambda+1}^{n-n_i} d_{\dots}^p \\ E_{\dots}^{\lambda\mu} &= - \sum_{p=\lambda+1}^{n-n_i} \sum_{q=1}^{\mu} e_{\dots}^{pq} \\ F_{\dots}^{\lambda\mu\nu} &= + \sum_{p=\lambda+1}^{n-n_i} \sum_{q=1}^{\mu} \sum_{r=1}^{\nu} f_{\dots}^{pqr}, \end{aligned} \quad (1.39)$$

where the signs on the right are the opposite of those in (1.37). If the limits on a second superscript are modified the sign will be reversed again, and so on.

## 1.8 Lattice dynamical connection

### 1.8.1 Inner elastic constants and longwave coupling constants

Certain of the inner elastic constants are related to parameters that occur in conventional lattice dynamics and may be discovered by going to the longwave limit. This is equivalent to considering the motion of rigid sublattices.

The variables are the displacements  $\vec{u}^\alpha$  of all  $n$  sublattices from their equilibrium positions and the potential energy per unit initial volume may be written

$$V = V_0 + \Phi_i^\alpha u_i^\alpha + \frac{1}{2} \Phi_{ij}^{\alpha\beta} u_i^\alpha u_j^\beta + \frac{1}{6} \Phi_{ijk}^{\alpha\beta\gamma} u_i^\alpha u_j^\beta u_k^\gamma + \dots \quad \alpha, \beta, \gamma = 1, 2, \dots, n \quad (1.40)$$

where  $\Phi_i^\alpha \equiv (\partial V / \partial u_i^\alpha)_0$  etc., the derivatives being taken at equilibrium. The first step towards the desired comparison is a change from sublattice variable  $\vec{u}^\alpha$  to interlattice variables. This is done by defining  $n - 1$  interlattice displacements  $\vec{z}^\lambda$  by analogy with the first layer of the scheme in Table 1.2, but with all displacements non-zero:

$$\vec{z}^\lambda = \vec{u}^{\lambda+1} - \vec{u}^\lambda \quad \lambda = 1, 2, \dots, n - 1 \quad (1.41)$$

An additional variable is required to produce an invertible transformation between the two approaches. This is provided by  $\vec{z}^n$ , the displacement of the centre of mass:

$$\vec{z}^n = m^p \vec{u}^p / M \quad (1.42)$$

where  $m^p$  is the mass of an atom on sublattice  $p$  and  $M = \sum_{p=1}^n m^p$  is the mass of the entire basis.

The inverse of the coordinate transformation is then

$$u_i^\alpha = Q^{\alpha\lambda} z_i^\lambda \quad \alpha, \lambda = 1, 2, \dots, n \quad (1.43)$$

where

$$Q = \begin{bmatrix} \mu_1 - 1 & \mu_2 - 1 & \cdots & \mu_{n-1} - 1 & 1 \\ \mu_1 & \mu_2 - 1 & \cdots & \mu_{n-1} - 1 & 1 \\ \vdots & \vdots & \vdots & \vdots & \vdots \\ \mu_1 & \mu_2 & \cdots & \mu_{n-1} - 1 & 1 \\ \mu_1 & \mu_2 & \cdots & \mu_{n-1} & 1 \end{bmatrix} \quad (1.44)$$

is an  $n \times n$  matrix in which  $\mu_k = \left( \sum_{p=1}^k m^p \right) / M$ .

The corresponding differential operator applied to the potential energy density  $V$  gives

$$\frac{\partial V}{\partial z_i^\lambda} = \tilde{Q}^{\lambda\alpha} \frac{\partial V}{\partial u_i^\alpha}. \quad (1.45)$$

Because the vibrational energy of a crystal is small compared to its potential energy, the crystal potential energy density,  $V$ , is a good first approximation to the free energy per unit initial volume,  $\rho_0 F$  (Wallace 1972, p.60). The displacements  $\vec{z}^\lambda$  (apart from  $\vec{z}^n$ ) may also be identified with the  $\vec{\zeta}^\lambda$  in the absence of finite strain (i.e.  $H = I$ ) so that if (1.45) is evaluated at equilibrium the following result is obtained:

$$D_i^\lambda = \tilde{Q}^{\lambda\alpha} \Phi_i^\alpha \quad (1.46)$$

and, by extension,

$$E_{ij}^{\lambda\mu} = \tilde{Q}^{\lambda\alpha} \tilde{Q}^{\mu\beta} \Phi_{ij}^{\alpha\beta} \quad (1.47)$$

and

$$F_{ijk}^{\lambda\mu\nu} = \tilde{Q}^{\lambda\alpha} \tilde{Q}^{\mu\beta} \tilde{Q}^{\nu\gamma} \Phi_{ijk}^{\alpha\beta\gamma} \quad (1.48)$$

where  $\lambda, \mu$  and  $\nu$  run from 1 to  $n - 1$  and  $\alpha, \beta$  and  $\gamma$  from 1 to  $n$ .

As shown earlier all the  $D_i^\lambda$  vanish as a result of equilibrium conditions, hence all the  $\Phi_i^\alpha$  in (1.46) are zero, as would be expected from purely lattice dynamical considerations.

The motion of the centre of mass does not contribute to the potential energy of the crystal so the remaining constants, implied by the addition of  $\vec{z}^n$  to the set of variables, all vanish. Thus, since  $\tilde{Q}^{n\alpha} = 1$  for all  $\alpha$ ,

$$D_i^n = \sum_{\alpha} \Phi_i^\alpha = 0 \quad (1.49)$$

$$E_{ij}^{\lambda n} = \tilde{Q}^{\lambda\alpha} \left( \sum_{\beta} \Phi_{ij}^{\alpha\beta} \right) = 0 \quad (1.50)$$

and

$$F_{ijk}^{\lambda\mu n} = \tilde{Q}^{\lambda\alpha} \tilde{Q}^{\mu\beta} \left( \sum_{\gamma} \Phi_{ijk}^{\alpha\beta\gamma} \right) = 0, \quad (1.51)$$

corresponding to standard results on the coupling constants.

### 1.8.2 The secular equation and optic mode frequencies

The kinetic energy per unit initial volume may be written

$$T = \frac{1}{2} \rho^{\alpha\beta} \dot{u}_i^\alpha \dot{u}_i^\beta \quad (1.52)$$

where  $\rho^{\alpha\beta}$  is a diagonal density matrix in which  $\rho^{\alpha\alpha}$  is that part of the equilibrium crystal density due to the atoms on sublattice  $\alpha$  [30]. The Lagrangian per unit initial volume in the harmonic approximation is obtained by subtracting from  $T$  the quadratic terms in  $V$ . Standard procedures may then be used to obtain the  $3n$  equations

$$\left[ \Phi_{ij}^{\alpha\beta} - \omega^2 \rho^{\alpha\beta} \delta_{ij} \right] u_j^\beta = 0. \quad (1.53)$$

If the left-hand side is premultiplied by  $\tilde{Q}$  and  $\vec{u}$  is replaced by  $Q\vec{z}$  the equations become

$$\left[ E_{ij}^{\lambda\mu} - \omega^2 K^{\lambda\mu} \delta_{ij} \right] z_j^\mu = 0 \quad (1.54)$$

where  $K = \tilde{Q}\rho Q$  is a new density matrix (no longer diagonal) and  $\rho$  is a diagonal  $n \times n$  matrix given by

$$\rho = \rho_0 \begin{bmatrix} \mu_1 & \cdot & \cdots & \cdot & \cdot \\ \cdot & \mu_2 - \mu_1 & \cdots & \cdot & \cdot \\ \vdots & \vdots & \vdots & \vdots & \vdots \\ \cdot & \cdot & \cdots & \mu_{n-1} - \mu_{n-2} & \cdot \\ \cdot & \cdot & \cdots & \cdot & 1 - \mu_{n-1} \end{bmatrix}. \quad (1.55)$$

These equations have a non-trivial solution only for those values of  $\omega^2$  that satisfy the secular equation

$$|E_{ij}^{\lambda\mu} - \omega^2 K^{\lambda\mu} \delta_{ij}| = 0. \quad (1.56)$$

In this  $3n \times 3n$  determinant  $\omega^2$  no longer occurs along only the main diagonal. There are however three rows and three columns, corresponding to  $\lambda = n$  and  $\mu = n$  which contain zeroes except where they intersect on the main diagonal where the element  $-\omega^2 K^{nn}$  (i.e.  $-\rho_0 \omega^2$ ) occurs. These triply degenerate roots,  $\omega = 0$ , correspond to the acoustic modes at the zone centre and may be removed from the determinant leaving a  $3(n-1) \times 3(n-1)$  secular equation whose eigenvalues correspond to the longwave limit of the  $3(n-1)$  optic mode frequencies.

If  $n > 2$  then to each value of  $\omega^2$  there corresponds an eigenvector given by

$$E_{ij}^{\lambda\mu} z_j^\mu = \omega^2 K^{\lambda\mu} z_i^\mu. \quad (1.57)$$

If  $n = 2$  the eigenvectors are indeterminate.

## 1.9 Rationale

This Chapter has been concerned with dressing up some old ideas in new clothing. Vocabulary and notation, closely related to that of ordinary elasticity, has been introduced in an effort to make the unity of the subject more readily apparent.

Elastic constant measurements alone reveal nothing of the ‘inner’ aspects of the material. Fortunately there are various experimental techniques which reveal valuable information. Firstly the inelastic scattering of X-rays and neutrons, infra-red and Raman spectroscopy, can all be used for the determination of optic mode frequencies in the longwave limit. Secondly the strain dependence of the intensity of the elastic scattering of X-rays or neutrons from single crystals can be used to determine components of the internal strain tensor. After publishing the papers that form the basis of this and Chapter 2 I led a group specializing in this technique and produced results for a number of group IV elements and III-V compounds. These are mentioned briefly in Chapter 3 where the method, with specific reference to cubic diamond, is described. Thirdly, access to some

---

of the third-order inner elastic constants is possible in principle through the strain dependence of the above phenomena. It is doubtful if any of the techniques are yet sufficiently accurate to provide meaningful results, however.

## References

- [1] T. H. K. Barron, T. G. Gibbons and R. W. Munn, *J. Phys. C: Solid St. Phys.* **4**, 2805 (1971)
- [2] G. R. Barsch, *J. Appl. Phys.* **39**, 3780 (1968)
- [3] M. Born and K. Huang, *Dynamical Theory of Crystal Lattices* (Oxford: Clarendon Press, 1954)
- [4] M. Born, *Atomtheorie des festen Zustandes* (Leipzig: Teubner, 1923)
- [5] K. Brugger, *Phys. Rev.* **133**, A1611 (1964)
- [6] K. Brugger, *J. Appl. Phys.* **36**, 759 (1965)
- [7] K. Brugger, *J. Appl. Phys.* **36**, 768 (1965)
- [8] A. L. Cauchy, *Exercices de Mathématique*, **4** (1829)
- [9] A. Chapman, *Proc. Roy. Inst. of Great Britain*, **67**, 239 (1996)
- [10] C. S. G. Cousins, *Proc. Phys. Soc.*, **91**, 235 (1967)
- [11] C. S. G. Cousins, *J. Phys. C (Proc. Phys. Soc.)*, **1**, 478 (1968)
- [12] C. S. G. Cousins, *J. Phys. C (Solid St. Phys.)*, **2**, 765 (1969)
- [13] C. S. G. Cousins, *J. Phys. C:Solid St. Phys.*, **3**, 1677 (1970)
- [14] C. S. G. Cousins, *J. Phys. C:Solid St. Phys.*, **3**, L197 (1970)
- [15] C. S. G. Cousins, *J. Phys. F: Metal Phys.*, **2**, 1 (1972)
- [16] C. S. G. Cousins, *J. Phys. C:Solid St. Phys.*, **5**, L201 (1972)
- [17] C. S. G. Cousins, *J. Phys. C:Solid St. Phys.*, **11**, 4867 (1978)
- [18] C. S. G. Cousins, *J. Phys. C:Solid St. Phys.*, **11**, 4881 (1978)
- [19] K. Fuchs, *Proc. Roy. Soc.* **A153**, 622 (1936)
- [20] E. R. Fuller and E. R. Naimon, *Phys. Rev.* **B6**, 3609 (1972)
- [21] R. A. H. Hamilton and J. E. Parrott, *J. Phys. C (Proc. Phys. Soc.)* **1**, 829 (1968)

- 
- [22] R. Hooke, *A description of Helioscopes and some other Instruments* (London, 1676)
- [23] R. Hooke, *De Potentia Restitutiva or of Spring Explaining the Power of Springing Bodies* (London, 1678)
- [24] P. N. Keating, *Phys. Rev.* **145**, 637 (1966)
- [25] G. Kirchhoff, *Acad. Wiss. Wien Sitzungberichte*, **IX** (1852)
- [26] J. E. Lennard-Jones, *Proc. Roy. Soc. A*, **106**, 709 (1924)
- [27] J. E. Lennard-Jones, *J. E., Physica* **IV**, 941, (1937)
- [28] W. Ludwig, in *Springer Tracts in Modern Physics*, Volume 43 (1967)
- [29] E. Madelung, *Phys. Zeit.*, **19**, 524 (1918)
- [30] J. W. Martin, *J. Phys. C:Solid St. Phys.* **8**, 2869 (1975)
- [31] F. D. Murnaghan, *Finite Deformation of an Elastic Solid* (New York: Wiley, 1951)
- [32] C. L. Navier, *Mémoires Acad. Sci. Inst. France* (1827)
- [33] J. Nye, *Physical Properties of Crystals*, (Oxford: University Press, 1957 and, with additional material, 1985)
- [34] S. Poisson, *Mémoires Acad. Sci. Inst. France* (1829)
- [35] A. Segmüller, *Phys. kondens. Materie* **3**, 18 (1964)
- [36] R. Srinivasan, *Phys. Rev.* **144**, 620 (1966)
- [37] A. J. B. de St. Venant, *Comptes Rendus Acad. Sci. Paris*, **24** (1847)
- [38] R. N. Thurston, in *Encyclopedia of Physics*, ed. S. Flügge Vol. VIa/4 *Mechanics of Solids IV*, ed. C. Truesdell (Springer 1974)
- [39] D. C. Wallace, *Thermodynamics of Crystals* (New York: Wiley, 1972)

## Chapter 2

### Symmetry of inner elastic constants

A space group is an infinite, spatially periodic, arrangement of symmetry elements having the property that the operation of any particular element carries all the remaining elements into similar elements. At least one complete sample of the arrangement is contained within a limited region of space, a unit cell, and points within this region can be specified by coordinates with respect to some conventionally located reference axes. Every space group has a unique spectrum of sets of equivalent points (Wyckoff sets) of varying degrees of symmetry. A complete description of all space groups is given in the encyclopædic *International Tables of Crystallography, Volume A*, [8]. Conventions for the settings of Cartesian axes with respect to the symmetry elements are given in *Standards on Piezoelectric Crystals*, [11], a work that is far more general than its title suggests.

A crystal structure belongs to a particular space group if entire Wyckoff sets are populated by atoms or ions of the same species. The connection between this description and that in terms of interpenetrating sublattices is simple: every sublattice corresponds to a distinct point in one of the occupied sets. By investigating the effect of symmetry operations on individual points the effect on the sublattices is revealed.

Perfect crystals belong to one of 230 space groups, of which 73 are symmorphic and 157 are non-symmorphic. A space group is said to be symmorphic if, apart from the translations, the generating symmetry operations leave one common point fixed. Thus only the point-group operations are permitted: rotations, reflections, inversions and roto-inversions: together with the identity these form a group of order  $g$

$$\Gamma = \{A^{(s)}\}, \quad (2.1)$$

where the  $A^{(s)}$  are  $3 \times 3$  orthogonal matrices ( $g$  in all). Non-symmorphic space groups are those that possess the space operations of screw axes and/or glide planes. Their symmetry operations are represented by augmented  $4 \times 4$  partitioned matrices which form a group

$$\Gamma = \left\{ \left\{ A^{(s)} | \vec{t} \right\} \right\} = \left\{ \left[ \begin{array}{cc} A^{(s)} & \vec{t} \\ 0 & 1 \end{array} \right] \right\} \quad (2.2)$$

where  $\vec{t}$  is a  $3 \times 1$  column vector representing a fractional translation. These operators act on  $4 \times 1$  column vectors  $[\vec{r}_i/1]$  in which ordinary lattice vectors  $\vec{r}_i$  supply the first three elements.

## 2.1 Point-group symmetry analysis

As far as material tensors are concerned screw axes and glide planes are invisible. Symmetry properties are determined by the directions of the axes, not by the precise position of their origin. In principle the non-zero components of a tensor of rank  $r$  and any relations between them are obtained by invoking the tensor transformation law for every symmetry operator  $A^{(s)}$ :

$$T_{ijk..} = a_{ip}^{(s)} a_{jq}^{(s)} a_{kr}^{(s)} .. T_{pqr..} \quad (2.3)$$

where the  $a_{ip}^{(s)}$  etc. are the elements of  $A^{(s)}$ . The transformation law applies to tensors in uncontracted form. It can be modified provided care is taken. In practice a large number of vanishing components in the orthorhombic, tetragonal and cubic classes can be inferred by direct inspection. In particular, if one of the  $A^{(s)}$  is the inversion then

$$T_{ijk..} = (-1)^r T_{ijk..} \quad (2.4)$$

and tensors of odd rank vanish. Thus, as expected, the  $d$ ,  $D$ ,  $f$  and  $F$  tensors are restricted to the 21 non-centrosymmetric point groups. By their nature the tensors  $e$  and  $E$  are also limited to these groups even though in general tensors of even rank can be defined for all 32 point groups. The rhombohedral and hexagonal classes are rather labour-intensive and, again, require care. Symmetry analysis and direct inspection methods are fully described in [10] where complete results are given for the SOECs. These apply equally to the partial elastic constants introduced in the previous Chapter. Corresponding results for TOECs (and thus for partial TOECs also) are given in [2].

The analysis applies to each distinct sublattice tensor and inner elastic constant and has been carried out with the results displayed in the following six Tables. With one exception the results relate to the standard settings of axes set out in [11] and [12]. The exception relates to the point group  $\bar{6}m2$  where it was recommended that the  $0x_1$  axis be set parallel to a twofold axis. As I showed in [4], this violates two principles that underlie the recommendations: in fact the  $0x_1$  axis should be set perpendicular to a mirror plane  $m$ , a rotation of the axes through  $30^\circ$  about  $0x_3$ .

The maximum number of independent components that may be possessed by a tensor of a particular form for a particular point group may be found by group-theoretical methods. The numbers found here agree in all cases with the expectations listed in Table VIII(a) in [1, ch. 7] if the tensors  $d_i^\alpha$ ,  $d_{iJ}^\alpha$ ,  $d_{iJK}^\alpha$ ,  $e_{ij}^{\alpha\beta}$ ,  $e_{iJK}^{\alpha\beta}$  and  $f_{ijk}^{\alpha\beta\gamma}$  are identified with Properties number 2, 5, 11, 4, 9 and 6 respectively for the cases where  $\alpha$ ,  $\beta$  and  $\gamma$  are all different. If two or more sublattice indices are equal commutative relations may reduce the number still further. Table 2.7 displays this information.

The Tables in the compilation of [13] can be compared with the ones presented here after some minor adjustments, such as symmetrizing the fifth-order polar tensors for comparison with my Table 2.3. Strangely Thurston's footnote to his Table 16.5 states that a  $-30^\circ$  rotation of axes about  $0x_3$  is required for the point groups 3,  $32$  and  $3m$  as well as  $\bar{6}m2$  in order to conform to the standards

Table 2.1: Non-zero components of the tensors  $d_i^\alpha$  and  $D_i^\lambda$ 

Point group	$i$
1	1, 2, 3
$m$	1, 3
2	2
$mm2$ , 4, $4mm$ , 3, $3m$ , 6, $6mm$	3
$222$ , $\bar{4}$ , $\bar{4}2m$ , $422$ , 23, $\bar{4}3m$ , $432$ , 32, $\bar{6}$ , $\bar{6}m2$ , $622$	none

Table 2.2: Non-zero components of the tensors  $d_{iJ}^\alpha$ ,  $D_{iJ}^\lambda$  and  $A_{iJ}^\lambda$ 

Point group	$iJ$
1	All 18 possible pairs
$m$	11, 12, 13, 15, 24, 26, 31, 32, 33, 35
2	14, 16, 21, 22, 23, 25, 34, 36
$mm2$	15, 24, 31, 32, 33
$222$	14, 25, 36
4	14=-25, 15=24, 31=32, 33
$\bar{4}$	14=25, 15=-24, 31=-32, 36
$4mm$	15=24, 31=32, 33
$\bar{4}2m$	14=25, 36
$422$	14=-25
23, $\bar{4}3m$	14=25=36
$432$	None
3	Sets A, B, C and D (see below)
$3m$	Sets C and D
32	Sets A and B
6	Sets B and C
$\bar{6}$	Sets A and D
$6mm$	Set C
$\bar{6}m2$	Set D
$622$	Set B
Set A	11=-12=-26
Set B	14=-25
Set C	15=24, 31=32, 33
Set D	16=21=-22

Table 2.3: Non-zero components of the tensors  $d_{iJK}^\alpha$ ,  $D_{iJK}^\lambda$  and  $A_{iJK}^\lambda$ . Only components with  $J \leq K$  are shown as  $d_{iJK}^\alpha \equiv d_{iKJ}^\alpha$  etc.

Point group	$iJK$	
1	All 63 possible triplets	
$m$	Sets A(2), B(1) and B(3) (see below)	
2	Sets A(1), A(3) and B(2)	
$mm2$	115, 125, 135, 146, 214, 224, 234, 256, 311, 312, 313, 322, 323, 333, 344, 355, 366	
222	114, 124, 134, 156, 215, 225, 235, 246, 316, 326, 336, 345	
4	Sets C(−) and D(+), 312, 333, 366	
$\bar{4}$	Sets C(+) and D(−), 336, 345	
$4mm$	Set D(+), 312, 333, 366	
$\bar{4}2m$	Set C(+), 336, 345	
422	Set C(−)	
23	Sets E, F and G	
$\bar{4}3m$	Sets E, F and G with F=G	
432	Sets F and G with F=−G	
3	Sets H, I, J and K	6 Sets J and K
$3m$	Sets I and K	$\bar{6}$ Sets H and I
32	Sets H and J	$6mm$ Set K $\bar{6}m2$ Set I $622$ Set J
Set A(p)	p14, p16, p24, p26, p34, p36, p45, p56	
Set B(q)	q11, q12, q13, q15, q22, q23, q25, q33, q35, q44, q46, q55, q66	
Set C(±)	114=±225, 124=±215, 134=±235, 156=±246, 316=±326	
Set D(±)	115=±224, 125=±214, 135=±234, 146=±256, 311=±322, 313=±323, 344=±355	
Set E	114=225=336, 156=246=345	
Set F	124=235=316	
Set G	134=215=326	
Set H	111= $\frac{1}{2}\{(216)+3(226)\}$ , 112=166= $\frac{1}{2}\{226-216\}$ , 122= $\frac{1}{2}\{3(216)+(226)\}$ , 113=−123=−236, 144=−155=245, 315=−325=−346	
Set I	211= $\frac{1}{2}\{(116)+3(126)\}$ , 212=266= $\frac{1}{2}\{116-126\}$ , 222=− $\frac{1}{2}\{3(116)+(126)\}$ , 213=−223=136, 244=−255=−145, 314=−324=356	
Set J	114=−225, 124=−215, 134=−235, 156=−246=− $\frac{1}{2}\{114-124\}$	
Set K	115=224, 125=214, 135=234, 146=256= $\frac{1}{2}\{115-125\}$ , 311=322=312 + 2(366), 313=323, 344=355, 333	

Table 2.4: Non-zero components of the tensors  $e_{ij}^{\alpha\beta}$  and  $E_{ij}^{\lambda\mu}$ 

Point group	$ij$
1	All 9 possible pairs
$m, 2$	11, 22, 33, 13, 31
$mm2, 222$	11, 22, 33
$4, \bar{4}, 3, 6, \bar{6}$	11=22, 33, 12=-21
$4mm, \bar{4}2m, 422, 32, 3m, 6mm, \bar{6}m2, 622$	11=22, 33
$23, \bar{4}3m, 432$	11=22=33

Table 2.5: Non-zero components of the tensors  $e_{ijK}^{\alpha\beta}$  and  $E_{ijK}^{\lambda\mu}$ 

Point group	$ijK$
1	All 54 possible triplets
$m, 2$	Sets A(1), A(2), A(3), A(5), B(4) and B(6) (see below)
$mm2, 222$	111, 112, 113, 221, 222, 223, 331, 332, 333, 126, 135, 216, 234, 315, 324
$4, \bar{4}$	Sets C and D
$4mm, \bar{4}2m, 422$	Set C
23	Sets E, F, G, H, I
$432, \bar{4}3m$	Sets E, F, G, H, I with F=G and H=I
3	Sets J, K, L and M
$32, 3m$	Sets J and L
$6, \bar{6}$	Sets J and K
$6mm, \bar{6}m2, 622$	Set J
Set A(P)	11P, 13P, 22P, 31P, 33P
Set B(Q)	12Q, 21Q, 23Q, 32Q
Set C	111=222, 112=221, 113=223, 126=216, 234=315, 331=332, 333
Set D	116=-226, 121=-212, 122=-211, 123=-213, 134=-235, 314=-325
Set E	111=222=333
Set F	112=223=331
Set G	113=221=332
Set H	126=234=315
Set I	135=216=324
Set J	111=222, 112=221, 126=216= $\frac{1}{2}\{111-112\}$ , 113=223, 135=234, 315=324, 331=332, 333
Set K	121=-212, 122=-211, 116=-226= $\frac{1}{2}\{122-121\}$ , 123=-213, 134=-235, 314=-325
Set L	114=125=215=-224, 136=231=-232, 316=321=-322
Set M	-115=124=214=225, 131=-132=-236, 311=-312=-326

Table 2.6: Non-zero components of the tensors  $f_{ijk}^{\alpha\beta\gamma}$  and  $F_{ijk}^{\lambda\mu\nu}$ 

Point group	$ijk$
1	All 27 possible triplets
$m$	Sets A(1), A(3) and B(2) (see below)
2	Sets A(2), B(1) and B(3)
$mm2$	113, 131, 223, 232, 311, 322, 333
222	123, 132, 213, 231, 312, 321
4	Sets C(+) and D(-), 333
$\bar{4}$	Sets C(-) and D(+)
$4mm$	Set C(+), 333
$\bar{4}2m$	Set D(+)
422	Set D(-)
23	Sets E and F
$\bar{4}3m$	Sets E and F with E=F
432	Sets E and F with E=-F
3	Sets G, H, I and J
$3m$	Sets H and I
32	Sets G and J
6	Sets I and J
$\bar{6}$	Sets G and H
$6mm$	Set I
$\bar{6}m2$	Set H
622	Set J
Set A(p)	p11, p13, p22, p31, p33
Set B(q)	q12, q21, q23, q32
Set C( $\pm$ )	113= $\pm$ 223, 131= $\pm$ 232, 311= $\pm$ 322
Set D( $\pm$ )	123= $\pm$ 213, 132= $\pm$ 231, 312= $\pm$ 321
Set E	123=231=312
Set F	132=213=321
Set G	-111=122=212=221
Set H	112=121=211=-222
Set I	113=223, 131=232, 311=322, 333
Set J	123=-231, 132=-231, 312=-321

in [11]. This is incorrect—it restores and compounds the inconsistency that I exposed in [4]. Consistency requires that the non-zero components of a tensor in class  $\bar{6}m2$  be a subset of those of the same tensor in class  $3m$ , from which  $\bar{6}m2$  is derived by the addition of further symmetry elements. Similar arguments relate  $6mm$  to  $3m$  and  $622$  to  $32$ . The net conclusion is that the results for the point groups  $3$  and  $\bar{6}m2$  are correctly given but that two sets of non-zero components should be exchanged between  $32$  and  $3m$ , namely sets I and H in Table 2.3. Thurston’s results for a third-rank polar tensor in his Table 16.3 is marred only by the  $\bar{6}m2$  problem—the matrix should have its upper and middle rows interchanged.

Table 2.7: Total number of independent elements for each tensor by crystal class.

Point group	$d_i^\alpha$ $D_i^\lambda$	$d_{iJ}^\alpha$ $A_{iJ}^\lambda, D_{iJ}^\lambda$	$d_{iJK}^\alpha$ $A_{iJK}^\lambda, D_{iJK}^\lambda$	$e_{ij}^{\alpha\beta}$ $E_{ij}^{\lambda\mu}$	$e_{ijK}^{\alpha\beta}$ $E_{ijK}^{\lambda\mu}$	$f_{ijk}^{\alpha\beta\gamma}$ $F_{ijk}^{\lambda\mu\nu}$
1	3	18	63	9	54	27
$m$	2	10	34	5	28	14
2	1	8	29	5	28	13
$mm2$	1	5	17	3	15	7
222	0	3	12	3	15	6
4	1	4	15	3	14	7
$\bar{4}$	0	4	14	3	14	6
$4mm$	1	3	10	2	8	4
$\bar{4}2m$	0	2	7	2	8	3
422	0	1	5	2	8	3
23	0	1	4	1	5	2
$\bar{4}3m$	0	1	3	1	3	1
432	0	0	1	1	3	1
3	1	6	21	3	18	9
$3m$	1	4	13	2	10	5
32	0	2	8	2	10	4
6	1	4	11	3	12	7
$\bar{6}$	0	2	10	3	12	2
$6mm$	1	3	8	2	7	4
$\bar{6}m2$	0	1	5	2	7	1
622	0	1	3	2	7	3

In Appendix B are listed the transformation matrices that convert tensor components from the standard settings in the above Tables to the variant settings most commonly encountered.

## 2.2 Transformation of sublattice indices

So far the structure of the tensors has been elucidated in a macroscopic spirit—i.e. without regard for the effect of space group operations on the sublattice indices or interlattice indices. When these microscopic considerations are taken into account they lead, if  $n > 2$ , to further simplification. For this purpose the sublattice indices 1 to  $n$  are allotted to the different atoms in the basis. This procedure is arbitrary but can at least be made methodical by numbering all the atoms in a particular Wyckoff set sequentially and, if appropriate, by taking the least populated Wyckoff sets first. As an illustration here are the assignments for the hexagonal allotropes of diamond and graphite. In both cases the space group is  $P6_3/mmc$  and the hexagonal unit cell is defined by the three vectors  $\vec{a}_1 = a[1, 0, 0]$ ,  $\vec{a}_2 = a[-\frac{1}{2}, \frac{\sqrt{3}}{2}, 0]$  and  $\vec{a}_3 = c[0, 0, 1]$ , where  $a$  and  $c$  are the lattice parameters.

Table 2.8: Assignment of sublattice indices to the atomic sites in the hexagonal allotropes. The colon separates the non-equivalent pairs in  $hG$ .

Structure	Wyckoff sets	Site symmetry	Atomic coordinates at sublattice number			
			1	2	3	4
$hD$	f	$3m$	$(\frac{1}{3} \frac{2}{3} z)$	$(\frac{2}{3} \frac{1}{3} \bar{z})$	$(\frac{1}{3} \frac{2}{3} \frac{1}{2} - z)$	$(\frac{2}{3} \frac{1}{3} \frac{1}{2} + z)$
$hG$	d : b	$\bar{6}m2$	$(\frac{1}{3} \frac{2}{3} \frac{3}{4})$	$(\frac{2}{3} \frac{1}{3} \frac{1}{4})$	:	$(0 \ 0 \ \frac{3}{4})$ $(0 \ 0 \ \frac{1}{4})$

There is in group theory a theorem [9] which asserts that every finite group is isomorphic with a suitable group of permutations<sup>1</sup>. In the present context the group of point operations that transform the various atoms into one another is precisely matched by the group of permutations of the associated sublattice indices. The following Table, brought forward from Chapter 4, illustrates this for the hexagonal allotropes. The space group is of order 24 and for hexagonal diamond there

Table 2.9: Permutations of sublattice indices corresponding to spacegroup symmetry operations for the hexagonal structures.  $\vec{t}$  is the fractional translation column vector  $[0/0/\frac{1}{2}]$ .

Symmetry operations in space group $P6_3/mmc$						Subgroup with row 1	Permutations $hD$	Permutations $hG$
$\{1 0\}$	$\{3^+ 0\}$	$\{3^- 0\}$	$\{m 0\}$	$\{m' 0\}$	$\{m'' 0\}$	$R3m$	(1)(2)(3)(4)	(1)(2) : (3)(4)
$\{i 0\}$	$\{\bar{3}^+ 0\}$	$\{\bar{3}^- 0\}$	$\{2 0\}$	$\{2' 0\}$	$\{2'' 0\}$	$P\bar{3}m1$	(12)(34)	(12) : (34)
$\{2_z \vec{t}\}$	$\{6^+ \vec{t}\}$	$\{6^- \vec{t}\}$	$\{c \vec{t}\}$	$\{c' \vec{t}\}$	$\{c'' \vec{t}\}$	$P6_3mc$	(14)(23)	(12) : (34)
$\{m_z \vec{t}\}$	$\{\bar{6}^+ \vec{t}\}$	$\{\bar{6}^- \vec{t}\}$	$\{2_o \vec{t}\}$	$\{2_l \vec{t}\}$	$\{2_\mu \vec{t}\}$	$P\bar{6}m2$	(13)(24)	(1)(2) : (3)(4)

<sup>1</sup>In fact I discovered this for myself and excitedly reported it to the number theorist Bob Odoni over the snooker table one lunchtime. I had rather mixed feelings on being told that Cayley (1854) had preceded me by more than a century!

is a single Wyckoff set of 4 atoms. The identity and 5 other operations do not permute the indices. This is represented by enclosing each index singly in parentheses. A coset of 6 operations interchanges sublattices 1 and 2 and, simultaneously, 3 and 4. Two further cosets behave similarly. The hexagonal graphite structure has two Wyckoff sets of 2 atoms. The identity and 11 other elements produce no permutation whilst the coset of 12 elements permutes each pair. The sequence of indices within parentheses is termed a cycle.

### 2.3 Transformation of interlattice indices

To avoid unnecessary complexity it will be assumed from here on that no sublattice sites possess inversion symmetry.

In a structure formed from  $n$  sublattices there are  $n(n - 1)/2$  interlattice indices relating the sublattices in pairs of which  $n - 1$  at most are needed to label independent tensors. This conclusion, from Chapter 1, can only be arrived at in the general case by detailed analysis. The simplest way to approach the issue is to use triangular tableaux again, rather than the complicated mesh of semi-circles used in [5]. A scheme for the indices when  $n = 4$  is set out in Table 2.10. In the upper left tableau the assignments follow the prescription of the definition of inner displacement in Chapter 1. The other three tableaux illustrate the effect of the permutations shown, and correspond to the symmetry operations of Table 2.9: the pair on the left representing  $hG$  and all four representing  $hD$ . Certain of the indices are shown barred indicating the polar character of the index assignment: thus  $\bar{\zeta}^4$  which is defined as  $\bar{w}^3 - \bar{w}^1$  initially is equivalent to  $\bar{w}^2 - \bar{w}^4$  via the permutation (14)(23), i.e. to  $-\bar{\zeta}^5$ . This can be written as  $\bar{\zeta}^5$  in the spirit of crystallographic practice.

Table 2.10: Allocation of interlattice indices and the effect on them of the permutations indicated

$hD$ and $hG$				$hD$			
(1)(2)(3)(4)				(14)(23)			
1	2	3	4	4	3	2	1
1	2	3		$\bar{3}$	$\bar{2}$	$\bar{1}$	
	4	5			$\bar{5}$	$\bar{4}$	
		6			$\bar{6}$		
(12)(34)				(13)(24)			
2	1	4	3	3	4	1	2
$\bar{1}$	6		$\bar{3}$	3	$\bar{6}$	1	
	5	4			$\bar{4}$	$\bar{5}$	
		2			$\bar{2}$		

### 2.3.1 Indices connecting sublattices in distinct Wyckoff sets

Pairs of sublattice indices taken one from each of two Wyckoff sets  $u$  and  $v$  give rise to  $n_u n_v$  interlattice indices.

The effect of a symmetry operation on an interlattice index  $\lambda$  is completely determined by the simultaneous permutations of the sublattice indices  $u_i$  and  $v_p$ . Consider first the case where  $u$  and  $v$  are distinct (although they may be of the same type). Denoting the space group and its order by  $\Gamma$  and  $\gamma$  respectively it can readily be seen that a subgroup  $U_{ii}$  of  $\Gamma$ , of order  $\gamma/n_u$ , exists that leaves  $u_i$  invariant. The elements of this subgroup are those whose equivalent permutations contain  $u_i$  in cycles of unit order, i.e.  $(u_i)$ . The remaining elements of  $\Gamma$  can be grouped into  $n_u - 1$  cosets  $U_{ij}$ , also of  $\gamma/n_u$  elements, that transform  $u_i$  into  $u_j$ . The elements of these cosets are those whose permutations contain cycles in which  $u_i$  is followed immediately by  $u_j$  (including cycles that commence with  $u_j$  and end with  $u_i$ ). Similarly  $\Gamma$  can be decomposed into a subgroup  $V_{pp}$ , of order  $\gamma/n_v$ , that leaves  $v_p$  invariant and  $n_v - 1$  cosets  $V_{pq}$  that transform  $v_p$  into  $v_q$ .

The two sublattice indices  $u_i$  and  $v_p$  and their associated interlattice index  $\lambda$  are left invariant by a subgroup  $G^\lambda$  of  $\Gamma$ , of order  $g_\lambda$ , consisting of those elements common to  $U_{ii}$  and  $V_{pp}$ : thus

$$G^\lambda = U_{ii} \cap V_{pp} \quad (2.5)$$

and

$$1 \leq g_\lambda \leq \min(\gamma/n_u, \gamma/n_v) \quad (2.6)$$

since  $G^\lambda$  certainly contains the identity but no more elements than are present in the smaller subgroup.  $G^\lambda$  is called the stabilizer of  $\lambda$ .

The non-zero components of tensors carrying a single index  $\lambda$  and any relations between them are given by considering the set of equations, one for each element in  $G^\lambda$ , of the form

$$T_{ijk..}^\lambda = a_{ip}^{(s)} a_{jq}^{(s)} a_{kr}^{(s)} .. T_{pqr..}^\lambda \quad (2.7)$$

where the  $a_{ip}^{(s)}$  etc. are elements of the point operation in  $\Gamma_s$ . This procedure defines  $n_u n_v$  tensors of a given kind. Except in the simplest structures many of these tensors are interdependent, being related by those elements of  $\Gamma$  that change the interlattice indices. Let  $\lambda'$  be the index that relates the sublattices  $u_j$  and  $v_q$ . Then  $\lambda$  is transformed into  $\lambda'$  by the elements that are common to the cosets  $U_{ij}$  and  $V_{pq}$ : if this set is denoted by  $H^{\lambda\lambda'}$  then

$$H^{\lambda\lambda'} = U_{ij} \cap V_{pq} \quad (2.8)$$

with the proviso that  $j = i$  and  $q = p$  are not taken together. If this is not an empty set the the tensor with index  $\lambda'$  is totally determined by that with index  $\lambda$  according to

$$T_{ijk..}^{\lambda'} = a_{ip}^{(s)} a_{jq}^{(s)} a_{kr}^{(s)} .. T_{pqr..}^\lambda \quad (2.9)$$

where the  $a_{ip}^{(s)}$  etc. are elements of any one point operation in  $H^{\lambda\lambda'}$ . If the set is empty the two tensors are independent.

To determine the precise number,  $p_{uv}$ , of independent tensors of a given kind it is necessary to decompose the set of interlattice indices into mutually exclusive subsets, each subset containing a complete collection of related indices. The number of these subsets is the number sought. A particular subset containing  $\lambda$  is called the orbit of  $\lambda$  under  $\Gamma$  and is denoted by  $O^\lambda$ . If the number of elements in  $O^\lambda$  is  $o_\lambda$  then it can be shown that

$$o_\lambda = \gamma / g_\lambda \quad (2.10)$$

[7, p.63]. A preliminary look at the bounds of  $p_{uv}$  is instructive. The bounds on  $g_\lambda$  given in (2.6) can be inserted into (2.10) to give

$$\max(n_u, n_v) \leq o_\lambda \leq \gamma. \quad (2.11)$$

Now  $\sum o_\lambda = n_u n_v$ , so upper and lower bounds on  $p_{uv}$  will be obtained by assuming orbits of equal size, each containing either the upper or the lower bound of  $o_\lambda$ . This yields

$$n_u n_v / \gamma \leq p_{uv} \leq \min(n_u, n_v). \quad (2.12)$$

Two definite conclusions may be drawn from (2.12): (i) if the set  $v$  is a general set (i.e. has as many elements as the order of the group) then  $n_v = \gamma$  and  $p_{uv} = n_u$  and (ii) if the set  $u$  consists of a single member then  $p_{uv} = 1$  irrespective of  $n_v$ .

The exact value of  $p_{uv}$  can be determined using a matrix representation of the permutations. Let  $P_u(\Gamma_s)$  be an  $n_u \times n_u$  matrix with units in positions  $(i, j)$  if  $\Gamma_s$  carries  $u_i$  into  $u_j$  and zeroes elsewhere. The character  $\chi_u(\Gamma_s)$  of the matrix is given by

$$\chi_u(\Gamma_s) = \text{tr } P_u(\Gamma_s) \quad (2.13)$$

and a theorem of Frobenius and Burnside states that the number of orbits of  $u_i$  is given by

$$q_u = \frac{1}{\gamma} \sum_{\Gamma_s \in \Gamma} \chi_u(\Gamma_s). \quad (2.14)$$

The permutations of a second Wyckoff set  $v$  can be represented in a similar way in terms of the  $n_v \times n_v$  matrices  $P_v(\Gamma_s)$ .

These two representations of  $\Gamma$  may be used to create a third by forming the tensor product of  $P_u(\Gamma_s)$  and  $P_v(\Gamma_s)$ . This defines an  $n_u n_v \times n_u n_v$  matrix of which a specific element is given by

$$(P_{uv}(\Gamma_s))_{(i,p),(j,q)} = (P_u(\Gamma_s))_{ij} (P_v(\Gamma_s))_{pq}. \quad (2.15)$$

This new representation reveals the behaviour of the ordered pair  $(u_i, v_j)$  under the operation  $\Gamma_s$ , and thus the behaviour of the interlattice index  $\lambda$  corresponding to that pair. The number of orbits of  $\lambda$  is given by (2.14):

$$p_{uv} = \frac{1}{\gamma} \sum_{\Gamma_s \in \Gamma} \chi_{uv}(\Gamma_s). \quad (2.16)$$

It follows from (2.15), by setting  $j = i$  and  $q = p$  and then summing over  $i$  and  $p$ , that

$$\text{tr } P_{uv}(\Gamma_s) = \text{tr } P_u(\Gamma_s) \cdot \text{tr } P_v(\Gamma_s) \quad (2.17)$$

so that, by (2.13),

$$\chi_{uv}(\Gamma_s) = \chi_u(\Gamma_s) \chi_v(\Gamma_s) \quad (2.18)$$

and finally, by (2.16)

$$p_{uv} = \frac{1}{\gamma} \sum_{\Gamma_s \in \Gamma} \chi_u(\Gamma_s) \chi_v(\Gamma_s). \quad (2.19)$$

If the set  $u$  and  $v$  are both of the same kind, say  $u$ , then (2.19) becomes

$$p_{uu} = \frac{1}{\gamma} \sum_{\Gamma_s \in \Gamma} \chi_u^2(\Gamma_s). \quad (2.20)$$

### 2.3.2 Indices connecting sublattices within a single Wyckoff set

With some modification the above arguments can be used for the case where the interlattice indices relate to sublattice indices from the same Wyckoff set. Firstly there are no indices relating a sublattice to itself, so the  $n_u^2$  intersections obtained by setting  $V_{pp} = U_{pp}$  in (2.5) are reduced by  $n_u$ , since the  $n_u$  cases in which  $p = i$  must be excluded. Secondly, because of the polar nature of the definition of inner displacement briefly noted in Section 2.3, the remaining  $n_u(n_u - 1)$  fall into two equal groups—the set  $\{\lambda\}$  and the set  $\{\bar{\lambda}\}$ . Tensors labelled with an odd number of indices are related by

$$T_{ijk..}^{\bar{\lambda}} = -T_{ijk..}^{\lambda} \quad (2.21)$$

and clearly only one member of each  $\lambda/\bar{\lambda}$  pair is required, reducing the number of interlattice indices to  $n_u(n_u - 1)/2$ .

Analogous to (2.5) the stabilizers of  $\lambda$  and  $\bar{\lambda}$  are given by

$$G^\lambda = G^{\bar{\lambda}} = U_{ii} \cap U_{pp} \quad (2.22)$$

with

$$1 \leq g_\lambda = g_{\bar{\lambda}} \leq \gamma/n_u \quad (2.23)$$

and the tensors carrying a single interlattice index have the form derived by applying (2.7) as before.

A systematic set of  $\lambda$ , all positive integers, is implicit in the definition of inner displacement. This does not however eliminate the set of  $\bar{\lambda}$  from the problem because all symmetry operations not contained in  $U_{ii}$  transform some  $\lambda$ s into  $\bar{\lambda}$ s. This is easily shown by looking at the permutation corresponding to such a symmetry operation. It contains at least one cycle of length greater than unity and in this cycle there is a largest sublattice index, say  $\ell$ . Suppose that  $\ell$  is flanked by  $x$  and  $y$  so the cycle contains the sequence  $(..x\ell y..)$ . The symmetry operation will convert the interlattice

index related to  $x$  and  $\ell$ , which will be of  $\lambda$ -type because  $x < \ell$ , into that related to  $\ell$  and  $y$ , which will be of  $\bar{\lambda}$ -type since  $\ell > y$ . Equation (2.8) now gives rise to two possibilities:

$$H^{\lambda\lambda'} = H^{\bar{\lambda}\bar{\lambda}'} = U_{ij} \cap U_{pq} \quad (2.24)$$

in cases where  $i < p, j < q$  and the simultaneous equalities  $i = j$  and  $p = q$  are rejected and

$$H^{\lambda\bar{\lambda}'} = H^{\bar{\lambda}\lambda'} = U_{ij} \cap U_{pq} \quad (2.25)$$

in cases where  $i < p$  and  $j > q$ . Corresponding to the non-empty sets of (2.25) the transformation (2.9) relating  $T_{ijk..}^{\lambda'}$  to  $T_{pqr..}^{\lambda}$  can be modified by (2.21) to give

$$T_{ijk..}^{\lambda'} = -a_{ip}^{(s)} a_{jq}^{(s)} a_{kr}^{(s)} \dots T_{pqr..}^{\lambda}. \quad (2.26)$$

Thus a transformation from  $\lambda$  to  $\bar{\lambda}'$  is equivalent to one from  $\lambda$  to  $\lambda'$  combined with a change of sign.

All the orbits of  $\lambda$  certainly contain both barred and unbarred indices so it follows that the number,  $p_u$ , of independent interlattice indices can be obtained from (2.12) by setting  $n_v = n_u$  and removing unity from both bounds, one orbit disappearing because no sublattice is displaced relative to itself. Thus

$$(n_u^2/\gamma) - 1 \leq p_u \leq n_u - 1. \quad (2.27)$$

Two definite conclusions may be drawn from (2.27): (i) that  $p_u = \gamma - 1$  if  $u$  is a general set and (ii) that  $p_u = 1$  if  $n_u = 2$ . The exact expression follows from the results (2.14) and (2.20) using the matrix representation of permutations:

$$p_u = p_{uu} - q_u = \frac{1}{\gamma} \sum_{\Gamma_s \in \Gamma} (\chi_u^2(\Gamma_s) - \chi_u(\Gamma_s)). \quad (2.28)$$

## 2.4 In conclusion

General results in the manner of those for point group symmetry are not possible for the interlattice indices. Even with the same space group and the same number of atoms in the basis the outcomes for two different crystals can be very different.

Thus, referring to  $hG$  in Table 2.9, it can be seen that  $\chi_d(\Gamma_s) = \chi_b(\Gamma_s) = 2$  for the six  $\Gamma_s$  in row 1 and the six in row 4. Since  $\gamma = 24$  (2.19) reveals a single orbit of  $p_{db} = 2$  elements ( $\lambda = 2$  or 6 and  $\lambda = 4$  or 5), and (2.28) reveals two orbits of  $p_d = p_b = 1$  element each ( $\lambda = 1$ ) and ( $\lambda = 3$ ).

The results for  $hD$  are  $\chi_f(\Gamma_s) = 4$  for just the six  $\Gamma_s$  in row 1, and there is a single orbit with  $p_f = 3$  elements ( $\lambda = 1$  or 3,  $\lambda = 2$  or 6 and  $\lambda = 4$  or 5).

---

## References

- [1] S. Bhagavantam, *Crystal Symmetry and Physical Properties* (London: Academic Press, 1966)
- [2] K. Brugger, *J. Appl. Phys.* **36**, 759 (1965)
- [3] A. Cayley, *Phil. Mag.* **7**, 40 (1854)
- [4] C. S. G. Cousins, *J. Phys. C: Solid St. Phys.* **5**, L201 (1972)
- [5] C. S. G. Cousins, *J. Phys. C: Solid St. Phys.* **11**, 4867 (1978)
- [6] C. S. G. Cousins, *J. Phys. C: Solid St. Phys.* **11**, 4881 (1978)
- [7] J. A. Green, *Sets and Groups*, (London: Routledge and Kegan Paul, 1965)
- [8] *International Tables for Crystallography*, Vol.A (Kluwer Academic Publishers, Dordrecht, 1990)
- [9] W. Ledermann, *Introduction to the Theory of Finite Groups* (Edinburgh: Oliver and Boyd, 1957)
- [10] J. Nye, *Physical Properties of Crystals*, (Oxford: University Press, 1957)
- [11] *Standards on Piezoelectric Crystals* Proc. Inst. Radio Engrs. **37**, 1378 (1949)
- [12] *Standards on Piezoelectric Crystals* Proc. Inst. Radio Engrs. **46**, 764 (1958)
- [13] R. N. Thurston, in *Encyclopedia of Physics*, ed. S. Flügge Vol. VIa/4 *Mechanics of Solids IV*, ed. C. Truesdell (Springer 1974)

## Chapter 3

### Experimental interlude: the internal strain parameter of cubic diamond

#### 3.1 Introduction

Inner displacement ceased to be an abstruse theoretical concept when Kleinman delivered a paper entitled *Covalent bonding in semiconductors* to the 1962 Conference on Semiconductors held appropriately, but before my time, at Exeter. He drew attention to some problems relating to energy band calculations and covalency in silicon under uniaxial stress in the [111] direction [11]. The central atom in each tetrahedral group may participate in bond-bending with minimal stretching, bond-stretching with minimal bending or in something in between. Since the central atom moves along the body-diagonal of the cube to an extent *not* controlled by macroscopic elasticity he suggested that the displacement be measured by looking at the X-ray structure factor of the 200 reflection under stress. For a strain  $\epsilon = 0.003$  he predicted  $F_{200} \approx 0.04\zeta_K$  where  $0 \leq \zeta_K \leq 1$ , an easily measurable structure factor.  $\zeta_K$  has ever since been known as the Kleinman internal strain parameter. Experimental work was quickly undertaken and results announced for germanium [18] and silicon [19]. Additional analysis was provided in [20]. No further work was published for ten years when two papers on GaAs appeared [12, 13]. What seemed a reasonable result I realized later, after developing a detailed theory for zincblende-structure material, to be totally unreliable [1].

It was in 1980 that I set up the group<sup>1</sup> that made, as far as I know, all but one of the subsequent internal strain parameter measurements so far published: Si [2, 4], Ge [3, 4], GaAs [5], cD [6] and InSb [7]. The exception was the Si measurement of d'Amour *et al.* [9] which appeared simultaneously with ours. All these materials had either the diamond or the zincblende structure: simple high-symmetry structures with only two atoms in the basis and a single internal strain tensor with one independent component. All the measurements were difficult and it was due to my obsession with sublattice displacement that they were undertaken. Si and Ge were certainly the easiest because large, high-quality single crystals could be obtained. GaAs and InSb were

---

<sup>1</sup>My co-workers for some or all of the time were Brian Sheldon and Roy Meads at Exeter, Leif Gerward and Birger Selsmark at the Technical University of Denmark and Janus Staun Olsen of the Ørsted Institute, Copenhagen University

more difficult because they were brittle and thus less able to sustain sufficiently large stress. The problem with *cD* was its very small X-ray form factor (a neutron diffraction method would have been much better) and an internal strain predicted to be about six times smaller than Si or Ge: nevertheless we succeeded.

In fact *cD* is the only one of the allotropes under discussion whose internal strain tensor could have been determined. The following account illustrates the principles of how it was done but without including the more mundane theoretical and experimental details.

### 3.2 Inner displacement due to uniaxial stress

At the level of experiment the distinction between the infinitesimal and the finite strain approaches vanishes. Equation (1.9) can thus be shorn of superscripts and higher-order terms to give

$$\delta_i = A_{iJ}\epsilon_J. \quad (3.1)$$

Hooke's law in its simplest manifestation is

$$\epsilon_J = S_{JK}\sigma_K \quad (3.2)$$

whence

$$\delta_i = A_{iJ}S_{JK}\sigma_K. \quad (3.3)$$

The forms of  $A$  and  $S$  for *cD* are

$$A = \begin{bmatrix} 0 & 0 & 0 & A_{14} & 0 & 0 \\ 0 & 0 & 0 & 0 & A_{14} & 0 \\ 0 & 0 & 0 & 0 & 0 & A_{14} \end{bmatrix} \quad (3.4)$$

and

$$S = \begin{bmatrix} S_{11} & S_{12} & S_{12} & 0 & 0 & 0 \\ S_{12} & S_{11} & S_{12} & 0 & 0 & 0 \\ S_{12} & S_{12} & S_{11} & 0 & 0 & 0 \\ 0 & 0 & 0 & S_{44} & 0 & 0 \\ 0 & 0 & 0 & 0 & S_{44} & 0 \\ 0 & 0 & 0 & 0 & 0 & S_{44} \end{bmatrix}. \quad (3.5)$$

The components of a stress of magnitude  $\sigma$  parallel to the unit vector  $\vec{\ell} = [\ell_1, \ell_2, \ell_3]$  are given by

$$\sigma_K = \ell_i \ell_j \sigma, \quad (3.6)$$

where  $ij$  is the Voigt contraction of  $K$  and where  $\sigma$  is positive for a tensile stress and negative for a compressive one. Combining (3.4), (3.5) and (3.6) converts (3.3) into

$$\begin{bmatrix} \delta_1 \\ \delta_2 \\ \delta_3 \end{bmatrix} = A_{14} S_{44} \sigma \begin{bmatrix} \ell_2 \ell_3 \\ \ell_3 \ell_1 \\ \ell_1 \ell_2 \end{bmatrix}. \quad (3.7)$$

This equation is deceptively simple and its interpretation is not intuitive. If the stress axis is parallel to a  $\bar{4}$  axis then two of the  $\ell_i$  are zero and  $\vec{\delta} = 0$ . If just one of the  $\ell_i$  is zero then  $\vec{\delta} \cdot \vec{\ell} = 0$  and the inner displacement is perpendicular to the stress axis and maximizes if the non-zero direction cosines are each of magnitude  $1/\sqrt{2}$ . If none of the  $\ell_i$  is zero then  $\vec{\delta} \cdot \vec{\ell} = 3A_{14}S_{44}\sigma\ell_1\ell_2\ell_3$  which is maximized simultaneously with  $|\vec{\delta}|$  if the magnitudes of the  $\ell_i$  are each  $1/\sqrt{3}$ . These different situations are illustrated in the following Figure.

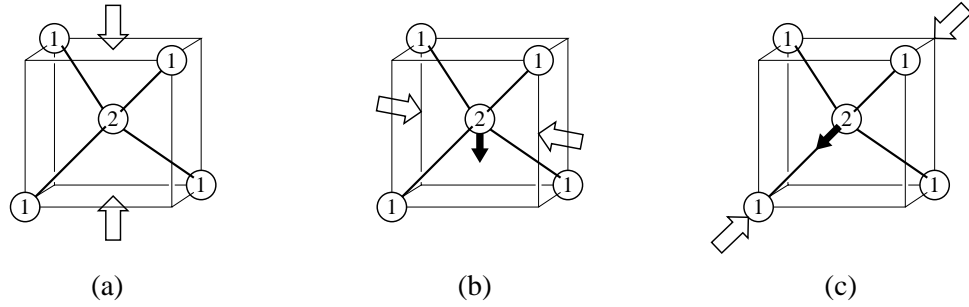


Figure 3.1: The inner displacement of the central atom in the tetrahedral cluster induced by uniaxial stresses along different axes. (a)  $\sigma \parallel [001]$ ,  $\vec{\delta} = 0$ ; (b)  $\sigma \parallel [1\bar{1}0]$ ,  $\vec{\delta} \parallel [001]$ ; (c)  $\sigma \parallel [111]$ ,  $\vec{\delta} \parallel [111]$ .

The displacement of atoms on sublattice 2 relative to those on sublattice 1 due to the application of uniaxial stress is thus given by

$$u_i = \epsilon_{ij}R_j + \delta_i \quad (3.8)$$

where  $\vec{R}$  is the vector from an atom on 1 to an atom on 2.

### 3.3 Change in structure factor due to inner displacement

The internal strain parameters are obtained from intensity measurements of X-ray reflections. Because the crystal is under stress the appropriate diffraction theory is the ‘kinematic’ theory in which reflection intensity is proportional to the square of the structure factor.

The X-ray structure factor for Bragg diffraction from planes whose reflection vector is  $\vec{H}$  is

$$F_H = f[1 + \exp(2\pi i\vec{H} \cdot \vec{R})], \quad (3.9)$$

where  $\vec{R} = (a/4)[1\ 1\ 1]$  is the position vector of the second carbon atom in the basis relative to the first and  $f$  is the atomic scattering factor of a carbon atom.

In the conventional cubic description the components  $(h, k, \ell)$  in  $\vec{H} = (1/a)(h, k, \ell)$  must be all odd or all even and the square of the structure factor becomes

$$|F_H|_0^2 = 32f^2(1 + \cos \phi_H), \quad (3.10)$$

where

$$\phi_H = 2\pi\vec{H} \cdot \vec{R} = \frac{\pi}{2}(h + k + \ell) \quad (3.11)$$

and the subscript zero denotes the unstrained crystal.

If the crystal is strained  $\vec{R}$  undergoes a change due to the macroscopic deformation and an additional change due to inner displacement. The first of these effectively cancels with the covariant deformation of  $\vec{H}$  and (3.10) is replaced by

$$|F_H|_\sigma^2 = 32f^2[1 + \cos(\phi_H + \psi_H)], \quad (3.12)$$

where

$$\psi_H(\sigma, \ell) = 2\pi \vec{H} \cdot \vec{\delta} = \frac{2\pi}{a} A_{14} S_{44} \sigma (h\ell_2\ell_3 + k\ell_3\ell_1 + \ell\ell_1\ell_2). \quad (3.13)$$

The effect of inner displacement on the square of the structure factor is presented, to lowest order, in Table 3.1.

Table 3.1: Effect of stress on structure factor

Reflection type	Unstressed	Stressed	
$h + k + \ell$	$ F_H/8f _0^2$	$ F_H/8f _\sigma^2 -  F_H/8f _0^2$	$\Delta I/I_0$
$4n$	1	$-\psi_H^2/4$	$-\psi_H^2/4$
$4n + 1$	$\frac{1}{2}$	$-\psi_H/2$	$-\psi_H$
$4n + 2$	0	$\psi_H^2/4$	
$4n + 3$	$\frac{1}{2}$	$\psi_H/2$	$\psi_H$

It can be seen that the allowed reflections show varying behaviour: the fractional intensity changes are linear in  $\psi_H$  for the  $(4n + 1)$ - and  $(4n + 3)$ -type reflections but are opposite in direction. For the  $4n$ -type the fractional change is quadratic in  $\psi_H$  and probably very difficult to detect. Two kinds of  $(4n + 2)$ -type reflection may be distinguished: if each of  $h$ ,  $k$  and  $\ell$  is of the form  $(4n + 2)$  the reflection is forbidden if the atoms are spherically symmetric and vibrate harmonically, otherwise it is weak. Such is the case for the 222 reflection in  $cD$  where tetrahedral symmetry induces asphericity and appreciable anharmonicity is present. If only one of  $h$ ,  $k$  or  $\ell$  is  $(4n + 2)$ -type and the others are  $4n$ -type, then space group symmetry forbids the reflection strictly. The 002 and 006 reflections are in this category. If stress is applied suitably these reflections are weakly induced with an intensity that varies quadratically with  $\psi_H$ .

In a nutshell the internal strain parameter is obtained from the stress-dependence of the intensities,  $I_w$  and  $I_s$ , of a weak reflection and a strong reflection. For  $cD$  the 006 and 008 reflections were used and the parameter obtained from

$$A_{14} \propto \frac{a}{3\pi S_{44} \sqrt{I_s^*}} \frac{d\sqrt{I_w}}{d\sigma}, \quad (3.14)$$

where a multiplier involving temperature factors, X-ray polarization, mass attenuation coefficient and other configuration-dependent parameters is needed to produce equality and  $I_s^*$  is a limiting high-stress value.

### 3.4 X-ray methods

The original experiments [18, 19, 9] on Si and Ge used characteristic  $K_\alpha$  radiation from conventional X-ray tubes. This is the angle-dispersive method and requires sample rotation between the measurements of the two reflections. There is thus the danger that the two reflections are actually from slightly different regions of the crystal and therefore sample different conditions of crystal quality. This particular problem is avoided if the energy-dispersive method is used. The full Bremsstrahlung distribution from the tube is used and the crystal reflects those energies in the beam that satisfy the Bragg law for the working angle selected. Diffracted beams are collected by a solid-state detector and the constituent photons sorted by energy into a multi-channel analyzer. Typically a 40 keV range of photons will be divided with near-perfect linearity between 2048 channels. Thus a series of harmonics may be obtained together: the  $002n$  reflections at photon energies  $E_n$  given by

$$E_n = n \frac{hc}{2d_{002} \sin \theta}. \quad (3.15)$$

All my group's measurements were made this way except for *cD*. The very small atomic scattering factor of carbon and the anticipated small internal strain made it desirable to use synchrotron radiation. Experiments were carried out on Station 9.1 of the Synchrotron Radiation Source at Daresbury and on the Energy-Dispersive Scattering Station at HASYLAB-DESY in Hamburg. The details that follow relate to the latter source.

### 3.5 Experimental details

A series of horizontal and vertical slits limit the cross-section of the horizontally-polarized synchrotron radiation (SR) to a  $100 \times 100 \mu\text{m}^2$  square.

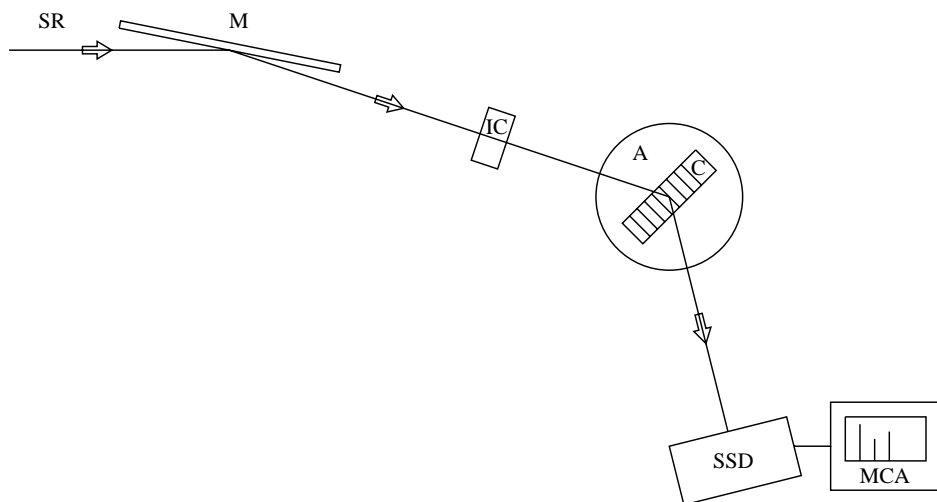


Figure 3.2: The layout of the components in the determination of the internal strain parameter of *cD*.

An ionization chamber (IC) is used to monitor the incident beam intensity and the diffracted radiation is collected by a solid-state detector (SSD) linked to a multi-channel analyzer (MCA). The sample (C) is held between the anvils (A) of the press in the configuration of Figure 3.1(b), turned so that the stress axis  $[1\bar{1}0]$  is vertical and the  $002n$  reflection vectors are horizontal. Transmission geometry was used so that errors due to surface distortion were minimized if not eliminated. The function of the mirror (M) is explained below.

### 3.5.1 Sample

This was a type IIA diamond cuboid with approximate dimensions  $2 \times 1 \times 3 \text{ mm}^3$  corresponding to the  $[001]$ ,  $[110]$  and  $[1\bar{1}0]$  directions. A type IIA diamond has an exceptionally low nitrogen content compared to 98% of natural diamonds which contain up to 0.3% nitrogen.

### 3.5.2 Uniaxial press

Stressing a sample of the hardest substance known requires special measures. Our press consisted of a maraged steel frame holding a hydraulic cell and a pair of anvils made of a sintered material based on tungsten carbide. The sample was gripped over its  $(1\bar{1}0)$  faces with zirconium shims to accommodate any residual surface irregularity. The highest stress attained in the experiment was 6.2 GPa.

### 3.5.3 Working angle

With white X-rays the beam can be incident at any angle  $\theta$  and the crystal will diffract the energies that satisfy the Bragg equation. Careful choice of angle is required, however, in order to avoid multiple diffraction that could otherwise totally confuse and invalidate the measurement. This phenomenon was first described by Renninger[17], who called it *Umweganregung* or ‘detour radiation’, and much later developed by me and my coworkers [8] in relation to energy-dispersive X-ray methods and the 222 reflection in Si. Briefly if the indices of three reflections  $\vec{H}_i = (1/a)(h_i, k_i, \ell_i)$  satisfy

$$(h_1, k_1, \ell_1) + (h_2, k_2, \ell_2) = (h, k, \ell) \quad (3.16)$$

then if  $\vec{H}$  and either  $\vec{H}_1$  or  $\vec{H}_2$  both lie on the Ewald sphere the  $(\vec{H}_1, \vec{H}_2)$ -pair cooperate to simulate a  $\vec{H}$  reflection. If the latter is weak and the components of the pair are medium or strong the intensity of the weak reflection will be swamped if the scattering planes for  $\vec{H}$  and the  $(\vec{H}_1, \vec{H}_2)$ -pair coincide. Rotation of the crystal about  $\vec{H}$  brings this condition into and out of being. By determining the scattering plane orientations for all potentially damaging pairs,  $(113, \bar{1}\bar{1}3)$ ,  $(1\bar{1}3, \bar{1}13)$ ,  $(131, \bar{1}\bar{3}5)$  etc., we discover optimum Bragg angles for observing an unadulterated 006 reflection. The one we chose was  $\theta = 34.4^\circ$ , an angle that allows the stress axis to be set normal to the scattering plane with a comfortable tolerance of  $\pm 5^\circ$ .

### 3.5.4 Beam-tailoring by total external reflection

The high intensity of the synchrotron beam and the limited maximum count-rate achievable by a solid-state detector makes it desirable to cut out as much of the beam as possible, leaving just those energies required for the 006 and 008 reflections and maximizing the proportion of the diffracted beam due to the 006 reflection. This situation is closely approached by exploiting the total reflection of X-rays which occurs at very small glancing angles and is due to the X-ray refractive index being just less than unity. A gold-plated mirror, M in Fig. 3.2, is used to intercept the synchrotron beam and eliminate photons whose energies exceed 30 keV. The reflected component is then diffracted, in transmission geometry, by the sample and only the 004, 006 and 008 reflections are collected. Furthermore the beam intensity at 18.6 keV, where the 006 occurs, is considerably greater than it is at 24.8 keV, where the 008 occurs, thereby strongly enhancing the diffracted intensity of the weaker reflection.

## 3.6 Result

We found

$$A_{14} = -0.111 \pm 0.018 \text{ \AA} \quad \text{and} \quad \zeta_K = 0.125 \pm 0.020 \quad (3.17)$$

which agreed nicely with the later, and more sophisticated, calculations in a series of studies. Musgrave found  $\zeta_K = 0.268$  using a simple valence-force-field model [15]; Keating's original model [10] gave  $\zeta_K = 0.21$ ; Lawætz used elastic constants and the Raman frequency to predict  $\zeta_K = 0.23$  [14] and Weber obtained  $\zeta_K = 0.12$  using his bond-charge model [21]. Nielsen's calculations of  $\zeta_K = 0.108$  (and  $\zeta_K = 0.093$ ) using an *ab initio* pseudopotential are discussed later, in Chapter 6.

## References

- [1] C. S. G. Cousins, Acta Cryst. **A40**, 116 (1984)
- [2] C. S. G. Cousins, L. Gerward, J. Staun Olsen, B. Selsmark, and B. J. Sheldon, J. Appl. Cryst. **15**, 154 (1982)
- [3] C. S. G. Cousins, L. Gerward, K. Nielsen, J. Staun Olsen, B. Selsmark, B. J. Sheldon and G. E. Webster, J. Phys. C:Solid St. Phys., **15**, L651 (1982)
- [4] C. S. G. Cousins, L. Gerward, J. Staun Olsen, B. Selsmark, and B. J. Sheldon, J. Phys. C:Solid St. Phys., **20**, 29 (1987)
- [5] C. S. G. Cousins, L. Gerward, J. Staun Olsen, B. Selsmark, B. J. Sheldon and G. E. Webster, Semicond. Sci. Technol. **4**, 333 (1989)

- 
- [6] C. S. G. Cousins, L. Gerward, J. Staun Olsen and B. J. Sheldon, *J. Phys. C:Condens. Matter*, **1**, 4511 (1989)
- [7] C. S. G. Cousins, L. Gerward, J. Staun Olsen, S. A. Sethi and B. J. Sheldon, *phys. stat. sol. (a)* **126**, 135 (1991)
- [8] C. S. G. Cousins, L. Gerward and J. Staun Olsen, *phys. stat. sol. (a)* **48**, 113 (1978)
- [9] H. d'Amour, W. Denner, H. Schulz and M. Cardona, *J. Appl. Cryst.* **15**, 148 (1982)
- [10] P. N. Keating, *Phys. Rev.* **145**, 637 (1966)
- [11] L. Kleinman, *Phys. Rev.* **128**, 2614 (1962)
- [12] C. N. Koumelis and E. K. Rozis, *Acta Cryst.* **A31**, 84 (1975); erratum: *Acta Cryst.* **A32**, 170 (1976)
- [13] C. N. Koumelis, G. E. Zardas, C. A. Londos and D. K. Leventouri, *Acta Cryst.* **A32**, 306 (1976)
- [14] P. Lawætz, *phys. stat. sol. (b)* **57**, 535 (1973)
- [15] M. J. P. Musgrave, *Proc. Roy. Soc.* **A272**, 503 (1963)
- [16] O. H. Nielsen, *Phys. Rev.* **B34**, 5808 (1986)
- [17] M. Renninger, *Z. Phys.* **106**, 147 (1937)
- [18] A. Segmüller, *Phys. Letts.* **4**, 277 (1963)
- [19] A. Segmüller, *Phys. kondens Materie* **3**, 18 (1964)
- [20] A. Segmüller and H. R. Neyer, *Phys. kondens Materie*, **4**, 63 (1965)
- [21] W. Weber, *Phys. Rev.* **B15**, 4789 (1977)

## Chapter 4

### Inner elastic constants, internal strain tensors, zone-centre optic mode frequencies and their pressure dependence

Carbon is particularly rich in the number of its allotropes: besides the common forms of diamond and graphite there is a hexagonal form (lonsdaleite) of the former, a rhombohedral form of the latter and the fullerenes, of which  $C_{60}$  is the most famous example. A number of hypothetical metastable forms have also been proposed: graphyne, a layer structure in which benzene rings are arranged in 6-fold coordination, by Baughman *et al.* [1]; H6, a three-dimensional network of  $sp^2$ -bonded carbon atoms capable of continuous transformation to *cD* without bond-breaking, by Tamor and Hass [15]; and a group of other purely  $sp^2$ -bonded structures, such as R6 (space group  $R\bar{3}m$ ), consisting of 8-membered rings in chair conformation; BCT8, 8-membered boat-shaped rings ( $I4_1md$ ); and SC24, a simple-cubic structure with 6-membered rings ( $Pn\bar{3}m$ ) by Jungnickel *et al.* [8] in the quest to develop a nitrogen-dopable, and thus *n*-type, material.

This and the next Chapter contain a full description of the elasticity, through third order, of two diamond and two graphite allotropes of carbon. They pave the way for detailed individual studies in the four subsequent Chapters. To be fully comprehensive it is necessary to look at as many related properties as possible: not solely macroscopic elastic constants, but optic-mode frequencies, their stress- and/or pressure-dependence, and internal strain. In other words it is necessary to focus on microscopic aspects—the consequences of the relative movements of sublattices—that were given detailed treatment in the first two Chapters.

A full symmetry analysis of the sublattice tensors and inner elastic constants is given, for each structure, in Sec. 4.1. The results for cubic diamond (*cD*), some of which have been published before [4, 11], are given here in two versions: in standard form and in a non-conventional form, obtained by transformation of axes, which will facilitate comparison with rhombohedral graphite (*rG*) and with intermediate structures along the possible solid-state transformation path from *rG* to *cD* [6, 9], as treated in Chapter 9.

General expressions for the linear and quadratic internal strain tensors are given in Sec. 4.2. The independent components of the linear tensors are presented for all four allotropes. Those of the quadratic tensor are given only for *cD* and *hG*.

The frequencies of optic modes at the zone centre and their eigenvectors are treated in Sec. 4.3 via a secular equation that relates to the optic modes alone. Explicit solutions for each allotrope are given. The variation of frequency with strain can be followed if the secular equation for the strained crystal can be obtained. This is possible in terms of effective inner elastic constants that are defined in a way similar to that used for the macroscopic elastic constants. Results are listed for each allotrope in Sec. 4.4. Finally expressions for the pressure-dependence of the optic mode frequencies have been deduced and presented in Sec. 4.5.

#### 4.1 Symmetry

The essential geometry of the structures—the space groups, primitive unit cell vectors, atomic coordinates and the allocation of sublattice indices—is summarised in Table 4.1.

Table 4.1: Essential geometry and the assignment of sublattice indices to the atomic sites in the various structures. In *cD*  $a$  is the lattice parameter of the cubic cell; in *rG*  $a$  and  $c$  are the lattice parameters of the non-primitive triple hexagonal cell and  $\rho = c/a$  is the axial ratio.

	<i>cD</i>	<i>rG</i>	<i>hD</i>	<i>hG</i>
Space group	$Fd\bar{3}m$	$R\bar{3}m$	$P6_3/mmc$	
Unit cell vectors	$\vec{a}_1$ $\frac{a}{2}[0, 1, 1]$ $\vec{a}_2$ $\frac{a}{2}[1, 0, 1]$ $\vec{a}_3$ $\frac{a}{2}[1, 1, 0]$	$\frac{a}{6}[3, \sqrt{3}, 2\rho]$ $\frac{a}{6}[-3, \sqrt{3}, 2\rho]$ $\frac{a}{3}[0, -\sqrt{3}, \rho]$	$a[1, 0, 0]$ $a[-\frac{1}{2}, \frac{\sqrt{3}}{2}, 0]$ $a[0, 0, \rho]$	
Wyckoff sites	a	c	f	d : b
Site symmetry	$\bar{4}3m$	$3m$	$3m$	$\bar{6}m2$
Sublattice indices	1 $-(\frac{1}{8} \frac{1}{8} \frac{1}{8})$ 2 $(\frac{1}{8} \frac{1}{8} \frac{1}{8})$ 3 4	$-(u \ u \ u)$ $(u \ u \ u)$	$(\frac{1}{3} \frac{2}{3} z)$ $(\frac{2}{3} \frac{1}{3} 1 - z)$ $(\frac{1}{3} \frac{2}{3} \frac{1}{2} - z)$ $(\frac{2}{3} \frac{1}{3} \frac{1}{2} + z)$	$(\frac{1}{3} \frac{2}{3} \frac{3}{4}) :$ $(\frac{2}{3} \frac{1}{3} \frac{1}{4}) :$ $:(0 \ 0 \ \frac{3}{4})$ $:(0 \ 0 \ \frac{1}{4})$

To make comparison easy the four structures are shown in Fig. 4.1 in relation to hexagonal cells: triple cells for *cD* and *rG* (with  $u = \frac{1}{6}$ ) and primitive ones for *hD* (with  $z = \frac{1}{16}$ ) and *hG*.

Although the inner elastic constants are free of redundancy, a certain arbitrariness has been introduced: a relabelling of the sublattices will lead to a shuffling of values of the components of the tensors. For this reason it is much simpler to treat the symmetry of the sublattice tensors  $d$ ,  $e$  and  $f$  and subsequently to deduce that of the inner elastic constants  $D$ ,  $E$  and  $F$ . The simpler part has already been done. The forms of the individual tensors of the  $d^\alpha$ ,  $e^{\alpha\beta}$  and  $f^{\alpha\beta\gamma}$  families, their non-zero components and any interdependencies, have been extracted from Tables 2.1 through 2.6

in Chapter 2 at the appropriate point group and are presented in Tables 4.2 and 4.3. Some additional simplification follows from the commutative nature of differentiation:  $e_{ij}^{\alpha\beta} = e_{ji}^{\alpha\beta}$  when  $\alpha = \beta$ ,  $d_{iJK}^{\alpha} = d_{iKJ}^{\alpha}$  and several similar relations for  $f_{ijk}^{\alpha\beta\gamma}$ .

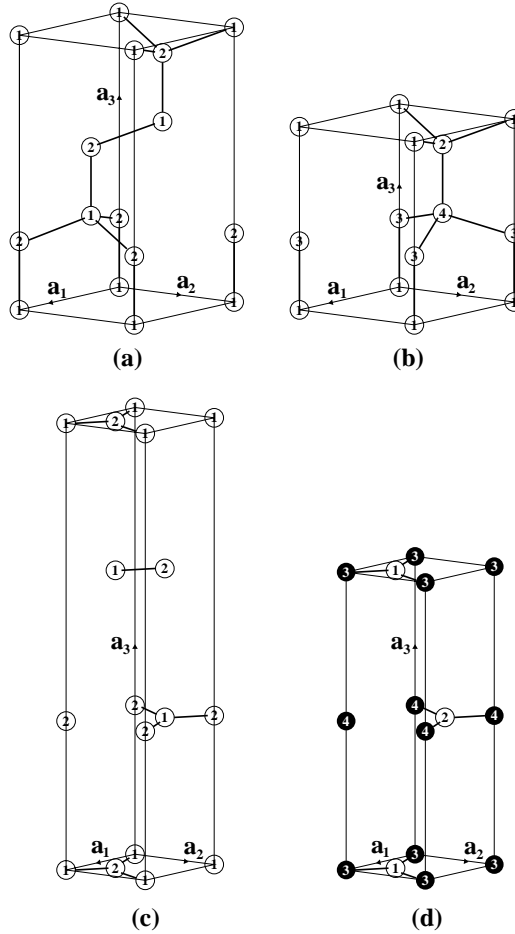


Figure 4.1: Unit cells of four carbon allotropes. In (a) a triple hexagonal cell is used for  $cD$  to facilitate comparison with  $hD$  in (b). In (c) a triple cell is used similarly for  $rG$  to contrast its layer structure (ABCA) with that of  $hG$  (ABA) in (d). In  $hG$  the distinction between non-equivalent pairs of atoms is made by colour.  $sp^3$  or  $sp^2$  bonds have been emphasised.

Table 4.2: The symmetry of the individual sublattice tensors in  $cD$ : the non-zero components and their interrelationships.  $\alpha$ ,  $\beta$  and  $\gamma$  take the values 1 or 2.

$d_{14}^{\alpha} = d_{25}^{\alpha} = d_{36}^{\alpha}$	$f_{123}^{\alpha\beta\gamma} = f_{132}^{\alpha\beta\gamma} = f_{213}^{\alpha\beta\gamma} = f_{231}^{\alpha\beta\gamma} = f_{312}^{\alpha\beta\gamma} = f_{321}^{\alpha\beta\gamma}$
$e_{11}^{\alpha\beta} = e_{22}^{\alpha\beta} = e_{33}^{\alpha\beta}$	$e_{111}^{\alpha\beta} = e_{222}^{\alpha\beta} = e_{333}^{\alpha\beta}$
$d_{114}^{\alpha} = d_{225}^{\alpha} = d_{336}^{\alpha}$	$e_{112}^{\alpha\beta} = e_{113}^{\alpha\beta} = e_{221}^{\alpha\beta} = e_{223}^{\alpha\beta} = e_{331}^{\alpha\beta} = e_{332}^{\alpha\beta}$
$d_{124}^{\alpha} = d_{134}^{\alpha} = d_{215}^{\alpha} = d_{235}^{\alpha} = d_{316}^{\alpha} = d_{326}^{\alpha}$	$e_{126}^{\alpha\beta} = e_{135}^{\alpha\beta} = e_{216}^{\alpha\beta} = e_{234}^{\alpha\beta} = e_{315}^{\alpha\beta} = e_{324}^{\alpha\beta}$
$d_{156}^{\alpha} = d_{246}^{\alpha} = d_{345}^{\alpha}$	

Table 4.3: The symmetry of the individual sublattice tensors in  $rG$ ,  $hD$  and  $hG$ : the non-zero components of each and their interrelationships.  $\alpha$ ,  $\beta$  and  $\gamma$  take the values 1 or 2 in  $rG$ ; 1, 2, 3 or 4 in  $hD$  and  $hG$ .

$hG$ (left column), $rG$ and $hD$ (both columns)	
$\bar{6}m2$	$6mm$
$d_{16}^\alpha = d_{21}^\alpha = -d_{22}^\alpha$	$d_3^\alpha$ $d_{15}^\alpha = d_{24}^\alpha$ $d_{31}^\alpha = d_{32}^\alpha$ $d_{33}^\alpha$
$d_{116}^\alpha = -\frac{1}{4}(d_{211}^\alpha + 3d_{222}^\alpha)$ $d_{126}^\alpha = \frac{1}{4}(3d_{211}^\alpha + d_{222}^\alpha)$	$d_{115}^\alpha = d_{224}^\alpha$ $d_{125}^\alpha = d_{214}^\alpha$
$d_{136}^\alpha = d_{213}^\alpha = -d_{223}^\alpha$	$d_{135}^\alpha = d_{234}^\alpha$
$d_{145}^\alpha = -d_{244}^\alpha = d_{255}^\alpha$	$d_{146}^\alpha = d_{256}^\alpha = \frac{1}{2}(d_{115}^\alpha - d_{125}^\alpha)$
$d_{212}^\alpha = d_{266}^\alpha = \frac{1}{2}(d_{116}^\alpha - d_{126}^\alpha)$	$d_{311}^\alpha = d_{322}^\alpha = d_{312}^\alpha + 2d_{366}^\alpha$
$d_{314}^\alpha = -d_{324}^\alpha = d_{356}^\alpha$	$d_{313}^\alpha = d_{323}^\alpha$ $d_{333}^\alpha$ $d_{344}^\alpha = d_{355}^\alpha$
$f_{112}^{\alpha\beta\gamma} = f_{121}^{\alpha\beta\gamma} = f_{211}^{\alpha\beta\gamma} = -f_{222}^{\alpha\beta\gamma}$	$f_{113}^{\alpha\beta\gamma} = f_{223}^{\alpha\beta\gamma}$ $f_{131}^{\alpha\beta\gamma} = f_{232}^{\alpha\beta\gamma}$ $f_{311}^{\alpha\beta\gamma} = f_{322}^{\alpha\beta\gamma}$ $f_{333}^{\alpha\beta\gamma}$
$\bar{6}m2, 6mm, \text{ part of } 3m \dots$	$\dots \text{ rest of } 3m$
$e_{11}^{\alpha\beta} = e_{22}^{\alpha\beta}$ $e_{33}^{\alpha\beta}$	
$e_{111}^{\alpha\beta} = e_{222}^{\alpha\beta}$ $e_{112}^{\alpha\beta} = e_{221}^{\alpha\beta}$ $e_{113}^{\alpha\beta} = e_{223}^{\alpha\beta}$	
$e_{126}^{\alpha\beta} = e_{216}^{\alpha\beta} = \frac{1}{2}(e_{111}^{\alpha\beta} - e_{112}^{\alpha\beta})$	$e_{114}^{\alpha\beta} = e_{125}^{\alpha\beta} = e_{215}^{\alpha\beta} = -e_{214}^{\alpha\beta}$
$e_{135}^{\alpha\beta} = e_{234}^{\alpha\beta}$	$e_{136}^{\alpha\beta} = e_{231}^{\alpha\beta} = -e_{232}^{\alpha\beta}$
$e_{315}^{\alpha\beta} = e_{324}^{\alpha\beta}$	$e_{316}^{\alpha\beta} = e_{321}^{\alpha\beta} = -e_{322}^{\alpha\beta}$
$e_{331}^{\alpha\beta} = e_{332}^{\alpha\beta}$ $e_{333}^{\alpha\beta}$	

### 4.1.1 Cubic diamond and rhombohedral graphite

A major simplification occurs for structures in which the basis comprises two atoms only, so that  $n = 2$ . Then  $\lambda$ ,  $\mu$  and  $\nu$  take only the value 1 and the superscripts on  $D$ ,  $E$  and  $F$  become redundant. It also follows that the summations in (1.37) disappear, leaving only single terms on the right involving  $p = q = r = 1$  and giving the simplest possible general set of independent components:

$$\begin{aligned} D_{i..} &= -d_{i..}^1 \\ E_{ij.} &= e_{ij.}^{11} \\ F_{ijk} &= -f_{ijk}^{111}. \end{aligned} \quad (4.1)$$

A full collection of specific independent components is shown in Table 4.4 and the complete collection of all non-zero components is obtained by collating the entries in this Table with those in Tables 4.2 and 4.3. The alternative description of the inner elasticity of  $cD$  that will facilitate comparison with the intermediate structures along the  $cD$  to  $rG$  transformation path is produced by a rotation of axes. The matrix

$$a = \begin{bmatrix} \frac{1}{\sqrt{2}} & -\frac{1}{\sqrt{2}} & 0 \\ \frac{1}{\sqrt{6}} & \frac{1}{\sqrt{6}} & -\frac{2}{\sqrt{6}} \\ \frac{1}{\sqrt{3}} & \frac{1}{\sqrt{3}} & \frac{1}{\sqrt{3}} \end{bmatrix} \quad (4.2)$$

transforms the usual  $cD$  coordinate system ( $0x_1$ ,  $0x_2$  and  $0x_3$  along  $[100]$ ,  $[010]$  and  $[001]$  respectively) to one in which  $0x'_1$  lies along  $[1\bar{1}0]$ ,  $0x'_2$  along  $[11\bar{2}]$  and  $0x'_3$  along  $[111]$ . Tensors in the new system are related to those in the old by the transformation law [13]

$$T'_{ijk\dots} = a_{ip} a_{jq} a_{kr} \dots T_{pqr\dots} \quad (4.3)$$

The tensors that are in contracted form must first be uncontracted, then transformed, then re-contracted. These results have been added to Table 4.4. Rotation of axes cannot increase the actual number of independent components of any tensor. The apparent increase conceals numerous relations between the members of the modified set.

### 4.1.2 Hexagonal diamond and hexagonal graphite

The space group symmetry of  $hD$  and  $hG$  was briefly introduced in the previous Chapter. Both allotropes belong to the space group  $P6_3/mmc$ , (no. 194 in the International Tables for Crystallography [7]), which is non-symmorphic, indicating the presence of screw and glide symmetry elements. The 24 symmetry elements are represented by augmented  $4 \times 4$  partitioned matrices

$$\{R_i|\vec{t}\} = \begin{bmatrix} R_i & \vec{t} \\ \mathbf{0} & 1 \end{bmatrix} \quad (4.4)$$

where the  $R_i$  are  $3 \times 3$  point symmetry operations and  $\vec{t}$  is a  $3 \times 1$  column vector representing the fractional translation associated with  $R_i$ . Half the operations have  $\vec{t} = [0/0/0]$  and half have  $\vec{t} = [0/0/\frac{1}{2}]$ .

Table 4.4: Independent components of the inner elastic constants:  $cD$  in columns 1 and 4, and  $rG$  in columns 2 and 5. For columns 3 and 6  $cD$  is referred to a quasi-rhombohedral system ( $0x'_1$  along  $[1\bar{1}0]$ ,  $0x'_2$  along  $[11\bar{2}]$  and  $0x'_3$  along  $[111]$ ): linear combinations of elements from columns 1 or 4 are equivalent to the elements in columns 2 or 5. The full sets of non-zero components are obtained by reading columns 1 and 4, and 2 and 5, in conjunction with the relations in Tables 4.2 and 4.3.

$cD$	$rG$	quasi- $rD$	$cD$	$rG$	quasi- $rD$
	$D_3$	$\equiv 0$			
$D_{14}$	$D_{16}$	$\sqrt{\frac{2}{3}}D_{14}$	$F_{123}$	$F_{112}$	$\frac{2}{\sqrt{6}}F_{123}$
	$D_{15}$	$-\frac{1}{\sqrt{3}}D_{14}$		$F_{113}$	$-\frac{1}{\sqrt{3}}F_{123}$
	$D_{31}$	$-\frac{1}{\sqrt{3}}D_{14}$		$F_{333}$	$\frac{2}{\sqrt{3}}F_{123}$
	$D_{33}$	$\frac{2}{\sqrt{3}}D_{14}$			
$E_{11}$	$E_{11}$	$E_{11}$			
	$E_{33}$	$E_{11}$			
$D_{114}$	$D_{116}$	$\frac{1}{\sqrt{6}}(D_{114} + D_{124} + 2D_{156})$	$E_{111}$	$E_{111}$	$\frac{1}{2}(E_{111} + E_{112} + 2E_{126})$
$D_{124}$	$D_{126}$	$\frac{1}{3\sqrt{6}}(-D_{114} + 7D_{124} - 2D_{156})$	$E_{112}$	$E_{112}$	$\frac{1}{6}(E_{111} + 5E_{112} - 2E_{126})$
$D_{156}$	$D_{136}$	$\frac{2}{3\sqrt{6}}(2D_{114} + D_{124} - 2D_{156})$	$E_{126}$	$E_{113}$	$\frac{1}{3}(E_{111} + 2E_{112} - 2E_{126})$
	$D_{145}$	$\frac{2}{3\sqrt{6}}(-D_{114} + D_{124} + D_{156})$		$E_{126}$	$\frac{1}{6}(E_{111} - E_{112} + 4E_{126})$
	$D_{314}$	$\frac{1}{3\sqrt{6}}(D_{114} - D_{124} + 2D_{156})$		$E_{135}$	$\frac{1}{3}(E_{111} - E_{112} + E_{126})$
	$D_{115}$	$-\frac{1}{2\sqrt{3}}(D_{114} + D_{124} + 2D_{156})$		$E_{331}$	$\frac{1}{3}(E_{111} + 2E_{112} - 2E_{126})$
	$D_{125}$	$\frac{1}{6\sqrt{3}}(-5D_{114} - D_{124} + 2D_{156})$		$E_{333}$	$\frac{1}{3}(E_{111} + 2E_{112} + 4E_{126})$
	$D_{135}$	$\frac{1}{3\sqrt{3}}(D_{114} - 4D_{124} + 2D_{156})$		$E_{114}$	$\frac{1}{3\sqrt{2}}(E_{111} - E_{112} - 2E_{126})$
	$D_{311}$	$-\frac{2}{\sqrt{3}}D_{124}$		$E_{136}$	$\frac{1}{3\sqrt{2}}(E_{111} - E_{112} - 2E_{126})$
	$D_{312}$	$-\frac{2}{3\sqrt{3}}(2D_{114} + D_{124} - 2D_{156})$			
	$D_{313}$	$\frac{1}{3\sqrt{3}}(D_{114} + 2D_{124} - 4D_{156})$			
	$D_{333}$	$\frac{4}{3\sqrt{3}}(D_{114} + 2D_{124} + 2D_{156})$			
	$D_{344}$	$\frac{1}{3\sqrt{3}}(-2D_{114} + 2D_{124} - D_{156})$			

The position coordinates and the indices assigned to the sublattices are shown in Table 4.1. In Table 4.5 are shown the permutations of the sublattice indices induced by the 24 operations of the space group.

Table 4.5: Permutations of sublattice indices corresponding to spacegroup symmetry operations for the hexagonal structures.  $\vec{t}$  is the fractional translation column vector  $[0/0/\frac{1}{2}]$ . The colon separates the non-equivalent pairs in  $hG$ .

Symmetry operations in						Subgroup with row 1	Permutations	
space group $P6_3/mmc$							$hD$	$hG$
$\{1 0\}$	$\{3^+ 0\}$	$\{3^- 0\}$	$\{m 0\}$	$\{m' 0\}$	$\{m'' 0\}$	$R3m$	(1)(2)(3)(4)	(1)(2) : (3)(4)
$\{i 0\}$	$\{\bar{3}^+ 0\}$	$\{\bar{3}^- 0\}$	$\{2 0\}$	$\{2' 0\}$	$\{2'' 0\}$	$P\bar{3}m1$	(12)(34)	(12) : (34)
$\{2_z \vec{t}\}$	$\{6^+ \vec{t}\}$	$\{6^- \vec{t}\}$	$\{c \vec{t}\}$	$\{c' \vec{t}\}$	$\{c'' \vec{t}\}$	$P6_3mc$	(14)(23)	(12) : (34)
$\{m_z \vec{t}\}$	$\{\bar{6}^+ \vec{t}\}$	$\{\bar{6}^- \vec{t}\}$	$\{2_o \vec{t}\}$	$\{2_l \vec{t}\}$	$\{2_r \vec{t}\}$	$P\bar{6}m2$	(13)(24)	(1)(2) : (3)(4)

The latter divide into four subsets of six operations. Those in the first row form a subgroup of point symmetry  $3m$  and leave the sublattice indices in  $hD$  unchanged. Those in the first and fourth rows together form a subgroup of point symmetry  $\bar{6}m2$  and leave the  $hG$  indices unchanged. This determines the fundamental form of the individual sublattice tensors and indicates that those in  $hD$  will have more non-zero components than those in  $hG$ . The two structures therefore require individual treatment.

#### 4.1.2.1 Hexagonal diamond

The components of the  $d$  and  $f$  tensors in  $hD$  are divided conveniently into mutually exclusive  $\bar{6}m2$  and  $6mm$  sets, as shown in Table 4.3. The operations in rows 1 and 2 of the Table 4.5 together constitute the subgroup  $P\bar{3}m1$ . Because half the operations interchange the sublattice indices  $1 \leftrightarrow 2$  and  $3 \leftrightarrow 4$  simultaneously the point group  $\bar{3}m$  determines the non-zero elements of sum tensors such as  $d_{i..}^1 + d_{i..}^2$ . Since  $\bar{3}m$  is centrosymmetric *all* elements of sum tensors bearing an odd number of superscripts vanish. Thus

$$\begin{aligned} d_{i..}^1 + d_{i..}^2 &= 0 \\ d_{i..}^3 + d_{i..}^4 &= 0. \end{aligned}$$

The operations in rows 1 and 3 similarly comprise the subgroup  $P6_3mc$ , with row 3 operations producing the interchanges  $1 \leftrightarrow 4$  and  $2 \leftrightarrow 3$ . The point group  $6mm$  now determines the non-zero elements of sum tensors such as  $d_{i..}^1 + d_{i..}^4$ . Finally operations in rows 1 and 4 together constitute the subgroup  $P\bar{6}m2$ , with row 4 operations producing the interchanges  $1 \leftrightarrow 3$  and  $2 \leftrightarrow 4$ . The point group  $\bar{6}m2$  now determines the non-zero elements of sum tensors such as  $d_{i..}^1 + d_{i..}^3$ . Thus the following deductions can be made:

$$\begin{aligned}
d_{i..}^1 + d_{i..}^3 &= -(d_{i..}^2 + d_{i..}^4) \neq 0 && \bar{6}m2 \text{ elements} \\
&= 0 && 6mm \text{ elements} \\
d_{i..}^1 + d_{i..}^4 &= -(d_{i..}^2 + d_{i..}^3) \neq 0 && 6mm \text{ elements} \\
&= 0 && \bar{6}m2 \text{ elements.}
\end{aligned}$$

In summary

$$d_{i..}^1 = -d_{i..}^2 = \pm d_{i..}^3 = \mp d_{i..}^4$$

with the upper(lower) signs applicable to  $\bar{6}m2(6mm)$  elements. In conjunction with (1.37) or (1.39) and (1.38) these give independent, zero and dependent components as follows

$$\begin{aligned}
D_{i..}^1 &= -d_{i..}^1 \\
D_{i..}^2 &= 0 \\
D_{i..}^3 &= \pm D_{i..}^1,
\end{aligned} \tag{4.5}$$

with the same interpretation of signs.

Similarly it is possible to use the above arguments to generate sixteen relations that are satisfied by the  $f$  tensors:

$$\begin{aligned}
f_{ijk}^{111} &= -f_{ijk}^{222} = \pm f_{ijk}^{333} = \mp f_{ijk}^{444} \\
f_{ijk}^{112} &= -f_{ijk}^{221} = \pm f_{ijk}^{334} = \mp f_{ijk}^{443} \\
&\vdots && \vdots && \vdots \\
f_{ijk}^{144} &= -f_{ijk}^{233} = \pm f_{ijk}^{322} = \mp f_{ijk}^{411}.
\end{aligned}$$

Equations (1.37), (1.38) and (1.39) are then invoked many times to establish a preliminary *maximum* number of independent components (13) and a minimum number of dependent components (also 13)

$$\begin{aligned}
F_{ijk}^{\lambda\mu\nu} &= -\sum_{p=1}^{\lambda} \sum_{q=1}^{\mu} \sum_{r=1}^{\nu} f_{ijk}^{pqr} && \lambda\mu\nu < 222 \\
F_{ijk}^{222} &= 0 \\
F_{ijk}^{\lambda\mu\nu} &= \pm F_{ijk}^{4-\lambda, 4-\mu, 4-\nu} && \lambda\mu\nu > 222,
\end{aligned} \tag{4.6}$$

reading  $\lambda\mu\nu$  as a 3-digit number and with the same interpretation of  $\pm$  as before. There is only a single independent sublattice tensor component in the  $\bar{6}m2$  set, which may be taken as  $f_{222}^{\alpha\beta\gamma}$ . As the three subscripts are equal the commutative property of differentiation implies that all components with permuted superscripts are equal. This property carries over to the inner elastic constants  $F_{ijk}^{\lambda\mu\nu}$  and reduces the number of independent constants to three and renders six more zero. For the  $6mm$  set the component  $f_{333}^{\alpha\beta\gamma}$  gives the same result. The remaining three independent components each

permit the interchange of a different pair of superscripts. The net result is that six  $F_{113}^{\lambda\mu\nu}$  may be chosen as independent and the remaining  $F_{131}^{\lambda\mu\nu}$  and  $F_{311}^{\lambda\mu\nu}$  components related to them. All these results are embodied in Table 4.6.

All the components of the second-order  $e$  tensors and most of those of the third order belong in common to  $3m$ ,  $\bar{3}m$ ,  $\bar{6}m2$  and  $6mm$  symmetry, the remainder to  $\bar{3}m$  and  $3m$  only. The difference between these sets lies in the effect of the symmetry operations on the signs of individual components: in the main set the (uncontracted) subscript sequences have the form  $ii$ ,  $iiii$ ,  $ijjj$  or  $ijij$  and the components do not change sign under any operation; in the residual set the sequences are  $ijk$ ,  $ijik$ ,  $ijii$  or  $ijkk$  (one 3 and an odd number of 2s, in fact) and the components change sign under operations in rows 3 and 4 of Table 4.5. In the main set attention therefore focuses on difference tensors, such as  $e_{ij}^{11} - e_{ij}^{22}$ , whose signs are reversed by operations in rows 2, 3 and 4 of the Table. This shows that all such difference tensors are null and thus that

$$\begin{aligned} e_{ij}^{11} &= e_{ij}^{22} = \pm e_{ij}^{33} = \pm e_{ij}^{44} \\ e_{ij}^{12} &= e_{ij}^{21} = \pm e_{ij}^{34} = \pm e_{ij}^{43} \\ e_{ij}^{13} &= e_{ij}^{24} = \pm e_{ij}^{31} = \pm e_{ij}^{42} \\ e_{ij}^{14} &= e_{ij}^{23} = \pm e_{ij}^{32} = \pm e_{ij}^{41} \end{aligned}$$

where the plus signs are taken throughout. The residual set of third-order terms gives rise to the minus signs via the nullification of sum tensors, such as  $e_{ij}^{11} + e_{ij}^{33}$  and  $e_{ij}^{23} + e_{ij}^{32}$ , by the operations of rows 3 and 4 in Table 4.5.

The inner elastic constants follow from (1.37) or (1.39) and (1.38). Independent and dependent constants for the main set are

$$\begin{aligned} E_{ij}^{11} &= e_{ij}^{11} \\ E_{ij}^{12} &= e_{ij}^{11} + e_{ij}^{12} \\ E_{ij}^{13} &= -e_{ij}^{14} \\ E_{ij}^{22} &= 2E_{ij}^{12} \\ E_{ij}^{21} &= E_{ij}^{23} = E_{ij}^{32} = E_{ij}^{12} \\ E_{ij}^{31} &= E_{ij}^{13} \\ E_{ij}^{33} &= E_{ij}^{11} \end{aligned} \tag{4.7}$$

and for the residual set are

$$\begin{aligned} E_{ij}^{11} &= e_{ij}^{11} \\ E_{ij}^{13} &= -e_{ij}^{14} \\ E_{ij}^{12} &= E_{ij}^{21} = E_{ij}^{22} = E_{ij}^{23} = E_{ij}^{32} = 0 \\ E_{ij}^{31} &= -E_{ij}^{13} \\ E_{ij}^{33} &= -E_{ij}^{11} \end{aligned} \tag{4.8}$$

This concludes the analysis for  $hD$ .

Table 4.6: Interrelation of components of the inner elastic constants of  $hD$ . The left-hand elements in column 1 and the lower part of column 2, associated with the subscript sequence in column 2 if any, may be taken as an independent set. The full sets of non-zero components are obtained by reading columns 1 and 2 in conjunction with the appropriate relations in Table 4.3. All components  $D_{iJ}^2$ ,  $D_{iJK}^2$  and  $F_{ijk}^{222}$  are zero.

$D_3^1 = -D_3^3$	
$D_{16}^1 = D_{16}^3$	
$D_{iJ}^1 = -D_{iJ}^3$	$iJ = 15, 31, 33$
$E_{ii}^{11} = E_{ii}^{33}$	$ii = 11, 33$
$E_{ii}^{12} = E_{ii}^{21} = \frac{1}{2}E_{ii}^{22} = E_{ii}^{23} = E_{ii}^{32}$	"
$E_{ii}^{13} = E_{ii}^{31}$	"
$D_{iJK}^1 = D_{iKJ}^1 = D_{iJK}^3 = D_{iKJ}^3$	$iJK = 116, 126, 136, 145, 314$
$D_{iJK}^1 = D_{iKJ}^1 = -D_{iJK}^3 = -D_{iKJ}^3$	$iJK = 115, 125, 135, 311, 312, 313, 333, 344$
$E_{ijK}^{11} = E_{ijK}^{33}$	$ijK = 111, 112, 113, 126, 135, 315, 331, 333$
$E_{ijK}^{12} = E_{ijK}^{21} = \frac{1}{2}E_{ijK}^{22} = E_{ijK}^{23} = E_{ijK}^{32}$	"
$E_{ijK}^{13} = E_{ijK}^{31}$	"
$E_{ijK}^{11} = -E_{ijK}^{33}$	$ijK = 114, 136, 316$
$E_{ijK}^{13} = -E_{ijK}^{31}$	$ijK = 136, 316$
$F_{112}^{111} = F_{112}^{333}$	
$F_{112}^{112} = F_{112}^{121} = F_{112}^{122} = F_{112}^{211} = F_{112}^{212} = F_{112}^{221}$	
$\quad = F_{112}^{123} = F_{112}^{132} = F_{112}^{213} = F_{112}^{231} = F_{112}^{312} = F_{112}^{321}$	
$\quad = F_{112}^{223} = F_{112}^{232} = F_{112}^{233} = F_{112}^{322} = F_{112}^{323} = F_{112}^{332}$	
$F_{112}^{113} = F_{112}^{131} = F_{112}^{133} = F_{112}^{311} = F_{112}^{313} = F_{112}^{331}$	
$F_{113}^{111} = -F_{113}^{333}$	
$F_{113}^{112} = F_{113}^{122} = F_{113}^{212} = -F_{113}^{232} = -F_{113}^{322} = -F_{113}^{332}$	
$F_{113}^{113} = -F_{113}^{331}$	
$F_{113}^{121} = F_{113}^{211} = -F_{113}^{233} = -F_{113}^{323}$	
$F_{113}^{123} = F_{113}^{213} = -F_{113}^{231} = -F_{113}^{321}$	
$F_{113}^{131} = -F_{113}^{133} = F_{113}^{311} = -F_{113}^{313}$	
$F_{113}^{221} = -F_{113}^{223}$	
$F_{333}^{111} = -F_{333}^{333}$	
$F_{333}^{112} = F_{333}^{121} = F_{333}^{122} = F_{333}^{211} = F_{333}^{212} = F_{333}^{221}$	
$\quad = -F_{333}^{223} = -F_{333}^{232} = -F_{333}^{233} = -F_{333}^{322} = -F_{333}^{323} = -F_{333}^{332}$	
$F_{333}^{113} = F_{333}^{131} = -F_{333}^{133} = F_{333}^{311} = -F_{333}^{313} = -F_{333}^{331}$	

#### 4.1.2.2 Hexagonal graphite

The arguments for *hG* are largely a repeat of those above but with outcomes that differ because the basis consists of two non-equivalent pairs rather than a single quartet. All the individual *d*, *e* and *f* tensors have  $\bar{6}m2$  symmetry. Operations in rows 1 to 4 combined constitute  $P6_3/mmc$  and all elements of sum tensors, such as  $d_{i..}^1 + d_{i..}^2$ , vanish as the associated point group  $6/mmm$  is centrosymmetric. Thus

$$\begin{aligned}d_{i..}^1 + d_{i..}^2 &= 0 \\d_{i..}^3 + d_{i..}^4 &= 0\end{aligned}$$

with no further interrelations. Thus, using (1.37) and (1.38),

$$\begin{aligned}D_{i..}^1 &= -d_{i..}^1 \\D_{i..}^2 &= 0 \\D_{i..}^3 &= +d_{i..}^4\end{aligned}\tag{4.9}$$

giving two independent inner elastic constants where *hD* had one.

For the *f* tensors there are sixteen pairs of relations:

$$\begin{aligned}f_{ijk}^{111} &= -f_{ijk}^{222} & f_{ijk}^{333} &= -f_{ijk}^{444} \\f_{ijk}^{112} &= -f_{ijk}^{221} & f_{ijk}^{334} &= -f_{ijk}^{443} \\&\vdots & &\vdots \\f_{ijk}^{144} &= -f_{ijk}^{233} & f_{ijk}^{322} &= -f_{ijk}^{411}.\end{aligned}$$

In conjunction with (1.37), (1.38) and (1.39) it is found that the independent and zero elements are

$$\begin{aligned}F_{ijk}^{111} &= -f_{ijk}^{111} \\F_{ijk}^{112} &= -(f_{ijk}^{111} + f_{ijk}^{112}) \\F_{ijk}^{113} &= +f_{ijk}^{114} \\F_{ijk}^{123} &= +(f_{ijk}^{114} + f_{ijk}^{124}) \\F_{ijk}^{133} &= -f_{ijk}^{144} \\F_{ijk}^{223} &= -(f_{ijk}^{144} + f_{ijk}^{244}) \\F_{ijk}^{333} &= +f_{ijk}^{444} \\F_{ijk}^{222} &= 0.\end{aligned}\tag{4.10}$$

The numerous dependent elements, related by permutation of superscripts for the reason given above for *hD*, are displayed in Table 4.7.

The analysis of the *e* and *E* tensors follows that of the main group in *hD* though with a slightly different outcome:

$$E_{ij.}^{11} = e_{ij.}^{11}$$

$$\begin{aligned}
E_{ij.}^{12} &= e_{ij.}^{11} + e_{ij.}^{12} \\
E_{ij.}^{13} &= -e_{ij.}^{14} \\
E_{ij.}^{22} &= 2E_{ij.}^{12} \\
E_{ij.}^{21} &= E_{ij.}^{23} = E_{ij.}^{32} = E_{ij.}^{12} \\
E_{ij.}^{31} &= -e_{ij.}^{41} \\
E_{ij.}^{33} &= e_{ij.}^{44}.
\end{aligned} \tag{4.11}$$

Table 4.7: Interrelation of components of the inner elastic constants of  $hG$ . The left-hand elements in column 1, associated with the subscript sequence in column 2 if any, may be taken as an independent set. The full sets of non-zero components are obtained by reading columns 1 and 2 in conjunction with the appropriate relations in Table 4.3. All components  $D_{iJ}^2$ ,  $D_{iJK}^2$  and  $F_{ijk}^{222}$  are zero.

$D_{16}^1$	
$D_{16}^3$	
$E_{ii}^{11}$	$ii = 11, 33$
$E_{ii}^{12} = E_{ii}^{21} = \frac{1}{2}E_{ii}^{22} = E_{ii}^{23} = E_{ii}^{32}$	"
$E_{ii}^{13} = E_{ii}^{31}$	"
$E_{ii}^{33}$	"
$D_{iJK}^1 = D_{iKJ}^1$	$iJK = 116, 126, 136, 145, 212, 314$
$D_{iJK}^3 = D_{iKJ}^3$	$iJK = 116, 126, 136, 145, 212, 314$
$E_{ijK}^{11}$	$ijK = 111, 112, 113, 126, 135, 315, 331, 333$
$E_{ijK}^{12} = E_{ijK}^{21} = \frac{1}{2}E_{ijK}^{22} = E_{ijK}^{23} = E_{ijK}^{32}$	"
$E_{ijK}^{13} = E_{ijK}^{31}$	"
$E_{ijK}^{33}$	"
$F_{112}^{111}$	
$F_{112}^{112} = F_{112}^{121} = F_{112}^{122} = F_{112}^{211} = F_{112}^{212} = F_{112}^{221}$	
$F_{112}^{113} = F_{112}^{131} = F_{112}^{311}$	
$F_{112}^{123} = F_{112}^{132} = F_{112}^{213} = F_{112}^{231} = F_{112}^{312} = F_{112}^{321}$	
$F_{112}^{133} = F_{112}^{313} = F_{112}^{331}$	
$F_{112}^{223} = F_{112}^{232} = F_{112}^{322} = F_{112}^{233} = F_{112}^{323} = F_{112}^{332}$	
$F_{112}^{333}$	

## 4.2 Internal strain tensors

The symmetry of these tensors is the same as that of the  $D^\lambda$  tensors and the elements that are non-zero for the structures under discussion can be read from Tables 4.4, 4.6 or 4.7 as appropriate (except that the condition  $A_{i,j}^2 = 0$  does not always apply, as shown below). In principle these tensors may be determined experimentally by analysing x-ray diffraction from stressed single crystals. In practice the measurements are either difficult because the effect is very small, as in *cD* [5], or impossible because a sufficiently large single crystal cannot be obtained, as in *hG*, *rG* and *hD*. Theoretically their values may be obtained from the internal equilibrium conditions given in equations (1.22) and (1.24) in Chapter 1.

Only the independent linear tensor components are given for *rG* and *hD* in the following lists.

### 4.2.1 Cubic diamond

Equation (1.22) yields a single linear component given by

$$A_{14} = -D_{14}/E_{11} \quad (4.12)$$

and (1.24) gives three quadratic components

$$\begin{aligned} A_{114} &= -G_{114}/E_{11} \\ A_{124} &= -G_{124}/E_{11} \\ A_{156} &= -G_{156}/E_{11} \end{aligned} \quad (4.13)$$

in which

$$\begin{aligned} G_{114} &= D_{114} + A_{14}E_{111} \\ G_{124} &= D_{124} + A_{14}E_{112} \\ G_{156} &= D_{156} + 2A_{14}E_{126} + (A_{14})^2E_{123}. \end{aligned} \quad (4.14)$$

### 4.2.2 Rhombohedral graphite

The four independent linear tensor components are

$$\begin{aligned} A_{16} &= -D_{16}/E_{11} \\ A_{15} &= -D_{15}/E_{11} \\ A_{31} &= -D_{31}/E_{33} \\ A_{33} &= -D_{33}/E_{33}. \end{aligned} \quad (4.15)$$

### 4.2.3 Hexagonal diamond

The solutions of (1.22) for  $hD$ , invoking the dependencies to be found in Table 4.6, lead to

$$\begin{aligned} A_{16}^1 &= A_{16}^3 = -D_{16}^1 / (E_{11}^{11} - E_{11}^{12} + E_{11}^{13}) \\ A_{15}^1 &= -A_{15}^3 = -D_{15}^1 / (E_{11}^{11} - E_{11}^{13}) \\ A_{31}^1 &= -A_{31}^3 = -D_{31}^1 / (E_{33}^{11} - E_{33}^{13}) \\ A_{33}^1 &= -A_{33}^3 = -D_{33}^1 / (E_{33}^{11} - E_{33}^{13}) \end{aligned} \quad (4.16)$$

with  $A_{iJ}^2 = -\frac{1}{2}(A_{iJ}^1 + A_{iJ}^3)$  giving

$$\begin{aligned} A_{16}^2 &= -A_{16}^1 \\ A_{15}^2 &= A_{31}^2 = A_{33}^2 = 0. \end{aligned} \quad (4.17)$$

### 4.2.4 Hexagonal graphite

The independence of  $D^1$  and  $D^3$  leads to similarly independent  $A^1$  and  $A^3$  given by

$$A_{16}^1 = \frac{(E_{11}^{33} - \frac{1}{2}E_{11}^{12})D_{16}^1 - (E_{11}^{13} - \frac{1}{2}E_{11}^{12})D_{16}^3}{(E_{11}^{13} - \frac{1}{2}E_{11}^{12})^2 - (E_{11}^{11} - \frac{1}{2}E_{11}^{12})(E_{11}^{33} - \frac{1}{2}E_{11}^{12})} \quad (4.18)$$

and

$$A_{16}^3 = \frac{(E_{11}^{11} - \frac{1}{2}E_{11}^{12})D_{16}^3 - (E_{11}^{13} - \frac{1}{2}E_{11}^{12})D_{16}^1}{(E_{11}^{13} - \frac{1}{2}E_{11}^{12})^2 - (E_{11}^{11} - \frac{1}{2}E_{11}^{12})(E_{11}^{33} - \frac{1}{2}E_{11}^{12})}. \quad (4.19)$$

As for  $hD$ , the solutions of (1.22) for  $hG$ , invoking the dependencies to be found in Table 4.7, lead to

$$A_{iJ}^2 = -\frac{1}{2}(A_{iJ}^1 + A_{iJ}^3). \quad (4.20)$$

The inner displacement is confined to the basal plane.

For the quadratic internal strain the solutions of (1.24) are

$$A_{iJK}^1 = \frac{(E_{ii}^{33} - \frac{1}{2}E_{ii}^{12})G_{iJK}^1 - (E_{ii}^{13} - \frac{1}{2}E_{ii}^{12})G_{iJK}^3}{(E_{ii}^{13} - \frac{1}{2}E_{ii}^{12})^2 - (E_{ii}^{11} - \frac{1}{2}E_{ii}^{12})(E_{ii}^{33} - \frac{1}{2}E_{ii}^{12})} \quad (4.21)$$

and

$$A_{iJK}^3 = \frac{(E_{ii}^{11} - \frac{1}{2}E_{ii}^{12})G_{iJK}^3 - (E_{ii}^{13} - \frac{1}{2}E_{ii}^{12})G_{iJK}^1}{(E_{ii}^{13} - \frac{1}{2}E_{ii}^{12})^2 - (E_{ii}^{11} - \frac{1}{2}E_{ii}^{12})(E_{ii}^{33} - \frac{1}{2}E_{ii}^{12})}. \quad (4.22)$$

Five pairs of solutions, with  $A_{iJK}^2 = -\frac{1}{2}(A_{iJK}^1 + A_{iJK}^3)$ , correspond to the following composite expressions, in which summation over repeated superscripts is implied,

$$\begin{aligned} G_{136}^\lambda &= D_{136}^\lambda + E_{113}^{\lambda\mu} A_{16}^\mu \\ G_{145}^\lambda &= D_{145}^\lambda \\ G_{211}^\lambda &= D_{211}^\lambda + 2E_{112}^{\lambda\mu} A_{16}^\mu - F_{112}^{\lambda\mu\nu} A_{16}^\mu A_{16}^\nu \\ G_{222}^\lambda &= D_{222}^\lambda - 2E_{111}^{\lambda\mu} A_{16}^\mu - F_{112}^{\lambda\mu\nu} A_{16}^\mu A_{16}^\nu \\ G_{314}^\lambda &= D_{314}^\lambda + E_{315}^{\lambda\mu} A_{16}^\mu. \end{aligned} \quad (4.23)$$

### 4.3 The zone-centre optic modes

The relationship of the  $E^{\lambda\mu}$  tensors to the more familiar coupling constants  $\Phi^{\alpha\beta}$  was demonstrated in Chapter 1

$$E_{ij}^{\lambda\mu} = \tilde{Q}^{\lambda\alpha} \Phi_{ij}^{\alpha\beta} Q^{\beta\mu} \quad (4.24)$$

and shown to lead to a secular equation relating to optic modes alone:

$$|E_{ij}^{\lambda\mu} - \omega^2 K^{\lambda\mu} \delta_{ij}| = 0 \quad (4.25)$$

where  $K^{\lambda\mu} = \tilde{Q}^{\lambda\alpha} \rho^{\alpha\beta} Q^{\beta\mu}$ . The matrices  $Q$  and  $\rho$  defined in (1.44) and (1.55) are much simplified because all atoms in the basis of any allotrope are equal. This leads to  $\mu_k = k/n$  and  $\rho = (\rho_0/n)I_n$ , where  $I_n$  is the  $n \times n$  unit matrix.

In general to each value of  $\omega^2$  there corresponds an eigenvector given by

$$E_{ij}^{\lambda\mu} z_j^\mu = \omega^2 K^{\lambda\mu} z_i^\mu. \quad (4.26)$$

For  $cD$  and  $rG$  it is indeterminate whilst for  $hD$  and  $hG$  it is  $Z$ , a triad of relative sublattice displacement vectors  $\vec{z}$ :  $Z = [\vec{z}^1, \vec{z}^2, \vec{z}^3]$ .

Where relevant the mode frequencies have been labeled with subscripts  $R$  or  $I$  to indicate Raman or infra-red activity.

#### 4.3.1 Cubic diamond and rhombohedral graphite

For both  $cD$  and  $rG$   $Q$  is the column vector  $[-\frac{1}{2}/\frac{1}{2}]$  and  $K$  reduces to the scalar  $\rho_0/4$ . As  $E$  is diagonal the secular equation for optic modes reduces to

$$|E_{11} - \frac{1}{4}\rho_0\omega^2|^3 = 0$$

for  $cD$ , giving the triply-degenerate frequency

$$\omega_R^2(T_{2g}) = \frac{4}{\rho_0} E_{11}. \quad (4.27)$$

The eigenvectors are indeterminate: a set such as  $\vec{z} = [1, 0, 0]$ ,  $\vec{z} = [0, 1, 0]$  and  $\vec{z} = [0, 0, 1]$  could be chosen to represent an LO mode and two TO modes in the limit  $\vec{k} \rightarrow 0$  along one of the cubic axes. For  $rG$  the equation reduces to

$$|E_{11} - \frac{1}{4}\rho_0\omega^2|^2 |E_{33} - \frac{1}{4}\rho_0\omega^2| = 0$$

giving a doubly-degenerate frequency

$$\omega_R^2(E_g) = \frac{4}{\rho_0} E_{11} \quad (4.28)$$

with eigenvectors  $\vec{z} = [\cos \theta, \sin \theta, 0]$  with arbitrary  $\theta$  and a non-degenerate one

$$\omega_R^2(A_{1g}) = \frac{4}{\rho_0} E_{33} \quad (4.29)$$

whose eigenvector is  $\vec{z} = [0, 0, 1]$ . This and two values of  $\theta$  differing by  $\pi/2$  will then represent an LO mode and two TO modes in the limit  $k \rightarrow 0$  along the unique axis or any direction perpendicular to it. All other directions see a mixing of longitudinal and transverse character.

### 4.3.2 Hexagonal diamond

When  $n = 4$   $Q$  and  $K$  are given by

$$Q = \frac{1}{4} \begin{bmatrix} -3 & -2 & -1 \\ 1 & -2 & -1 \\ 1 & 2 & -1 \\ 1 & 2 & 3 \end{bmatrix}$$

and

$$K = \frac{\rho_0}{16} \begin{bmatrix} 3 & 2 & 1 \\ 2 & 4 & 2 \\ 1 & 2 & 3 \end{bmatrix}.$$

The resulting secular equation is a product of three  $3 \times 3$  subdeterminants

$$|\Delta_1| |\Delta_2| |\Delta_3| = 0$$

where the matrix  $\Delta_i$  is

$$\Delta_i = \begin{bmatrix} E_{ii}^{11} - \frac{3}{16}\rho_0\omega^2 & E_{ii}^{12} - \frac{1}{8}\rho_0\omega^2 & E_{ii}^{13} - \frac{1}{16}\rho_0\omega^2 \\ E_{ii}^{12} - \frac{1}{8}\rho_0\omega^2 & 2(E_{ii}^{12} - \frac{1}{8}\rho_0\omega^2) & E_{ii}^{12} - \frac{1}{8}\rho_0\omega^2 \\ E_{ii}^{13} - \frac{1}{16}\rho_0\omega^2 & E_{ii}^{12} - \frac{1}{8}\rho_0\omega^2 & E_{ii}^{33} - \frac{3}{16}\rho_0\omega^2 \end{bmatrix}$$

and symmetry imposes  $\Delta_1 = \Delta_2$ . Each of the subdeterminants factorizes into a linear and quadratic part: the repeated determinant has the roots

$$\begin{aligned} \omega^2(E_{2u}) &= \frac{8}{\rho_0} E_{11}^{12} \\ \omega_R^2(E_{1g}) &= \frac{8}{\rho_0} (E_{11}^{11} - E_{11}^{13}) \\ \omega_R^2(E_{2g}) &= \frac{8}{\rho_0} (E_{11}^{11} - E_{11}^{12} + E_{11}^{13}) \end{aligned} \quad (4.30)$$

resulting in three degenerate pairs of frequencies. The third determinant has the same form and gives

$$\begin{aligned} \omega^2(B_{1u}) &= \frac{8}{\rho_0} E_{33}^{12} \\ \omega_R^2(A_{1g}) &= \frac{8}{\rho_0} (E_{33}^{11} - E_{33}^{13}) \\ \omega^2(B_{2g}) &= \frac{8}{\rho_0} (E_{33}^{11} - E_{33}^{12} + E_{33}^{13}) \end{aligned} \quad (4.31)$$

for the remaining frequencies.

The  $i$ th components of the  $\vec{z}^\lambda$  for a specific mode are the solutions of  $|\Delta_i[z_i^1, z_i^2, z_i^3]| = 0$  when  $\omega^2$  in  $\Delta_i$  has been replaced by its eigenvalue. The results for the above modes are

$$\begin{aligned}
 Z(E_{2u}) &= [[0, 0, 0], [\cos \theta, \sin \theta, 0], [0, 0, 0]] \\
 Z(E_{1g}) &= \left[ \left[ \frac{1}{\sqrt{2}} \cos \theta, \frac{1}{\sqrt{2}} \sin \theta, 0 \right], [0, 0, 0], \left[ -\frac{1}{\sqrt{2}} \cos \theta, -\frac{1}{\sqrt{2}} \sin \theta, 0 \right] \right] \\
 Z(E_{2g}) &= \left[ \left[ \frac{1}{\sqrt{3}} \cos \theta, \frac{1}{\sqrt{3}} \sin \theta, 0 \right], \left[ -\frac{1}{\sqrt{3}} \cos \theta, -\frac{1}{\sqrt{3}} \sin \theta, 0 \right], \left[ \frac{1}{\sqrt{3}} \cos \theta, \frac{1}{\sqrt{3}} \sin \theta, 0 \right] \right] \\
 Z(B_{1u}) &= [[0, 0, 0], [0, 0, 1], [0, 0, 0]] \\
 Z(A_{1g}) &= \left[ \left[ 0, 0, \frac{1}{\sqrt{2}} \right], [0, 0, 0], \left[ 0, 0, -\frac{1}{\sqrt{2}} \right] \right] \\
 Z(B_{2g}) &= \left[ \left[ 0, 0, \frac{1}{\sqrt{3}} \right], [0, 0, -\frac{1}{\sqrt{3}}], \left[ 0, 0, \frac{1}{\sqrt{3}} \right] \right].
 \end{aligned}
 \tag{4.32}$$

Vibrational patterns corresponding to these eigenvectors are shown in Fig. 4.2.

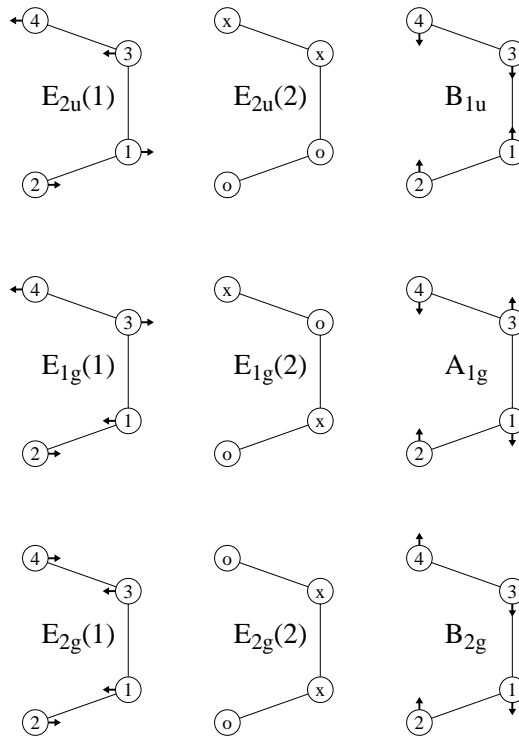


Figure 4.2: A representative set of vibration patterns for hD. x and o indicate motions into and out of the page.

### 4.3.3 Hexagonal graphite

The hexagonal allotropes have identical complements of  $E_{ii}^{\lambda\mu}$  components and thus the same secular equation. The only difference arises from the dependency  $E_{ii}^{11} = E_{ii}^{33}$  that holds for  $hD$  but not for  $hG$ . This is responsible for the slightly more complicated expressions that follow. The three degenerate pairs of frequencies are given by

$$\begin{aligned}\omega_I^2(E_{1u}) &= \frac{8}{\rho_0} E_{11}^{12} \\ \omega_R^2(E_{2g2}) &= \frac{4}{\rho_0} \left[ E_{11}^{11} - E_{11}^{12} + E_{11}^{33} + E_{11}^\dagger \right] \\ \omega_R^2(E_{2g1}) &= \frac{4}{\rho_0} \left[ E_{11}^{11} - E_{11}^{12} + E_{11}^{33} - E_{11}^\dagger \right]\end{aligned}\quad (4.33)$$

where

$$(E_{11}^\dagger)^2 = (E_{11}^{12} - 2E_{11}^{13})^2 + (E_{11}^{11} - E_{11}^{33})^2$$

and the three non-degenerate frequencies by

$$\begin{aligned}\omega_I^2(A_{2u}) &= \frac{8}{\rho_0} E_{33}^{12} \\ \omega_R^2(B_{1g2}) &= \frac{4}{\rho_0} \left[ E_{33}^{11} - E_{33}^{12} + E_{33}^{33} + E_{33}^\dagger \right] \\ \omega_R^2(B_{1g1}) &= \frac{4}{\rho_0} \left[ E_{33}^{11} - E_{33}^{12} + E_{33}^{33} - E_{33}^\dagger \right]\end{aligned}\quad (4.34)$$

where

$$(E_{33}^\dagger)^2 = (E_{33}^{12} - 2E_{33}^{13})^2 + (E_{33}^{11} - E_{33}^{33})^2.$$

The eigenvectors for the  $E_{1u}$  and  $A_{2u}$  modes have the same form as their  $hD$  counterparts. The remainder are slightly less constrained: the parameters  $a$  and  $b$  are, in every case, arbitrary.

$$\begin{aligned}Z(E_{1u}) &= [[0, 0, 0], [\cos\theta, \sin\theta, 0], [0, 0, 0]] \\ Z(E_{2g2}) &= \left[ [a \cos\theta, a \sin\theta, 0], \left[ \frac{1}{2}(b-a) \cos\theta, \frac{1}{2}(b-a) \sin\theta, 0 \right], [-b \cos\theta, -b \sin\theta, 0] \right] \\ Z(E_{2g1}) &= \left[ [a \cos\theta, a \sin\theta, 0], \left[ -\frac{1}{2}(a+b) \cos\theta, -\frac{1}{2}(a+b) \sin\theta, 0 \right], [b \cos\theta, b \sin\theta, 0] \right] \\ Z(A_{2u}) &= [[0, 0, 0], [0, 0, 1], [0, 0, 0]] \\ Z(B_{1g2}) &= \left[ [0, 0, a], [0, 0, \frac{1}{2}(b-a)], [0, 0, -b] \right] \\ Z(B_{1g1}) &= \left[ [0, 0, a], [0, 0, -\frac{1}{2}(a+b)], [0, 0, b] \right].\end{aligned}\quad (4.35)$$

Vibrational patterns corresponding to these eigenvectors are shown in Fig. 4.3.

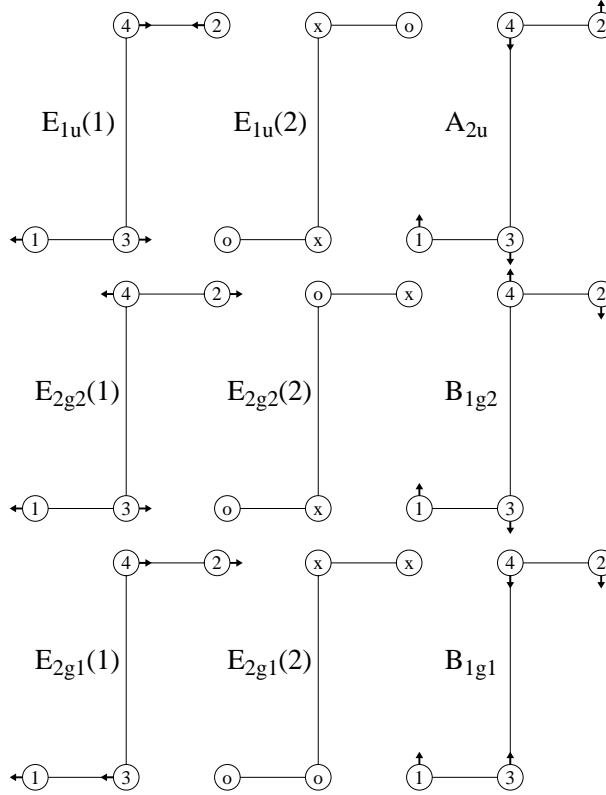


Figure 4.3: A representative set of vibration patterns for  $hG$ .  $x$  and  $o$  indicate motions into and out of the page.

The present approach has been checked against the traditional lattice dynamical treatment of  $hG$  by Maradudin [10]. After allowing for a different labelling of sublattices agreement is total.

#### 4.4 Effective inner elastic constants

When an initially-strained crystal is further deformed its energy can be expressed in two ways: either in terms of the additional deformation and effective elastic constants or in terms of the overall deformation and the elastic constants of the crystal in the unstrained state. The procedure is described fully, in the context of the macroscopic elastic constants, by Wallace in [16, Sec. 8] and is readily extended to cover the microscopic constants.

The effective  $E$  tensors, denoted by  $\bar{E}_{ij}^{\lambda\mu}$ , may be used in the secular equation (with the appropriate density  $\rho$ ) to obtain the optic mode frequencies in stressed crystals. Strains can be chosen to introduce off-diagonal elements and remove degeneracies. Phonon deformation parameters, which characterise the strain dependence of the frequency [3, 14], are easily derived from the  $\bar{E}$  tensors below. It will be seen that these expressions can be very lengthy. The results for the simplest case, that of hydrostatic pressure, are presented in Sec. 4.5.

## 4.4.1 Cubic diamond

$$\begin{aligned}
\bar{E}_{11} &= E_{11}(1 + \eta_1 - \eta_2 - \eta_3) + E_{111}\eta_1 + E_{112}(\eta_2 + \eta_3) \\
\bar{E}_{22} &= E_{11}(1 - \eta_1 + \eta_2 - \eta_3) + E_{111}\eta_2 + E_{112}(\eta_1 + \eta_3) \\
\bar{E}_{33} &= E_{11}(1 - \eta_1 - \eta_2 + \eta_3) + E_{111}\eta_3 + E_{112}(\eta_1 + \eta_2) \\
\bar{E}_{12} &= (E_{11} + E_{126} + A_{14}F_{123})\eta_6 \\
\bar{E}_{13} &= (E_{11} + E_{126} + A_{14}F_{123})\eta_5 \\
\bar{E}_{23} &= (E_{11} + E_{126} + A_{14}F_{123})\eta_4.
\end{aligned} \tag{4.36}$$

## 4.4.2 Rhombohedral graphite

$$\begin{aligned}
\bar{E}_{11} &= E_{11}(1 + \eta_1 - \eta_2 - \eta_3) + E_{111}\eta_1 + E_{112}\eta_2 + E_{113}\eta_3 + E_{114}\eta_4 \\
&\quad + F_{112}A_{16}(\eta_1 - \eta_2) + F_{113}(A_{31}(\eta_1 + \eta_2) + A_{33}\eta_3) \\
\bar{E}_{12} &= \bar{E}_{21} = E_{11}\eta_6 + E_{114}\eta_5 + E_{126}\eta_6 + F_{112}A_{16}\eta_6 \\
\bar{E}_{13} &= \frac{1}{2}(E_{11} + E_{33})\eta_5 + E_{135}\eta_5 + E_{136}\eta_6 + F_{113}A_{16}\eta_6 \\
\bar{E}_{22} &= E_{11}(1 - \eta_1 + \eta_2 - \eta_3) + E_{111}\eta_2 + E_{112}\eta_1 + E_{113}\eta_3 - E_{114}\eta_4 \\
&\quad - F_{112}A_{16}(\eta_1 - \eta_2) + F_{113}(A_{31}(\eta_1 + \eta_2) + A_{33}\eta_3) \\
\bar{E}_{23} &= \frac{1}{2}(E_{11} + E_{33})\eta_4 + E_{135}\eta_4 + E_{136}(\eta_1 + \eta_2) + F_{113}A_{16}(\eta_1 - \eta_2) \\
\bar{E}_{31} &= \frac{1}{2}(E_{11} + E_{33})\eta_5 + E_{315}\eta_5 + E_{316}\eta_6 + F_{113}A_{16}\eta_6 \\
\bar{E}_{32} &= \frac{1}{2}(E_{11} + E_{33})\eta_4 + E_{315}\eta_4 + E_{316}(\eta_1 + \eta_2) + F_{113}A_{16}(\eta_1 - \eta_2) \\
\bar{E}_{33} &= E_{33}(1 - \eta_1 - \eta_2 + \eta_3) + E_{331}(\eta_1 + \eta_2) + E_{333}\eta_3 + F_{333}(A_{31}(\eta_1 + \eta_2) + A_{33}\eta_3).
\end{aligned} \tag{4.37}$$

## 4.4.3 Hexagonal diamond

$$\begin{aligned}
\bar{E}_{11}^{\lambda\mu} &= E_{11}^{\lambda\mu}(1 + \eta_1 - \eta_2 - \eta_3) + E_{111}^{\lambda\mu}\eta_1 + E_{112}^{\lambda\mu}\eta_2 + E_{113}^{\lambda\mu}\eta_3 + E_{114}^{\lambda\mu}\eta_4 \\
&\quad + F_{112}^{\lambda\mu\nu}A_{16}^\nu(\eta_1 - \eta_2) + F_{113}^{\lambda\mu\nu}(A_{31}^\nu(\eta_1 + \eta_2) + A_{33}^\nu\eta_3) \\
\bar{E}_{12}^{\lambda\mu} &= \bar{E}_{21}^{\lambda\mu} = E_{11}^{\lambda\mu}\eta_6 + E_{114}^{\lambda\mu}\eta_5 + E_{126}^{\lambda\mu}\eta_6 + F_{112}^{\lambda\mu\nu}A_{16}^\nu\eta_6 \\
\bar{E}_{13}^{\lambda\mu} &= \frac{1}{2}(E_{11}^{\lambda\mu} + E_{33}^{\lambda\mu})\eta_5 + E_{135}^{\lambda\mu}\eta_5 + E_{136}^{\lambda\mu}\eta_6 + F_{131}^{\lambda\mu\nu}A_{16}^\nu\eta_6 \\
\bar{E}_{22}^{\lambda\mu} &= E_{11}^{\lambda\mu}(1 - \eta_1 + \eta_2 - \eta_3) + E_{111}^{\lambda\mu}\eta_2 + E_{112}^{\lambda\mu}\eta_1 + E_{113}^{\lambda\mu}\eta_3 - E_{114}^{\lambda\mu}\eta_4 \\
&\quad - F_{112}^{\lambda\mu\nu}A_{16}^\nu(\eta_1 - \eta_2) + F_{113}^{\lambda\mu\nu}(A_{31}^\nu(\eta_1 + \eta_2) + A_{33}^\nu\eta_3) \\
\bar{E}_{23}^{\lambda\mu} &= \frac{1}{2}(E_{11}^{\lambda\mu} + E_{33}^{\lambda\mu})\eta_4 + E_{135}^{\lambda\mu}\eta_4 + E_{136}^{\lambda\mu}(\eta_1 + \eta_2) + F_{131}^{\lambda\mu\nu}A_{16}^\nu(\eta_1 - \eta_2) \\
\bar{E}_{31}^{\lambda\mu} &= \frac{1}{2}(E_{11}^{\lambda\mu} + E_{33}^{\lambda\mu})\eta_5 + E_{315}^{\lambda\mu}\eta_5 + E_{316}^{\lambda\mu}\eta_6 + F_{311}^{\lambda\mu\nu}A_{16}^\nu\eta_6 \\
\bar{E}_{32}^{\lambda\mu} &= \frac{1}{2}(E_{11}^{\lambda\mu} + E_{33}^{\lambda\mu})\eta_4 + E_{315}^{\lambda\mu}\eta_4 + E_{316}^{\lambda\mu}(\eta_1 + \eta_2) + F_{311}^{\lambda\mu\nu}A_{16}^\nu(\eta_1 - \eta_2) \\
\bar{E}_{33}^{\lambda\mu} &= E_{33}^{\lambda\mu}(1 - \eta_1 - \eta_2 + \eta_3) + E_{331}^{\lambda\mu}(\eta_1 + \eta_2) + E_{333}^{\lambda\mu}\eta_3 \\
&\quad + F_{333}^{\lambda\mu\nu}(A_{31}^\nu(\eta_1 + \eta_2) + A_{33}^\nu\eta_3).
\end{aligned} \tag{4.38}$$

#### 4.4.4 Hexagonal graphite

$$\begin{aligned}
\bar{E}_{11}^{\lambda\mu} &= E_{11}^{\lambda\mu}(1 + \eta_1 - \eta_2 - \eta_3) + E_{111}^{\lambda\mu}\eta_1 + E_{112}^{\lambda\mu}\eta_2 + E_{113}^{\lambda\mu}\eta_3 + F_{112}^{\lambda\mu\nu}A_{16}^{\nu}(\eta_1 - \eta_2) \\
\bar{E}_{12}^{\lambda\mu} &= \bar{E}_{21}^{\lambda\mu} = E_{11}^{\lambda\mu}\eta_6 + E_{126}^{\lambda\mu}\eta_6 + F_{112}^{\lambda\mu\nu}A_{16}^{\nu}\eta_6 \\
\bar{E}_{13}^{\lambda\mu} &= \frac{1}{2}(E_{11}^{\lambda\mu} + E_{33}^{\lambda\mu})\eta_5 + E_{135}^{\lambda\mu}\eta_5 \\
\bar{E}_{22}^{\lambda\mu} &= E_{11}^{\lambda\mu}(1 - \eta_1 + \eta_2 - \eta_3) + E_{111}^{\lambda\mu}\eta_2 + E_{112}^{\lambda\mu}\eta_1 + E_{113}^{\lambda\mu}\eta_3 - F_{112}^{\lambda\mu\nu}A_{16}^{\nu}(\eta_1 - \eta_2) \\
\bar{E}_{23}^{\lambda\mu} &= \frac{1}{2}(E_{11}^{\lambda\mu} + E_{33}^{\lambda\mu})\eta_4 + E_{135}^{\lambda\mu}\eta_4 \\
\bar{E}_{31}^{\lambda\mu} &= \frac{1}{2}(E_{11}^{\lambda\mu} + E_{33}^{\lambda\mu})\eta_5 + E_{315}^{\lambda\mu}\eta_5 \\
\bar{E}_{32}^{\lambda\mu} &= \frac{1}{2}(E_{11}^{\lambda\mu} + E_{33}^{\lambda\mu})\eta_4 + E_{315}^{\lambda\mu}\eta_4 \\
\bar{E}_{33}^{\lambda\mu} &= E_{33}^{\lambda\mu}(1 - \eta_1 - \eta_2 + \eta_3) + E_{331}^{\lambda\mu}(\eta_1 + \eta_2) + E_{333}^{\lambda\mu}\eta_3.
\end{aligned} \tag{4.39}$$

### 4.5 The pressure dependence of the optic mode frequencies

Under hydrostatic pressure  $\eta_4 = \eta_5 = \eta_6 = 0$ ,  $\eta_1 = \eta_2 = \eta_3 = -kp$  for cD and  $\eta_1 = \eta_2 = -k_a p$ ,  $\eta_3 = -k_c p$  in the remaining three cases, where  $k$ ,  $k_a$  and  $k_c$  are linear compressibilities. These strains are inserted into the effective constants above, the effective constants into the appropriate eigenvalue equations (again with the appropriate density, which is also pressure-dependent) and the latter differentiated with respect to  $p$ . No degeneracies are lifted by hydrostatic pressure.

Some composite constants are defined below in order to shorten the lengths of some of the expressions in  $hG$  and  $hD$ .

#### 4.5.1 Cubic diamond

$$\frac{d\omega_R^2(T_{2g})}{dp} = -\frac{4k}{\rho_0} (2E_{11} + E_{111} + 2E_{112}). \tag{4.40}$$

#### 4.5.2 Rhombohedral graphite

$$\begin{aligned}
\frac{d\omega_R^2(E_g)}{dp} &= -\frac{4}{\rho_0} (k_a(2E_{11} + E_{111} + E_{112} + 2F_{113}A_{31}) + k_c(E_{113} + F_{113}A_{33})) \\
\frac{d\omega_R^2(A_{1g})}{dp} &= -\frac{4}{\rho_0} (2k_a(E_{331} + F_{333}A_{31}) + k_c(2E_{33} + E_{333} + F_{333}A_{33})).
\end{aligned} \tag{4.41}$$

#### 4.5.3 Hexagonal diamond

The composite constants are

$$\begin{aligned}
E_{ii}^{aa} &\equiv E_{ii}^{11} - E_{ii}^{12} + E_{ii}^{13} \\
E_{ii}^{bb} &\equiv E_{ii}^{11} - E_{ii}^{13}
\end{aligned}$$

$$\begin{aligned} F_{i3}^{aa\nu} &\equiv F_{i3}^{11\nu} - F_{i3}^{12\nu} + F_{i3}^{13\nu} \\ F_{i3}^{bb\nu} &\equiv F_{i3}^{11\nu} - F_{i3}^{13\nu} \end{aligned}$$

and the pressure derivatives are

$$\begin{aligned} \frac{d\omega^2(E_{2u})}{dp} &= -\frac{8}{\rho_0} (k_a(2E_{11}^{12} + E_{111}^{12} + E_{112}^{12} + 2F_{113}^{12\nu} A_{31}^\nu) + k_c(E_{113}^{12} + F_{113}^{12\nu} A_{33}^\nu)) \\ \frac{d\omega_R^2(E_{1g})}{dp} &= -\frac{8}{\rho_0} (k_a(2E_{11}^{aa} + E_{111}^{aa} + E_{112}^{aa} + 2F_{113}^{aa\nu} A_{31}^\nu) + k_c(E_{113}^{aa} + F_{113}^{aa\nu} A_{33}^\nu)) \\ \frac{d\omega_R^2(E_{2g})}{dp} &= -\frac{8}{\rho_0} (k_a(2E_{11}^{bb} + E_{111}^{bb} + E_{112}^{bb} + 2F_{113}^{bb\nu} A_{31}^\nu) + k_c(E_{113}^{bb} + F_{113}^{bb\nu} A_{33}^\nu)) \end{aligned} \quad (4.42)$$

and

$$\begin{aligned} \frac{d\omega^2(B_{1u})}{dp} &= -\frac{8}{\rho_0} (2k_a(E_{331}^{12} + F_{333}^{12\nu} A_{31}^\nu) + k_c(2E_{33}^{12} + E_{333}^{12} + F_{333}^{12\nu} A_{33}^\nu)) \\ \frac{d\omega_R^2(A_{1g})}{dp} &= -\frac{8}{\rho_0} (2k_a(E_{331}^{aa} + F_{333}^{aa\nu} A_{31}^\nu) + k_c(2E_{33}^{aa} + E_{333}^{aa} + F_{333}^{aa\nu} A_{33}^\nu)) \\ \frac{d\omega^2(B_{2g})}{dp} &= -\frac{8}{\rho_0} (2k_a(E_{331}^{bb} + F_{333}^{bb\nu} A_{31}^\nu) + k_c(2E_{33}^{bb} + E_{333}^{bb} + A_{33}^\nu F_{333}^{bb\nu})). \end{aligned} \quad (4.43)$$

#### 4.5.4 Hexagonal graphite

The composite constant is

$$E_{ii}^{cc} \equiv E_{ii}^{11} - E_{ii}^{12} + E_{ii}^{33}$$

and the pressure derivatives are

$$\begin{aligned} \frac{d\omega_I^2(E_{1u})}{dp} &= -\frac{8}{\rho_0} (k_a(2E_{11}^{12} + E_{111}^{12} + E_{112}^{12}) + k_c E_{113}^{12}) \\ \frac{d\omega_R^2(E_{2g2})}{dp} &= -\frac{4}{\rho_0} \left( k_a(2(E_{11}^{cc} + E_{11}^\dagger) + E_{111}^{cc} + E_{112}^{cc}) + k_c E_{113}^{cc} + \frac{d\bar{E}_{11}^\dagger}{dp} \right) \\ \frac{d\omega_R^2(E_{2g1})}{dp} &= -\frac{4}{\rho_0} \left( k_a(2(E_{11}^{cc} - E_{11}^\dagger) + E_{111}^{cc} + E_{112}^{cc}) + k_c E_{113}^{cc} - \frac{d\bar{E}_{11}^\dagger}{dp} \right) \end{aligned} \quad (4.44)$$

where

$$\begin{aligned} \frac{d\bar{E}_{11}^\dagger}{dp} &= \frac{E_{11}^{12} - 2E_{11}^{13}}{E_{11}^\dagger} (k_a(E_{111}^{12} - 2E_{111}^{13} + E_{112}^{12} - 2E_{112}^{13}) + k_c(E_{113}^{12} - 2E_{113}^{13})) \\ &\quad + \frac{E_{11}^{11} - E_{11}^{33}}{E_{11}^\dagger} (k_a(E_{111}^{11} - E_{111}^{33} + E_{112}^{11} - E_{112}^{33}) + k_c(E_{113}^{11} - E_{113}^{33})) \end{aligned}$$

and

$$\begin{aligned}
\frac{d\omega_I^2(A_{2u})}{dp} &= -\frac{8}{\rho_0} (2k_a E_{331}^{12} + k_c (2E_{33}^{12} + E_{333}^{12})) \\
\frac{d\omega_R^2(B_{1g2})}{dp} &= -\frac{4}{\rho_0} \left( 2k_a E_{331}^{cc} + k_c (2(E_{33}^{cc} + E_{33}^\dagger) + E_{333}^{cc}) + \frac{d\bar{E}_{33}^\dagger}{dp} \right) \\
\frac{d\omega_R^2(B_{1g1})}{dp} &= -\frac{4}{\rho_0} \left( 2k_a E_{331}^{cc} + k_c (2(E_{33}^{cc} - E_{33}^\dagger) + E_{333}^{cc}) - \frac{d\bar{E}_{33}^\dagger}{dp} \right)
\end{aligned} \tag{4.45}$$

where

$$\begin{aligned}
\frac{d\bar{E}_{33}^\dagger}{dp} &= \frac{E_{33}^{12} - 2E_{33}^{13}}{E_{33}^\dagger} (2k_a (E_{331}^{12} - 2E_{331}^{13}) + k_c (E_{333}^{12} - 2E_{333}^{13})) \\
&\quad + \frac{E_{33}^{11} - E_{33}^{33}}{E_{33}^\dagger} (2k_a (E_{331}^{11} - E_{331}^{33}) + k_c (E_{333}^{11} - E_{333}^{33})).
\end{aligned}$$

## 4.6 Summary

The different microscopic tensors that arise in connection with the elasticity and with the frequencies and eigenvectors of the zone-centre optic modes in four carbon allotropes have been analysed in detail. Expressions for the internal strain tensor components have also been derived and may be seen to relate to the frequencies of the Raman-active modes. This illustrates a general symmetry requirement, first given by Miller and Axe, in [12], that only Raman-active modes contribute to the internal strain part of the elastic constants. These results are carried forward to the next Chapter where the macroscopic elasticity of the four allotropes is subjected to similar detailed treatment.

Finally the effective inner elastic constants under arbitrary strain have been determined and used to obtain the pressure derivatives of the optic mode frequencies.

## References

- [1] R. H. Baughman, H. Eckhardt and M. Kertesz, *J. Chem. Phys.* **87**, 6687 (1987)
- [2] K. Brugger, *Phys. Rev.* **133**, A1611 (1964)
- [3] F. Cerdeira, C. J. Buchenauer, F. H. Pollak and M. Cardona, *Phys. Rev.* **B5**, 580 (1972)
- [4] C. S. G. Cousins, *J. Phys. C:Solid St. Phys.* **15**, 1857 (1982)
- [5] C. S. G. Cousins, L. Gerward, J. Staun Olsen and B. J. Sheldon, *J.Phys: Condens.Matter* **1**, 4511 (1989)
- [6] S. Fahy, S. G. Louie and M. L. Cohen, *Phys. Rev.* **B34**, 1191 (1986)

- 
- [7] *International Tables for Crystallography*, Vol.A (Kluwer Academic Publishers, Dordrecht, 1990)
- [8] G. Jungnickel, P. K. Sitch, Th. Frauenheim, B. R. Eggen, M. I. Heggie, C. D. Latham and C. S. G. Cousins, *Phys. Rev. B* **57**, R661 (1998)
- [9] M. Kertesz and R. Hoffmann, *J. Solid State Chem.* **54**, 313 (1984)
- [10] A. A. Maradudin, *Phys. Rev. B* **13**, 658 (1976)
- [11] J. W. Martin, *J. Phys. C:Solid St. Phys.* **8**, 2869 (1975)
- [12] P. B. Miller and J. D. Axe, *Phys. Rev.* **163**, 924 (1967)
- [13] J. F. Nye, *Physical Properties of Crystals*, (Oxford: University Press, 1957)
- [14] A. K. Sood, E. Anastassakis and M. Cardona, *Phys. Stat. Sol. (b)* **129**, 505 (1985)
- [15] M. A. Tamor and K. C. Hass, *J. Mater. Res.* **5**, 2273 (1990)
- [16] D. C. Wallace in *Solid State Physics* edited by H. Ehrenreich, F. Seitz and D. Turnbull (Academic Press, New York and London, 1970), Volume 25

## Chapter 5

### Total elastic constants, compressibilities and pressure derivatives

#### 5.1 Anatomy of the macroscopic constants

The treatment of crystal equilibrium presented in Chapter 1 leads to expressions for the total elastic constants in terms of partial and inner elastic constants, and internal strain tensors.

Apart from  $cD$ , treated in [2], there has been no previous analysis of the composition of the elastic constants of any of the other allotropes, all of which have a rich complement of inner elastic constants.

Some constants may be selected as independent and these constitute the set that must be evaluated in order to get a full description of the elasticity. They are presented for  $hD$  and  $hG$  in Table 5.1, and for  $cD$  and  $rG$  in Table 5.2. Also shown in the latter are the elastic constants of  $cD$  transformed to a quasi-rhombohedral system of axes, a form suitable for considering the  $cD$  to  $rG$  solid-state transition.

Table 5.1: The symmetry of the elastic constants of  $hD$  and  $hG$ . The odd columns contain the components of each constant that have been selected as independent and the even columns contain the relationships between them and the remaining non-zero components ones.

$C_1$	$C_2 = C_1$	$C_{111}$	$C_{112} = C_{111} - C_{166} - 3C_{266}$
$C_3$		$C_{113}$	$C_{122} = C_{111} - 2C_{166} - 2C_{266}$
		$C_{133}$	$C_{222} = C_{111} + C_{166} - C_{266}$
$C_{11}$	$C_{22} = C_{11}$	$C_{333}$	$C_{123} = C_{113} - 2C_{366}$
$C_{12}$	$C_{23} = C_{13}$	$C_{144}$	$C_{223} = C_{113}$
$C_{13}$	$C_{55} = C_{44}$	$C_{244}$	$C_{233} = C_{133}$
$C_{33}$	$C_{66} = \frac{1}{2}(C_{11} - C_{12})$	$C_{344}$	$C_{155} = C_{244}$
$C_{44}$		$C_{166}$	$C_{255} = C_{144}$
		$C_{266}$	$C_{355} = C_{344}$
		$C_{366}$	$C_{456} = \frac{1}{2}(C_{244} - C_{144})$

Table 5.2: Top: The symmetry of the elastic constants of  $cD$ . Odd columns show the components selected as independent, even columns the relationships between them and the remaining non-zero components. Bottom: The symmetry of the elastic constants of  $rG$ . First two columns as for  $cD$ . The third column shows the elastic constants of quasi- $rD$  in terms of those of  $cD$ .

		$cD$
$C_1$	$C_2 = C_3 = C_1$	$C_{111}$ $C_{222} = C_{333} = C_{111}$
		$C_{112}$ $C_{113} = C_{122} = C_{133} = C_{223} = C_{233} = C_{112}$
$C_{11}$	$C_{22} = C_{33} = C_{11}$	$C_{123}$
$C_{12}$	$C_{13} = C_{23} = C_{12}$	$C_{144}$ $C_{255} = C_{366} = C_{144}$
$C_{44}$	$C_{55} = C_{66} = C_{44}$	$C_{155}$ $C_{166} = C_{244} = C_{266} = C_{344} = C_{355} = C_{155}$
		$C_{456}$
		$rG$
$C_1$	$C_2 = C_1$	$C_1$
$C_3$		$C_1$
$C_{11}$	$C_{22} = C_{11}$	$(C_{11} + C_{12} + 2C_{44})/2$
$C_{12}$	$C_{66} = (C_{11} - C_{12})/2$	$(C_{11} + 5C_{12} - 2C_{44})/6$
$C_{13}$	$C_{23} = C_{13}$	$(C_{11} + 2C_{12} - 2C_{44})/3$
$C_{33}$		$(C_{11} + 2C_{12} + 4C_{44})/3$
$C_{44}$	$C_{55} = C_{44}$	$(C_{11} - C_{12} + C_{44})/3$
$C_{14}$	$C_{24} - C_{56} = -C_{14}$	$(C_{11} - C_{12} - 2C_{44})/3\sqrt{2}$
$C_{111}$	$C_{112} = C_{111} - C_{166} - 3C_{266}$	$(C_{111} + 3C_{112} + 12C_{155})/4$
$C_{113}$	$C_{122} = C_{111} - 2C_{166} - 2C_{266}$	$(C_{111} + 4C_{112} + C_{123} + 2C_{144} - 4C_{155})/6$
$C_{133}$	$C_{222} = C_{111} + C_{166} - C_{266}$	$(C_{111} - 3C_{112} + 2C_{123} - 8C_{456})/9$
$C_{333}$	$C_{123} = C_{113} - 2C_{366}$	$(C_{111} + 6C_{112} + 2C_{123} + 12C_{144} + 24C_{155} + 16C_{456})/9$
$C_{144}$	$C_{223} = C_{113}$	$(C_{111} + 3C_{112} - 4C_{123} + 9C_{144} - 3C_{155} - 2C_{456})/18$
$C_{244}$	$C_{233} = C_{133}$	$(C_{111} - C_{112} + C_{144} + C_{155} + 2C_{456})/6$
$C_{344}$	$C_{155} = C_{244}$	$(C_{111} - C_{123} - 3C_{144} + 6C_{155} - 2C_{456})/9$
$C_{166}$	$C_{255} = C_{144}$	$(C_{111} - C_{112} + 4C_{144} + 4C_{155} + 8C_{456})/12$
$C_{266}$	$C_{355} = C_{344}$	$(C_{111} + 3C_{112} - 4C_{123} - 12C_{144} + 36C_{155} - 8C_{456})/36$
$C_{366}$	$C_{456} = (C_{244} - C_{144})/2$	$(C_{111} - C_{123} + 12C_{144} - 8C_{456})/18$
$C_{114}$	$C_{224} = -(C_{114} + 2C_{124})$	$(C_{111} + C_{112} - 2C_{123} - 4C_{144} - 4C_{155})/6\sqrt{2}$
$C_{124}$	$C_{156} = (C_{114} + 3C_{124})/2$	$(C_{111} - 3C_{112} + 2C_{123} - 8C_{456})/18\sqrt{2}$
$C_{134}$	$C_{256} = (C_{114} - C_{124})/2$	$(C_{111} - C_{123} - 6C_{155} + 4C_{456})/9\sqrt{2}$
$C_{444}$	$C_{234} = -C_{356} = -C_{134}$	$-(C_{111} - 3C_{112} + 2C_{123} + 3C_{144} - 3C_{155} - 2C_{456})/9\sqrt{2}$
	$C_{446} = C_{124}$	
	$C_{455} = -C_{444}$	
		quasi- $rD$

The final expressions for  $C_{IJ}$  and  $C_{IJK}$  as sums of partial and inner elastic constants were given in Chapter 1. They are recapitulated here with extra definitions that simplify the presentation for the individual allotropes:

$$\begin{aligned} C_{IJ} &= C_{IJ}^0 - A_{iI}^\lambda A_{jJ}^\mu E_{ij}^{\lambda\mu} \\ &= C_{IJ}^0 - \Delta_{IJ} \end{aligned} \quad (5.1)$$

and

$$\begin{aligned} C_{IJK} &= C_{IJK}^0 + A_{iI}^\lambda D_{iJK}^\lambda + A_{iJ}^\lambda D_{iIK}^\lambda + A_{iK}^\lambda D_{iIJ}^\lambda \\ &\quad + A_{iI}^\lambda A_{jJ}^\mu E_{ijK}^{\lambda\mu} + A_{iI}^\lambda A_{jK}^\mu E_{ijJ}^{\lambda\mu} + A_{iJ}^\lambda A_{jK}^\mu E_{ijI}^{\lambda\mu} \\ &\quad + A_{iI}^\lambda A_{jJ}^\mu A_{kK}^\nu F_{ijk}^{\lambda\mu\nu} \\ &= C_{IJK}^0 + \Delta_{IJK}. \end{aligned} \quad (5.2)$$

The expressions for the non-zero components  $\Delta_{IJ}$  and  $\Delta_{IJK}$  for the different allotropes are obtained by taking appropriate sets of independent non-zero inner elastic constants and internal strain tensor components from Tables 4.4, 4.6 and 4.7 in Chapter 1.

The considerable differences between the two hexagonal allotropes is a direct consequence of the different site symmetries in the two structures: the two distinct pairs of equivalent sites in  $hG$  each have  $\bar{6}m2$  symmetry whereas the four equivalent sites in  $hD$  have the lower  $3m$  symmetry.

### 5.1.1 Cubic diamond

At the second order

$$\Delta_{44} = (A_{14})^2 E_{11} \quad (5.3)$$

and at the third

$$\begin{aligned} \Delta_{144} &= 2A_{14}D_{114} + (A_{14})^2 E_{111} \\ \Delta_{155} &= 2A_{14}D_{124} + (A_{14})^2 E_{112} \\ \Delta_{456} &= 3A_{14}D_{156} + 3(A_{14})^2 E_{126} + (A_{14})^3 F_{123}. \end{aligned} \quad (5.4)$$

### 5.1.2 Rhombohedral graphite

At the second order

$$\begin{aligned} \Delta_{11} &= (A_{31})^2 E_{33} + (A_{16})^2 E_{11} \\ \Delta_{12} &= (A_{31})^2 E_{33} - (A_{16})^2 E_{11} \\ \Delta_{13} &= A_{31} A_{33} E_{33} \\ \Delta_{33} &= (A_{33})^2 E_{33} \\ \Delta_{44} &= (A_{15})^2 E_{11} \\ \Delta_{14} &= A_{15} A_{16} E_{11}. \end{aligned} \quad (5.5)$$

At the third order

$$\begin{aligned}
\Delta_{111} &= 3A_{16}D_{211} + 3A_{31}D_{311} \\
&\quad + 3(A_{16})^2E_{112} + 6A_{16}A_{31}E_{136} + 3(A_{31})^2E_{331} \\
&\quad - (A_{16})^3F_{112} + 3(A_{16})^2A_{15}F_{113} + (A_{31})^3F_{333} \\
\Delta_{113} &= 2A_{16}D_{136} + A_{33}D_{311} + 2A_{31}D_{313} \\
&\quad + (A_{16})^2E_{113} + 2A_{16}A_{33}E_{136} + 2A_{31}A_{33}E_{331} \\
&\quad + (A_{31})^2E_{333} + (A_{16})^2A_{33}F_{113} + (A_{31})^2A_{33}F_{333} \\
\Delta_{133} &= 2A_{33}D_{313} + A_{31}D_{333} + (A_{33})^2E_{331} + 2A_{31}A_{33}E_{333} + A_{31}(A_{33})^2F_{333} \\
\Delta_{333} &= 3A_{33}D_{333} + 3(A_{33})^2E_{333} + (A_{33})^3F_{333} \\
\Delta_{144} &= -A_{16}D_{145} + 2A_{15}D_{125} + A_{31}D_{344} + 2A_{31}A_{15}E_{315} + (A_{15})^2E_{112} \\
&\quad - A_{16}(A_{15})^2F_{112} + A_{31}(A_{15})^2F_{113} \\
\Delta_{244} &= A_{16}D_{145} + 2A_{15}D_{115} + A_{31}D_{344} + 2A_{31}A_{15}E_{315} + (A_{15})^2E_{111} \\
&\quad + A_{16}(A_{15})^2F_{112} + A_{31}(A_{15})^2F_{113} \\
\Delta_{344} &= 2A_{15}D_{135} + A_{33}D_{344} + 2A_{33}A_{15}E_{315} + (A_{15})^2E_{113} + A_{33}(A_{15})^2F_{113} \quad (5.6) \\
\Delta_{166} &= -A_{16}(D_{211} + 2D_{222}) + \frac{1}{2}A_{31}(D_{311} - D_{312}) \\
&\quad + (A_{16})^2(2E_{111} - E_{112}) + 2A_{31}A_{16}E_{136} \\
&\quad + (A_{16})^3F_{112} + A_{31}(A_{16})^2F_{113} \\
\Delta_{266} &= A_{16}(2D_{211} + D_{222}) + \frac{1}{2}A_{31}(D_{311} - D_{312}) \\
&\quad - (A_{16})^2(E_{111} - 2E_{112}) + 2A_{31}A_{16}E_{136} \\
&\quad - (A_{16})^3F_{112} + A_{31}(A_{16})^2F_{113} \\
\Delta_{366} &= 2A_{16}D_{136} + \frac{1}{2}A_{33}(D_{311} - D_{312}) \\
&\quad + (A_{16})^2E_{113} + 2A_{33}A_{16}E_{136} + A_{33}(A_{16})^2F_{113} \\
\Delta_{114} &= 2A_{16}D_{125} + A_{15}D_{211} \\
&\quad + 2A_{16}A_{15}E_{112} + 2A_{31}A_{15}E_{136} \\
&\quad - (A_{16})^2A_{15}F_{112} + 2A_{16}A_{15}A_{31}F_{113} \\
\Delta_{124} &= -A_{16}D_{125} + A_{15}D_{212} + A_{31}D_{314} \\
&\quad + A_{16}A_{15}(E_{111} - E_{112}) + (A_{16})^2A_{15}F_{112} \\
\Delta_{134} &= A_{16}D_{135} + A_{15}D_{136} + A_{33}D_{314} \\
&\quad + A_{16}A_{15}(E_{113} + E_{135}) + A_{33}A_{15}E_{136} + A_{16}A_{15}A_{33}F_{113} \\
\Delta_{444} &= -3A_{15}D_{145} - (A_{15})^3F_{112}
\end{aligned}$$

### 5.1.3 Hexagonal diamond

In Chapter 4 it was useful to define some composite constants in order to simplify expressions for the pressure derivatives of the optic mode frequencies. A similar need arises here. The composite constants are

$$\begin{aligned}
E_{ij}^{aa} &\equiv E_{ij}^{11} - E_{ij}^{12} + E_{ij}^{13} \\
E_{ij}^{bb} &\equiv E_{ij}^{11} - E_{ij}^{13} \\
F_{112}^{11a} &\equiv F_{112}^{111} - 3F_{112}^{112} + 3F_{112}^{113} \\
F_{113}^{1bb} &\equiv F_{113}^{111} - F_{113}^{113} - 2F_{113}^{121} + 2F_{113}^{123} + 2F_{113}^{131} + F_{113}^{221} \\
F_{113}^{1cc} &\equiv F_{113}^{111} - 2F_{113}^{131} - F_{113}^{113}
\end{aligned}$$

At the second order

$$\begin{aligned}
\Delta_{11} &= 2(A_{31}^1)^2 E_{33}^{bb} + 2(A_{16}^1)^2 E_{11}^{aa} \\
\Delta_{12} &= 2(A_{31}^1)^2 E_{33}^{bb} - 2(A_{16}^1)^2 E_{11}^{aa} \\
\Delta_{13} &= 2A_{31}^1 A_{33}^1 E_{33}^{bb} \\
\Delta_{33} &= 2(A_{33}^1)^2 E_{33}^{bb} \\
\Delta_{44} &= 2(A_{15}^1)^2 E_{11}^{bb}.
\end{aligned} \tag{5.7}$$

At the third order

$$\begin{aligned}
\Delta_{111} &= 6A_{16}^1 D_{211}^1 + 6A_{31}^1 D_{311}^1 + 6(A_{16}^1)^2 E_{112}^{aa} + 12A_{16}^1 A_{31}^1 E_{136}^{bb} \\
&\quad + 6(A_{31}^1)^2 E_{331}^{bb} - 2(A_{16}^1)^3 F_{112}^{11a} + 6(A_{16}^1)^2 A_{31}^1 F_{113}^{1bb} + 2(A_{31}^1)^3 (F_{333}^{111} - 3F_{333}^{113}) \\
\Delta_{113} &= 4A_{16}^1 D_{136}^1 + 2A_{33}^1 D_{311}^1 + 4A_{31}^1 D_{313}^1 + 2(A_{16}^1)^2 E_{113}^{aa} + 4A_{16}^1 A_{33}^1 E_{136}^{bb} + 4A_{31}^1 A_{33}^1 E_{331}^{bb} \\
&\quad + 2(A_{31}^1)^2 E_{333}^{bb} + 2(A_{16}^1)^2 A_{33}^1 F_{113}^{1bb} + 2(A_{31}^1)^2 A_{33}^1 (F_{333}^{111} - 3F_{333}^{113}) \\
\Delta_{133} &= 4A_{33}^1 D_{313}^1 + 2A_{31}^1 D_{333}^1 + 2(A_{33}^1)^2 E_{331}^{bb} + 4A_{31}^1 A_{33}^1 E_{333}^{bb} + 2A_{31}^1 (A_{33}^1)^2 (F_{333}^{111} - 3F_{333}^{113}) \\
\Delta_{333} &= 6A_{33}^1 D_{333}^1 + 6(A_{33}^1)^2 E_{333}^{bb} + 2(A_{33}^1)^3 (F_{333}^{111} - 3F_{333}^{113}) \\
\Delta_{144} &= -2A_{16}^1 D_{145}^1 + 4A_{15}^1 D_{125}^1 + 2A_{31}^1 D_{344}^1 + 4A_{31}^1 A_{15}^1 E_{315}^{bb} + 2(A_{15}^1)^2 E_{112}^{bb} \\
&\quad - 2A_{16}^1 (A_{15}^1)^2 (F_{112}^{111} - F_{112}^{113}) + 2A_{31}^1 (A_{15}^1)^2 F_{113}^{1cc} \\
\Delta_{244} &= 2A_{16}^1 D_{145}^1 + 4A_{15}^1 D_{115}^1 + 2A_{31}^1 D_{344}^1 + 4A_{31}^1 A_{15}^1 E_{315}^{bb} + 2(A_{15}^1)^2 E_{111}^{bb} \\
&\quad + 2A_{16}^1 (A_{15}^1)^2 (F_{112}^{111} - F_{112}^{113}) + 2A_{31}^1 (A_{15}^1)^2 F_{113}^{1cc} \\
\Delta_{344} &= 4A_{15}^1 D_{135}^1 + 2A_{33}^1 D_{344}^1 + 4A_{33}^1 A_{15}^1 E_{315}^{bb} + 2(A_{15}^1)^2 E_{113}^{bb} + 2A_{33}^1 (A_{15}^1)^2 F_{113}^{1cc} \\
\Delta_{166} &= -2A_{16}^1 (D_{211}^1 + 2D_{222}^1) + A_{31}^1 (D_{311}^1 - D_{312}^1) + 2(A_{16}^1)^2 (2E_{111}^{aa} - E_{112}^{aa}) \\
&\quad + 4A_{31}^1 A_{16}^1 E_{136}^{bb} + 2(A_{16}^1)^3 F_{112}^{11a} + 2A_{31}^1 (A_{16}^1)^2 F_{113}^{1bb} \\
\Delta_{266} &= 2A_{16}^1 (2D_{211}^1 + D_{222}^1) + A_{31}^1 (D_{311}^1 - D_{312}^1) - 2(A_{16}^1)^2 (E_{111}^{aa} - 2E_{112}^{aa}) \\
&\quad + 4A_{31}^1 A_{16}^1 E_{136}^{bb} - 2(A_{16}^1)^3 F_{112}^{11a} + 2A_{31}^1 (A_{16}^1)^2 F_{113}^{1bb} \\
\Delta_{366} &= 4A_{16}^1 D_{136}^1 + A_{33}^1 (D_{311}^1 - D_{312}^1) + 2(A_{16}^1)^2 E_{113}^{aa} + 4A_{33}^1 A_{16}^1 E_{136}^{bb} + 2A_{33}^1 (A_{16}^1)^2 F_{113}^{1bb}
\end{aligned} \tag{5.8}$$

### 5.1.4 Hexagonal graphite

The following composite constants are useful:

$$\begin{aligned} E_{11}^{1c} &\equiv E_{11}^{11} - \frac{1}{2}E_{11}^{12} \\ E_{11}^{3c} &\equiv E_{11}^{33} - \frac{1}{2}E_{11}^{12} \\ F_{112}^{1cc} &\equiv \frac{1}{4}F_{112}^{112} - F_{112}^{123} + F_{112}^{133} \end{aligned}$$

At the second order, after using  $E_{11}^{22} = 2E_{11}^{12} = 2E_{11}^{23}$  and  $A_{16}^2 = -\frac{1}{2}(A_{16}^1 + A_{16}^3)$  (see Chapter 4), we obtain

$$\begin{aligned} \Delta_{11} &= (A_{16}^1)^2 E_{11}^{1c} + (A_{16}^3)^2 E_{11}^{3c} \\ &\quad + 2A_{16}^1 A_{16}^3 (E_{11}^{13} - \frac{1}{2}E_{11}^{12}) \\ \Delta_{12} &= -\Delta_{11} \end{aligned} \quad (5.9)$$

At the third order

$$\begin{aligned} \Delta_{111} &= 3A_{16}^1 D_{211}^1 + 3A_{16}^3 D_{211}^3 + 3(A_{16}^1)^2 E_{112}^{1c} + 3(A_{16}^3)^2 E_{112}^{3c} + 6A_{16}^1 A_{16}^3 (E_{112}^{13} - \frac{1}{2}E_{112}^{12}) \\ &\quad - (A_{16}^1)^3 (F_{112}^{111} - \frac{3}{4}F_{112}^{112}) - \frac{3}{4}(A_{16}^1)^2 A_{16}^3 F_{112}^{223} - 3A_{16}^1 (A_{16}^3)^2 F_{112}^{1cc} - (A_{16}^3)^3 (F_{112}^{333} - \frac{3}{4}F_{112}^{223}) \\ \Delta_{113} &= 2A_{16}^1 D_{136}^1 + 2A_{16}^3 D_{136}^3 + (A_{16}^1)^2 E_{113}^{1c} + (A_{16}^3)^2 E_{113}^{3c} + 2A_{16}^1 A_{16}^3 (E_{113}^{13} - \frac{1}{2}E_{113}^{12}) \\ \Delta_{144} &= -A_{16}^1 D_{145}^1 - A_{16}^3 D_{145}^3 \\ \Delta_{244} &= -\Delta_{144} \\ \Delta_{166} &= -A_{16}^1 (D_{211}^1 + 2D_{222}^1) - A_{16}^3 (D_{211}^3 + 2D_{222}^3) + (A_{16}^1)^2 (2E_{111}^{1c} - E_{112}^{1c}) \\ &\quad + (A_{16}^3)^2 (2E_{111}^{3c} - E_{112}^{3c}) + 2A_{16}^1 A_{16}^3 (2E_{111}^{13} - E_{112}^{13} - E_{111}^{12} + \frac{1}{2}E_{112}^{12}) \\ &\quad + (A_{16}^1)^3 (F_{112}^{111} - \frac{3}{4}F_{112}^{112}) + (A_{16}^3)^3 (F_{112}^{333} - \frac{3}{4}F_{112}^{223}) + \frac{3}{4}(A_{16}^1)^2 A_{16}^3 F_{112}^{223} + 3A_{16}^1 (A_{16}^3)^2 F_{112}^{1cc} \\ \Delta_{266} &= A_{16}^1 (2D_{211}^1 + D_{222}^1) + A_{16}^3 (2D_{211}^3 + D_{222}^3) + (A_{16}^1)^2 (2E_{112}^{1c} - E_{111}^{1c}) \\ &\quad + (A_{16}^3)^2 (2E_{112}^{3c} - E_{111}^{3c}) + 2A_{16}^1 A_{16}^3 (2E_{112}^{13} - E_{111}^{13} - E_{112}^{12} + \frac{1}{2}E_{111}^{12}) \\ &\quad - (A_{16}^1)^3 (F_{112}^{111} - \frac{3}{4}F_{112}^{112}) - (A_{16}^3)^3 (F_{112}^{333} - \frac{3}{4}F_{112}^{223}) - \frac{3}{4}(A_{16}^1)^2 A_{16}^3 F_{112}^{223} - 3A_{16}^1 (A_{16}^3)^2 F_{112}^{1cc} \\ \Delta_{366} &= \Delta_{113} \end{aligned} \quad (5.10)$$

## 5.2 Compliances and compressibilities

Measurements of lattice parameter and volume change under pressure by means of X-ray or neutron diffraction may be used to extract elasticity information from crystals too small to subject to more conventional techniques, such as ultrasonics. The primary quantities obtained are the harmonic and anharmonic linear compressibilities,  $k_I$  and  $K_I$ , defined implicitly in the extended form of Hooke's law (in which  $\delta_J = 1$  if  $J = 1, 2$  or  $3$  and is zero otherwise):

$$\begin{aligned} \eta_I &= -pS_{IJ}\delta_J + \frac{1}{2}p^2 S_{IJK}\delta_J\delta_K \\ &= -k_I p + \frac{1}{2}K_I p^2. \end{aligned} \quad (5.11)$$

The compliances,  $S_{IJ}$  and  $S_{IJK}$ , have the same patterns of independent components as the  $C_{IJ}$  and  $C_{IJK}$  and can thus be read from Tables 5.1 and 5.2. The relations of dependence however are slightly different: each occurrence of a subscript 4, 5 or 6 must be associated with a factor of 2 (see [4]), thus for instance

$$C_{222} = C_{111} + C_{166} - C_{266}$$

has the analogue

$$S_{222} = S_{111} + 4S_{166} - 4S_{266}.$$

### 5.2.1 Cubic diamond

When  $\eta_1 = \eta_2 = \eta_3$  we have (dropping subscripts)

$$k = S_{11} + 2S_{12} \quad (5.12)$$

and

$$K = S_{111} + 6S_{112} + S_{123}. \quad (5.13)$$

On setting  $2\eta_1 = 2\eta_2 = 2\eta_3 = \Delta a^2/a_0^2$  we obtain

$$\Delta a/a_0 = -kp + \frac{1}{2}(K - k^2)p^2 \quad (5.14)$$

for the change in lattice parameter.

The exact expression for the volume  $V$  of a finitely strained crystal is

$$\left(\frac{V}{V_0}\right)^2 = \det(I + 2\eta) \quad (5.15)$$

and leads to volume change given by

$$\frac{\Delta V}{V_0} = -3kp + \frac{3}{2}(K + k^2)p^2. \quad (5.16)$$

### 5.2.2 Hexagonal diamond, hexagonal graphite and rhombohedral graphite

For the axial allotropes, in which  $2\eta_1 = 2\eta_2 = \Delta a^2/a_0^2$  and  $2\eta_3 = \Delta c^2/c_0^2$ , there are two compressibilities of each kind:

$$\begin{aligned} k_a &= S_{11} + S_{12} + S_{13} \\ k_c &= 2S_{13} + S_{33} \\ K_a &= S_{111} + 2S_{112} + 2S_{113} + S_{122} + 2S_{123} + S_{133} \\ K_c &= 2S_{113} + 2S_{123} + 4S_{133} + S_{333}. \end{aligned} \quad (5.17)$$

The lattice parameters change as

$$\begin{aligned}\Delta a/a_0 &= -k_a p + \frac{1}{2}(K_a - k_a^2)p^2 \\ \Delta c/c_0 &= -k_c p + \frac{1}{2}(K_c - k_c^2)p^2\end{aligned}\quad (5.18)$$

and the volume as

$$\frac{\Delta V}{V_0} = -k_v p + \frac{1}{2}(K_v + 4k_a k_c - k_c^2)p^2 \quad (5.19)$$

where  $k_v = 2k_a + k_c$  and  $K_v = 2K_a + K_c$ .

### 5.3 Effective elastic constants and their pressure derivatives

Ultrasonic velocity measurements made on an initially-stressed crystal yield effective elastic constants. When such a crystal is further deformed its energy can be expressed either in terms of the additional deformation and the effective elastic constants or in terms of the overall deformation and the elastic constants of the crystal in the unstrained state. The procedure is described fully for arbitrary strain in [6, Sec. 8]. The expressions so obtained are differentiated to give the pressure derivatives of the second-order constants.

#### 5.3.1 Cubic diamond

The effective constants are

$$\begin{aligned}\bar{C}_{11} &= C_{11}(1 + 3\eta_1 - \eta_2 - \eta_3) + C_{111}\eta_1 + C_{112}(\eta_2 + \eta_3) \\ \bar{C}_{12} &= C_{12}(1 + \eta_1 + \eta_2 - \eta_3) + C_{112}(\eta_1 + \eta_2) + C_{123}\eta_3 \\ \bar{C}_{44} &= C_{44}(1 - \eta_1 + \eta_2 + \eta_3) + C_{144}\eta_1 + C_{155}(\eta_2 + \eta_3).\end{aligned}\quad (5.20)$$

Differentiation of the above, after setting  $\eta_1 = \eta_2 = \eta_3 = -kp$ , gives the following pressure derivatives:

$$\begin{aligned}-C'_{11} &= k(C_{11} + C_{111} + 2C_{112}) \\ -C'_{12} &= k(C_{12} + 2C_{112} + C_{123}) \\ -C'_{44} &= k(C_{44} + C_{144} + 2C_{155}).\end{aligned}\quad (5.21)$$

#### 5.3.2 Hexagonal diamond and hexagonal graphite

For both allotropes the effective constants are

$$\begin{aligned}\bar{C}_{11} &= C_{11}(1 + 3\eta_1 - \eta_2 - \eta_3) + C_{111}\eta_1 + C_{112}\eta_2 + C_{113}\eta_3 \\ \bar{C}_{12} &= C_{12}(1 + \eta_1 + \eta_2 - \eta_3) + C_{112}\eta_1 + C_{122}\eta_2 + C_{123}\eta_3 \\ \bar{C}_{13} &= C_{13}(1 + \eta_1 - \eta_2 + \eta_3) + C_{113}\eta_1 + C_{123}\eta_2 + C_{133}\eta_3\end{aligned}\quad (5.22)$$

$$\begin{aligned}\bar{C}_{33} &= C_{33}(1 - \eta_1 - \eta_2 + 3\eta_3) + C_{133}(\eta_1 + \eta_2) + C_{333}\eta_3 \\ \bar{C}_{44} &= C_{44}(1 - \eta_1 + \eta_2 + \eta_3) + C_{144}\eta_1 + C_{244}\eta_2 + C_{344}\eta_3.\end{aligned}$$

Differentiation, after setting  $\eta_1 = \eta_2 = -k_a p$  and  $\eta_3 = -k_c p$ , then gives the following pressure derivatives:

$$\begin{aligned}-C'_{11} &= k_a(2C_{11} + C_{111} + C_{112}) + k_c(-C_{11} + C_{113}) \\ -C'_{12} &= k_a(2C_{12} + C_{112} + C_{122}) + k_c(-C_{12} + C_{123}) \\ -C'_{13} &= k_a(C_{113} + C_{123}) + k_c(C_{13} + C_{133}) \\ -C'_{33} &= 2k_a(-C_{33} + C_{133}) + k_c(3C_{33} + C_{333}) \\ -C'_{44} &= k_a(C_{144} + C_{244}) + k_c(C_{44} + C_{344}).\end{aligned}\tag{5.23}$$

It was not possible, using the above procedure, to reproduce the expressions for the effective elastic constants of hexagonal crystals under isotropic pressure given in [5].

### 5.3.3 Rhombohedral graphite

The effective constants are

$$\begin{aligned}\bar{C}_{11} &= C_{11}(1 + 3\eta_1 - \eta_2 - \eta_3) + C_{111}\eta_1 + C_{112}\eta_2 + C_{113}\eta_3 + C_{114}\eta_4 \\ \bar{C}_{12} &= C_{12}(1 + \eta_1 + \eta_2 - \eta_3) + C_{14}\eta_4 + C_{112}\eta_1 + C_{122}\eta_2 + C_{123}\eta_3 + C_{124}\eta_4 \\ \bar{C}_{13} &= C_{13}(1 + \eta_1 - \eta_2 + \eta_3) + C_{14}\eta_4 + C_{113}\eta_1 + C_{123}\eta_2 + C_{133}\eta_3 + C_{134}\eta_4 \\ \bar{C}_{33} &= C_{33}(1 - \eta_1 - \eta_2 + 3\eta_3) + C_{133}(\eta_1 + \eta_2) + C_{333}\eta_3 + C_{334}\eta_4 \\ \bar{C}_{44} &= C_{44}(1 - \eta_1 + \eta_2 + \eta_3) - C_{14}\eta_4 + C_{144}\eta_1 + C_{244}\eta_2 + C_{344}\eta_3 + C_{444}\eta_4 \\ \bar{C}_{14} &= C_{14}(1 + \eta_1) + \frac{1}{2}(C_{12} + C_{13})\eta_4 + C_{114}\eta_1 + C_{124}\eta_2 + C_{134}\eta_3 + C_{144}\eta_4.\end{aligned}\tag{5.24}$$

As  $\eta_4 = 0$  under hydrostatic pressure their pressure derivatives are simply the same as those of  $hD$  and  $hG$  augmented by

$$-C'_{14} = k_a(C_{14} + C_{114} + C_{124}) + k_c C_{134}.\tag{5.25}$$

## 5.4 Summary

Starting with the general results in Chapter 1 the composition of the second- and third-order elastic constants of the four carbon allotropes in terms of their inner elastic constants and internal strain tensors has been presented. Certain properties derived from these constants, such as compliances, compressibilities and the pressure derivatives, are closely related to parameters that can be obtained directly by X-ray or neutron diffraction or from ultrasonic velocity measurements. These have also been exposed explicitly.

**References**

- [1] K. Brugger, *Phys. Rev.* **133**, A1611 (1964)
- [2] C. S. G. Cousins, *J.Phys.C:Solid St. Phys.* **15**, 1857 (1982)
- [3] K. Fuchs, *Proc. Roy. Soc.* **A153**, 622 (1936)
- [4] J. F. Nye, *Physical Properties of Crystals*, (Oxford: University Press, 1957)
- [5] R. Ramji Rao and R. Srinivasan, *Phys. Status Solidi* **31**, K39 (1969)
- [6] D. C. Wallace in *Solid State Physics* edited by H. Ehrenreich, F. Seitz and D. Turnbull (Academic Press, New York and London, 1970), Volume 25

## Chapter 6

### Cubic diamond: optimization of an anharmonic Keating model and its subsequent modification

#### 6.1 Introduction

Over the years a number of valence-force-field approaches have been developed and/or used to treat elasticity [9, 10, 11, 13, 16, 24], lattice dynamics [14, 23] and piezo-Raman spectroscopy [1, 3, 4, 8] in covalently bonded materials. These range from Keating's original 2-parameter model [10] dealing with harmonic properties to the massive 21-term database of Vanderbilt *et al.* [24] that handles harmonic, third-order and fourth-order anharmonic properties of silicon.

In the desire to achieve a good description of both harmonic and third-order anharmonic properties of cubic diamond with the smallest number of parameters I have chosen to develop and optimize the original Keating model [10, 11] by including only such further interactions as were strictly necessary.

Most of the formal aspects of the elasticity of *cD* have been covered in Chapters 4 and 5. The key results are summarised in Sec. 6.2, together with an elegant representation of the compliances. Sec. 6.3 extends the previous results concerning the optic mode frequency to cover the uniaxial stress-dependence of the frequencies (phonon deformation potentials) so that a wealth of experimental data [1, 3, 4, 8] can be considered.

Previous applications of the Keating model are reviewed in Sec. 6.4 and the method is extended to include all three nearest-neighbour 3-body interactions at the second order. The optimization of the four parameters of its harmonic part is carried out. It is shown that the bond-bending parameter obtained this way always contains implicitly a 4-body contribution that cannot be separated from the normal 3-body contribution by consideration of elasticity alone. Separation is achieved by fitting phonon frequencies at the *X* and *L* points of the Brillouin zone.

Additionally six anharmonic terms have been considered at the third order [1, 11]. In an exact fit of these to experimental values of the three pressure derivatives of the second-order elastic constants and of the three phonon deformation potentials that describe the stress dependencies of the Raman frequency [1, 8] it was found that one parameter was insignificant. For the optimized anharmonic

potential the other five force constants were fitted by least squares with almost no change in values. The full array of results is summarized in Sec. 6.5. Finally in Sec. 6.6 the elasticity of  $cD$  is expressed relative to rhombohedral axes. When compared with the standard cubic approach this reveals the drawback to the Keating model: namely that the parameters depend on some unit cell dimension. The situation is avoided by redefining the strain so that all parameters at the second and third order have the dimension of energy. The modified parameters have the virtue that they are then transferable between structures.

## 6.2 Elastic constants, compliances and pressure derivatives

The total elastic constants are given by

$$\begin{aligned} C_{11} &= C_{11}^0 \\ C_{12} &= C_{12}^0 \\ C_{44} &= C_{44}^0 - (A_{14})^2 E_{11} \end{aligned} \quad (6.1)$$

at the second order and by

$$\begin{aligned} C_{111} &= C_{111}^0 \\ C_{112} &= C_{112}^0 \\ C_{123} &= C_{123}^0 \\ C_{144} &= C_{144}^0 + 2A_{14}D_{114} + (A_{14})^2 E_{111} \\ C_{155} &= C_{155}^0 + 2A_{14}D_{124} + (A_{14})^2 E_{112} \\ C_{456} &= C_{456}^0 + 3A_{14}D_{156} + 3(A_{14})^2 E_{126} + (A_{14})^3 F_{123} \end{aligned} \quad (6.2)$$

at the third, where

$$A_{14} = -D_{14}/E_{11} \quad (6.3)$$

is the internal strain parameter.

Second-order compliances  $S_{IJ}$  enter the general expressions for the effective elastic constants that are needed in the anharmonic parametrization. They are obtained from the stiffnesses  $C_{IJ}$  through the following relations, [18]

$$\begin{aligned} k \equiv S_{11} + 2S_{12} &= 1/(C_{11} + 2C_{12}) \\ k' \equiv S_{11} - S_{12} &= 1/(C_{11} - C_{12}) \\ k'' \equiv S_{44} &= 1/C_{44}. \end{aligned} \quad (6.4)$$

The abbreviations  $k$ ,  $k'$ , and  $k''$  serve to simplify the following expressions for the third-order compliances [5], which take a particularly neat form as a result of the high symmetry of  $cD$ :

$$K = S_{111} + 6S_{112} + 2S_{123} = -k^3(C_{111} + 6C_{112} + 2C_{123})$$

$$\begin{aligned}
S_{111} - 3S_{112} + 2S_{123} &= -k_r^3(C_{111} - 3C_{112} + 2C_{123}) \\
S_{111} - S_{123} &= -kk_r^2(C_{111} - C_{123}) \\
S_{144} + 2S_{155} &= -kk_r^2(C_{144} + 2C_{155}) \\
S_{144} - S_{155} &= -k_r k_r^2(C_{144} - C_{155}) \\
S_{456} &= -k_r^3 C_{456}.
\end{aligned} \tag{6.5}$$

where  $k$  and  $K$  are the harmonic and anharmonic linear compressibilities respectively.

The hydrostatic pressure derivatives of the elastic constants are given by

$$\begin{aligned}
C'_{11} &= -k(C_{11} + C_{111} + 2C_{112}) \\
C'_{12} &= -k(C_{12} + 2C_{112} + C_{123}) \\
C'_{44} &= -k(C_{44} + C_{144} + 2C_{244})
\end{aligned} \tag{6.6}$$

and

$$B' = -\frac{1}{3} - \frac{k}{3}(C_{111} + 6C_{112} + 2C_{123}), \tag{6.7}$$

where the bulk modulus  $B = (C_{11} + 2C_{12}) = 1/3k$ .

### 6.3 The zone-centre optical modes

The general approach to optic mode frequencies given in Chapter 4 led to the following expressions for the triply-degenerate Raman frequency

$$\omega_0^2(T_{2g}) = \frac{4}{\rho_0} E_{11} = \frac{a^3}{2m} E_{11} \tag{6.8}$$

and its pressure derivative

$$\left( \frac{d\omega^2(T_{2g})}{dp} \right)_0 = -\frac{4k}{\rho_0} (2E_{11} + E_{111} + 2E_{112}) \tag{6.9}$$

where  $\rho_0$  is the equilibrium density,  $m$  is the mass of a carbon atom and  $k$  the linear compressibility.

#### 6.3.1 The secular equation under stress

The effective inner elastic constants,  $\bar{E}$ , for arbitrary strain are given by (4.37).

The secular equation for the optical modes under a stress  $\sigma$  is

$$\left| \bar{E}_{ij} - \frac{\rho}{4} \omega^2 \right| = 0 \tag{6.10}$$

in which

$$\frac{\rho_0}{\rho} = 1 + k\sigma. \tag{6.11}$$

The phonon deformation potentials that describe the stress-dependence of the mode frequencies depend on the stress derivatives of both  $\bar{E}_{ij}$  and  $\rho$ .

Under hydrostatic pressure  $p$  the effective constants are

$$\bar{E}_{11} = \bar{E}_{22} = \bar{E}_{33} = E_{11}(1 + pk) - pk(E_{111} + 2E_{112}) \quad (6.12)$$

and the eigenvalues remain triply degenerate with

$$\omega_H^2 = \frac{4}{\rho} \bar{E}_{11}. \quad (6.13)$$

For a uniaxial stress  $\sigma$  in the direction  $\vec{\ell}$  the stress components are given by  $\sigma_J = \sigma \ell_i \ell_j$ , where  $J$  is the conventional contraction of  $ij$ . Hooke's law,  $\eta_I = S_{IJ} \sigma_J$ , can now be used to eliminate  $\eta_I$  from the effective inner elastic constants in favour of  $\sigma \ell_i \ell_j$  and derivatives with respect to stress found. Three situations are relevant to the work described here:

#### 6.3.1.1 $\sigma$ along [001]

This is a tetragonal deformation and the effective  $E$  tensor now has two different diagonal components:

$$\begin{aligned} \bar{E}_{11} &= \bar{E}_{22} = E_{11}(1 - \sigma S_{11}) + \sigma(S_{12}E_{111} + (S_{11} + S_{12})E_{112}) \\ \bar{E}_{33} &= E_{11}(1 - \sigma(2S_{12} - S_{11})) + \sigma(S_{11}E_{111} + 2S_{12}E_{112}). \end{aligned} \quad (6.14)$$

The eigenvalues consist of a doublet and a singlet given by

$$\omega_d^2 = \frac{4}{\rho} \bar{E}_{11} \quad (6.15)$$

and

$$\omega_s^2 = \frac{4}{\rho} \bar{E}_{33}. \quad (6.16)$$

#### 6.3.1.2 $\sigma$ along [111]

This is a trigonal deformation in which

$$\begin{aligned} \bar{E}_{11} &= \bar{E}_{22} = \bar{E}_{33} = E_{11}(1 - \frac{1}{3}\sigma(S_{11} + 2S_{12})) + \frac{1}{3}\sigma(S_{11} + 2S_{12})(E_{111} + 2E_{112}) \\ \bar{E}_{12} &= \bar{E}_{13} = \bar{E}_{23} = \frac{1}{3}\sigma S_{44}(E_{11} + E_{126} + A_{14}F_{123}) \end{aligned} \quad (6.17)$$

The eigenvalues are

$$\omega_d^2 = \frac{4}{\rho} (\bar{E}_{11} - \bar{E}_{12}) \quad (6.18)$$

and

$$\omega_s^2 = \frac{4}{\rho} (\bar{E}_{11} + 2\bar{E}_{12}). \quad (6.19)$$

### 6.3.1.3 $\sigma$ along [1 1 0]

In this orthorhombic deformation an off-diagonal component is introduced:

$$\begin{aligned}\bar{E}_{11} &= \bar{E}_{22} = E_{11}(1 - \sigma S_{12}) + \frac{1}{2}\sigma((S_{11} + S_{12})E_{111} + (S_{11} + 3S_{12})E_{112}) \\ \bar{E}_{12} &= \frac{1}{2}\sigma S_{44}(E_{11} + E_{126} + A_{14}F_{123}) \\ \bar{E}_{33} &= E_{11}(1 - \sigma S_{11}) + \sigma(S_{12}E_{111} + (S_{11} + S_{12})E_{112}).\end{aligned}\quad (6.20)$$

Degeneracy has now been removed and three eigenvalues are obtained:

$$\omega_{\pm}^2 = \frac{4}{\rho}(\bar{E}_{11} \pm \bar{E}_{12}) \quad (6.21)$$

and

$$\omega_3^2 = \frac{4}{\rho}\bar{E}_{33}. \quad (6.22)$$

### 6.3.2 Phonon deformation potentials

There are several different *ad hoc* definitions and notations used to describe the strain dependence of the optic mode frequencies at the zone centre [4, 20]:  $K_{ij} \equiv \partial\omega^2/\partial\eta_{ij}$  and  $\tilde{K}_{ij} \equiv \partial\ln\omega^2/\partial\eta_{ij} = (1/\omega_0^2)K_{ij}$  are general expressions whilst  $p = K_{11}$ ,  $q = K_{12}$  and  $r = K_{44}$  are parameters specific to cubic symmetry. When the eigenvalue expressions in the previous subsections are differentiated with respect to stress, relations precisely the same as those given in [4] are obtained with

$$\begin{aligned}\frac{p}{2\omega_0^2} &= 1 + \frac{E_{111}}{2E_{11}} \\ \frac{q}{2\omega_0^2} &= \frac{E_{112}}{2E_{11}} \\ \frac{r}{\omega_0^2} &= 1 + \frac{E_{126} + A_{14}F_{123}}{E_{11}},\end{aligned}\quad (6.23)$$

together with the mode Grüneisen parameter

$$\gamma_G = -\frac{1}{3} \left( 1 + \frac{E_{111} + 2E_{112}}{2E_{11}} \right). \quad (6.24)$$

A slightly different approach has been adopted by Nielsen [17] who defines a *phonoelastic tensor*  $\Omega$  as the square root of the dynamical matrix. Elements of this tensor, expanded in powers of  $\eta$ , then combine to give frequencies under strain. Certain of the linear coefficients then correspond to phonon deformation potentials:  $\Omega_{11}$ ,  $\Omega_{12}$  and  $2\Omega_{44}$  corresponding to the lefthand sides of the three members of (6.23) above.

## 6.4 The Keating model

The Keating formalism [10] models the strain energy only and does not provide values for the cohesive energy or the lattice parameter,  $a$  ( $=3.567 \text{ \AA}$ ). The value of  $a$  is assumed when forming the strain variables  $\Delta_{ij} \equiv (\vec{r}^i \cdot \vec{r}^j - \vec{r}^{i0} \cdot \vec{r}^{j0})$ , where  $i$  and  $j$  label atoms neighbouring a particular reference atom,  $s$ , and  $i0$  and  $j0$  label the unstrained configuration.

The connection between  $\Delta_{ij}$ , the finite strain tensor  $\eta$  and the inner displacement vector  $\vec{\zeta}$  follows from the definition of homogeneous deformation. If  $H$  is the deformation gradient matrix then  $\vec{r}^i = H \vec{r}^{i0} \pm \tilde{H}^{-1} \vec{\zeta}$ , where the sign depends on which sublattice the reference atom lies on,

$$\Delta_{ii} = 2r_p^{i0} \eta_{pq} r_q^{i0} \pm 2r_p^{i0} \zeta_p + \zeta_p \zeta_p \quad (6.25)$$

and

$$\Delta_{ij} = 2r_p^{i0} \eta_{pq} r_q^{j0} \pm (r_p^{i0} + r_p^{j0}) \zeta_p + \zeta_p \zeta_p \quad (6.26)$$

where terms of order three and higher have been omitted.

### 6.4.1 Harmonic interactions

The harmonic energy per cell derives here from a nearest-neighbour 2-body interaction, three nearest-neighbour 3-body interactions and a certain 4-body interaction. It takes the form, [19],

$$E^{(2)} = \frac{1}{a^2} \sum_{s=1}^2 \sum_{i=1}^4 \left( \alpha \Delta_{ii}^2 + \sum_{j=1}^4{}' (\beta \Delta_{ij}^2 + \frac{1}{2} \sigma (\Delta_{ii} + \Delta_{jj}) \Delta_{ij} + \tau \Delta_{ii} \Delta_{jj} + \kappa \Delta_{ij} \Delta_{ik}) \right) \quad (6.27)$$

where the prime on the summation over  $j$  indicates that  $j \neq i$ . The  $\kappa$  term is related to the  $f_{\phi\phi^*}$  valence force field parameter introduced by McMurry *et al.* [14] as an essential ingredient in the treatment of the flattening of the transverse acoustic dispersion curves towards the  $X$  and  $L$  points in the Brillouin zone. It relates to a chain of three bonds in a  $180^\circ$  dihedral-angle configuration. The absence of a summation over  $k$  arises as follows. The bonds labelled  $j$  and  $k$  are attached to opposite ends of bond  $i$  and are parallel. Under homogeneous deformation the outer bonds are strained in the same way, forcing the two angles of the chain to change in the same way. This results in  $\Delta_{ij} \Delta_{ik} = \Delta_{ij}^2$  and the interaction becomes formally indistinguishable from the simple 3-body bond-bending interaction. Elastic constants and the zone-centre frequency cannot be used to separate  $\beta$  from  $\kappa$ . However the expressions for some of the phonon frequencies at the zone boundary mix  $\beta$  and  $\kappa$  in different proportions thereby enabling the separation to be made.

The second-order elastic, inner elastic and internal strain parameters are given by the following, in which  $\beta^*$  denotes  $\beta + \kappa$ :

$$\begin{aligned} C_{11} &= \frac{1}{a} (\alpha + 3\beta^* - \sigma + 3\tau) \\ C_{12} &= \frac{1}{a} (\alpha - \beta^* - \sigma + 3\tau) \end{aligned}$$

$$\begin{aligned}
B &= \frac{1}{a}(\alpha + \frac{1}{3}\beta^* - \sigma + 3\tau) \\
C_{44}^0 &= \frac{1}{a}(\alpha + \beta^* - \sigma - \tau) \\
D_{14} &= \frac{4}{a^2}(\alpha - \beta^* - \tau) \\
E_{11} &= \frac{16}{a^3}(\alpha + \beta^* + \sigma - \tau) \\
A_{14} &= -\frac{a}{4} \left( \frac{\alpha - \beta^* - \tau}{\alpha + \beta^* + \sigma - \tau} \right) \\
\zeta_K &= -\frac{4}{a}A_{14}
\end{aligned} \tag{6.28}$$

where  $B$  is the bulk modulus,  $\zeta_K$  is the Kleinman internal strain parameter and the remaining total second-order constant,  $C_{44}$ , is given by (6.1).

In addition, because  $\Delta_{ii}$  and  $\Delta_{ij}$  contain terms in  $\zeta^2$ , the ‘harmonic’ energy contains small anharmonic contributions via  $E_{111}$  and  $E_{112}$ . These are given by

$$E_{111}^{(2)} = E_{112}^{(2)} = \frac{16}{a^3}(\alpha - \beta^* + \sigma + 3\tau) \tag{6.29}$$

Initially the model was limited to the  $\alpha$  and  $\beta^*$  terms alone and applied to Group IV elements and III-V semiconductors [10, 13]. The targets for fitting were  $C_{11}$ ,  $C_{12}$  and  $C_{44}$ .

Table 6.1: Parametrization of the harmonic part of the Keating model. As explained in the text all fits of ‘ $\beta$ ’ to experimental data are in fact fits of  $\beta + \kappa$ : this is indicated below by the use of  $\beta^*$ . Units are GPa for  $C_{IJ}$  and  $B$ , GPa  $\text{\AA}^{-2}$  for  $E_{11}$ , and GPa  $\text{\AA}$  for  $\alpha$  etc.

	$\leftarrow \alpha, \beta^*$ fittings				$\rightarrow \alpha, \beta^*, \tau$		$\alpha, \beta^*, \sigma$		Present work	
	Exact				LSq	?	Exact	Exact	LSq	Observed
$C_{11}$	Fit	Fit	756	433	990	1051	Fit	Fit	1072	1079(5) <sup>a</sup>
$C_{12}$	Fit	-199	Fit	447	69	100	Fit	Fit	131	124(5) <sup>a</sup>
$E_{11}$	756	Fit	Fit	Fit	666	770	Fit	Fit	562	553.4(8) <sup>b</sup>
$C_{44}$	576	350	567	-13	520	589	593	Fit	574	578(2) <sup>a</sup>
$B$	(Fit)	226	335	Fit	376	417	(Fit)	(Fit)	445	442(4) <sup>a</sup>
$\zeta_K$	0.206	-0.45	0.28	1.02	0.131	0.20	0.12	0.074	0.093	0.125(20) <sup>c</sup>
$\alpha$	1294	430	1006	1582	1068	1304	1056	987	1009	
$\beta^*$	852	1140	564	-12.2	821	848	852	852	840	
$\sigma$							-238	-250	-234	
$\tau$						-33		19	21	

<sup>a</sup> Reference [15]   <sup>b</sup> Reference [25]   <sup>c</sup> Reference [6]

Values of  $\alpha$  and  $\beta^*$  deduced from  $C_{11}$  and  $C_{12}$  [15] gave  $C_{44}$  to better than 0.3% [10]. This very encouraging result hid a 37% error in  $E_{11}$  or a 17% error in the Raman frequency  $\omega_0$  [25]. It also

predicted a value of 0.21 for  $\zeta_K$ . This was later measured by my research collaborators and the much smaller value of  $0.125 \pm 0.020$  obtained [6]. With more experimental data available different fits can be made and these are listed in Table 6.1. For columns 2 through 5 two data are used to determine  $\alpha$  and  $\beta^*$  and the implications set out: at least one quantity is very poorly predicted each time and  $\zeta_K$  in particular is bad. In column 6 a least-squares fit to four data by Anastassakis *et al.* [1] leads to  $\alpha = 1068 \text{ GPa \AA}$  and  $\beta^* = 821 \text{ GPa \AA}$ . This gives a value of  $\zeta_K$  close to that measured, though  $\omega_0$  is still 10% too large and  $C_{12}$  is 44% too small.

The first extension of the Keating model to include an additional interaction was made by Bashenov *et al.* [2] who introduced (using  $\gamma$ ) the term denoted here by  $\tau$ . Column 7 lists the quoted values; the precise method of calculation is unclear.

The case for the inclusion of the other 3-body term was discussed by Rucker and Methfessel [19]. They pointed out that a good agreement for  $C_{11}$ ,  $C_{12}$ ,  $C_{44}$  and  $\omega_0$  in diamond could be obtained using just  $\alpha$ ,  $\beta^*$  and  $\sigma$  ( $\gamma$  in their paper) whereas it appeared important to introduce  $\tau$  to improve the fit to the phonon dispersion in Si and Ge. Column 8 shows the result of this fitting. Each fit generates a unique relation for  $\zeta_K$  in terms of the fitted parameters—in this case

$$1 - 2\zeta_K = \left( \frac{4a(C_{11} - 3C_{12})}{M\omega_0^2} \right)^{1/2}. \quad (6.30)$$

This gives a value  $\zeta_K = 0.102$  that is close to a theoretical calculation [17] and reasonably close to experiment [6]. The predicted value for  $C_{44}$  is now 593 GPa, much closer to the observed 578 GPa.

The inclusion of both extra terms will now be considered. Inversion of the earlier equations for  $C_{11}$ ,  $C_{12}$ ,  $E_{11}$  and  $D_{14}$  (as  $\zeta_K E_{11}$ ) yields

$$\begin{aligned} \alpha &= \frac{a}{8}(C_{11} + C_{12}) + \frac{a^3}{64}E_{11}(1 + 2\zeta_K) \\ \beta^* &= \frac{a}{4}(C_{11} - C_{12}) \\ \sigma &= -\frac{a}{2}(C_{11} - C_{12}) + \frac{a^3}{16}E_{11}(1 - \zeta_K) \\ \tau &= -\frac{a}{8}(C_{11} - 3C_{12}) + \frac{a^3}{64}E_{11}(1 - 2\zeta_K). \end{aligned} \quad (6.31)$$

These then imply

$$1 - \zeta_K = \left( \frac{8a(C_{11} - C_{12} - C_{44})}{M\omega_0^2} \right)^{1/2} \quad (6.32)$$

giving  $\zeta_K = 0.074$ , a value that is somewhat lower than either the measured value or theoretical predictions. If the tolerances on the experimental data are taken into account a range of values is obtained:  $\zeta_K = 0.074 \pm 0.009$ . Although this is not quite enough to bracket the experimental range there are reasons, discussed in Sec. 6.5, for supposing that the experimental value may have been slightly overestimated. This 4-parameter fit is listed in column 9. A least squares solution involving the observed value of  $\zeta_K$  produces the fitting shown in column 10.

To check further the quality of the fits and to resolve the  $\beta/\kappa$  problem involves consideration of the zone-boundary phonons [21]. At the  $X$  point these have frequencies given by

$$\begin{aligned}
M\omega_{LO,LA}^2 &= 4\alpha + 8\beta + 4\tau + 4\kappa \\
&= 4\alpha + 8\beta^* + 4\tau - 4\kappa \\
M\omega_{TO}^2 &= 8\alpha - 8\tau \\
M\omega_{TA}^2 &= 8\beta \\
&= 8\beta^* - 8\kappa
\end{aligned} \tag{6.33}$$

and at the  $L$  point by

$$\begin{aligned}
M\omega_{LO}^2 &= 2\alpha + 13\beta + \sigma + 4\tau + 4\kappa \\
&= 2\alpha + 13\beta^* + \sigma + 4\tau - 9\kappa \\
M\omega_{LA}^2 &= 6\alpha + \beta - 3\sigma \\
&= 6\alpha + \beta^* - 3\sigma - \kappa \\
M\omega_{TO}^2 &= 8\alpha + 4\beta + 4\sigma - 8\tau + 4\kappa \\
&= 8\alpha + 4\beta^* + 4\sigma - 8\tau \\
M\omega_{TA}^2 &= 4\beta \\
&= 4\beta^* - 4\kappa.
\end{aligned} \tag{6.34}$$

Table 6.2: Phonon frequencies  $f(\equiv \omega/2\pi)$  at the  $\Gamma$ ,  $X$  and  $L$  points. Units: THz for  $f$ , GPa Å for  $\beta^*$  etc.

Point	Mode	Exact fit		Least-sq. fit		Observed <sup>a</sup>
$\Gamma$	LO,TO	39.93	39.93	40.23	40.23	39.93
$X$	LO,LA	37.09	35.36	37.09	35.45	35.80
	TO	31.36	31.36	31.68	31.68	32.39
	TA	29.41	24.78	29.20	24.78	24.04
$L$	LO	40.42	36.77	40.29	36.80	37.21
	LA	30.91	30.40	31.05	30.57	31.00
	TO	35.90	35.90	36.21	36.21	36.25
	TA	20.80	17.52	20.65	17.52	16.55
$\beta^*$		852		840		
$\beta$		605		605		
$\kappa$		0	247	0	235	

<sup>a</sup> Reference [25]: errors are estimated at 2-3%

Columns 3, 5 and 7 in Table 6.2 show the frequencies predicted using the four parameters  $\alpha$ ,  $\beta^*$ ,  $\sigma$  and  $\tau$  (i.e. with no explicit  $\kappa$  term), in both exact and least-squares versions, and those observed. The least-squares fit appears to be very slightly better.

The TO modes, which have no explicit  $\kappa$  component, are well predicted with errors of only -2% and -0.1%. Apart from one the remainder are overestimated: in particular the errors in the TA modes are 22% at  $X$  and 25% at  $L$ . This characteristic failure to pick up the flattening of the TA modes near the boundary is markedly reduced by setting  $\kappa = 247 \text{ GPa \AA}$  in the exact and  $\kappa = 235 \text{ GPa \AA}$  in the least-squares fittings to give the values listed in columns 4 and 6: the errors in the TA modes are now 3% and 6% respectively and the separation of  $\beta^*$  has now been achieved with  $\beta = 605 \text{ GPa \AA}$  in each case.

With the simple model under consideration there is no way to improve all the zone-boundary frequencies. I showed in [7] that the most general force constant fitting to nearest and next-nearest neighbour interactions [12] imposes a condition on the calculated frequencies:

$$2(\omega_{LA}^2 - \omega_{LO}^2 + \omega_{TO}^2 - \omega_{TA}^2)_L = 3(\omega_{TO}^2 - \omega_{TA}^2)_X. \quad (6.35)$$

Observed values do not satisfy this equation: the left- and right-hand sides differ from their mean by 6%, a figure that suggests that the above fit is as good as it can be.

The inner elastic constants and internal strain parameters are collected together in summary Table 6.4 in Sec. 6.5 and the decomposition of the calculated constants and the associated compliances are shown in summary Tables 6.5 and 6.6.

#### 6.4.2 Anharmonic interactions

Keating extended his method to the anharmonic régime [11] by considering the  $\gamma$ ,  $\delta$  and  $\epsilon$  terms in the following expression for the anharmonic energy per cell

$$E^{(3)} = \frac{8}{3a^3} \sum_{s=1}^2 \sum_{i=1}^4 \left( \gamma \Delta_{ii}^3 + \sum_{j=1}^4 \left( \delta \Delta_{ij}^3 + \frac{3}{2} \epsilon (\Delta_{ii} + \Delta_{jj}) \Delta_{ij}^2 + \frac{3}{2} \eta (\Delta_{ii}^2 + \Delta_{jj}^2) \Delta_{ij} + 3\theta \Delta_{ii} \Delta_{ij} \Delta_{jj} + \frac{3}{2} \xi \Delta_{ii} \Delta_{jj} (\Delta_{ii} + \Delta_{jj}) \right) \right) \quad (6.36)$$

where all nearest-neighbour 2-body and 3-body interactions have been written down. He successfully applied this model to fitting the third-order elastic constants of Si and Ge. The direct measurement of these constants for diamond would be extremely difficult for several reasons and has probably not been attempted. Nevertheless experimental data are available that relate to the third-order elastic constants, through pressure derivatives of second-order constants, [15] and to third-order inner elastic constants, in the form of stress derivatives of the Raman frequency [8]. The pattern of analysis used here is essentially the same as the one developed in [1]. The latter work however involved only a 2-parameter harmonic fitting and this affects, in principle, the fits to  $E_{111}$

and  $E_{112}$  and causes poorly fitted quantities ( $E_{11}$ ,  $B$  and, perhaps,  $\zeta_K$ ) to distort the anharmonic fitting.

The third-order elastic and inner elastic constants are given by the following expressions:

$$\begin{aligned}
C_{111} &= \gamma - \delta + 9\epsilon - 3\eta - 3\theta + 9\xi \\
C_{112} &= \gamma - \delta + \epsilon - 3\eta - 3\theta + 9\xi \\
C_{123} &= \gamma + 3\delta - 3\epsilon - 3\eta - 3\theta + 9\xi \\
C_{144}^0 &= \gamma + \delta - \epsilon - 3\eta + \theta + \xi \\
C_{155}^0 &= \gamma - \delta + 3\epsilon - 3\eta - 3\theta + \xi \\
C_{456}^0 &= \gamma - 3\eta + 3\theta - 3\xi \\
D_{114} &= \frac{4}{a}(\gamma - \delta - \epsilon - \eta + 3\theta + \xi) \\
D_{124} &= \frac{4}{a}(\gamma + \delta - \epsilon - \eta + \theta + \xi) \\
D_{156} &= \frac{4}{a}(\gamma - \eta + \theta - 3\xi) \\
E_{111}^{(3)} &= \frac{16}{a^2}(\gamma + \delta + 3\epsilon + \eta + 5\theta + \xi) \\
E_{112}^{(3)} &= \frac{16}{a^2}(\gamma - \delta - \epsilon + \eta + \theta + \xi) \\
E_{126} &= \frac{16}{a^2}(\gamma + \eta - \theta - 3\xi) \\
F_{123} &= \frac{64}{a^3}(\gamma + 3\eta - 3\theta - 3\xi).
\end{aligned} \tag{6.37}$$

The full  $E_{111}$  and  $E_{112}$  are then given by

$$\begin{aligned}
E_{111} &= E_{111}^{(2)} + E_{111}^{(3)} \\
E_{112} &= E_{112}^{(2)} + E_{112}^{(3)}
\end{aligned} \tag{6.38}$$

and the remaining total third-order constants,  $C_{144}$ ,  $C_{155}$  and  $C_{456}$ , by expressions in (6.2).

The target quantities related to the pressure derivatives of the second-order constants are  $C_{111} + 2C_{112}$ ,  $2C_{112} + C_{123}$  and  $C_{144} + 2C_{155}$ , given by (6.6), where values of  $C'_{IJ}$  have been derived from [15]. The latter work actually determines pressure derivatives of ultrasonic wave propagation coefficients and their  $C'_{11}$  and  $C'_{44}$  values must be increased by unity and  $C'_{12}$  decreased by unity for consistency with the definitions in (6.6). The targets related to the phonon deformation potentials are  $E_{111} + 2E_{112}$ ,  $E_{111} - E_{112}$  and  $E_{126} + A_{14}F_{123}$ , given by (6.23), where values of  $p$ ,  $q$  and  $r$  have been deduced from [8] and  $E_{11}$  and  $A_{14}$  have been carried forward from the least-squares harmonic fit. The (equal) values of  $E_{111}^{(2)}$  and  $E_{112}^{(2)}$  arising from the fitting of the harmonic energy should be removed from the first of the above three targets. This quantity is, however, very small: for the exact fitting it is  $-20.6 \text{ GPa \AA}$  and a minute  $-0.4 \text{ GPa \AA}$  for the least-squares fitting.

Table 6.3: Parametrization of the anharmonic part of the Keating model using pressure derivatives of the second-order elastic constants and the phonon deformation potentials. All input quantities are dimensionless. The units for  $\gamma$  etc. are GPa

Input	Ref. [8]	Ref. [1]	Present work	Observed	
$C'_{11}$	7.31		Fit	6.97	6.98(70) <sup>a</sup>
$C'_{12}$	3.23		Fit	2.09	2.06(70) <sup>a</sup>
$C'_{44}$	4.40	3.95	Fit	3.98	3.98(30) <sup>a</sup>
$(C'_{11} - C'_{12})/2$		2.45			2.46(10) <sup>a</sup>
$(C'_{11} + C'_{12} + 2C'_{44})/2$		8.65			8.50(60) <sup>a</sup>
$(p + 2q)/2\omega_0^2$	-3.35	-3.19	Fit	-3.18	-3.18(24) <sup>b</sup>
$(p - q)/2\omega_0^2$	-0.50	-0.52	Fit	-0.52	-0.52(8) <sup>b</sup>
$r/\omega_0^2$	-1.2	-1.89	Fit	-1.88	-1.9(2) <sup>b</sup>
$\gamma$	-1670	-1478	-1200	-1198	
$\delta$	95	140	164	166	
$\epsilon$	-499	-654	-567	-566	
$\eta$		-227	-139	-138	
$\theta$		181	145	143	
$\xi$			0.55		

<sup>a</sup> Reference [15]    <sup>b</sup> Reference [8]

With six targets and six force constants an exact fitting is possible. This gives a value for  $\xi$  (0.55 GPa) that is over 250 times smaller than the next smallest. It quantifies and confirms the observation in [1] that this term, which indicates anharmonic crosstalk between contiguous bonds, should probably be small. When  $\xi$  is neglected and the remaining five constants fitted by least-squares the new values differ from the old by no more than 1.4%. The results of these fittings are displayed in Table 6.3 together with the earlier fitting based on two harmonic terms and three anharmonic ones [8], and that of [1]. Differences between the present results and those in [1] are initially puzzling since the same basic approach and the same input data have been used in each case. Small differences are to be expected as a consequence of the use of different values of  $\zeta_K$ ,  $E_{11}$  and  $B$ . The force constants derived in [1] are consistent with the values of the third-order constants and with the three phonon deformation potentials but return values of 5.21, 3.32 and 11.33 for the three pressure derivatives on which they are supposed to be based. A clue is provided by Eqs. (7) in [1] where two of the three expressions contain twice the correct contribution of second-order constants: in fact all three derivatives have been so used. The error arises from the inappropriate use of equations developed by Thurston and Brugger [22] to facilitate the determination of third-order elastic constants from ultrasonic measurements by including compensation for changes in specimen

dimensions under stress.

One of the conclusions drawn in [1] was that the force constants  $\eta$  and  $\theta$  made a relatively small contribution to the elastic constants but were crucial to fitting the phonon deformation potentials. The present results make this point even more strongly: the two constants almost completely cancel and provide less than 0.5% of the elastic constants.

All the calculated anharmonic constants have been entered in Tables 6.4 and 6.6 in the next Section.

## 6.5 Summary of results

The inner elastic constants and internal strain parameters are shown in Table 6.4. Most of these are appearing for the first time.

Table 6.4: The inner elastic constants and internal strain parameters. Units are GPa  $\text{\AA}^{-1}$  for  $D$ , GPa  $\text{\AA}^{-2}$  for  $E$ , GPa  $\text{\AA}^{-3}$  for  $F$  and  $\text{\AA}$  for  $A$ .

Inner elastic constants					Internal strain			
$D_{14}$	46.6	$E_{11}$	561.9		$A_{14}$	-0.083		
					$\zeta_K$	0.093	0.108 <sup>a</sup>	
$D_{114}$	-259	$E_{111}$	-2705		$A_{114}$	0.06	1.39 <sup>a</sup>	
$D_{124}$	-529	$E_{112}$	-998		$A_{124}$	0.79	1.11 <sup>a</sup>	
$D_{156}$	-1028	$E_{126}$	-1860	$F_{123}$	-2879	$A_{156}$	1.32	1.96 <sup>a</sup>

<sup>a</sup> Reference [17]

Only  $E_{11}$  and  $A_{14}/\zeta_K$  are known experimentally (see Table 6.1). The calculated value of  $E_{11}$  is just 1.5% too large whereas  $\zeta_K$  at 0.093 is somewhat smaller than the 0.125 measured. The only other calculation of  $\zeta_K$  is due to Nielsen [17] who used local density functional theory with *ab initio* pseudopotentials. It is intriguing that the value he obtained in the course of fitting all the elastic constants to the LDA output was 0.092(2), essentially the same as the present one. The value he actually reported, 0.108(1), was obtained by a quite separate, albeit more direct, calculation. The possibility that the experimental value is too large follows from the fact that the sample was subjected to a uniaxial stress of 6.2 GPa parallel to  $[1, 1, 0]$ . This is large enough to induce quadratic components in the inner displacement and leads to an effective parameter

$$\zeta_K = -\frac{4}{a} (A_{14} + \sigma(S_{12}A_{114} + (S_{11} + S_{12})A_{124})). \quad (6.39)$$

Inserting calculated values shows that the experiment probably yielded too high a value in the ratio 0.087 to 0.083. This would reduce  $\zeta_K$  to 0.119, a shift of 5%, well within the already large

experimental uncertainty. At the third order the present values are rather less than those obtained in [17].

The decomposition of the elastic constants into partial and internal contributions is shown in Tables 6.5 and 6.6.

Table 6.5: The second-order elastic constants: stiffnesses are in GPa, compliances are in (TPa)<sup>-1</sup>.

$C_{IJ}$	Present work			Observed	<i>Ab initio</i>			Observed	
	Partial	Internal	Total	Ref. [15]	Ref. [17]	Ref. [19]	$S_{IJ}$	Total	Ref. [15]
$C_{11}$	1072.3		1072.3	1079(5)	1050(10)	1104.	$S_{11}$	0.958	0.949(5)
$C_{12}$	130.7		130.7	124(5)	127(4)	149.	$S_{12}$	-0.104	-0.098(3)
$C_{44}$	577.8	-3.9	574.0	578(2)	550(5)	581.	$S_{44}$	1.742	1.730(6)

Table 6.6: The third-order elastic constants: stiffnesses are in GPa, compliances are in (TPa)<sup>-2</sup>.

$C_{IJK}$	Present work			$\gamma, \delta, \epsilon$ fit	<i>Ab initio</i>		$S_{IJK}$	Total
	Partial	Internal	Total	Ref. [8]	Ref. [17]			
$C_{111}$	-6475.		-6475.	-6260	-6300(300)	$S_{111}$	4.609	
$C_{112}$	-1947.		-1947.	-2260	-800(100)	$S_{112}$	0.936	
$C_{123}$	982.		982.	112	0(400)	$S_{123}$	-1.698	
$C_{144}$	91.	24.	115.	-674	0(300)	$S_{144}$	-2.230	
$C_{155}$	-3079.	81.	-2998.	-2860	-2600(100)	$S_{155}$	7.808	
$C_{456}$	-355.	219.	-135.	-823	-1300(100)	$S_{456}$	0.716	

At the second order additional *ab initio* calculations, in which the full-potential linear muffin-tin orbital (FP-LMTO) method has been used, are available [19]. These are clearly of similar quality to those in [17]. In spite of its simplicity the 4-parameter Keating model clearly matches the predictions of more sophisticated calculations with regard to elastic constants and the zone-centre phonons.

At the third order the present results are quite similar to the previous 3-parameter fit of Grimditch *et al.* [8] This is expected as it is known that the extra two parameters introduced in [1] and used here have their major impact on the phonon deformation potentials. Nielsen's calculations provide the only theoretical comparison. These have been included even though they are quoted to only 2 significant figures. The two largest constants,  $C_{111}$  and  $C_{155}$ , are in reasonable agreement with this work but  $C_{456}$  seems rather inflated, the present value is much more in keeping with the relative size of this constant in other diamond-structure materials.

The calculated compliances are essentially of the same quality as the stiffnesses. They can be used directly to give the linear compressibilities at second and third order:  $k = 0.749$  TPa<sup>-1</sup> and

$K = 6.83 \text{ TPa}^{-2}$ . The corresponding volume compressibilities are  $k_v = 3k = 2.25 \text{ TPa}^{-1}$  and  $K_v = 3K = 20.5 \text{ TPa}^{-2}$ .

## 6.6 A modified Keating model

There is a drawback to the use of the Keating model: its parameters are not transferable. This fact appears to have passed unnoticed because the model has been applied exclusively to structures with the same atomic configuration, i.e. the tetrahedral arrangement common to diamond and zincblende. The problem arises from Keating's inclusion of the structure-specific lattice parameter  $a$  into his definition of strain [10]. It manifests itself most clearly in the attempt to account for the elasticity of  $hD$  which should be almost the same as that of  $cD$  insofar as the atoms in the two structures have precisely the same nearest neighbour configuration. The issue is resolved by a simple redefinition of strain.

### 6.6.1 Cubic diamond referred to rhombohedral axes

The simplest way to illustrate the non-transferability problem is to refer the elasticity of  $cD$  to rhombohedral axes. If these are taken to be  $Ox_1 \parallel [1\bar{1}0]$ ,  $Ox_2 \parallel [11\bar{2}]$  and  $Ox_3 \parallel [111]$  the resulting sets of elastic and inner elastic constants have the forms appropriate to the rhombohedral Laue group RI. Each set divides into two subsets: the group of elements that correspond to hexagonal symmetry and the group of elements that disappear if there is no rhombohedral symmetry. The transformed partial elastic and inner elastic constants are given in terms of the cubic constants by the expressions listed in Table 4.4 and Table 5.2. Total elastic constants transform in the same way as the partial constants because any inner elastic contributions to them transform compatibly.

The Keating parameters are not tensor components and there is no rule for their transformation. The Keating expressions for the partial and inner elastic constants can be transformed, however, and give rise, for example, to

$$C_{11}^0 = \frac{2}{a}(\alpha + \beta^* - \sigma + \tau)$$

etc., where  $a$  is the lattice parameter of the cubic unit cell. The harmonic energy per cell in the cubic system is given by (6.27). This energy does not change when the axes are rotated and nor do the  $\Delta_{ii}$  and  $\Delta_{ij}$ , being differences of scalar products and thus independent of coordinate system. Yet we would not expect to find  $a$  appearing in the equation if we were starting directly from the rhombohedral description, which involves a unit cell containing six atoms and lattice parameters  $a_h = a/\sqrt{2}$  and  $c_h = \sqrt{3}a$ , see Fig. 4.1. If (6.27) is used with  $a_h$  in place of  $a$  (explicitly in the initial factor and implicitly in  $\Delta_{ii}$  and  $\Delta_{ij}$ ) it is necessary to halve the harmonic Keating parameters to regain acceptable second-order constants, the same bulk modulus for example. Similarly, for the anharmonic energy and third-order constants, division by  $2\sqrt{2}$  is necessary. Using the parameters



### 6.6.2 Recasting the energy expressions

The simplest satisfactory solution emerges if the  $a^{-2}$  and  $a^{-3}$  factors are removed from  $E^{(2)}$  and  $E^{(3)}$ . Additionally a cosmetic alteration in the coefficients of individual terms in  $E^{(2)}$  and  $E^{(3)}$  will remove various powers of 2 whose presence is due to Keating's use of  $a/2$  in place of  $a$  in his original definition of strain. The modified energies per cell become

$$E^{(2)} = \frac{1}{2} \sum_{s=1}^2 \sum_{i=1}^4 \left( \alpha \Delta_{ii}^2 + \sum_{j=1}^4 ' (\beta^* \Delta_{ij}^2 + \sigma (\Delta_{ii} + \Delta_{jj}) \Delta_{ij} + \tau \Delta_{ii} \Delta_{jj}) \right) \quad (6.40)$$

and

$$E^{(3)} = \frac{1}{2} \sum_{s=1}^2 \sum_{i=1}^4 \left( \gamma \Delta_{ii}^3 + \sum_{j=1}^4 ' (\delta \Delta_{ij}^3 + \epsilon (\Delta_{ii} + \Delta_{jj}) \Delta_{ij}^2 + \eta (\Delta_{ii}^2 + \Delta_{jj}^2) \Delta_{ij} + \theta \Delta_{ii} \Delta_{ij} \Delta_{jj} + \xi \Delta_{ii} \Delta_{jj} (\Delta_{ii} + \Delta_{jj})) \right) \quad (6.41)$$

where the prime on the summation indicates that  $j \neq i$ . The previous notation has been retained so that confusion is avoided: expressions for elastic constants will change (as shown below) but the conceptual foundation of the model remains the same.

### 6.6.3 Modified Keating parameters

Identification of the old and the new energy expressions indicates how the parameters of the model must be modified: for example

$$\alpha_{\text{mod}} = \frac{2}{a^2} \alpha \quad (6.42)$$

and

$$\gamma_{\text{mod}} = \frac{16}{3a^3} \gamma. \quad (6.43)$$

The modified results for all the parameters deduced for cD by least squares fitting in Sec. 6.4 are listed in Table 6.9 in two different units.

Table 6.9: Modified Keating parameters

	Previous	Modified	
$\alpha$	1009 GPa Å	158.6 GPa Å <sup>-1</sup>	0.990 eV Å <sup>-4</sup>
$\beta^*$	840	132.0	0.824
$\sigma$	-234	-18.4	-0.115
$\tau$	21	3.3	0.021
$\gamma$	-1198 GPa	-140.8 GPa Å <sup>-3</sup>	-0.879 eV Å <sup>-6</sup>
$\delta$	166	19.5	0.122
$\epsilon$	-566	-99.7	-0.623
$\eta$	-138	-24.3	-0.152
$\theta$	143	50.6	0.316

### 6.6.4 Modified cubic diamond referred to cubic axes

All that remains is to collect together the modified expressions for the different categories of elastic constant. Powers of  $4/a$  in the unmodified expressions for the inner elastic constants and the internal strain arose from components of the unstretched bond and are replaced here by powers of  $\sqrt{3}/r_0$ . At the second order

$$\begin{aligned}
C_{11} &= \frac{a}{2}(\alpha + 3\beta^* - 2\sigma + 3\tau) \\
C_{12} &= \frac{a}{2}(\alpha - \beta^* - 2\sigma + 3\tau) \\
B &= \frac{a}{2}(\alpha + \frac{1}{3}\beta^* - 2\sigma + 3\tau) \\
C_{44}^0 &= \frac{a}{2}(\alpha + \beta^* - 2\sigma - \tau) \\
D_{14} &= \frac{a\sqrt{3}}{2r_0}(\alpha - \beta^* - \tau) \\
E_{11} &= \frac{a}{2r_0^2}(\alpha + \beta^* + 2\sigma - \tau) \\
A_{14} &= -\frac{r_0}{\sqrt{3}}\left(\frac{\alpha - \beta^* - \tau}{\alpha + \beta^* + 2\sigma - \tau}\right) \\
\zeta_K &= -\frac{\sqrt{3}}{r_0}A_{14}
\end{aligned} \tag{6.44}$$

where  $r_0$  is the equilibrium bond length. Also

$$E_{111}^{(2)} = E_{112}^{(2)} = \frac{a}{2r_0^2}(\alpha - \beta^* + 2\sigma + 3\tau) \tag{6.45}$$

represent the anharmonic contribution to the harmonic energy.

At the third order

$$\begin{aligned}
C_{111} &= \frac{3a^3}{16}(\gamma - \delta + 6\epsilon - 2\eta - \theta + 6\xi) \\
C_{112} &= \frac{a^3}{16}(3\gamma - 3\delta + 2\epsilon - 6\eta - 3\theta + 18\xi) \\
C_{123} &= \frac{3a^3}{16}(\gamma + 3\delta - 2\epsilon - 2\eta - \theta + 6\xi) \\
C_{144}^0 &= \frac{a^3}{16}(3\gamma + 3\delta - 2\epsilon - 6\eta + \theta + 2\xi) \\
C_{155}^0 &= \frac{a^3}{16}(3\gamma - 3\delta + 6\epsilon - 6\eta - 3\theta + 2\xi) \\
C_{456}^0 &= \frac{3a^3}{16}(\gamma - 2\eta + \theta - 2\xi) \\
D_{114} &= \frac{a^3\sqrt{3}}{16r_0}(3\gamma - 3\delta - 2\epsilon - 2\eta + 3\theta + 2\xi) \\
D_{124} &= \frac{a^3\sqrt{3}}{16r_0}(3\gamma + 3\delta - 2\epsilon - 2\eta + \theta + 2\xi)
\end{aligned} \tag{6.46}$$

$$\begin{aligned}
D_{156} &= \frac{a^3 \sqrt{3}}{16 r_0} (3\gamma - 2\eta + \theta - 6\xi) \\
E_{111}^{(3)} &= \frac{a^3}{16 r_0^2} (3\gamma + 3\delta + 6\epsilon + 2\eta + 5\theta + 2\xi) \\
E_{112}^{(3)} &= \frac{a^3}{16 r_0^2} (3\gamma - 3\delta - 2\epsilon + 2\eta + \theta + 2\xi) \\
E_{126} &= \frac{a^3}{16 r_0^2} (3\gamma + 2\eta - \theta - 6\xi) \\
F_{123} &= \frac{a^3}{16 r_0^3} (3\gamma + 6\eta - 3\theta - 6\xi).
\end{aligned}$$

The full  $E_{111}$  and  $E_{112}$  are then given by

$$\begin{aligned}
E_{111} &= E_{111}^{(2)} + E_{111}^{(3)} \\
E_{112} &= E_{112}^{(2)} + E_{112}^{(3)}
\end{aligned} \tag{6.47}$$

as before.

## 6.7 Summary

The original goal of finding a simple model to characterize both the harmonic and anharmonic aspects of the elasticity of diamond has been achieved: the 4/5-parameter harmonic model provides an excellent fit to the second-order experimental data and the 5-parameter anharmonic fitting predicts third-order elastic constants that are in reasonable agreement with both a previous 3-parameter model and an *ab initio* calculation. Fewer parameters always lead to a poorer fit.

The single unexpected outcome has been the implication, supported by an earlier *ab initio* calculation, that the internal strain parameter,  $\zeta_K$ , is possibly even smaller than observed, where it is already less than 25% of the values found for other group IV elements and III-V semiconductors.

Finally the Keating model has been recast in a form that makes the parameters characteristic of the bonds alone, and not dependent on the dimensions of the unit cell chosen to describe the structure. This means that the elasticity of *c*D can be referred to rhombohedral axes without altering the model parameters and that these parameters can be transferred unchanged to *h*D, as exemplified in Chapter 8.

## References

- [1] E. Anastassakis, A. Cantarero and M. Cardona, *Phys. Rev.* **B41**, 7529 (1990)
- [2] V. K. Bashenov, D. I. Marvakov and A. M. Mutal, *phys. stat. sol. (b)* **86**, K7, (1978)
- [3] M. I. Bell, *phys. stat. sol. (b)* **53**, 675 (1972)

- 
- [4] F. Cerdeira, C. J. Buchenauer, F. H. Pollak and M. Cardona, *Phys. Rev.* **B5**, 580 (1972)
- [5] C. S. G. Cousins, *J. Phys. C*, **1**, 835 (1968)
- [6] C. S. G. Cousins, L. Gerward, J. Staun Olsen and B. J. Sheldon,  
*J. Phys.:Condens.Matter* **1**, 4511 (1989)
- [7] C. S. G. Cousins, *J. Phys. C: Solid State Phys.*, **15**, 1857 (1982)
- [8] M. H. Grimsditch, E. Anastassakis and M. Cardona, *Phys. Rev.* **B18**, 901 (1978)
- [9] J. R. Guth, A. C. Hess, P. F. McMillan and W. T. Petuskey,  
*J. Phys.:Condens. Matter* **2**, 8007 (1990)
- [10] P. N. Keating, *Phys. Rev.* **145**, 637 (1966)
- [11] P. N. Keating, *Phys. Rev.* **149**, 674 (1966)
- [12] J. W. Martin, *J. Phys. C:Solid St. Phys.* **8**, 2858 (1975)
- [13] R. M. Martin, *Phys. Rev.* **B1**, 4005 (1970)
- [14] H. L. McMurry, A. W. Solbrig, Jr., J. K. Boyter and C. Noble,  
*J. Phys. Chem. Solids* **28**, 2359 (1967)
- [15] H. J. McSkimin and P. Andreatch, Jr., *J. Appl. Phys.* **43**, 2944 (1972)
- [16] M. J. P. Musgrave and J. A. Pople, *Proc. Roy. Soc. A***268**, 474 (1962)
- [17] O. H. Nielsen, *Physica* **139 & 140B**, 202 (1986); *Phys. Rev.* **B34**, 5808 (1986)
- [18] J. Nye, *Physical Properties of Crystals*, (Oxford: University Press, 1957 and, with additional material, 1985)
- [19] H. Rucker and M. Methfessel, *Phys. Rev.* **B52**, 11059 (1995)
- [20] A. K. Sood, E. Anastassakis and M. Cardona, *Phys. Stat. Sol. (b)* **129**, 505 (1985)
- [21] Z. Sui and I. P. Herman, *Phys. Rev.* **B48**, 17938 (1993)
- [22] R. N. Thurston and K. Brugger, *Phys. Rev.* **133**, A1604 (1964)
- [23] R. Tubino, L. Piseri and G. Zerbi, *J. Chem. Phys.* **56**, 1022 (1972)
- [24] D. Vanderbilt, S. H. Taole and S. Narasimhan, *Phys. Rev.* **B40**, 5657 (1989)
- [25] J. L. Warren, R. G. Wenzel and J. L. Yarnell, *Inelastic Scattering of Neutrons* (IAEA, Vienna, 1965), Vol. 1, p. 361

## Chapter 7

### Hexagonal graphite: review of data, previous calculations and a fit to the modified anharmonic Keating model

#### 7.1 Introduction

The (almost?) exclusive use of the Keating formalism in connection with cubic diamond- and zinc-blende-structure materials has led to its identification as a model of the covalent bond. In fact there is no ‘physical’ content in the Keating model—it is simply a way of associating strain derivatives of energy with the structural variables, interatomic separations and angles, that are thought likely to be significant for whatever reason. In this Chapter I extend the modified Keating model to hexagonal graphite.

The elasticity of *hG* is a challenge from both theoretical and experimental points of view on account of the extreme anisotropy of the structure. If the elasticity of *cD* is referred to cartesian axes with  $Ox_1 \parallel [1\bar{1}0]$  and  $Ox_3 \parallel [111]$  the greater part of the resulting quasi-rhombohedral set of elastic constants (given in full in Chapter 6, Tables 6.5 and 6.6) may be compared directly to the *hG* set. Both the differences and the similarities are startling: *hG*'s  $C_{33}$  at 38 GPa is a mere 3% of its *cD* equivalent, 1212 GPa, whilst the combination that relates to uniform strain within layers,  $C_{11} + C_{12}$ , is 1240 GPa in *hG* and 1270 GPa in *cD*. Thus *hG* is as stiff as *cD* within a layer but 30 times more compliant between layers. A consequence of this is the ease with which irregularity of stacking can take place and accounts for the fact that single crystalline regions of natural graphite are always both limited in extent and contain a mixture of the hexagonal and rhombohedral forms. Such material cannot be used for ultrasonic determinations of elastic constants but, in powder form, can be compressed and changes in the lattice parameters followed by X-ray diffraction, [22, 27]. In this way both second- and third-order compressibilities may be determined.

Second-order elastic constants may be obtained from ultrasonic experiments on compression-annealed pyrolytic graphite, [5, 11, 12]. This material consists of layers that are stacked with high precision (*c*-axes parallel within  $0.5^\circ$ ) but whose *a*-axes are distributed at random. In spite of this it is still possible to find the single-crystal constants because second-order elasticity is isotropic in the basal plane, rendering the randomness invisible. This isotropy does not extend to the third-

order elastic constants. Since the latter are usually measured by determining the uniaxial stress dependence of ultrasonic wave velocities through single crystals it is unlikely that they will be determined directly in the foreseeable future. Some combinations may be determined indirectly through the pressure dependence of the second-order constants, however.

The theoretical challenge arises from two sources. Firstly there is the relative complexity of the structure. The basis consists of four atoms, none of which occupies a site with inversion symmetry. Thus, as shown in Chapters 4 and 5, there are numerous inner elastic constants besides the 5 independent second-order and 10 independent third-order constants for a material belonging to Laue group HI. To extract a full complement of components using any model in which the energy is not a simple function of interatomic separations, unit cell volume etc., requires the calculation of the energy for more than 280,000 configurations! This makes the development of a parametrization of the bonding in *hG* highly desirable.

Secondly there is the anisotropy. It is often reasonable in the case of close-packed structures, such as the FCC and the HCP, to fit Lennard-Jones potentials to second-order elastic constants and to transfer the parameters to defect situations. This cannot be done for *hG*: there is no way to define a pair potential that can represent a binding energy of 5 eV/atom and a nearest-neighbour distance 1.42 Å within a layer as well as the values 0.02 eV/atom and 3.35 Å between layers, [7]. To improve the situation an empirical potential for carbon invoking 3-body contributions was introduced by Stillinger and Weber, [36], and Tersoff produced another that takes variable atomic coordination into account *via* a many-body term, [38], giving a reasonable account of the in-plane bonding. This was extended by Nordlund *et al.*, [34], who added an interaction to accommodate the weak interlayer bonding. A further development, due to Heggie, [19], resulted in a carbon potential capable of interpolating smoothly between  $sp^2$  and  $sp^3$  configurations. Part of this potential involved Keating-like terms, though these were limited to just the bond-stretching and bond-bending ones of the original [23] model. As the development and optimization of a Keating model has been so successful for *cD*, [3, 15, 23, 24] (and Chapter 6!) I felt it worthwhile to extend the ideas to *hG*. The elastic constants fall into two groups: one contributed to principally by the  $sp^2$ -bonding interactions within the graphene planes and the other by  $\pi$ -bonding between planes.

In Sec. 7.2 I review the experimental data and justify my model. The development of the model is carried out in Sec. 7.3 and the fitting and the results are presented and discussed in Sec. 7.4.

## 7.2 Modelling the elasticity

### 7.2.1 Appraisal of input data

#### 7.2.1.1 *At the second order*

The five second-order elastic constants of pyrolytic graphite were determined by Blakslée *et al.* [5] and three of these are taken as target values here. Revised values are used for  $C_{13}$  and  $C_{44}$ .

Values for  $C_{44}$  ranged from 0.18 to 0.35 GPa and are very small. They arise from the anomalously low velocities of transverse ultrasonic waves propagated along the  $c$ -axis and stem from the mobility of dislocations. When the latter is eliminated by neutron irradiation values up to 5 GPa are found. The high values are believed to be characteristic of ideal single crystal material. Sensitivity to the state of the crystal has been demonstrated by Grimsditch [16] using Brillouin surface scattering. He confirms the value  $5.05 \pm 0.35$  GPa found earlier for a sample of natural graphite [17] and confirms also what appeared at first sight to be a contradictory value  $3.25 \pm 0.015$  GPa, reported in [26] for highly oriented pyrolytic graphite. The difference is consistent with the influence of crystallite grain size on the speed of surface waves. The higher value has been adopted here.

Zhao and Spain [41] have used their compressibility data to probe the *linear* modulus  $B_a$  ( $\equiv 1/k_a$ ) and present a case for raising the value of  $C_{13}$  from 15 GPa to  $22 \pm 2$  GPa. Unfortunately they have inadvertently used the expression for the *planar* modulus! If their procedure is carried through correctly the value of  $C_{13}$  is lowered to  $7.9 \pm 3.5$  GPa.

Five of the six zone-centre optic mode frequencies are known of which two can be converted directly to inner elastic constant values. The  $E_{1u}$  mode [30, 31] at  $1587 \text{ cm}^{-1}$  (47.58 THz) gives  $E_{11}^{12} = 253.0 \text{ GPa } \text{\AA}^{-2}$  and the  $A_{2u}$  mode [32] at  $868 \text{ cm}^{-1}$  (26.0 THz) gives  $E_{33}^{12} = 75.66 \text{ GPa } \text{\AA}^{-2}$ .

### 7.2.1.2 At the third order

The anharmonic part of the potential determines the non-linear part of the compressibility and the pressure derivatives of the second-order constants and of the zone-centre optic mode frequencies.

The early work on the compressibility of graphite carried out by Lynch and Drickamer [27] has been examined and their tabulated values of  $a/a_0$  and  $c/c_0$  fitted to quartics in  $p$ . This gives for the linear compressibilities  $k_a = 14.4 \times 10^{-4} \text{ GPa}^{-1}$  and  $k_c = 2.24 \times 10^{-2} \text{ GPa}^{-1}$ . The former value is high compared to that derived by inversion of the  $C_{IJ}$ ,  $6.4 \times 10^{-4} \text{ GPa}^{-1}$ , and casts some doubt on the  $a(p)$  measurements. The value of  $k_c$  is much closer to the inversion value of  $2.7 \times 10^{-2} \text{ GPa}^{-1}$ . Other experiments [5, 12] gave  $(2.68 \pm 0.13) \times 10^{-2} \text{ GPa}^{-1}$  and  $(2.4 \pm 0.2) \times 10^{-2} \text{ GPa}^{-1}$ . The non-linear compressibilities are  $K_a = 2.8 \times 10^{-4} \text{ GPa}^{-2}$  and  $K_c = 4.66 \times 10^{-3} \text{ GPa}^{-2}$ . This value of  $K_a$  is actually rather large and indicates a perceptible non-linearity in the in-plane compressibility. Kelly [25] observes that this non-linear variation of  $a$  cannot be correct in the light of the work of Hershbach and Laurie [20], in which indirect information on the anharmonicity of in-plane bonds is obtained by analysing C-C bond force constants. Zhao and Spain [41] report that the pressures in [27] are probably overestimated increasingly with higher pressure, thereby introducing the suspect non-linearity into the pressure dependence of  $a$ . Their own work shows no such behaviour.

A more recent study of finely ground natural graphite by Hanfland *et al.* [18] presents com-

compressibility data *via* a one-dimensional analogue of the Murnaghan equation of state [29]:

$$r/r_0 = [(\beta'/\beta_0)p + 1]^{-1/\beta'}$$

where  $r$  is  $a$  or  $c$ ,  $\beta_0^{-1} = -(d \ln r / dp)_{p=0} = k_r$  is the linear compressibility and  $\beta'$  is the pressure derivative of  $\beta$ . The values  $k_a = 8.0 \times 10^{-4} \text{ GPa}^{-1}$  and  $k_c = 2.8 \times 10^{-2} \text{ GPa}^{-1}$  are implied. Expansion of the above expression to second order in  $p$  leads to the identification

$$\beta' = -2 + \frac{K_r}{k_r^2}$$

and their value of 10.8 for  $\beta'$  when  $r = c$  then implies that  $K_c = 10.0 \times 10^{-3} \text{ GPa}^{-2}$ .

The full set of pressure derivatives of second-order elastic constants was first presented by Gauster and Fritz [11]. The value of  $C'_{44}$  at 0.0023 was problematic, like  $C_{44}$  a victim of dislocation mobility. A later study [12] reassesses the derivative to be  $0.81 \pm 0.15$  and also raises the earlier value of  $C'_{33}$  from 9.6 to  $14.6 \pm 1.1$ .

The Raman shifts under pressure of the  $E_{2g}$  modes have been measured [18] and yield  $df/dp$  of 0.140 and 0.145  $\text{THz}(\text{GPa})^{-1}$  for the  $E_{2g2}$  and  $E_{2g1}$  modes respectively. Similar measurement [2] on the  $B_{1g1}$  mode gives  $df/dp = 0.572 \text{ THz}(\text{GPa})^{-1}$ .

### 7.2.2 Justification of model

As indicated in the Introduction it is the large anisotropy of graphite that makes the modelling of elastic constants particularly difficult. Most early work, as reviewed in Kelly, [25], concentrated on explaining the interlayer constants,  $C_{33}$ ,  $C_{44}$  and their pressure derivatives. In particular the experimental work of Blakslee *et al.* [5] and Green *et al.* [12] was followed by theoretical studies using, firstly, simple pairwise potentials (Lennard-Jones and exponential core) in [13] and, secondly, parabolic and other band models for the electronic contributions to the constants in [14].

In a separate investigation I have used the Ewald summation technique [10] to calculate the full spectrum of contributions to elastic and inner elastic constants through third order for all inverse powers of atomic separation from  $n = 4$  to  $n = 14$ . It was impossible (a) to combine any two of these in such a way that the structure was in equilibrium at the observed lattice parameters, i.e. with the first-order constants  $C_1$  and  $C_3$  simultaneously zero, or (b) to combine any three in such a way that  $C_1 = C_3 = 0$  without  $C_{33}$  being negative and  $C_{44}$  always far too small or negative. In addition all zone-centre optic mode frequencies involving the  $E_{33}^{\lambda\mu}$  were imaginary.

The notion that elastic constants may be simulated by *any* combination of pair potentials can be ruled out by reference to one of the two second-order Cauchy relations. Central forces within the graphene planes imply  $C_{11}^0 = 3C_{12}^0$ . The observed values are  $C_{11} = C_{11}^0 - \Delta = 1060 \text{ GPa}$  and  $C_{12} = C_{12}^0 + \Delta = 180 \text{ GPa}$ , where  $\Delta$  is the internal strain contribution. This gives  $C_{11}^0 = 930 \text{ GPa}$ ,  $C_{12}^0 = 310 \text{ GPa}$  and  $\Delta = -130 \text{ GPa}$ . A value of  $|\Delta|$  equal to 40% of  $C_{12}^0$  is unreasonably large, implying enormous internal strain in total contrast to  $cD$  where it is very small. Thus one expects

strong non-central forces within the layers. The second relation is  $C_{13} = C_{44}$ . As shown above the relevant values are  $C_{13} = 7.9 \pm 3.5$  GPa and  $C_{44} = 5.05 \pm 0.35$  GPa. Within the large experimental error the Cauchy relation is satisfied although the quoted value of  $C_{13}$  exceeds that of  $C_{44}$  by 60%. I therefore suspect and assume the presence of weak non-central forces between the layers.

Nemanich *et al.* [32] who reported the first experimental determination of the  $A_{2u}$  mode frequency,  $868 \text{ cm}^{-1}$ , drew attention to previous calculations based on various force field models in which frequencies in a wide range from  $600 \text{ cm}^{-1}$  to  $1300 \text{ cm}^{-1}$  were predicted. They asserted that the nature of the lattice dynamics of graphite is such that even a valence force model with bond-stretching, bond-bending and three-body terms cannot describe the  $A_{2u}$  mode: a four-body force, characterized by a puckering of the layer planes, is required. This problem is not found with the model developed here.

Nemanich *et al.* [30] measured the  $E_{2g2}$  frequency as well as that of the  $E_{1u}$  mode and found the splitting between them to be 150 GHz. They argued that to fit the  $\omega(E_{1u}) > \omega(E_{2g2})$  observation it is necessary to include second-nearest-neighbour out-of-plane interactions, a conclusion supported by Al-Jishi and Dresselhaus in their lattice-dynamical model [1]. Such interactions are included in this development.

### 7.3 The modified Keating model

The structure of  $hG$  is shown in Fig. 7.1 and fully described in Chapter 4.

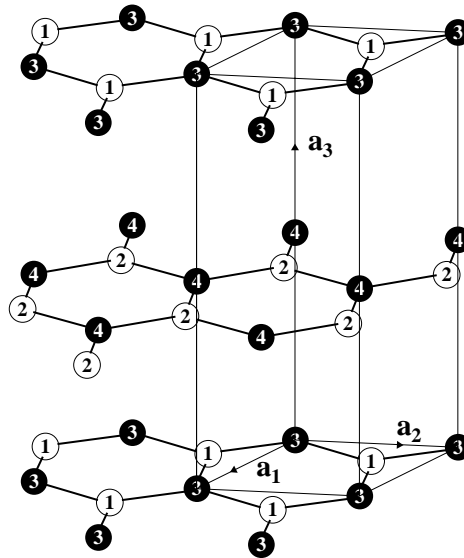


Figure 7.1: The structure of  $hG$  with a unit cell indicated.

I also use Bernal notation [4] in which the inequivalent sites are designated A (sublattices 3 and 4) and B (sublattices 1 and 2).

### 7.3.1 The strain variables

With four atoms in the basis the strain variables are more complicated than those of cD because of the three distinct inner displacement vectors,  $\vec{\zeta}^\lambda$ . The strains may be expressed as

$$\Delta_{ii} = 2r_p^{i0} \eta_{pq} r_q^{i0} + 2r_p^{i0} z_p^\pi + z_p^\pi z_p^\pi \quad (7.1)$$

and

$$\Delta_{ij} = 2r_p^{i0} \eta_{pq} r_q^{j0} + r_p^{i0} z_p^\rho + r_p^{j0} z_p^\pi + z_p^\rho z_p^\pi \quad (7.2)$$

where terms of order three and higher have been omitted and the significance of  $\vec{z}^\pi$  and  $\vec{z}^\rho$  is as follows. Consider the reference atom belonging to sublattice 2 in the central layer in Fig. 7.2. It has three bonds to atoms on sublattice 4 within the layer and four sets of three bonds to sublattices 1 and 3 in the layers above and below. When  $i$  refers to sublattice 1  $\vec{z}^\pi = -\vec{\zeta}^1$  (minus because a positive value indicates 2 relative to 1, 3 relative to 2 or 1, or 4 relative to 3, 2 or 1). Similarly when  $i$  refers to sublattice 3  $\vec{z}^\pi = +\vec{\zeta}^2$  and when it refers to sublattice 4 then  $\vec{z}^\pi = \vec{\zeta}^2 + \vec{\zeta}^3$  because ‘4 relative to 2’ is equivalent to ‘3 relative to 2’ plus ‘4 relative to 3’. Similarly for  $j$  and  $\vec{z}^\rho$ , and for the remaining reference atoms.

### 7.3.2 The model parameters

The electronic structure of graphite is successfully approached by the Slonczewski-Weiss-McClure (SWMcC) model [8, 9, 28, 35, 37] and leads to a parametrization in which the energy of  $\pi$ -bonding is associated with various vectors (AA', AB', BA' and BB') between adjacent layers, vectors (AA'' and BB'') between alternate layers, and with the nearest-neighbour in-plane vectors (AB and BA). Table 7.1 shows the SWMcC parameters deduced by Charlier, Gonze and Michenaud [8] in their first-principles study of the electronic properties of hG, together with a brief indication of

Table 7.1: The SWMcC model parameters  $\gamma_i$  (data and attribution taken from [8]) and the bond interactions selected for the Keating model.

$\gamma_i$	Value (eV)	Arising from	Bond-stretching	Bond-bending
$\gamma_0$	2.598	AB and BA in-plane interactions	AB BA	AB/AB BA/BA
$\gamma_1$	0.364	AA' interlayer interactions (determines width of $\pi$ bands at the K point)	AA'	AA'/AB'
$\gamma_4$	0.177	AB' and BA' interlayer interactions	AB' BA'	AB'/AB' BA'/BA'
$\gamma_3$	0.319	BB' interlayer interactions	BB'	BB'/BA'
$\gamma_5$	0.036	AA'' alternate layer interactions		
$\gamma_2$	-0.014	BB'' alternate layer interactions (determines $\pi$ band overlap)		
$\gamma_6$	-0.026	Chemical shift between A and B atoms		

the significance of these parameters, as given in their Appendix. This provides a guide to selecting specific sets of vectors to parametrise the elasticity of  $hG$ . Corresponding to the four largest parameters I focus initially on four sets: one planar and three interlayer.

1. The planar part of the energy per cell is modelled analogously to  $cD$ . The three nearest-neighbour A atoms to a B atom, see upper right portion of Fig. 7.2, give rise to three 2-body ‘bond-stretching’  $BA_i$  interactions, three 3-body ‘bond-bending’  $BA_i BA_j$  interactions and various couplings between them. The same number of interactions arise from each A atom. Up to four harmonic parameters ( $\alpha$ ,  $\beta$ ,  $\sigma$  and  $\tau$ ) and six anharmonic parameters ( $\gamma$ ,  $\delta$ ,  $\epsilon$ ,  $\eta$ ,  $\theta$  and  $\xi$ ) may be needed here.

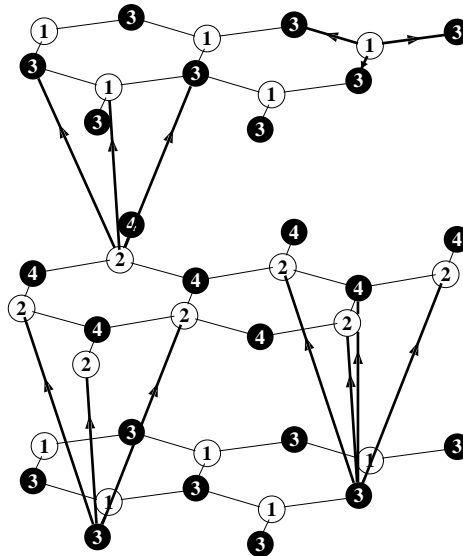


Figure 7.2: Configurations of bonds in the Keating model. Filled atoms are Bernal type A, empty atoms are type B. Upper right: three in-plane BA bonds. Lower right: an  $AA'$  and three  $AB'$  bonds. Lower left: three  $AB'$  bonds. Upper left: a  $BB'$  and two  $BA'$  bonds. The associated interactions are described in the text.

2. This set comprises the 2-body  $AA'_i$  interaction between nearest-neighbours (NN) in adjacent planes, see lower right portion of Fig. 7.2, and the 3-body interactions that couple the  $AA'_i$  with the three neighbouring oblique interlayer vectors  $AB'_j$ . Up to ten more parameters may be needed (with superscript ').
3. This set comprises the three 2-body  $AB'_i$  next-nearest neighbour (NNN) interlayer interactions and the three 3-body interactions involving  $AB'_i AB'_j$  pairs, see lower left portion of Fig. 7.2, together with the symmetrical group of 2-body  $BA'_i$  and 3-body  $BA'_i BA'_j$  interactions. Up to ten more parameters may be needed (with superscript '').
4. This set comprises the three 2-body  $BB'_i$  interaction between nearest-neighbours in adjacent

planes and the 3-body interactions that couple each  $BB'_i$  with the two closest neighbouring oblique interlayer vectors  $BA'_j$  see upper left portion of Fig. 7.2.

These sets are also shown in Table 7.1 in line with the SWMcC parameters  $\gamma_i$  with which they are associated. One set can be discarded, however, because of geometrical interdependence. This arises as follows. Starting and finishing at a B site there are several loops of four vectors, symbolically  $BB' + B'A + AA' + A'B = 0$ , which may be used to express all  $\Delta_{ii}$  and  $\Delta_{ij}$  belonging to set 4 in terms of the strain variables of the other three sets.

With a possible 12 harmonic and 18 anharmonic parameters arising from the remaining three sets I am loth to introduce the  $AA''$  and  $BB''$  interactions. In fact these involve vectors joining pairs of atoms on the same sublattice and their 'bond-stretching' aspect thus makes no contribution to the inner elastic constants.

### 7.3.3 The energy

The three sets of parameters defined above, together with the bookkeeping, result in expressions considerably lengthier than those relating to cD. Not all terms are destined for use. In keeping with the streamlining introduced in the modified model all numerical coefficients are unity. The halves outside the summations compensate for double counting. The second-order energy per unit cell is

$$\begin{aligned}
 E^{(2)} = & \frac{1}{2} \sum_{s=1}^4 \sum_{i=1}^3 \left( \alpha \Delta_{ii}^2 + \sum_{j=1}^3 ' (\beta \Delta_{ij}^2 + \sigma (\Delta_{ii} + \Delta_{jj}) \Delta_{ij} + \tau \Delta_{ii} \Delta_{jj}) \right. \\
 & \left. + \alpha'' \Delta_{ii}^2 + \sum_{j=1}^3 ' (\beta'' \Delta_{ij}^2 + \sigma'' (\Delta_{ii} + \Delta_{jj}) \Delta_{ij} + \tau'' \Delta_{ii} \Delta_{jj}) \right) \\
 & + \frac{1}{2} \sum_{s=3}^4 \sum_{i=1}^2 \left( \alpha' \Delta_{ii}^2 + \sum_{j=1}^3 (\beta' \Delta_{ij}^2 + \sigma' (\Delta_{ii} + \Delta_{jj}) \Delta_{ij} + \tau' \Delta_{ii} \Delta_{jj}) \right). \quad (7.3)
 \end{aligned}$$

The third-order energy per unit cell is

$$\begin{aligned}
 E^{(3)} = & \frac{1}{2} \sum_{s=1}^4 \sum_{i=1}^3 \left( \gamma \Delta_{ii}^3 + \sum_{j=1}^3 ' (\delta \Delta_{ij}^3 + \epsilon (\Delta_{ii} + \Delta_{jj}) \Delta_{ij}^2 \right. \\
 & \left. + \eta (\Delta_{ii}^2 + \Delta_{jj}^2) \Delta_{ij} + \theta \Delta_{ii} \Delta_{ij} \Delta_{jj} + \xi \Delta_{ii} \Delta_{jj} (\Delta_{ii} + \Delta_{jj}) \right) \\
 & + \gamma'' \Delta_{ii}^3 + \sum_{j=1}^3 ' (\delta'' \Delta_{ij}^3 + \epsilon'' (\Delta_{ii} + \Delta_{jj}) \Delta_{ij}^2 \\
 & \left. + \eta'' (\Delta_{ii}^2 + \Delta_{jj}^2) \Delta_{ij} + \theta'' \Delta_{ii} \Delta_{ij} \Delta_{jj} + \xi'' \Delta_{ii} \Delta_{jj} (\Delta_{ii} + \Delta_{jj}) \right) \\
 & + \frac{1}{2} \sum_{s=3}^4 \sum_{i=1}^2 \left( \gamma' \Delta_{ii}^3 + \sum_{j=1}^3 (\delta' \Delta_{ij}^3 + \epsilon' (\Delta_{ii} + \Delta_{jj}) \Delta_{ij}^2 \right. \\
 & \left. + \eta' (\Delta_{ii}^2 + \Delta_{jj}^2) \Delta_{ij} + \theta' \Delta_{ii} \Delta_{ij} \Delta_{jj} + \xi' \Delta_{ii} \Delta_{jj} (\Delta_{ii} + \Delta_{jj}) \right). \quad (7.4)
 \end{aligned}$$

## 7.3.4 The elastic constants

Every independent elastic and inner elastic constant has been obtained in terms of these parameters by applying the generalized method of homogeneous deformation (described in Appendix A) to a unit contribution of each Keating parameter in turn. Writing each constant  $M_i$  as a linear combination of Keating parameters  $K_j$  with coefficients  $\mu_j$  and a common factor  $F_i$ :  $M_i = F_i \times \sum \mu_j K_j$  gives the results set out in Tables 7.2, 7.3 and 7.4.

Table 7.2: Coefficients of the modified Keating parameters in the second-order partial and inner elastic constants. The common factors are expressed in terms of the lattice parameter  $a = 2.46 \text{ \AA}$  and the interlayer spacing  $d = 3.3495 \text{ \AA}$ .  $t$  stands for  $\sqrt{3}$ .

	Factor	Planar				Interlayer: NN				Interlayer: NNN			
		$\alpha$	$\beta$	$\sigma$	$\tau$	$\alpha'$	$\beta'$	$\sigma'$	$\tau'$	$\alpha''$	$\beta''$	$\sigma''$	$\tau''$
$C_{11}^0$	$2ta^2/3d$	1	1	-2	1					2	2	-4	2
$C_{12}^0$	$2ta^2/9d$	1	-1	-2	5					2	-2	-4	10
$C_{13}$	$4td/3$							2	2	4	-4	4	8
$C_{33}$	$16td^3/a^2$					$\frac{1}{3}$	2	4	2	2	4	8	4
$C_{44}$	$4td/3$						1	2		4	2	4	-4
$D_{16}^1$	$a/3d$	2	-2	-1	-2					4	-4	-2	-4
$D_{16}^3$	$a/3d$	-2	2	1	2			2		4	-4	-2	-4
$E_{11}^{11}$	$2t/3d$	2	1	2	-2					4	2	4	-4
$E_{11}^{12}$	$2t/3d$	2	1	2	-2					4	2	4	-4
$E_{11}^{13}$	$2t/3d$							1		4	2	4	-4
$E_{11}^{33}$	$2t/3d$	2	1	2	-2			2	2	4	2	4	-4
$E_{33}^{11}$	$4td/a^2$						1	2		4	8	16	8
$E_{33}^{12}$	$4td/a^2$						1	2		4	8	16	8
$E_{33}^{13}$	$4td/a^2$						2	4	2	4	8	16	8
$E_{33}^{33}$	$4td/a^2$					$\frac{4}{3}$	5	10	4	4	8	16	8
$E_{111,112,331}^{11(2)}$	$2t/3d$	2	-2	2	4					4	-4	4	8
$E_{111,112,331}^{12(2)}$	$2t/3d$	2	-2	2	4					4	-4	4	8
$E_{111,112,331}^{13(2)}$	$2t/3d$							1		4	-4	4	8
$E_{111,112,331}^{33(2)}$	$2t/3d$	2	-2	2	4			2	4	4	-4	4	8
$E_{113,333}^{11(2)}$	$8td/a^2$							1	1	2	4	8	4
$E_{113,333}^{12(2)}$	$8td/a^2$							1	1	2	4	8	4
$E_{113,333}^{13(2)}$	$8td/a^2$						1	2	1	2	4	8	4
$E_{113,333}^{33(2)}$	$8td/a^2$					$\frac{2}{3}$	2	5	1	2	4	8	4

The common factors have been expressed in terms of the interlayer spacing  $d$  rather than the lattice parameter  $c$  to facilitate comparison with the treatment of  $rG$  in Chapter 9.

Table 7.3: Coefficients of the modified Keating parameters in the third-order partial elastic constants and the  $D$  and  $F$  tensors. Numerical data as for Table 7.2

Factor	Planar						Interlayer: NN						Interlayer: NNN					
	$\gamma$	$\delta$	$\epsilon$	$\eta$	$\theta$	$\xi$	$\gamma'$	$\delta'$	$\epsilon'$	$\eta'$	$\theta'$	$\xi'$	$\gamma''$	$\delta''$	$\epsilon''$	$\eta''$	$\theta''$	$\xi''$
$C_{111}^0$	$ta^4/d$	1	-1	2	-2	-1	2						2	-2	4	-4	-2	4
$C_{113}^0$	$8ta^2d/3$								1	1			3	3	-2		-1	8
$C_{133}$	$32td^3/3$								1	2	1	3	3	-3		6	3	12
$C_{333}$	$32td^5/a^2$							1	6	12	12	6	6	12	24	24	12	24
$C_{144}^0$	$2ta^2d/9$								1	4			12	-12	-6		12	24
$C_{244}^0$	$2ta^2d/3$								1	4			12		2		4	-8
$C_{344}$	$8td^3/3$								3	6	8	2	4	12	6	12	24	
$C_{166}^0$	$ta^4/9d$	3		2	-6	1	-2						6		4	-12	2	-4
$C_{266}^0$	$ta^4/9d$	1	-4	6	-2	-3	2						2	-8	12	-4	-6	4
$C_{366}^0$	$8ta^2d/9$								1	1			3	6			-3	
$D_{136}^1$	$4ad/3$									2	2		6	-6	-6	6	-3	
$D_{136}^3$	$4ad/3$									2	4	1	2	6	-6	-6	6	-3
$D_{145}^1$	$2ad/3$									1	4		12	-3	-6	12	-12	-24
$D_{145}^3$	$2ad/3$									3	5	8	12	-3	-6	12	-12	-24
$D_{211}^1$	$a^3/3d$	3	3	-2	-3	-1	2						6	6	-4	-6	-2	4
$D_{211}^3$	$a^3/3d$	-3	-3	2	3	1	-2				2		6	6	-4	-6	-2	4
$D_{222}^1$	$a^3/3d$	-5	-1	2	5	-1	2						-10	-2	4	10	-2	4
$D_{222}^3$	$a^3/3d$	5	1	-2	-5	1	-2						-10	-2	4	10	-2	4
$D_{314}^1$	$2ad/3$									1	4		12	-12	-12	12	-6	
$D_{314}^3$	$2ad/3$									3	8	2	8	12	-12	-12	12	-6
$F_{112}^{111}$	$a/3d$	12	-3	-6	12	-12	-24						24	-6	-12	24	-24	-48
$F_{112}^{112}$	$a/3d$	12	-3	-6	12	-12	-24						24	-6	-12	24	-24	-48
$F_{112}^{113}$	$a/3d$									4			24	-6	-12	24	-24	-48
$F_{112}^{123}$	$a/3d$									4			24	-6	-12	24	-24	-48
$F_{112}^{133}$	$a/3d$									2	8		24	-6	-12	24	-24	-48
$F_{112}^{223}$	$a/3d$	-12	3	6	-12	12	24				8		24	-6	-12	24	-24	-48
$F_{112}^{333}$	$a/3d$	-12	3	6	-12	12	24			6	6	12	24	-6	-12	24	-24	-48

Table 7.4: Coefficients of the modified Keating parameters in the third-order  $E$  tensors. Numerical data as for Table 7.2

	Factor	Planar					Interlayer: NN					Interlayer: NNN								
		$\gamma$	$\delta$	$\epsilon$	$\eta$	$\theta$	$\xi$	$\gamma'$	$\delta'$	$\epsilon'$	$\eta'$	$\theta'$	$\xi'$	$\gamma''$	$\delta''$	$\epsilon''$	$\eta''$	$\theta''$	$\xi''$	
$E_{111}^{11(3)}$	$ta^2/3d$	6		1		2	-4						12		2		4	-8		
$E_{111}^{12(3)}$	$ta^2/3d$	6		1		2	-4						12		2		4	-8		
$E_{111}^{13(3)}$	$ta^2/3d$												12		2		4	-8		
$E_{111}^{33(3)}$	$ta^2/3d$	6		1		2	-4						12		2		4	-8		
$E_{112}^{11(3)}$	$ta^2/9d$	6	-6	-3		6	12						12	-12	-6		12	24		
$E_{112}^{12(3)}$	$ta^2/9d$	6	-6	-3		6	12						12	-12	-6		12	24		
$E_{112}^{13(3)}$	$ta^2/9d$									2			12	-12	-6		12	24		
$E_{112}^{33(3)}$	$ta^2/9d$	6	-6	-3		6	12		2	4			12	-12	-6		12	24		
$E_{113}^{11(3)}$	$4td/3$									4	4		12	6	12	24				
$E_{113}^{12(3)}$	$4td/3$									4	4		12	6	12	24				
$E_{113}^{13(3)}$	$4td/3$								2	6	1	4	12	6	12	24				
$E_{113}^{33(3)}$	$4td/3$								6	8	8	2	4	12	6	12	24			
$E_{135}^{11(3)}$	$2td/3$								2	8			24	12	24	48				
$E_{135}^{12(3)}$	$2td/3$								2	8			24	12	24	48				
$E_{135}^{13(3)}$	$2td/3$								4	12	2	8	24	12	24	48				
$E_{135}^{31(3)}$	$2td/3$								3	6	12		24	12	24	48				
$E_{135}^{33(3)}$	$2td/3$								9	16	16	6	8	24	12	24	48			
$E_{331}^{11(3)}$	$4td/3$								1	4			12	-12		24	12	48		
$E_{331}^{12(3)}$	$4td/3$								1	4			12	-12		24	12	48		
$E_{331}^{13(3)}$	$4td/3$								2	6	1	4	12	-12		24	12	48		
$E_{331}^{33(3)}$	$4td/3$								5	8	6	16	12	-12		24	12	48		
$E_{333}^{11(3)}$	$8td^3/a^2$								3	6	8	2	4	12	24	48	48	24	48	
$E_{333}^{12(3)}$	$8td^3/a^2$								3	6	8	2	4	12	24	48	48	24	48	
$E_{333}^{13(3)}$	$8td^3/a^2$								6	12	12	6	12	12	24	48	48	24	48	
$E_{333}^{33(3)}$	$8td^3/a^2$								4	15	30	32	14	28	12	24	48	48	24	48

## 7.4 The fitting and the results

As there is only a limited amount of experimental data it is not possible to fit more than a few parameters. Even with an excellent match to all data there is no guarantee of uniqueness. At the second order the interlayer constants are fitted first. The primary target data, see Table 7.5, are  $C_{13}$ ,  $C_{33}$ ,  $C_{44}$  and  $E_{33}^{12}$ , deduced from the frequency of the  $A_{2u}$  mode.

Table 7.5: Target data for the harmonic part of the modified Keating model. Units are GPa for  $C_{IJ}$  and GPa  $\text{\AA}^{-2}$  for  $E_{ii}$ .

Target	Experiment	Assumed	Fit
$C_{13}$	$7.9 \pm 3.5^a$		7.9
$C_{33}$	$36.5 \pm 1.0^b$		36.5
$C_{44}$	$5.05 \pm 0.35^c$		5.05
$E_{33}^{12}$	$75.66 \pm 0.09^d$		75.663
$E_{33}^{11} - E_{33}^{12} + E_{33}^{33}$		75.65	75.65
$\frac{1}{2}(C_{11}^0 + C_{12}^0)$	$620. \pm 28.$		620.
$\frac{1}{2}(A_{16}^3 - A_{16}^1)$		-0.082	-0.082
' $\zeta_K$ '		0.115	0.115
$C_{11}^0$		1063.85	1063.85
$C_{12}^0$		176.15	176.15
$C_{11}$	$1060. \pm 20.^b$		1060.
$C_{12}$	$180. \pm 20.^b$		180.
$E_{11}^{12}$	$253.0 \pm 0.5^e$		253.0
$E_{11}^{11} - E_{11}^{12} + E_{11}^{33}$	$251.6 \pm 0.5^e$		251.6

<sup>a</sup> Re-evaluation of conclusion drawn in Ref. [41]

<sup>b</sup> Ref. [5]   <sup>c</sup> Ref. [16]   <sup>d</sup> Ref. [32]   <sup>e</sup> Ref. [30]

In addition the combination  $E_{33}^{11} - E_{33}^{12} + E_{33}^{33}$  is tentatively deduced from the values of the frequencies of the  $B_{1g1}$  and the  $B_{1g2}$  modes. No experimental value exists for the latter but in the lattice dynamical literature [1, 33] it is shown as nearly degenerate with the  $A_{2u}$  mode—so a close value has been assumed. Interlayer interactions are responsible for the splitting between the  $E_{1u}$  and  $E_{2g2}$  modes. A near-perfect fit is found by scanning possible sets of parameters interactively using *Mathematica* software [39]. The parameters so found contribute to both  $C_{11}^0$  and  $C_{12}^0$ . These values are subtracted from the observed values and, together with the frequency of the  $E_{1u}$  mode, are used to determine the planar parameters. A degree of freedom exists because the experimental data does not fix the (unknown) internal strain. In view of the extremely small value found in cD I set this arbitrarily so that  $\frac{1}{2}(A_{16}^3 - A_{16}^1)$ , which governs the in-plane inner displacement, was equal to -0.082 and equivalent to a quasi-Kleinman parameter  $\zeta_K$  of 0.115. The harmonic parameters are listed in the upper part of Table 7.7.

The anharmonic parameters were fitted by a similar process using the target data in Table 7.6. The quality of the experimental data is mixed and it was very difficult at first to find a realistic fit at all.

Table 7.6: Target data for the anharmonic part of the modified Keating model. Units are  $\text{GPa}^{-2}$  for the  $K_i$  and  $\text{THzGPa}^{-1}$  for the  $f'$ . The  $C'_{IJ}$  are dimensionless.

Target	Experiment	Assumed	Fit
$C'_{13}$	$3.1 \pm 0.5^a$		3.2
$C'_{33}$	$9.6 \pm 0.8^a$		
	$15.2 \pm 1.1^b$	14.6	12.9
$C'_{44}$	$0.81 \pm 0.15^b$		1.9
$f'(E_{2g1})$	$0.145 \pm 0.012^c$		0.147
$f'(B_{1g1})$	$0.572 \pm 0.020^d$		0.673
$C'_{11}$	$39.0 \pm 3.9^a$		39.0
$C'_{12}$	$11.0 \pm 1.1^a$		11.0
$f'(E_{2g2})$	$0.140 \pm 0.001^c$		0.140
$10^6 K_a$	$282^e$ $1.92^c$	O(7.5)	8.0
$10^3 K_c$	$4.66^e$ $10.0^c$	O(10)	11.9

<sup>a</sup>Ref. [11] <sup>b</sup>Ref. [41] <sup>c</sup>Ref. [18] <sup>d</sup>Ref. [2] <sup>e</sup>Ref. [27]

Eventual success depended on solving two problems. The first of these occurred in the interlayer fit where a value near to zero was always predicted for  $f'_3$ , the pressure dependence of the frequency of the  $E_{2g1}$  mode [18], one of the more reliable pieces of experimental information. It was resolved when it was realised that  $C'_{44}$  and  $f'_3$  have identical dependence on the Keating parameters and that a fit could be achieved by raising the target value of  $C'_{44}$  from 0.81 to 1.9, about 60% of  $C'_{13}$ . This appears to be totally reasonable in that  $C'_{44}$  is about 60% of  $C'_{13}$ . The quantities  $C'_{33}$  and  $f'_6$  are similarly linked. Remarkably only three interlayer parameters are required and none of them involves bond-bending. The second problem is the prediction of the third-order compressibilities  $K_a$  and  $K_c$ . The former is heavily dominated by  $C'_{133}$  and the latter by  $C'_{333}$ . Although these stiffnesses are fully determined by the interlayer parameters the planar fit has to be obtained before  $K_a$  and  $K_c$  can be found. There is no reliable value for  $K_a$  but I have assumed that it will be similar to that of  $cD$  in view of the great similarity of the planar elasticity of  $hG$  to that of  $cD$ , to which attention was drawn in the Introduction. Interlayer fits that were otherwise satisfactory were discriminated by the planar fit value of  $K_a$ .

The planar fit is based on  $C'_{11}$ ,  $C'_{12}$ ,  $f'_2$  and  $K_a$ . These involve the six parameters in only four combinations:  $2\gamma + 3\theta$ ,  $\delta$ ,  $\epsilon + \theta - 4\xi$  and  $\eta + 2\theta - 4\xi$ . In addition there is a linear relation between the four targets limiting the number of planar parameters to three. I have set  $\eta = \theta = \xi = 0$  and solved for  $\gamma$ ,  $\delta$  and  $\epsilon$ . The results of the anharmonic fitting are summarized in the lower half of Table 7.7.

Table 7.7: The modified Keating parameters. Note the smaller units for the anharmonic interlayer parameters.

	Planar		Interlayer					
	GPa Å <sup>-1</sup>	eV Å <sup>-4</sup>	GPa Å <sup>-1</sup>	eV Å <sup>-4</sup>		GPa Å <sup>-1</sup>	eV Å <sup>-4</sup>	
$\alpha$	266.21	1.662	$\alpha'$	39.55	0.2469	$\alpha''$	3.231	0.0202
$\beta$	240.53	1.501	$\beta'$	3.005	0.0188	$\beta''$	0.288	0.0018
$\sigma$	30.12	0.188	$\sigma'$	-5.037	-0.0314			
$\tau$	53.50	0.334	$\tau'$	-6.120	-0.0382	$\tau''$	1.447	0.0090
	GPa Å <sup>-3</sup>	eV Å <sup>-6</sup>	MPa Å <sup>-3</sup>	meV Å <sup>-6</sup>		MPa Å <sup>-3</sup>	meV Å <sup>-6</sup>	
$\gamma$	-687.13	-4.289	$\gamma'$	211.3	1.312	$\gamma''$	-35.62	-0.2247
$\delta$	-961.91	-6.004						
$\epsilon$	-365.19	-2.279				$\xi''$	-6.05	-0.0378

The most striking feature of the parameters overall is their relative size. The harmonic ones drop roughly an order of magnitude in going from set to set:  $\alpha$  to  $\alpha'$  to  $\alpha''$ , for example. Whilst this is expected on the basis of the relative sizes of the various second-order elastic constants it is no guide to the startling anharmonic patterns. Firstly the expected order of magnitude increase in passing from harmonic to anharmonic planar parameters,  $\alpha$  to  $\gamma$  say, is totally reversed for the two interlayer sets. Secondly it appears that  $\gamma'$  is more than 3000 times smaller than  $\gamma$  implying that anharmonicity is almost exclusively a planar feature. Thirdly the planar set has bond-bending parameters of similar size to its bond-stretching ones in marked contrast to the interlayer sets where bond-stretching dominates.

The above fit translates into the internal strain tensors and inner elastic constants shown in Tables 7.8 and 7.9.

Table 7.8: The internal strain tensors in Å. The actual in-plane internal strain is given by  $A_{iJ}^1 + A_{iJ}^2$  in one layer and by  $A_{iJ}^2 + A_{iJ}^3$  in the other. These components are equal and opposite and the first of them is given in the fifth column.

$iJ$ .	$A_{iJ}^1$	$A_{iJ}^2$	$A_{iJ}^3$	$A_{iJ}^1 + A_{iJ}^2$
16	-1.21	1.29	-1.37	0.082
136	0.7	-0.7	0.7	0
145	7.1	-7.1	7.1	0
211	-53.8	78.2	-102.6	24.4
222	54.4	-79.3	104.2	-24.9
314	-1.2	1.2	-1.2	0

The value of the linear internal strain was arbitrarily pre-selected. The components of the quadratic internal strain have been included because they follow directly from the inner elastic constants, as shown in Chapter 4. They do not affect elasticity below the fourth order. From a formal perspective they appear well-behaved: for example the  $A_{1JK}^1 + A_{1JK}^2$  are all zero. This is certainly to be expected as  $y$ -components alone would be involved in the relative displacement of sublattices if A and B sites were equivalent. The  $A_{2JJ}^1 + A_{2JJ}^2$  are the only components that involve the planar parameters, hence their large values.

Table 7.9: The inner elastic constants. The  $D$  tensors are in  $\text{GPa } \text{\AA}^{-1}$ , the  $E$  tensors in  $\text{GPa } \text{\AA}^{-2}$  and the  $F$  tensors in  $\text{GPa } \text{\AA}^{-3}$

$D_{16}^1$	-19.5	$D_{16}^3$	20.0						
$D_{136}^1$	-2.4	$D_{136}^3$	-2.4						
$D_{145}^1$	-1.6	$D_{145}^3$	-1.6						
$D_{211}^1$	-6248.	$D_{211}^3$	6247.						
$D_{222}^1$	5434.	$D_{222}^3$	-5433.						
$D_{314}^1$	-2.4	$D_{314}^3$	-2.4						
$E_{11}^{11}$	253.0	$E_{11}^{12}$	253.0	$E_{11}^{13}$	0.92	$E_{11}^{33}$	251.6		
$E_{33}^{11}$	75.66	$E_{33}^{12}$	75.66	$E_{33}^{13}$	1.63	$E_{33}^{33}$	75.65		
$E_{111}^{11}$	-4562.	$E_{111}^{12}$	-4562.	$E_{111}^{13}$	5.9	$E_{111}^{33}$	-4574.		
$E_{112}^{11}$	1074.	$E_{112}^{12}$	1074.	$E_{112}^{13}$	6.1	$E_{112}^{33}$	1062.		
$E_{113}^{11}$	13.9	$E_{113}^{12}$	13.9	$E_{113}^{13}$	-1.7	$E_{113}^{33}$	13.9		
$E_{135}^{11}$	-3.4	$E_{135}^{12}$	-3.4	$E_{135}^{13}$	-3.4	$E_{135}^{31}$	-3.4	$E_{135}^{33}$	-3.4
$E_{331}^{11}$	114.7	$E_{331}^{12}$	114.7	$E_{331}^{13}$	0.7	$E_{331}^{33}$	102.8		
$E_{333}^{11}$	-45.0	$E_{333}^{12}$	-45.0	$E_{333}^{13}$	-60.5	$E_{333}^{33}$	27.8		
$F_{112}^{111}$	-775.9	$F_{112}^{112}$	-775.9	$F_{112}^{113}$	-0.1	$F_{112}^{123}$	-0.1		
$F_{112}^{133}$	-0.1	$F_{112}^{223}$	775.6	$F_{112}^{333}$	775.6				

The inner elastic constants clearly reflect the contrast just noted between constants that involve the planar parameters and those that don't.

The decomposition of the elastic stiffnesses and compliances is shown in Table 7.10. The five second-order constants selected as targets came from various sources, including a re-analysis of a previously modified value of  $C_{13}$ . Their inversion therefore generates a novel set of second-order compliances which, since the fitting procedure reproduced the experimental stiffnesses exactly, may be taken as the *de facto* experimental values also. Derived quantities, such as the compressibilities, follow directly, as shown in Chapter 5.

Table 7.10: The composition of the calculated elastic stiffnesses and the corresponding compliances and compressibilities. Stiffnesses are in GPa, second-order compliances in  $\text{TPa}^{-1}$  and third-order compliances in  $\text{TPa}^{-2}$ .

$IJ$	$\leftarrow$	$C_{IJ}$		$\rightarrow$	$S_{IJ}$ Total	$IJK$	$\leftarrow$	$C_{IJK}$		$\rightarrow$	$S_{IJK}$ Total
	Partial	Internal	Total	Partial			Internal	Total			
11	1063.85	-3.85	1060.0	0.973	111	-8629.8	-3022.5	-11672.3	7.0		
12	176.15	3.85	180.0	-0.164	113	-14.6	6.7	-7.9	-3.3		
13	7.9		7.9	-0.175	133	-125.4		-125.4	1.0		
33	36.5		36.5	27.48	333	-579.0		-579.0	11910.		
44	5.05		5.05	198.0	144	-4.5	-4.1	-8.6	-219.2		
					244	-9.0	4.1	-4.9	-382.3		
					344	-75.0		-75.0	80696.		
					166	-5874.8	-899.7	-6774.5	34.9		
					266	2039.5	-1070.3	968.1	-10.6		
					366	-3.4	6.8	3.4	-5.7		
			$k_a$	0.634				$K_a$	8.0		
			$k_c$	27.1				$K_c$	11906.		
			$k_v$	28.4				$K_v$	11922.		

The spectrum of the third-order stiffnesses of  $hG$  is shown, I believe, for the first time. The  $C_{IJK}$  display the now-familiar planar/interlayer contrast. Whereas the magnitudes of the internal strain contributions to the second-order constants were from 0.4 to 2%, at the third order they range from 15 to 200%. On inversion to compliances just two components dominate,  $S_{333}$  and  $S_{344}$ , as do  $S_{33}$  and  $S_{44}$  at the second order. The great disparity between  $S_{333}$  on the one hand and  $S_{111}$ ,  $S_{113}$  and  $S_{133}$  on the other is precisely what is needed to achieve the disparity between  $K_a$  and  $K_c$ .

The zone-centre optic mode properties are shown in Table 7.11. The modes and eigenvectors are described in Chapter 4. The two larger in-plane mode frequencies were targeted and there was no difficulty in reproducing the experimentally observed 150 GHz difference. In their Born-von Kármán lattice dynamical study [1], Al-Jishi and Dresselhaus found, in agreement with Nemanich *et al.* [30], that the above difference could be accounted for only by the inclusion of a second neighbour interlayer interaction. They further added that all the zone-centre frequencies and elastic constants, apart from  $C_{13}$ , could be fitted using only two interlayer and four planar neighbourhoods. To fit both  $C_{13}$ , which they took to be 15 GPa, and the frequency difference required extension to four interlayer neighbourhoods. Whether the value of 7.9 GPa that has been used here would have improved their fit is unknown: what I have shown is that all the second-order elastic constants and zone-centre frequencies can be fitted using one in-plane and two interlayer sets of interactions.

Table 7.11: The zone-centre optic modes. Experimental frequencies are given in both  $\text{cm}^{-1}$  and THz, the pressure derivatives in  $\text{THz GPa}^{-1}$ .

Mode	Eigenvector	Frequency $f$		Derivative $df/dp$	
		Experiment	Calculated	Experiment	Calculated
$E_{1u}$	$z_1^2 = 1, z_1^1 = z_1^3 = 0$	1587. <sup>a</sup>	47.58	47.58	0.142
$E_{2g_2}$	$z_2^2 = 1, z_2^1 = z_2^3 = 0$				
	$z_1^1 \approx -z_1^3 \approx \frac{1}{\sqrt{2}}, z_1^2 \approx 0$	1582. <sup>a</sup>	47.43	47.43	0.140 <sup>e</sup>
	$z_2^1 \approx -z_2^3 \approx \frac{1}{\sqrt{2}}, z_2^2 \approx 0$				
$E_{2g_1}$	$z_1^1 \approx -z_1^2 \approx z_1^3 \approx \frac{1}{\sqrt{3}}$	42. <sup>b</sup>	1.26	1.41	0.145 <sup>e</sup>
	$z_2^1 \approx -z_2^2 \approx z_2^3 \approx \frac{1}{\sqrt{3}}$				
$A_{2u}$	$z_3^2 = 1, z_3^1 = z_3^3 = 0$	868. <sup>c</sup>	26.02	26.02	-0.52
$B_{1g_2}$	$z_3^1 \approx -z_3^3 \approx \frac{1}{\sqrt{2}}, z_3^2 \approx 0$			25.74	-0.97
$B_{1g_1}$	$z_3^1 \approx -z_3^2 \approx z_3^3 \approx \frac{1}{\sqrt{3}}$	127. <sup>d</sup>	3.81	3.82	0.572 <sup>f</sup>

<sup>a</sup>Ref. [31] <sup>b</sup>Ref. [30] <sup>c</sup>Ref. [32] <sup>d</sup>Ref. [33] <sup>e</sup>Ref. [18] <sup>f</sup>Ref. [2]

The pressure derivatives of the frequencies were based on three experimental data, two of which were very well matched with the third overestimated by 18%. Of the remaining three derivatives that of the  $E_{1u}$  mode is clearly very reasonable. The other two are larger in magnitude and opposite in sign. The actual variation of frequency with pressure for all the modes is shown in Fig. 7.3.

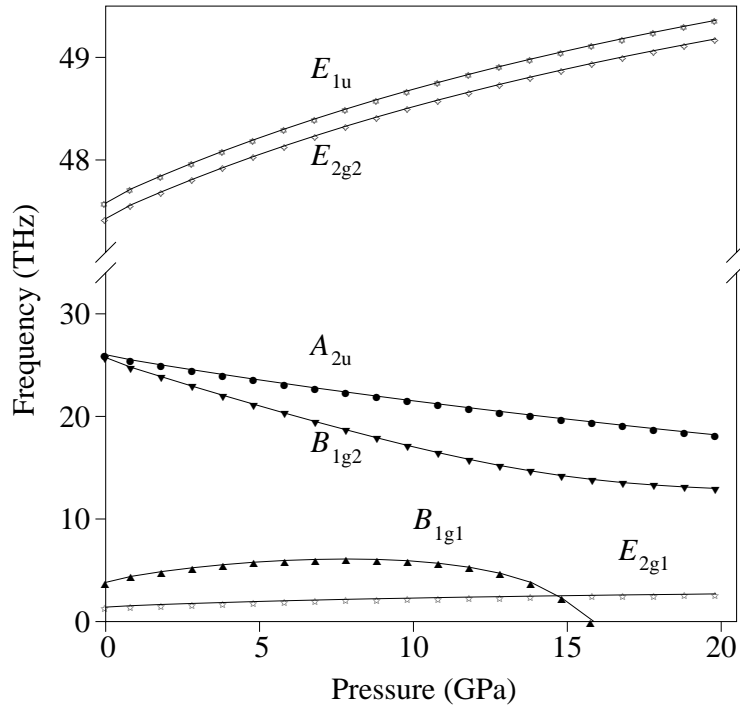


Figure 7.3: Pressure-dependence of the zone-centre optic-mode frequencies.

These results are particularly satisfying because they characterize the behaviour of a material approaching a pressure-induced phase transition: the axial modes  $A_{2u}$  and  $B_{1g2}$  show immediate softening whilst an initial hardening of  $B_{1g1}$  is followed by increasing softening from about 9 GPa. The frequency becomes zero, and the structure unstable, at 16 GPa. This value is perhaps a little high because of propagation of error from the overestimated value of the initial hardening.

Numerous investigations have shown that  $hG$  undergoes some sort of transition in just that range: Bundy and Kasper [6] achieved the first synthesis of  $hD$  by subjecting well-crystallized  $hG$  to a static pressure exceeding 13 GPa and temperature above 1000°C; Hanfland *et al.* [18] observed the  $E_{2g2}$  Raman line, noting a broadening that began at 9 GPa and the disappearance of the signal at 14 GPa; Yagi *et al.* [40] used a variety of high pressure devices and synchrotron radiation to clarify structural details of the transition, finding that it occurred at about 14 GPa and that the martensitically-transformed phase was  $hD$ .

## 7.5 Commentary

A widely-used alternative to valence force field or Keating models is the Tersoff potential for carbon [38]. Its parametrization was undertaken by optimizing a large number of cohesive energies of carbon polytypes, vacancy formation energies, together with the lattice constant and the bulk modulus of  $cD$ . The emphasis was thus on energy rather than energy derivatives. Recently an interlayer potential of the Tersoff type was proposed for graphite in [34]. I have tested this modified energy algorithm by incorporating it in place of the Keating energy algorithm. The results were poor. For example  $C_{11}$  was down by 60%,  $C_{12}$  was very negative and  $C_{33}$  was down by 75%. In addition  $C_{13}$  and  $C_{44}$  were essentially zero and some zone-centre frequencies were imaginary, results indicating insufficient bond-bending content in the interlayer modification. This highlights the importance of having realistic energy derivatives.

The Keating model is a simple vehicle for carrying such derivatives through third order. I believe that this is the first time the model has been extended rigorously to a non-cubic structure. As a preliminary it was necessary to review experimental data and an erroneous modification to  $C_{13}$  was identified and corrected. The parametrization is compact and involves only the nearest neighbours within a layer and the nearest- and next-nearest neighbours between layers. The quality of the harmonic fitting is very good, there was no difficulty in achieving a convincing fit, though it must be borne in mind that the fit is not unique. The planar parameters have substantial bond-bending character, qualitatively similar to those of  $cD$  (see Table 6.9), whilst the interlayer ones are biased in favour of bond-stretching.

A single target,  $C'_{44}$ , had to be changed (from 0.81 to 1.9) in order to obtain any credible anharmonic fitting. The final result is particularly impressive in three respects. Firstly it gives a good account of the pressure dependence of the remaining four second-order elastic constants, three optic-mode frequencies and the two third-order compressibilities in terms of just six parameters,

only one more than was necessary for  $cD$ . Secondly it gives an excellent account of the optic-mode behaviour to be expected of a material that undergoes a pressure-induced phase transition. Thirdly the huge contrast between the sizes of the planar and the interlayer parameters emphasises the difference between the covalent, strongly angularly-dependent, in-plane interaction and the weak, almost central, interlayer interaction.

At first sight it appears paradoxical that the *linear* variation of  $a$  (small  $K_a$ ) and the *quadratic* variation of  $c$  (large  $K_c$ ) as functions of pressure [27] should be associated with the *strong* planar and *weak* interlayer anharmonicities respectively. The paradox arises in the inversion of third-order stiffnesses to compliances and stems from the strong anisotropy of  $hG$ . Because  $C_{111}$  is so much larger than  $C_{333}$  the reciprocal nature of the inversion makes  $S_{111}$  very much smaller than  $S_{333}$  and so on. Thus  $K_c$  is dominated by *planar* anharmonicity,  $K_a$  by *interlayer* anharmonicity and the paradox is resolved. This argument will apply to other layer structures, such as  $hBN$ .

## References

- [1] R. Al-Jishi and G. Dresselhaus, Phys. Rev. **B26**, 4514 (1982)
- [2] B. Alzyab, C. H. Perry, C. Zahopoulos, O. A. Pringle and R. M. Nicklow, Phys. Rev. **B38**, 1544 (1988)
- [3] E. Anastassakis, A. Cantarero and M. Cardona, Phys. Rev. **B41**, 7529 (1990)
- [4] J. D. Bernal, Proc. R. Soc. London, Ser. A, **106**, 749 (1924)
- [5] O. L. Blakslee, D. G. Proctor, E. J. Seldin, G. B. Spence and T. Weng, J. Appl. Phys. **41**, 3373 (1970)
- [6] F. P. Bundy and J. S. Kasper, J. Chem. Phys. **46**, 3437 (1967)
- [7] J.-C. Charlier, X. Gonze and J.-P. Michenaud, Europhys. Lett., **28**, 403 (1994)
- [8] J.-C. Charlier, X. Gonze and J.-P. Michenaud, Phys. Rev. **B43**, 4579 (1991)
- [9] R. O. Dillon, I. L. Spain and J. W. McClure, J. Phys. Chem. Solids, **38**, 635 (1977)
- [10] P. P. Ewald, Ann. Physik **64**, 253 (1921)
- [11] W. B. Gauster and I. J. Fritz, J. Appl. Phys. **45**, 3309 (1974)
- [12] J. F. Green, P. Bolsaitis and I. L. Spain, J. Phys. Chem. Solids, **34**, 1927 (1973)
- [13] J. F. Green and I. L. Spain, J. Phys. Chem. Solids **34**, 2177 (1973)
- [14] J. F. Green and I. L. Spain, Phys. Rev. **B11**, 3935 (1975)

- 
- [15] M. H. Grimsditch, E. Anastassakis and M. Cardona, Phys. Rev. **B18**, 901 (1978)
- [16] M. Grimsditch, Phys. Status Solidi (b) **193**, K9 (1996)
- [17] M. Grimsditch, J. Phys. C **16**, L143 (1983)
- [18] M. Hanfland, H. Beister and K. Syassen, Phys. Rev. **B39**, 12598 (1989)
- [19] M. I. Heggie, J.Phys:Condens.Matter **3**, 3065 (1991)
- [20] D. R. Hershbach and V. W. Laurie, J. Chem. Phys. **35**, 458 (1961)
- [21] H. J. F. Jansen and A. J. Freeman, Phys. Rev. **B35**, 8207 (1987)
- [22] S. S. Kabalkina and L. F. Vereshchagin, Sov. Phys. Dokl., **5**, 373 (1960)
- [23] P. N. Keating, Phys. Rev. **145**, 637 (1966)
- [24] P. N. Keating, Phys. Rev. **149**, 674 (1966)
- [25] B. J. Kelly, *Physics of Graphite*, (Applied Science Publishers, London and New Jersey, 1981)
- [26] S. A. Lee and S. M. Lindsay, Phys. Status Solidi (b) **157**, K83 (1990)
- [27] R. W. Lynch and H. G. Drickamer, J. Chem. Phys. **44**, 181 (1966)
- [28] J. W. McClure, Phys. Rev. **108**, 612 (1957)
- [29] F. D. Murnaghan, Proc. Natl. Acad. Sci. **30**, 244 (1944)
- [30] R. J. Nemanich, G. Lucovsky and S. A. Solin in *Proceedings of the International Conference on Lattice Dynamics*, edited by M. Balkanski (Flammarion, Paris, 1975)
- [31] R. J. Nemanich, G. Lucovsky and S. A. Solin, Mater. Sci. Eng. **31**, 157 (1977)
- [32] R. J. Nemanich, G. Lucovsky and S. A. Solin, Solid State Comm. **23**, 117 (1977)
- [33] R. Nicklow, N. Wakabayashi and H. G. Smith, Phys. Rev. **B5**, 4951 (1972)
- [34] K. Nordlund, J. Keinonen and T. Mattila, Phys. Rev. Lett. **77**, 699 (1996)
- [35] J. C. Slonczewski and P. R. Weiss, Phys. Rev. **99**, 636(A) (1955); Phys. Rev. **109**, 272 (1958)
- [36] F. H. Stillinger and T. A. Weber, Phys. Rev. **B31**, 5262 (1985)
- [37] R. C. Tatar and S. Rabii, Phys. Rev. **B25**, 4126 (1982)
- [38] J. Tersoff, Phys. Rev. Lett. **61**, 2879 (1988), and Phys. Rev. **B39**, 5566 (1989)

- [39] Stephen Wolfram, *The Mathematica Book*, 4th ed. (Wolfram Media/Cambridge University Press, 1999)
- [40] T. Yagi, W. Utsumi, M. Yamakata, T. Kikegawa and O. Shimomura, *Rev. B***46**, 6031 (1992)
- [41] You Xiang Zhao and I. L. Spain, *Phys. Rev. B***40**, 993 (1989)

## Chapter 8

### Hexagonal diamond: elasticity and zone-centre optic modes *via* transferred Keating parameters

#### 8.1 Introduction

The possibility of a hexagonal form of diamond was first suggested by Kathleen Lonsdale in 1944 [7]. When a mineral having the expected X-ray diffraction pattern was subsequently found to comprise over 30% of the diamonds in the Canyon Diablo and Goalpara meteorites it was named lonsdaleite [4] in her honour. It was suggested that the mineral formed from crystalline graphite inclusions by impact shock, either on collision with Earth or by earlier collisions in space [5]. More recently there has been a different suggestion: various laboratory simulations seem to favour its formation by vapour deposition, most probably in a presolar, circumstellar condensation process [3]. It has also been found, again accompanying *cD*, as an inclusion in Vietnamese rubies [2]. Far less exotic but of more pertinence to this thesis, however, is its appearance in studies of *hG* under pressure. As briefly indicated in Chapter 7 *hG* undergoes a pressure-induced phase transition to *hD* at about 14 GPa, behaviour that is almost perfectly predicted by the modified Keating model to which the *hG* elasticity data has been fitted.

*hD* is more complex than *cD*, with more elastic constants at both second and third order, and with many more inner elastic constants. The formal details of the inner elastic constants and the zone-centre optic modes were treated in Chapter 4 and the anatomy of the total second- and third-order elastic constants in Chapter 5.

As both *cD* and *hD* are  $sp^3$ -bonded it is to be expected that total energies, bond lengths, and elastic constants will be very similar when compared in the appropriate manner. In fact some of the lattice properties of *cD* and *hD* have been calculated recently [11] by a total energy method using density functional theory within the local density approximation. Small differences in total energies, bond lengths, and bulk moduli reflect the fact that both structures have the same first- and second-neighbour environments, but different third-neighbour ones. The frequencies of zone-centre optic phonons were also calculated: the triple-degeneracy of the *cD* Raman mode was partially lifted and the frequencies of the *hD* modes were about 2% smaller than their cubic counterpart.

## 8.2 The hexagonal diamond structure

Even though the Keating model is limited to first- and second-neighbours small differences can still be accommodated as a result of the lower symmetry of  $hD$ . The extra degree of freedom, resulting from two lattice parameters in place of one, allows the equality of the four bond lengths to be relaxed: the axial bond may differ in length from the three non-axial bonds. The structures of the two diamond allotropes are described in Chapter 4.

### 8.2.1 The quasi- $cD$ case

This case, in which the atomic volume and all bond lengths are taken to be the same as those in  $cD$ , is depicted in Fig. 8.1.

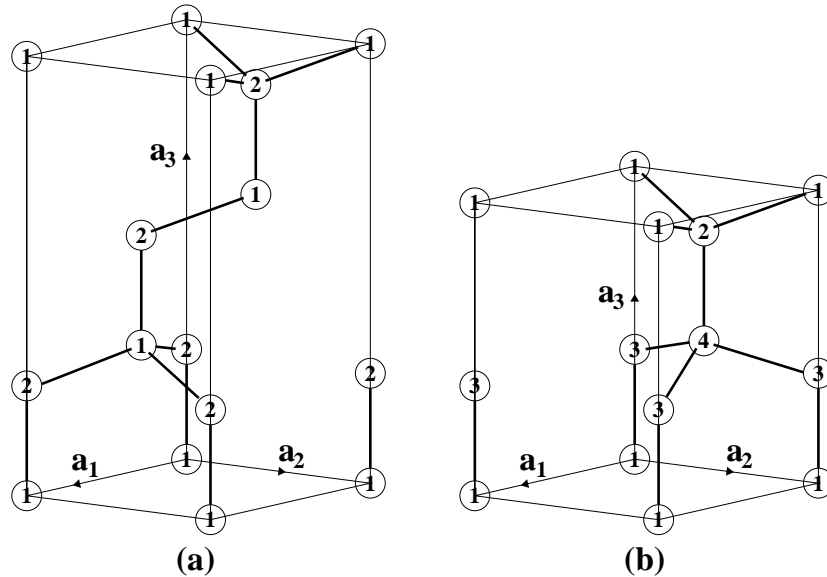


Figure 8.1: (a) The triple-hexagonal cell for  $cD$  and (b) the primitive hexagonal cell of  $hD$ . The numbers indicate the distinct sublattices on which the atoms lie.

Taking  $a_c = 3.567 \text{ \AA}$  the lattice parameters in the quasi- $cD$  case are  $a = a_c / \sqrt{2} = 2.5222 \text{ \AA}$  and  $c = 2a_c / \sqrt{3} = 4.1188 \text{ \AA}$ . The volume per atom  $\Omega_0 = \sqrt{3}ca^2/8 = 5.6731 \text{ \AA}^3$ . The common bond length is given by

$$r_0 = \frac{3}{8}c = \sqrt{\frac{3}{8}}a \quad (8.1)$$

and has the value  $1.5446 \text{ \AA}$ .

### 8.2.2 The actual $hD$ case

The detailed study of the  $hG$  to  $hD$  transformation undertaken in [12] reveals a small departure from the quasi- $cD$  case. The lattice parameters extrapolated to ambient pressure are  $a = 2.513(6) \text{ \AA}$  and  $c = 4.171(5) \text{ \AA}$ , indicating a slight decrease in the value of  $a$  but a 1.3% expansion in  $c$ . The

$c/a$  ratio goes up from the ideal 1.6330 to 1.66 and remains constant to at least 30 GPa pressure. In this case three bond lengths are given by

$$r_{0a} = \sqrt{\frac{1}{3}a^2 + 4z^2c^2} \quad (8.2)$$

and the fourth by

$$r_{0c} = \frac{1}{2}(1 - 4z)c \quad (8.3)$$

where  $z$  is the structural coordinate that is equal to 1/16 in the quasi-cD case, see Table 2.8. The measurements undertaken in [12] are not sufficient to give this parameter. If it is assumed that the structure retains equal bond lengths then  $r_{0a} = r_{0c} = 1.5474 \text{ \AA}$  and  $z$ , which is given by  $1 - 8z = 4a^2/3c^2$ , changes from 0.0625 to 0.0645. This scenario seems unlikely—it appears to take no advantage of the extra degree of freedom available. On the other hand the assumption that  $z$  remains at 1/16 produces a marked inequality of bond lengths:  $r_{0a} = 1.5417 \text{ \AA}$  and  $r_{0c} = 1.5641 \text{ \AA}$ , a difference of 1.5%. The actual behaviour of  $hD$  probably lies somewhere in between. Calculations for both these extremes are presented below, together with those for the quasi-cD case.

### 8.3 Modified Keating model

Now that the Keating model has been modified to use transferable parameters it is a simple matter to produce a complete description of the elasticity of  $hD$ .

#### 8.3.1 The strain variables

The strains in the modified model for  $hD$  are formally the same as those for  $hG$ :

$$\Delta_{ii} = 2r_p^{i0}\eta_{pq}r_q^{i0} + 2r_p^{i0}z_p^\pi + z_p^\pi z_p^\pi \quad (8.4)$$

and

$$\Delta_{ij} = 2r_p^{i0}\eta_{pq}r_q^{j0} + r_p^{i0}z_p^\rho + r_p^{j0}z_p^\pi + z_p^\rho z_p^\pi \quad (8.5)$$

where terms of order three and higher have been omitted. The significance of  $\vec{z}^\pi$  and  $\vec{z}^\rho$  is as follows. Consider the reference atom belonging to sublattice 2 in Fig. 8.1(b). It has three bonds to atoms on sublattice 1 and one bond to an atom on sublattice 4. When  $i$  refers to sublattice 1  $\vec{z}^\pi = -\vec{\zeta}^1$  (minus because a positive value indicates 2 relative to 1, 3 relative to 2 or 1, or 4 relative to 3, 2 or 1). If  $i$  refers to sublattice 4 then  $\vec{z}^\pi = \vec{\zeta}^2 + \vec{\zeta}^3$  (because 4 relative to 2 is equivalent to 3 relative to 2 plus 4 relative to 3). Similarly for  $j$  and  $\vec{z}^\rho$ , and for the remaining reference atoms.

#### 8.3.2 The energy

The expressions for the modified energies per cell are the same as those for  $cD$ , (6.40) and (6.41), except that the summations are now over four sublattices rather than two. The anharmonic term in

$\xi$  has been retained for the sake of formal completeness even though it was found to be insignificant *vis-à-vis*  $cD$ .

$$E^{(2)} = \frac{1}{2} \sum_{s=1}^4 \sum_{i=1}^4 \left( \alpha \Delta_{ii}^2 + \sum_{j=1}^4 ' (\beta^* \Delta_{ij}^2 + \sigma (\Delta_{ii} + \Delta_{jj}) \Delta_{ij} + \tau \Delta_{ii} \Delta_{jj}) \right) \quad (8.6)$$

and

$$E^{(3)} = \frac{1}{2} \sum_{s=1}^4 \sum_{i=1}^4 \left( \gamma \Delta_{ii}^3 + \sum_{j=1}^4 ' (\delta \Delta_{ij}^3 + \epsilon (\Delta_{ii} + \Delta_{jj}) \Delta_{ij}^2 + \eta (\Delta_{ii}^2 + \Delta_{jj}^2) \Delta_{ij} + \theta \Delta_{ii} \Delta_{ij} \Delta_{jj} + \xi \Delta_{ii} \Delta_{jj} (\Delta_{ii} + \Delta_{jj})) \right). \quad (8.7)$$

There is one important detail relating to the transferable parameters that needs attention: the value of  $\beta^*$ . In the analysis of  $cD$   $\beta^*$  was introduced as the combination  $\beta + \kappa$ , where  $\kappa$  represented the interactions of planar chains of three bonds, and the separation of  $\beta$  from  $\kappa$  was achieved by analysing phonon frequencies at the Brillouin zone boundary. In  $hD$  there are only nine chains per atom whereas  $cD$  has twelve. Thus where  $\beta^*$  was  $132.0 = 95.1 + 36.9 \text{ GPa } \text{\AA}^{-1}$  before it is replaced now by  $95.1 + \frac{3}{4} \times 36.9 = 122.8 \text{ GPa } \text{\AA}^{-1}$ .

Table 8.1: Modified Keating parameters

	Harmonic		Anharmonic		
	$\text{GPa } \text{\AA}^{-1}$	$\text{eV } \text{\AA}^{-4}$	$\text{GPa } \text{\AA}^{-3}$	$\text{eV } \text{\AA}^{-6}$	
$\alpha$	158.6	0.990	$\gamma$	-140.8	-0.879
$\beta^*$	122.8	0.767	$\delta$	19.5	0.122
$\sigma$	-18.4	-0.115	$\epsilon$	-99.7	-0.623
$\tau$	3.3	0.021	$\eta$	-24.3	-0.152
			$\theta$	50.6	0.316
			$\xi$	0.0	0.000

## 8.4 The partial and inner elastic constants

Expressions for the partial and inner elastic constants have been obtained by identifying the Keating energy density with the free energy per unit initial volume quoted in (1.10), ignoring first order terms. They have been confirmed by using the generalised method of homogeneous deformation, given in the Appendix, with a unit contribution from each of the model parameters in turn. As they are rather more numerous than those of  $hG$  they are presented in tabular form. The numerical coefficients relate only to the two cases where  $z = 1/16$ .

Table 8.2: Coefficients of the modified Keating parameters in the second-order partial and inner elastic constants and evaluation of the constants under the three régimes described in the text. The lattice parameters are  $a$  and  $c$ , and  $t$  is an abbreviation for  $\sqrt{3}$ . The coefficients are valid only for the  $z = 1/16$  cases.

Constant	Factor	$\alpha$	$\beta^*$	$\sigma$	$\tau$	Quasi-cD	$r_{0a} \neq r_{0c}$	$r_{0a} = r_{0c}$
							$z = 0.0625$	$z = 0.0645$
$C_{11}^0$	$4ta^2/3c$	1	1	-2	1	1146.	1132.	1132.
$C_{12}^0$	$4ta^2/9c$	1	-1	-2	5	106.0	104.7	104.7
$C_{13}^0$	$tc/12$	1	-1	-2	11	64.8	66.1	67.4
$C_{33}^0$	$tc^3/32a^2$	7	5	-14	5	1188.	1252.	1247.
$C_{44}^0$	$tc/12$	1	5	-2	-1	479.0	488.7	490.1
$D_{16}^1$	$2a/3c$	-2	2	1	2	-34.1	-33.8	-33.8
$D_{15}^1$	$t/3$	-1	1		1	-18.8	-18.9	-23.4
$D_{31}^1$	$t/3$	-1	1		1	-18.8	-18.9	-19.1
$D_{33}^1$	$tc^2/8a^2$	1	-1		-1	37.6	39.1	29.6
$E_{11}^{11}$	$4t/3c$	2	2	3	-2	280.9	279.4	279.4
$E_{11}^{12}$	$4t/3c$		1			68.8	68.5	68.5
$E_{11}^{13}$	$4t/3c$			-1		10.3	10.2	10.2
$E_{33}^{11}$	$tc/8a^2$	8	11	6	-2	350.7	360.4	361.4
$E_{33}^{12}$	$tc/8a^2$	6	1	-6		166.0	170.6	169.2
$E_{33}^{13}$	$tc/8a^2$		3	-10	6	80.2	82.4	83.2
$E_{111,112}^{11(2)}$	$4t/3c$	2	-2	3	6	20.4	20.3	20.3
$E_{111,112}^{12(2)}$	$4t/3c$				2	3.7	3.7	3.7
$E_{111,112}^{13(2)}$	$4t/3c$			-1		10.3	10.2	10.2
$E_{113}^{11(2)}$	$tc/8a^2$	4	-1	3	12	139.1	143.0	145.0
$E_{113}^{12(2)}$	$tc/8a^2$	3		-3	1	149.8	153.9	151.4
$E_{113}^{13(2)}$	$tc/8a^2$		3	-5		129.0	132.6	134.4
$E_{331}^{11(2)}$	$tc/2a^2$	2	-2	3	6	20.4	20.3	20.3
$E_{331}^{12(2)}$	$tc/2a^2$				2	3.7	3.7	3.7
$E_{331}^{13(2)}$	$tc/2a^2$			-1		10.3	10.2	10.2
$E_{333}^{11(2)}$	$3tc^3/64a^4$	4	-1	3	12	139.1	143.0	145.0
$E_{333}^{12(2)}$	$3tc^3/64a^4$	3		-3	1	149.8	153.9	151.4
$E_{333}^{13(2)}$	$3tc^3/64a^4$		3	-5		129.0	132.6	134.4

Table 8.3: Coefficients of the modified Keating parameters in the third-order partial elastic constants and the  $D$  and  $F$  tensors.

Constant	Factor	$\gamma$	$\delta$	$\epsilon$	$\eta$	$\theta$	$\xi$	Quasi-cD	$r_{0a} \neq r_{0c}$	$r_{0a} = r_{0c}$
									$z = 0.0625$	$z = 0.0645$
$C_{111}^0$	$2ta^4/c$	1	-1	2	-2	-1	2	-12317.	-12118.	-12118.
$C_{113}^0$	$tca^2/24$	3	3	-2	-6	-1	26	-130.5	-132.6	153.6
$C_{133}$	$tc^3/128$	1	-1	6	-2	-17	70	-1484.2	-1558.4	-1595.7
$C_{333}$	$3tc^5/1024a^2$	61	-13	46	-122	-13	46	-10520.	-11411.	-11148.
$C_{144}^0$	$tca^2/24$	1	-1	1	-2	1	2	-304.4	-309.4	-308.8
$C_{244}^0$	$tca^2/24$	3		5	-6	1	-2	-1370.8	-1393.3	-1421.8
$C_{344}$	$tc^3/128$	1	-13	22	-2	-9	6	-2832.9	-2974.6	-2978.3
$C_{166}^0$	$2ta^4/9c$	3		2	-6	1	-2	-1609.7	-1583.8	-1583.8
$C_{266}^0$	$2ta^4/9c$	1	-4	6	-2	-3	2	-3482.0	-3425.8	-3425.8
$C_{366}^0$	$tca^2/24$	1	2		-2	-1	6	-196.0	-199.2	-216.3
$D_{116}^1$	$2a^3/3c$	-3		1	3	-1	2	517.4	511.0	511.0
$D_{126}^1$	$2a^3/3c$	-1	-2	1	1	1	-2	73.2	72.3	72.3
$D_{136}^1$	$ca/16$	-2	2	2	2	1	-12	80.0	81.6	89.7
$D_{145}^1$	$ca/32$	-4	1	-4	4	4	8	352.8	360.0	369.1
$D_{314}^1$	$ca/16$	-2	2	-1	2	1		274.3	279.8	283.8
$D_{115}^1$	$ta^2/6$	-3		1	2	-1	2	410.5	412.0	442.7
$D_{125}^1$	$ta^2/18$	-3	3	3	2	-2	-6	-11.3	-11.3	-5.9
$D_{135}^1$	$tc^2/96$	-3	-15	6	2	9	-18	-19.3	-20.0	3.7
$D_{311}^1$	$ta^2/6$	-3	-3	2	2	1	-2	305.2	306.3	321.9
$D_{312}^1$	$ta^2/18$	-3	3	6	2	-3	-18	-19.4	-19.5	-20.0
$D_{313}^1$	$tc^2/96$	-3	3	-6	2	-3	30	269.2	279.1	279.8
$D_{333}^1$	$tc^4/64a^2$	15	3	-6	-10	3	-6	-1298.	-1390.	-1234.
$D_{344}^1$	$tc^2/96$	-18	12		2	-9	6	47.0	48.7	79.0
$F_{112}^{111}$	$2a/3c$	-4	1	1	-6	4	8	1019.	1012.	1012.
$F_{112}^{112}$	$2a/3c$			-2				81.4	81.0	81.0
$F_{112}^{113}$	$2a/3c$			-1	2			20.9	20.8	20.8
$F_{113}^{111}$	$t/4$	-8	-3	-2	-12	4	8	708.9	716.6	746.6
$F_{113}^{112}$	$t/6$		-3	4		6		-1.6	-1.5	-1.0
$F_{113}^{113}$	$t/12$		-9	2	4		-24	-65.0	-65.7	-67.0
$F_{113}^{121}$	$t/12$		3	8		6		-4.2	-4.0	-2.8
$F_{113}^{123}$	$t/4$		-3			2		2.6	2.5	1.8
$F_{113}^{131}$	$t/6$			-2	2	-3		-28.6	-29.0	-30.0
$F_{113}^{221}$	$t/6$		6	4				-6.8	-6.6	-4.6
$F_{333}^{111}$	$3tc^2/64a^2$	32	9	-14	12	-20	-40	-1078.	-1121.	-1043.
$F_{333}^{112}$	$tc^2/32a^2$	54	3	-10		6	-36	-740.8	-778.6	-738.4
$F_{333}^{113}$	$tc^2/64a^2$		9	-14	-52	12	24	194.8	205.1	196.5

Table 8.4: Coefficients of the modified Keating parameters in the third-order  $E$  tensors.

Constant	Factor	$\gamma$	$\delta$	$\epsilon$	$\eta$	$\theta$	$\xi$	Quasi-cD		
								$r_{0a} \neq r_{0c}$ $z = 0.0625$	$r_{0a} = r_{0c}$ $z = 0.0645$	
$E_{111}^{11(3)}$	$4ta^2/3c$	3		1	1	1	-2	-1769.	-1753.	-1753.
$E_{111}^{12(3)}$	$2ta^2/3c$			1				-177.9	-176.3	-176.3
$E_{111}^{13(3)}$	$4ta^2/3c$				-1			86.7	85.9	85.9
$E_{112}^{11(3)}$	$4ta^2/9c$	3	-3	-1	3	6		-301.9	-259.3	-259.3
$E_{112}^{12(3)}$	$2ta^2/9c$			1				-59.3	-58.8	-58.8
$E_{112}^{13(3)}$	$4ta^2/9c$				-1			28.9	28.7	28.7
$E_{113}^{11(3)}$	$tc/24$	6	-6	10	2	9	36	-461.7	-472.8	-501.4
$E_{113}^{12(3)}$	$tc/24$		-9	10				-348.9	-357.2	-354.5
$E_{113}^{13(3)}$	$tc/24$			6	-2	-9		-298.7	-305.9	-305.7
$E_{135}^{11(3)}$	$tc/96$	24	21	82	8	6	-24	-820.4	-840.0	-863.6
$E_{135}^{12(3)}$	$tc/48$		-9	20		-6		-367.8	-376.6	-374.3
$E_{135}^{13(3)}$	$tc/96$		-27	18	-8	-18	24	-225.9	-231.3	-230.8
$E_{331}^{11(3)}$	$tc/24$	6	-6	7	2	9	48	-372.7	-381.7	-398.7
$E_{331}^{12(3)}$	$tc/24$			1		-6	36	-119.8	-122.7	-126.6
$E_{331}^{13(3)}$	$tc/24$			3	-2	-9	12	-209.8	-214.7	-212.7
$E_{333}^{11(3)}$	$tc^3/256a^2$	168	-51	106	-52	-12	-24	-2561.	-2717.	-2651.
$E_{333}^{12(3)}$	$tc^3/256a^2$	162	-9	46	-216	-6	36	-1682.	-1779.	-1723.
$E_{333}^{13(3)}$	$tc^3/256a^2$		-27	90	-164	-36	120	-545.6	-577.2	-603.1
$E_{114}^{11}$	$a/12$	12	-3	-12	4	-12	-24	-263.8	-265.7	-282.3
$E_{136}^{11}$	$a/12$	12	-12	-15	4	-6	-12	-174.1	-175.4	-186.4
$E_{136}^{13}$	$a/4$			-1			4	62.9	63.4	62.7

## 8.5 The internal strain parameters

Using the appropriate inner elastic constants in (4.16) yields the internal strain parameters that are shown in Table 8.5. The accidental degeneracy displayed by the quasi-cD parameters is removed on passing to real  $hD$ . If  $A_{16}^1$  is to be compared with the  $A_{14}$  of cD both parameters need to be scaled: the former by  $a/2$ , the latter by  $a_c/4$ , these being the projections of the bonds along the  $Ox_1$  axes. This gives the values 0.121 and 0.093 respectively. Without the  $\beta^*$  adjustment  $A_{16}^1 = 0.117$  which scales to 0.093 as is to be expected. This shows that the  $\beta^*$  adjustment has a significant effect on the internal strain.

Table 8.5: The internal strain parameters. The final entry relates to cubic diamond. Units are Å.

Constant	Quasi-cD	$r_{0a} \neq r_{0c}$	$r_{0a} = r_{0c}$
		$z = 0.0625$	$z = 0.0645$
$A_{16}^1$	0.153	0.153	0.153
$A_{15}^1$	0.069	0.070	0.087
$A_{31}^1$	0.069	0.068	0.069
$A_{33}^1$	-0.139	-0.141	-0.107
$A_{14}$	0.083		

### 8.6 The total elastic constants and associated pressure derivatives

Armed with values of the internal strain and the inner elastic constants Eqs. (5.1), (5.2), (5.7) and (5.8) can be used to anatomize the macroscopic constants. Firstly I summarize in Table 8.6 the results for the total elastic constants at the second and third order, the bulk modulus and the pressure derivatives of the second-order constants for the three régimes under consideration.

Table 8.6: The second- and third-order elastic constants, the bulk modulus and the pressure derivatives of the second-order constants. Constants are in GPa, derivatives are dimensionless.

Constant	Quasi-cD	$r_{0a} \neq r_{0c}$	$r_{0a} = r_{0c}$	Constant	Quasi-cD	$r_{0a} \neq r_{0c}$	$r_{0a} = r_{0c}$
		$z = 0.0625$	$z = 0.0645$			$z = 0.0625$	$z = 0.0645$
$C_{11}$	1133.4	1119.2	1119.2	$C_{111}$	-11912.	-11720.	-11714.
$C_{12}$	113.8	112.4	112.4	$C_{113}$	-101.1	-102.7	-105.7
$C_{13}$	70.0	71.4	71.5	$C_{133}$	-1746.6	-1833.9	-1831.2
$C_{33}$	1177.2	1240.6	1240.7	$C_{333}$	-9662.2	-10481.	-10494.
$C_{44}$	476.4	486.0	486.0	$C_{144}$	-424.6	-431.5	-434.0
$B$	439.1	442.9	443.0	$C_{244}$	-1169.4	-1188.6	-1183.9
				$C_{344}$	-2831.0	-2972.6	-2974.6
$C'_{11}$	8.78	8.70	8.71	$C_{166}$	-1321.6	-1300.3	-1299.0
$C'_{12}$	1.54	1.54	1.53	$C_{266}$	-3432.5	-3377.1	-3375.8
$C'_{13}$	0.98	0.97	1.00	$C_{366}$	-214.7	-218.2	-219.7
$C'_{33}$	9.34	9.82	9.69				
$C'_{44}$	3.06	3.09	3.12				
$B'$	3.77	3.80	3.80				

There does not appear to be any distinct trend in the changes from column to column. The bulk modulus is in all cases very close to the observed cD value of 442 GPa. The fitted value of 445 GPa

drops to 439 GPa as a result of the  $\beta^*$  adjustment. The calculations in [11] give  $hD$  a bulk modulus 2.3% larger than that of  $cD$ , whilst the measurements of Yagi *et al.* give  $425 \pm 25$  GPa—equality within experimental error. The pressure derivative of the bulk modulus is about 2% larger than the value 3.72 found for  $cD$ . Secondly I single out the ‘unequal bonds’ régime to show, in Table 8.7, the full decomposition of all constants into partial and internal contributions, together with the elastic compliances and the compressibilities.

Table 8.7: The composition of the calculated elastic stiffnesses and the corresponding compliances and compressibilities for the ‘unequal bonds’ régime. Stiffnesses are in GPa, second-order compliances in  $\text{TPa}^{-1}$  and third-order compliances in  $\text{TPa}^{-2}$ .

$IJ$	$C_{IJ}$		$S_{IJ}$	$IJK$	$C_{IJK}$			$S_{IJK}$	
	←← Partial	→ Internal			→ Total	←← Partial	→ Internal		→ Total
11	1132.1	-12.9	1119.2	0.905	111	-12118.1	398.3	-11719.8	8.7
12	104.7	7.7	112.4	-0.088	113	-132.6	29.9	-102.7	-0.4
13	66.1	5.3	71.4	-0.047	133	-1558.4	275.5	-1833.9	0.7
33	1251.6	-11.0	1240.6	0.811	333	-11410.7	929.9	-10480.8	5.3
44	488.7	-2.7	486.0	2.058	144	-309.4	-122.1	-431.5	0.6
					244	-1393.3	204.7	-1188.6	3.8
					344	-2974.6	2.0	-2972.6	9.9
					166	-1583.8	283.5	-1300.3	3.4
					266	-3425.9	48.8	-3377.1	11.6
					366	-199.2	-19.0	-218.2	-0.2
			$k_a$	0.770				$K_a$	7.24
			$k_c$	0.717				$K_c$	6.56
			$k_v$	2.258				$K_v$	21.04

The inner elasticity contributes to every constant in  $hD$ , in marked contrast to the situation for  $cD$  and  $hG$ . The internal share varies between 0.5% and 7.5% for the second-order constants and between 0.1% and 30% for the third-order ones.

The compressibilities are no longer isotropic as they are in  $cD$  and in the quasi- $cD$  version of  $hD$ . The results for  $cD$ , from Chapter 6, are  $k = 0.749 \text{ TPa}^{-1}$ ,  $K = 6.83 \text{ TPa}^{-2}$ ,  $k_v = 2.25 \text{ TPa}^{-1}$ ,  $K_v = 20.5 \text{ TPa}^{-2}$ .

## 8.7 The zone-centre optic modes

The frequencies and eigenvectors follow from the analysis in Chapter 4 and are presented in Table 8.8. The calculated triply-degenerate  $T_{2g}$  mode frequency of 40.23 THz in  $cD$  corresponds to the triple degeneracy of the two  $E_{1g}$  and the  $A_{1g}$  modes at 39.49 THz in the quasi- $cD$  calculation.

The 1.8% lower value is due entirely to the reduced value of  $\beta^*$  and falls nicely in the middle of the range of 0.5% to 2.8% reduction observed in [6]. The  $E_{2g}$  frequency is well predicted, only exceeding the observed value by about 2%. For the Raman active modes the Keating model is in near-perfect agreement with the density functional calculations of Wu and Xu [11]. For the optically-inactive modes, however, the agreement is poorer. Calculations for the real  $hD$  case reveal no change in the three doubly-degenerate modes but show the lifting of the triple degeneracy by an increase in frequency of the  $A_{1g}$  mode of about 650 GHz. This is rather larger than the 270 GHz found in [11].

Table 8.8: The zone-centre optic modes. Experimental frequencies have been converted to THz. Comparative information for  $cD$  is given at the bottom.

Mode	Eigenvector	Experiment	Calculated $\rightarrow$		$r_{0a} \neq r_{0c}$	$r_{0a} = r_{0c}$
			Ref. [11]	Quasi- $cD$	$z = 0.0625$	$z = 0.0645$
$E_{1g}$	$z_1^1 = -z_1^3 = \frac{1}{\sqrt{2}}, z_1^2 = 0$ $z_2^1 = -z_2^3 = \frac{1}{\sqrt{2}}, z_2^2 = 0$	39.42–39.75 <sup>a</sup>	39.12	39.49	39.49	39.49
$E_{2g}$	$z_1^1 = -z_1^2 = z_1^3 = \frac{1}{\sqrt{3}}$ $z_2^1 = -z_2^2 = z_2^3 = \frac{1}{\sqrt{3}}$	35.08 <sup>b</sup> /35.22 <sup>c</sup>	35.77	35.80	35.80	35.80
$E_{2u}$	$z_1^2 = 1, z_1^1 = z_1^3 = 0$ $z_2^2 = 1, z_2^1 = z_2^3 = 0$		15.62	19.91	19.91	19.91
$A_{1g}$	$z_3^1 = -z_3^3 = \frac{1}{\sqrt{2}}, z_3^2 = 0$	39.42–39.75 <sup>a</sup>	39.39	39.49	40.13	40.15
$B_{2g}$	$z_3^1 = -z_3^2 = z_3^3 = \frac{1}{\sqrt{3}}$		37.56	39.07	39.71	39.94
$B_{1u}$	$z_3^2 = 1, z_3^1 = z_3^3 = 0$		33.55	30.93	31.44	31.31
$T_{2g}$		39.93 <sup>d</sup>	39.99	40.23		

<sup>a</sup>Ref. [6] <sup>b</sup>Ref. [9] <sup>c</sup>Ref. [8] <sup>d</sup>Ref. [10]

The pressure derivatives of the frequencies are shown in Table 8.9. Apart from the  $E_{2u}$  modes they all have approximately the same value as  $cD$ .

Table 8.9: Pressure-derivatives of optic-mode frequencies. The final entry relates to cubic diamond. Units are THz GPa<sup>-1</sup>.

Mode	Quasi- $cD$	$r_{0a} \neq r_{0c}$	$r_{0a} = r_{0c}$	Mode	Quasi- $cD$	$r_{0a} \neq r_{0c}$	$r_{0a} = r_{0c}$
		$z = 0.0625$	$z = 0.0645$			$z = 0.0625$	$z = 0.0645$
$E_{1g}$	0.098	0.099	0.099	$A_{1g}$	0.098	0.099	0.099
$E_{2g}$	0.092	0.092	0.092	$B_{2g}$	0.093	0.095	0.096
$E_{2u}$	0.032	0.031	0.031	$B_{1u}$	0.101	0.102	0.101
$T_{2g}$	0.097			$T_{2g}$	0.097		

The unexciting variation of frequency with pressure up to 20 GPa is presented in Fig. 8.2.

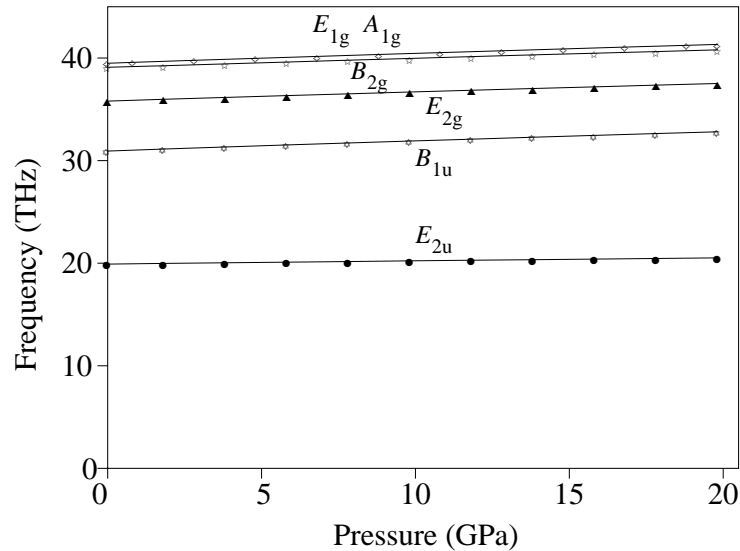


Figure 8.2: Pressure-dependence of the zone-centre optic-mode frequencies.

## 8.8 Summary and sting in the tail

It has been possible to provide a full and plausible picture of the elasticity of a material, about which very little is known, by transferring parameters from a well-characterized close relative. The adjustment of one of these parameters,  $\beta^*$ , in recognition of geometrical differences at the third-neighbour level, proved to be just what was required to give an accurate prediction of all three Raman frequencies. There is no obvious significant difference between the three structure régimes considered but...

...experiments have indicated [12] that the  $c/a$  ratio remains constant under pressure at 1.66, slightly greater than the quasi-cD value of 1.633, up to at least 30 GPa. This result generates a paradox. It implies that  $k_a > k_c$ , making the hD crystal more compressible in the  $Ox_1$  and  $Ox_2$  directions than it is in the  $Ox_3$  direction, in which case the application of pressure must increase the  $c/a$  ratio! The only way in which the ratio can remain constant is if  $k_a = k_c$ , and that implies the quasi-cD scenario. It may well turn out that the original synthesizers of hD, Bundy and Kasper [1], were nearer the mark with their values of  $a = 2.52 \text{ \AA}$ ,  $c = 4.12 \text{ \AA}$  and  $c/a = 1.635$ . Clearly more experimental work needs to be done to clarify this issue.

## References

- [1] F. P. Bundy and J. S. Kasper, *J. Chem. Phys.* **46**, 3437 (1967)

- 
- [2] N. Q. Dao, V. X. Quang, N. Q. Huy and J. P. Sylvestre, *Comptes Rendus de l'Académie des Sciences, Série II, Fascicule B*, **322**, 515 (1996)
- [3] T. L. Daulton, D. D. Eisenhour, T. J. Bernatowicz, R. S. Lewis and P. R. Buseck, *Geochimica et Cosmochimica Acta*, **60**, 4853 (1996)
- [4] C. Frondel and U. B. Marvin, *Nature* **214**, 587 (1967)
- [5] R. E. Hanneman, H. M. Strong and F. P. Bundy, *Science* **155**, 995 (1967)
- [6] D. S. Knight and W. B. White, *J. Mater. Res.* **4**, 385 (1989)
- [7] K. Lonsdale, *Nature* **153**, 669 (1944)
- [8] R. J. Nemanich, J. T. Glass, G. Lucovsky and R. E. Schroder, *J. Vac. Sci. Technol.* **A6**, 1783 (1988)
- [9] S. R. P. Silva, G. A. J. Amaratunga, E. K. H. Salje and K. M. Knowles, *J. Mater. Sci.* **29**, 4962 (1994)
- [10] J. L. Warren, R. G. Wenzel and J. L. Yarnell, *Inelastic Scattering of Neutrons* (IAEA, Vienna, 1965), Vol. 1, p. 361
- [11] B. R. Wu and J. Xu, *Phys. Rev.* **B57**, 13355 (1998)
- [12] T. Yagi, W. Utsumi, M. Yamakata, T. Kikegawa and O. Shimomura, *Rev.* **B46**, 6031 (1992)

## Chapter 9

### Rhombohedral graphite: elasticity, zone-centre optic modes and the *r*G-to-*c*D transformation *via* transferred Keating parameters

#### 9.1 Introduction

The Chapters of this thesis follow closely the chronological order of my involvement with their content. Up to this point I have believed in the existence of a rhombohedral allotrope because I have been aware of papers about it: the bandstructure treatment of Haering [8], the theoretical investigations of the *r*G-to-*c*D conversion by Kertesz and Hoffman [10] and Fahy *et al.* [4], and the comparative *ab initio* studies of a number of forms of graphite by Charlier *et al.* [3]. These papers refer to the fact that *r*G has never been isolated and state that it constitutes from 5 to 15% of most naturally-occurring graphite. Since an allotrope is defined as a *distinct crystalline form* of an element I think that *r*G may not be a genuine allotrope but that there is nevertheless *something* whose nature is worthy of study. To get a clearer idea of what it is one must return to the original structure investigations.

#### 9.2 Does the rhombohedral allotrope exist?

The original work of Lipson and Stokes [11] is frequently cited but, I suspect, rarely read. The authors were led to study an X-ray powder photograph of graphite that had been crystallized by arcing in order to elucidate some faint lines that could not be explained by the accepted structure of *h*G [2, 9, 12]. Such lines had been found quite generally in photographs from a wide variety of natural and artificial specimens. When the faint lines were indexed on the basis of a hexagonal cell they were found to have simple fractional  $\ell$  indices that were always multiples of  $\frac{2}{3}$ . The simplest way to explain the lines was to postulate a structure with a unit cell whose *c*-axis was  $\frac{3}{2}$  times as long as the usual one and to see the sample as a small amount of the new structure mixed with the ordinary one. Careful measurements of the intensities of all the lines showed that some had contributions from both structures, some were unique to the hexagonal form and some to the rhombohedral. Quantitatively, however, the enhancement of the intensities of the common lines was not quite right and Lipson and Stokes attempted to remove the new structure by digestion with

concentrated sulphuric and nitric acids. The faint lines were removed but the enhanced lines were as enhanced as before. It was concluded that the action of the acid had been ‘to rearrange the layers of atoms, rather than to remove the new structure’, a view supported by the broadening of lines with  $\ell$  non-zero (the regular arrangement of layers had been disturbed) and the unchanged width of lines with  $\ell$  zero (the integrity of planar layers had been preserved). They also concluded that there would always be a proportion of disordered material. All the intensity data would be consistent if their sample comprised 14% of the rhombohedral, 80% of the hexagonal and 6% of the disordered structures. The structure they proposed for *r*G is that given in Table 4.1 with  $a = 2.456 \text{ \AA}$ ,  $c = 10.044 \text{ \AA}$  and  $u = \frac{1}{6}$ . They did add a comment which as far as I know has been disregarded although, as I discuss later, it may well have some significance: *‘The parameter  $u$  cannot, of course, be determined exactly; we have chosen this value as it gives plane hexagonal rings. Actually the value  $u = 0.164$  would give slightly better agreement with the intensities, and this would mean that the atoms were  $\pm 0.03 \text{ \AA}$  out of the planes. The intensities, however, are too small for this point to be stated definitely.’*

The other major study was made by Freise and Kelly [6]. They deformed natural graphite single crystals and polycrystals at room temperature and coupled optical and electron microscopic investigations of these with X-ray investigations of the appearance and disappearance of the peaks corresponding to the rhombohedral form. Before detailing their own experiments they summarized earlier work on the dislocation structure of natural graphite: all total dislocations are observed to have Burgers vectors of the type  $a/3 \langle 11\bar{2}0 \rangle$ . In addition these dislocations are observed to split into partial dislocations with Burgers vectors of the type  $a/3 \langle 1\bar{1}00 \rangle$ . In a graphite crystal with the layer planes arranged in the hexagonal stacking sequence, the associated stacking fault becomes a region arranged in the rhombohedral stacking sequence. They report values of the stacking-fault energy centred on  $0.55 \text{ erg/cm}^2$  [1, 14], equivalent to  $0.09 \text{ meV}$  per atom in the plane.

Their first experiment showed that their starting material, both single crystal and polycrystalline samples, had no rhombohedral component. Next they compressed their single crystals along the *c*-axis between not-quite-parallel platens. This axial loading was necessary to enable shear to be applied in the basal plane without wholesale cleavage. No rhombohedral form was induced by shear. However, when they took filings from the single crystal, a process that involves much greater shear deformation, a large fraction of the rhombohedral form was detected. Extensive annealing studies were then carried out to characterize the rhombohedral domains. Directly after deformation they were about 10 layers thick. With increasing annealing temperature both the thickness of the domains and the volume fraction of the rhombohedral material decreased. The annealing behaviour is independent of time at a particular temperature, indicating that the disappearance of the rhombohedral form is not an activated process. The authors emphasize that randomly arranged isolated stacking faults will not give rise to rhombohedral reflections, only broadened hexagonal ones. The only regular arrangement that fits observation is one stacking fault on every other plane. Any other sequence must give rise to extra reflections, and these are not observed. They further

conclude, on the basis that the chance of finding 10 planes in the correct sequence is about 0.1%, that some ordered arrangement of dislocations occurs during deformation. Regions of rhombohedral stacking can become unobservable if just one or two dislocations glide through the stack. The work of Baker *et al.* [1] and Siems *et al.* [14] had shown that the total dislocations lying on the basal planes in graphite were always split into widely separated partial dislocations between 1000 and 2000 Å apart. This large separation means that a dislocation density of  $10^{12} \text{ cm}^{-2}$  will produce stacking faults over half the area of every layer plane. A larger density does not increase the proportion of stacking faults over a single plane. In the work under discussion the dislocation density in annealed samples was 100 to 1000 times smaller, and smaller still in the undeformed material.

All in all their work suggests that rhombohedral stacking

- is produced by severe basal shear;
- is around 10 layers thick;
- extends over an area of around  $2 \cdot 10^5$  unit rhombi;
- is limited to half a layer;
- is reduced by annealing (and completely removed if the temperature reaches  $3000^\circ\text{C}$ );
- and can be removed by dislocation glide.

This interpretation clearly explains why isolated rhombohedral graphite cannot be produced from hexagonal graphite. There is no true allotrope—just a mosaic distribution of microcrystalline defect regions embedded in the *hG* host. Each defect region is, however, large enough to justify theoretical study of its structure as a quasi-allotrope, and the rest of this Chapter is written in that spirit.

### 9.3 Cohesive energy

*hG* and *rG* consist of strongly-bonded graphene layers stacked under the influence of relatively weak forces in ABAB and ABCABC sequences respectively, to use a common description. One expects their energies to be very close and this turns out to be the case. Measured stacking fault energies in *hG* [1, 14] are always positive (around 0.09 meV/atom) showing that *hG* is the more stable allotrope. This is confirmed by energy calculations: for example, Furthmüller *et al.* find that the cohesive energy of *hG* exceeds that of *rG* by 0.9 meV/atom [7]. This value is reduced to a mere 0.11 meV/atom, suggestively close to the stacking fault energy, in the work of Charlier *et al.* [3].

There is a lack of calculations of the elasticity, though some naïve expectations have been expressed. Thus Fahy *et al.* [5] assert: ‘*Because the number of bonds between the layers is the same in rhombohedral graphite and in hexagonal graphite we expect their behavior under compression to be very similar.*’ The bonds between layers may be the same in number but their distributions are significantly different. The most important difference is a consequence of symmetry: in *hG*,

where each graphene layer is a mirror plane, the internal strain is entirely confined to those layers but in  $rG$ , whose only mirror planes are normal to the layers, the internal strain is free to occur along the unique axis as well. By taking the Keating parameters for  $hG$  and transferring them to  $rG$  it is possible to make good the previous lack.

### 9.3.1 Equilibrium structure

In Sec. 9.2 I drew attention to the tentative comment that the experimental results in [11] were better served by  $u = 0.164$  than by the planar value  $u = \frac{1}{6}$ . This implies buckling of  $\pm 0.03 \text{ \AA}$ , a shortening of the  $3.35 \text{ \AA}$  bond by 1.8%. A very simple picture, Figure 9.1, explains the origin of such buckling. An eclipsed atom in  $hG$ , say 3, has equal and opposite ‘large’ interlayer forces acting on it due to the eclipsing atoms above and below it, similarly an uneclipsed atom, say 1, experiences equal and opposite ‘small’ interlayer forces due to the non-eclipsing atoms above and below it. Both atoms have extremely large and balanced in-plane forces acting on them. No net forces act upwards or downwards and the integrity of the planes is ensured. Now consider those forces transferred to planar  $rG$ . No atoms are eclipsed on both sides and each atom has one ‘large’ and one ‘small’ interlayer force acting on it besides the very large in-plane forces. Atom 2 is drawn towards the atom below it and atom 1 towards the atom above. Small components of what were the in-plane forces will now be sufficient to augment the ‘small’ forces so that together they balance the ‘large’ forces.

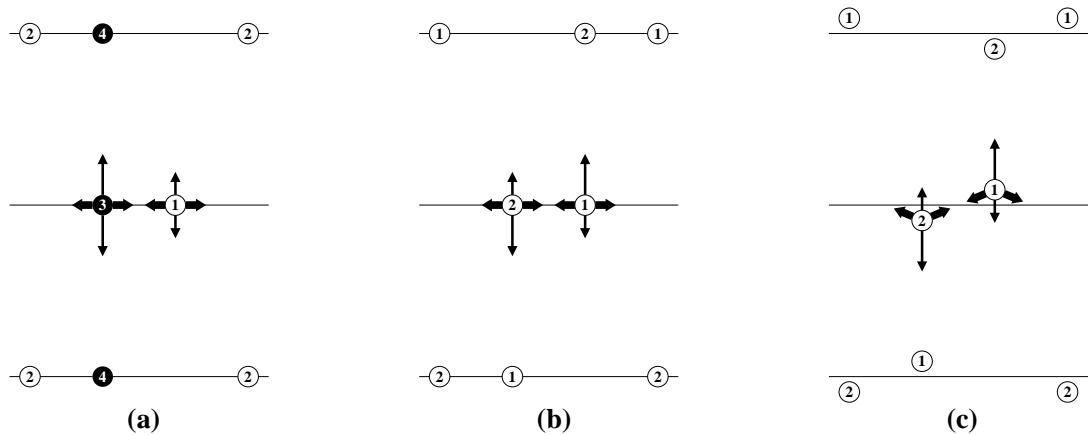


Figure 9.1: Force diagram for (a)  $hG$ , (b) planar  $rG$  and (c) buckled  $rG$

This could give rise to buckled  $rG$ , a structure near the beginning of a transformation path from  $rG$  to  $cD$ . However, an observable effect is unlikely. *Ab initio* calculations<sup>1</sup> of the total energy for a small range of values of  $u$  around the planar value show a minimum for  $u = 0.1666 \pm 0.0003$  which indicates that the net axial force on an atom is no greater than 0.2% of the in-plane force, a realistic figure that is consistent with the very small interlayer Keating parameters.

<sup>1</sup>I am most grateful to my colleague Professor G. P. Srivastava for making these calculations on my behalf.

### 9.4 Modified Keating model

The structure of  $rG$  is fully described in Chapter 4. Two layers are shown in Fig. 9.2 and the three sets of interactions corresponding to those used for  $hG$  are indicated. Bernal notation is no longer meaningful but it is useful to refer to the atoms on sublattices 1 and 2 by A and B, with superscript primes to indicate adjacent layers.

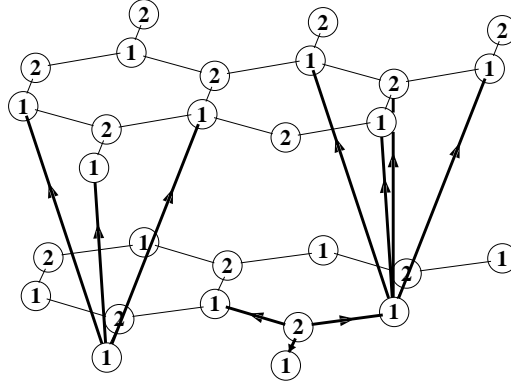


Figure 9.2: Configurations of bonds in the Keating model. The interactions are described in the text.

1. The planar part of the energy per cell is the same as that in  $hG$ . The three nearest-neighbour A atoms to a B atom, see lower centre portion of Fig. 9.2, give rise to three 2-body ‘bond-stretching’  $BA_i$  interactions, three 3-body ‘bond-bending’  $BA_i BA_j$  interactions and various couplings between them. The same number of interactions arise from each A atom. Four harmonic parameters ( $\alpha$ ,  $\beta$ ,  $\sigma$  and  $\tau$ ) and six anharmonic parameters ( $\gamma$ ,  $\delta$ ,  $\epsilon$ ,  $\eta$ ,  $\theta$  and  $\xi$ ) may be defined though not all of them are used.
2. This set comprises the 2-body  $AB'$  interaction between nearest-neighbours in adjacent planes, see right-hand portion of Fig. 9.2, and the 3-body interactions that couple  $AB'$  with the three neighbouring oblique interlayer vectors  $AA'_i$ . Unlike the  $hG$  case this set is limited to the plane above. There is a corresponding set of  $BA'$  interactions confined to the plane below. Ten more parameters may be defined (with superscript  $'$ , corresponding to the equivalent parameters in  $hG$ ).
3. This set comprises the three 2-body  $AA'_i$  interactions and the three 3-body interactions involving  $AA'_i AA'_j$  pairs, see left-hand portion of Fig. 9.2, together with the symmetrical group of 2-body  $BB'_i$  and 3-body  $BB'_i BB'_j$  interactions. There is a set of each above the plane and below the plane. Ten more parameters may be defined (with superscript  $''$ ).

In  $hG$  it was possible to ignore a potential fourth set of interactions,  $BB'$ , by noting a geometrical dependence between its strains and the strains of the other three sets. Any Keating parameters

associated with this set were implicitly included in the parametrization of the other sets. The corresponding case applies here through the numerous equivalences of the form  $B'B=B'A + AB$ . Because this is a different relation from the one in  $hG$  the implicit contribution of these interactions to the parameters above will also be different.

#### 9.4.1 The strain variables

The strains in the modified model for  $rG$  are the same as those for  $cD$ :

$$\Delta_{ii} = 2r_p^{i0}\eta_{pq}r_q^{i0} \pm 2r_p^{i0}\zeta_p + \zeta_p\zeta_p \quad (9.1)$$

and

$$\Delta_{ij} = 2r_p^{i0}\eta_{pq}r_q^{j0} \pm (r_p^{i0} + r_p^{j0})\zeta_p + \zeta_p\zeta_p \quad (9.2)$$

where terms of order three and higher have been omitted. Where the sign is undetermined the + sign is taken when the reference atom lies on sublattice 1, the – when it is on 2.

#### 9.4.2 The energy

The expressions for the modified energies per cell are the same as those for  $hG$  except that summations are now limited to two sublattices. As always the subscripts  $i$  and  $j$  are solely for the sake of bookkeeping—keeping in touch with the numbers of neighbours. Where, for the first time, there is only a single neighbour to consider (the  $AB'$  interaction set) the bond has been indicated by a subscript 1. The second-order energy per unit cell is

$$\begin{aligned} E^{(2)} = & \frac{1}{2} \sum_{s=1}^2 \sum_{i=1}^3 \left( \alpha \Delta_{ii}^2 + \sum_{j=1}^3 ' (\beta \Delta_{ij}^2 + \sigma (\Delta_{ii} + \Delta_{jj}) \Delta_{ij} + \tau \Delta_{ii} \Delta_{jj}) \right. \\ & \left. + \alpha'' \Delta_{ii}^2 + \sum_{j=1}^3 ' (\beta'' \Delta_{ij}^2 + \sigma'' (\Delta_{ii} + \Delta_{jj}) \Delta_{ij} + \tau'' \Delta_{ii} \Delta_{jj}) \right) \\ & + \frac{1}{2} \sum_{s=1}^2 \left( \alpha' \Delta_{11}^2 + \sum_{j=1}^3 (\beta' \Delta_{1j}^2 + \sigma' (\Delta_{11} + \Delta_{jj}) \Delta_{1j} + \tau' \Delta_{11} \Delta_{jj}) \right). \end{aligned} \quad (9.3)$$

The third-order energy per unit cell is

$$\begin{aligned} E^{(3)} = & \frac{1}{2} \sum_{s=1}^2 \sum_{i=1}^3 \left( \gamma \Delta_{ii}^3 + \sum_{j=1}^3 ' (\delta \Delta_{ij}^3 + \epsilon (\Delta_{ii} + \Delta_{jj}) \Delta_{ij}^2 + \eta (\Delta_{ii}^2 + \Delta_{jj}^2) \Delta_{ij} \right. \\ & \left. + \theta \Delta_{ii} \Delta_{ij} \Delta_{jj} + \xi \Delta_{ii} \Delta_{jj} (\Delta_{ii} + \Delta_{jj}) \right) \\ & + \gamma'' \Delta_{ii}^3 + \sum_{j=1}^3 ' (\delta'' \Delta_{ij}^3 + \epsilon'' (\Delta_{ii} + \Delta_{jj}) \Delta_{ij}^2 + \eta'' (\Delta_{ii}^2 + \Delta_{jj}^2) \Delta_{ij} \\ & \left. + \theta'' \Delta_{ii} \Delta_{ij} \Delta_{jj} + \xi'' \Delta_{ii} \Delta_{jj} (\Delta_{ii} + \Delta_{jj}) \right) \end{aligned} \quad (9.4)$$

$$\begin{aligned}
& + \frac{1}{2} \sum_{s=1}^2 \left( \gamma' \Delta_{11}^3 + \sum_{j=1}^3 (\delta' \Delta_{1j}^3 + \epsilon' (\Delta_{11} + \Delta_{jj}) \Delta_{1j}^2 + \eta' (\Delta_{11}^2 + \Delta_{jj}^2) \Delta_{1j} \right. \\
& \left. + \theta' \Delta_{11} \Delta_{1j} \Delta_{jj} + \xi' \Delta_{11} \Delta_{jj} (\Delta_{11} + \Delta_{jj}) \right).
\end{aligned}$$

Table 9.1: The modified Keating parameters.

	Planar		Interlayer					
	GPa Å <sup>-1</sup>	eV Å <sup>-4</sup>	GPa Å <sup>-1</sup>	eV Å <sup>-4</sup>	GPa Å <sup>-1</sup>	eV Å <sup>-4</sup>	GPa Å <sup>-1</sup>	eV Å <sup>-4</sup>
$\alpha$	266.21	1.662	$\alpha'$	39.55	0.2469	$\alpha''$	3.231	0.0202
$\beta$	240.53	1.501	$\beta'$	3.005	0.0188	$\beta''$	0.288	0.0018
$\sigma$	30.12	0.188	$\sigma'$	-5.037	-0.0314			
$\tau$	53.50	0.334	$\tau'$	-6.120	-0.0382	$\tau''$	1.447	0.0090
	GPa Å <sup>-3</sup>	eV Å <sup>-6</sup>	MPa Å <sup>-3</sup>	meV Å <sup>-6</sup>	MPa Å <sup>-3</sup>	meV Å <sup>-6</sup>		
$\gamma$	-687.13	-4.289	$\gamma'$	211.3	1.312	$\gamma''$	-35.62	-0.2247
$\delta$	-961.91	-6.004						
$\epsilon$	-365.19	-2.279				$\xi''$	-6.05	-0.0378

## 9.5 Elasticity of rhombohedral graphite

Expressions for the partial and inner elastic constants in terms of modified Keating parameters have been obtained for the planar  $rG$  structure, as they were for  $hG$ , by the method of homogeneous deformation. The second-order constants are presented in Table 9.2. At the third-order only those planar parameters that were non-zero in  $hG$ , and the bond-stretching interlayer parameters have been included in Table 9.3. Comparison with Tables 7.2, 7.3 and 7.4 shows that all the partial constants have the same expressions in both graphite allotropes. The most notable difference is the lack of any contribution to the inner elastic constants from the NNN interlayer interactions. This is because the  $AA'$  (and  $BB'$ ) connect points on the same sublattice. At the third order five of the six  $D_{iJK}$  that involve  $\xi'$  will be zero because the transferred parameters do not include it.

The partial and inner elastic constants derived from Tables 9.2 and 9.3, and checked by a homogeneous deformation calculation, are shown in Table 9.4. The large number of null  $D_{iJK}$  and  $E_{iJK}$  components is a pseudo-symmetry effect arising from the limited number of interactions taken in the model combined with the assumption of planar layers. A similar effect is shown by  $hD$  when the lattice parameters are chosen to give the quasi- $cD$  configuration: the linear compressibility becomes isotropic. A new feature is the appearance of additional anharmonic contributions,  $F_{113}^{(2)}$  and  $F_{333}^{(2)}$ , to the harmonic energy.

Table 9.2: Coefficients of the modified Keating parameters in the second-order partial and inner elastic constants. The common factors are expressed in terms of the lattice parameter  $a$  and the interlayer spacing  $d$ .  $t$  stands for  $\sqrt{3}$ .

	Factor	Planar				Interlayer: NN				Interlayer: NNN			
		$\alpha$	$\beta$	$\sigma$	$\tau$	$\alpha'$	$\beta'$	$\sigma'$	$\tau'$	$\alpha''$	$\beta''$	$\sigma''$	$\tau''$
$C_{11}^0$	$2ta^2/3d$	1	1	-2	1					2	2	-4	2
$C_{12}^0$	$2ta^2/9d$	1	-1	-2	5					2	-2	-4	10
$C_{13}^0$	$4td/3$							2	2	4	-4	4	8
$C_{33}^0$	$16td^3/a^2$					$\frac{1}{3}$	2	4	2	2	4	8	4
$C_{44}^0$	$4td/3$						1	2		4	2	4	-4
$C_{14}^0$	$2a/3$							1		4	-4	-2	-4
$D_{16}$	$2a/3d$	-2	2	1	2				1				
$D_{15}$	$4t/3$						1	1					
$D_{31}$	$4t/3$								1	2			
$D_{33}$	$4td^2/3a^2$					1	3	6	3				
$E_{11}$	$4t/3d$	2	1	2	-2		1						
$E_{33}$	$8td/3a^2$					2	3	6					
$E_{111,112,331}^{(2)}$	$4t/3d$	1	-1	1	2				1				
$E_{113,333}^{(2)}$	$8td/3a^2$					1		3	3				
$F_{113}^{(2)}$	$8t/3a^2$					2		3					
$F_{333}^{(2)}$	$8t/a^2$					2		3					

When the pseudo-symmetry is broken by the buckling of layers then  $u$  is no longer  $\frac{1}{6}$ , but smaller, and many coefficients that are zero (i.e. blank spaces) in Tables 9.2 and 9.3 will become non-zero, as will the associated constants.

The internal strain component common to the two allotropes is slightly different, as shown in Table 9.5, and the null value for  $A_{33}$  is another pseudo-symmetry consequence.

The full decomposition of the constants is given in Table 9.6. The overall picture reveals that the two graphite allotropes are remarkably similar. The calculated values of  $C_{11}$  and  $C_{12}$  in  $rG$  are a little smaller than they are in  $hG$  on account of the extra contributions of internal strain and this in turn makes  $k_a$  a little bigger than it is in  $hG$ . At the third order it is only  $C_{133}$  that is greatly changed by internal strain, but this gives  $S_{133}$  the value  $-40.1 \text{ TPa}^{-2}$  whereas it is  $+1.0 \text{ TPa}^{-2}$  in  $hG$ . This causes the one upset in the fitting: it produces a negative  $K_a$ . This was the most difficult target to fit in  $hG$  because, as explained in Chapter 7, it depends on the *interlayer* anharmonicity and particularly on the smallness of  $S_{133}$  relative to  $S_{333}$ . The remaining compressibilities  $k_c$ ,  $K_c$ ,  $k_v$  and  $K_v$  are essentially identical in the two allotropes.

Table 9.3: Coefficients of the modified Keating parameters in the third-order partial elastic constants and inner elastic constants. The common factors are expressed in terms of the lattice parameter  $a$  and the interlayer spacing  $d$ .  $t$  stands for  $\sqrt{3}$ .

	Factor	Planar			NN :Interlayer: NNN			
		$\gamma$	$\delta$	$\epsilon$	$\gamma'$	$\xi'$	$\gamma''$	$\xi''$
$C_{111}^0$	$ta^4/d$	1	-1	2			2	4
$C_{113}^0$	$8ta^2d/3$					1	3	8
$C_{133}^0$	$32td^3$					1	1	4
$C_{333}^0$	$32td^5/a^2$				1	12	6	24
$C_{144}^0$	$8ta^2d/3$						1	2
$C_{244}^0$	$8ta^2d/3$						3	-2
$C_{344}^0$	$32td^3/3$					1	3	
$C_{166}^0$	$ta^4/9d$	3		2			6	-4
$C_{266}^0$	$ta^4/9d$	1	-4	6			2	4
$C_{366}^0$	$8ta^2d/9$					2	3	
$C_{114}^0$	$4a^3/3$						3	2
$C_{124}^0$	$4a^3/3$						1	-2
$C_{134}^0$	$16ad^2/3$					2	3	
$C_{444}^0$	$16ad^2$						-1	2
$D_{116}$	$2a^3/3d$	-3		1				
$D_{126}$	$2a^3/3d$	-1	-2	1				
$D_{211}$	$2a^3/3d$	-3	-3	2				
$D_{222}$	$2a^3/3d$	5	1	-2				
$D_{314}$	$16ad/3$					1		
$D_{311}$	$8ta^2/3$					1		
$D_{312}$	$8ta^2/9$					1		
$D_{313}$	$64td^2/3$					1		
$D_{333}$	$32td^4/a^2$				1	6		
$D_{344}$	$32td^2/3$					1		
$E_{111}^{(3)}$	$2ta^2/3d$	6		1				
$E_{112}^{(3)}$	$2ta^2/3d$	2	-2	-1				
$E_{331}^{(3)}$	$32td/3$					1		
$E_{333}^{(3)}$	$32td^3/a^2$				1	2		
$F_{112}^{(3)}$	$2a/d$	-4	1	2				
$F_{333}^{(3)}$	$32td^2/a^2$				1			

Table 9.4: Calculated second- and third-order partial and inner elastic constants. Units are GPa for  $C_{IJ}^0$ ,  $\text{GPa \AA}^{-1}$  for  $D_{iJ}$ ,  $\text{GPa \AA}^{-2}$  for  $E_{ij}$ , and  $\text{GPa \AA}^{-3}$  for  $F_{ijk}$ .

Partial		Inner		Partial		Inner			
$C_{11}^0$	1063.85	$D_{16}$	39.5	$C_{111}^0$	-8630.4	$D_{116}$	5026.	$E_{111}$	-9148
$C_{12}^0$	176.15	$D_{15}$	-4.7	$C_{113}^0$	-14.6	$D_{126}$	6655.	$E_{112}$	2125
$C_{13}^0$	7.9	$D_{31}$	-39.9	$C_{133}^0$	-125.4	$D_{136}$	0.0	$E_{113}$	31.1
$C_{33}^0$	36.5	$D_{33}$	-0.04	$C_{333}^0$	-583.8	$D_{145}$	0.0	$E_{135}$	0.0
$C_{44}^0$	5.05			$C_{144}^0$	-4.5	$D_{314}$	0.0	$E_{331}$	216.1
$C_{14}^0$	1.6	$E_{11}$	502.8	$C_{244}^0$	-9.0	$D_{115}$	0.0	$E_{333}$	103.5
		$E_{33}$	148.0	$C_{344}^0$	-75.0	$D_{125}$	0.0	$E_{114}$	0.0
				$C_{166}^0$	-5875.2	$D_{135}$	0.0	$E_{136}$	0.0
				$C_{266}^0$	2039.6	$D_{311}$	0.0		
				$C_{366}^0$	-3.4	$D_{312}$	0.0	$F_{112}$	1552.
				$C_{114}^0$	-2.4	$D_{313}$	0.0	$F_{113}$	48.8
				$C_{124}^0$	-0.5	$D_{333}$	242.3	$F_{333}$	168.1
				$C_{134}^0$	-15.9	$D_{344}$	0.0		
				$C_{444}^0$	10.6				

Table 9.5: The internal strain tensors in  $\text{\AA}$ . The values for  $r\text{G}$  appear on the left. The actual in-plane internal strain in  $h\text{G}$  is shown on the right for comparison.

$iJ$	$A_{iJ}$	$A_{iJ}^2 + A_{iJ}^3$
16	-0.079	-0.083
15	0.009	
31	0.269	
33	0.000	

Table 9.6: The composition of the calculated elastic stiffnesses, the corresponding compliances and compressibilities and the pressure derivatives of the second-order stiffnesses. Stiffnesses are in GPa, second-order compliances in  $\text{TPa}^{-1}$  and third-order compliances in  $\text{TPa}^{-2}$ . The pressure derivatives are dimensionless.

$IJ$	$\leftarrow$	$C_{IJ}$		$\rightarrow$	$S_{IJ}$ Total	$IJK$	$\leftarrow$	$C_{IJK}$		$\rightarrow$	$S_{IJK}$ Total
	Partial	Internal	Total	Partial			Internal	Total			
11	1063.85	-13.86	1049.99	0.980	111	-8630.4	-2856.9	-11487.3	7.35		
12	176.15	-7.64	168.51	-0.157	113	-14.6	7.7	-6.9	-2.80		
13	7.90	-0.01	7.89	-0.178	133	-125.4	65.3	-60.1	-40.1		
33	36.5	0.0	36.5	27.47	333	-583.8	0.2	-583.6	12052.8		
44	5.05	-0.04	5.01	200.1	144	-4.5	0.2	-4.3	-226.6		
14	1.56	0.37	1.93	-0.438	244	-9.0	-0.8	-9.8	-339.2		
					344	-75.0	0.0	-75.0	82207.8		
					166	-5875.2	-853.4	-6728.6	35.1		
					266	2039.6	-1026.9	1012.7	-10.4		
					366	-3.4	0.2	-3.2	-5.0		
					114	-2.4	113.3	110.9	-20.9		
					124	-0.5	0.8	0.3	-4.6		
					134	-15.9	0.0	-15.9	-75.1		
					444	10.6	0.0	10.6	-84196.7		
			$k_a$	0.645				$K_a$	-31.2		
			$k_c$	27.1				$K_c$	11886.		
			$k_v$	28.4				$K_v$	11824.		
$C'_{11}$		38.8	(39.0)								
$C'_{12}$		10.9	(11.0)								
$C'_{13}$		3.2	(3.2)								
$C'_{33}$		13.1	(12.9)								
$C'_{44}$		1.9	(1.9)								
$C'_{14}$		0.4									

The first five pressure derivatives are essentially the same as the fitted values of the anharmonic targets for  $hG$ , shown in parentheses.

### 9.5.1 Zone-centre optic modes

The  $E_g$  mode in  $rG$  mimics the  $E_{2g2}$  mode of  $hG$  with a frequency of 47.43 THz and a pressure derivative of 0.14 THz/GPa. Likewise the  $A_{1g}$  mode mimics the  $B_{1g2}$  with values of 25.74 THz and

-0.97 THz/GPa. The behaviour under pressure is shown in Fig. 9.3 and indicates a phase transition in the vicinity of 22 GPa.

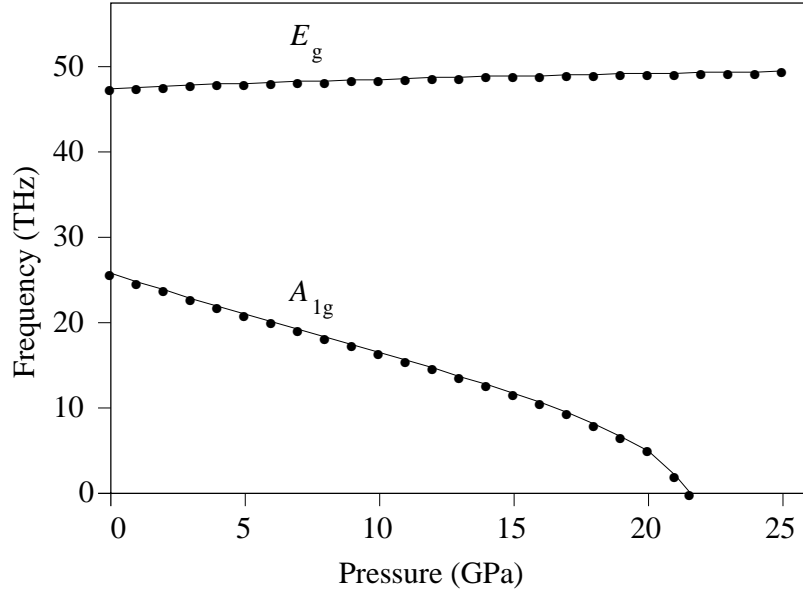


Figure 9.3: Pressure dependence of the zone-centre frequencies.

## 9.6 The *rG*-to-*cD* transformation

Although *rG* has never been isolated this has not inhibited study of its possible conversion to *cD*. A continuous transformation between the two structures can be envisaged because *cD* can be described by a primitive rhombohedral cell with two atoms in the basis in just the same way as *rG*. The quasi-*rD* picture is illustrated in Chapter 5. The top two rows of Table 9.7 show the lattice parameters (of the triple hexagonal cell), the volume (of the primitive rhombohedral cell) and the atomic coordinate of the two structures involved. Also listed are the lengths of the axial bonds,  $R$ , the non-axial bonds,  $r$ , and the buckling angle,  $\theta$ .

Table 9.7: End-points and transition-state parameters.

	$a$	$c$	$V_c$	$u$	$R$	$r$	$\theta$	$E_B$
<i>rG</i>	2.460	10.048	17.554	$\frac{1}{6}$	3.350	1.420	90.00	
<i>cD</i>	2.522	6.178	11.346	$\frac{1}{8}$	1.545	1.545	109.47	
Ref. [10]	2.519	6.684	12.243	0.139	1.86	1.50	104.2	0.6
Ref. [4](1)	2.513	7.088	12.920	0.182	2.07	1.48	101.4	0.33
Ref. [4](2)	2.372	6.770	11.0	0.155	2.1	1.38	97.0	

These latter parameters, indicated in Fig. 9.4, are related to the former by

$$R = 2uc, \quad (9.5)$$

$$r \cos \theta = 2c \left( u - \frac{1}{6} \right) \quad (9.6)$$

and

$$r \sin \theta = \frac{a}{\sqrt{3}}. \quad (9.7)$$

The volume per pair of atoms is

$$V_c = \frac{\sqrt{3}}{6} ca^2. \quad (9.8)$$

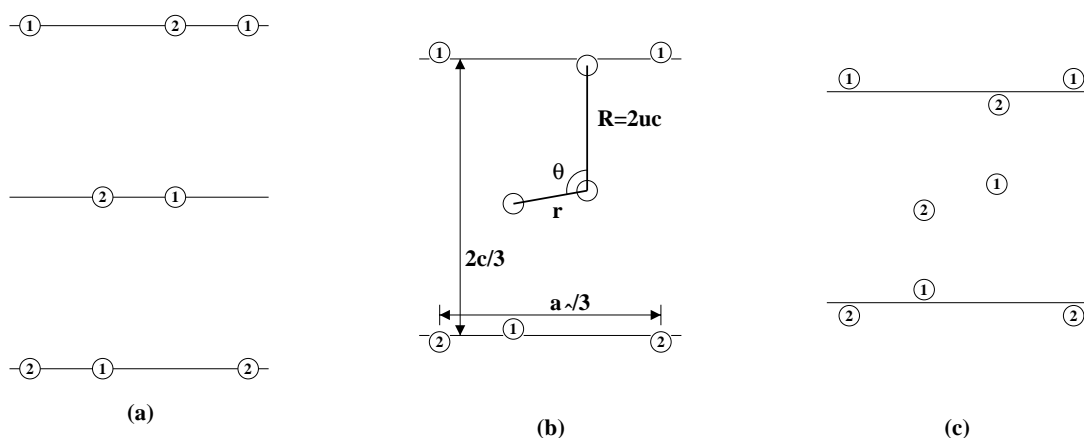


Figure 9.4:  $rG$ -to- $cD$  transformation path (a) initial  $rG$ , (b) intermediate stage, showing the essential parameters and (c) final  $cD$ .

$R$ ,  $r$  and  $\theta$  all change continuously during a concerted transformation and there is no uniquely constrained path. Several procedures may be followed. From a purely geometrical viewpoint the values of  $a$ ,  $c$  and  $u$  could be uniformly interpolated between their extreme values and  $R$ ,  $r$  and  $\theta$  calculated by the equations above. This would be to ignore the physics, though. One physical approach is to take the parameter of greatest change,  $R$ , and to interpolate it regularly between its extreme values. At each value the total energy is minimized with respect to  $r$  and  $\theta$ . The implied values of  $a$ ,  $c$  and  $u$  are then deduced. A second approach is to postulate a process such as hydrostatic compression, interpolate between the extremes of the cell volume  $V_c$  and minimize the associated enthalpy,  $E + pV_c$ , at each value. Both these approaches have been published and will now be briefly discussed and further illustrated by use of the Keating model.

### 9.6.1 Energy minimization calculations

In [10] Kertesz and Hoffmann presented an orbital model for this solid-state, high-pressure, transformation, relating it to chemical reactions having orbital symmetry constraints. They took  $R$  as

the independent reaction coordinate and optimized  $r$  and  $\theta$  at each value using extended Hückel band calculations. They identified a transition state at the maximum of the total energy versus  $R$  curve. This occurred at  $R = 1.86 \text{ \AA}$ ,  $r = 1.5 \text{ \AA}$  and  $\theta = 104.2^\circ$ . The energy barrier  $E_B$  was about  $0.6 \text{ eV/atom}$ . The transition state therefore occurs for  $a = 2.519 \text{ \AA}$ ,  $c = 6.684 \text{ \AA}$  and  $u = 0.139$ . These results have been entered in the third row of Table 9.7.

They used the small initial rate of increase of  $r$  with  $R$  to argue that the graphene layers do not buckle at low pressure. In connection with the (unstable) transition state they remark that it is customary to relate different solid-state structures by studies of hypothetical, sometimes unstable, structural models.

Fahy, Louie and Cohen [4] subsequently made a pseudopotential total-energy study of the transformation. In the first of two calculations they followed the rationale of the above work and found an energy barrier of  $0.33 \text{ eV/atom}$  when  $R = 2.07 \text{ \AA}$ ,  $r = 1.48 \text{ \AA}$  and  $\theta = 101.4^\circ$ . This result has been entered in row four of Table 9.7. In their study they follow the charge density in the plane of Fig. 9.4b along energy-minimizing path. They conclude, firstly, that only when  $R < 2.1 \text{ \AA}$  does the charge density between the layers become substantially inhomogeneous and accumulate along the axial bond and, secondly, that not until  $R < 1.8 \text{ \AA}$  does the double peak, characteristic of the  $sp^3$  bond in  $cD$ , appear.

The Keating model does not support energy minimization but does provide a means of following the elasticity and optic-mode frequency behaviour along a transformation path. In the following illustration  $R$  is taken as the independent variable and interpolated between its extremes. The lattice parameters are adjusted proportionately and the values of the other bondlengths and of the parameter  $u$  follow (this procedure is not as unphysical as the purely geometric variation mentioned earlier: effectively both  $c$  and  $uc$  are changed proportionately which means that  $u$  itself does not change very much initially; buckling is therefore slow to start, in keeping with the studies under discussion). The question of how the  $cD$  parametrization should merge with and ultimately replace the  $rG$  parametrization is answered by considering the charge density conclusions just reported. I take the Keating energy as

$$E = fE_{rG} + (1 - f)E_{cD} \quad (9.9)$$

where, with  $R_{\min} = 1.8$  and  $R_{\max} = 2.1$ , the switching function is

$$f = \begin{cases} 0 & \text{when } R < R_{\min}, \\ \frac{1}{2} - \frac{1}{2} \cos\left(\frac{\pi(R - R_{\min})}{R_{\max} - R_{\min}}\right) & \text{when } R_{\min} \leq R \leq R_{\max}, \\ 1 & \text{when } R_{\max} < R. \end{cases} \quad (9.10)$$

The results for the second-order elastic constants are illustrated in Fig. 9.5, for the internal strain parameters in Fig. 9.6 and for the zone-centre optic-mode frequencies in Fig. 9.7. Each display<sup>2</sup>

<sup>2</sup>I have inadvertently used  $R_{\min} = 1.7$  in the switching function when preparing these displays. The effect is of no great significance as the results are essentially qualitative.

is divided into three by the upper and lower limits of the switching function. On the left only the *rG* parameters are involved, any variations being due solely to the changes in the geometry of the cell, and on the right only *cD* parameters are involved. The mixing of the two régimes occurs in between.

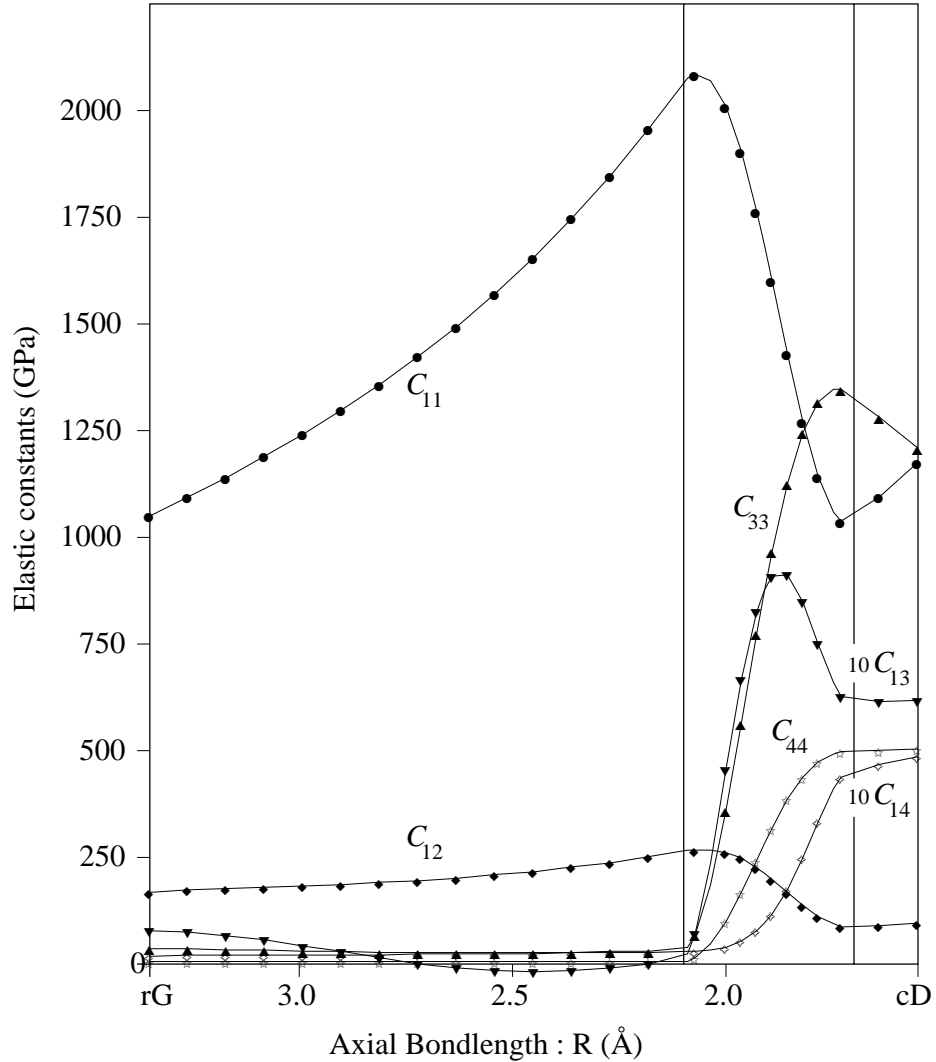


Figure 9.5: Second-order elastic constants along a transformation path.  $C_{13}$  and  $C_{14}$  are shown at  $\times 10$  magnification. Terminal values on the right are quasi-*rD* values.

It is partly the geometrical aspect of the partial constants, the disposition of  $a$  and  $d$  in the common factors in Table 9.2, and partly the internal strain that determines the overall variation of the total constants seen in the *rG* region. Thus both  $C_{11}^0$  and  $C_{12}^0$  increase as  $a^2/d$  and double in size as 68% of the path is traversed. Roughly equal contributions from inner displacement are subtracted from each, about 5% of  $C_{11}^0$  but 25% of  $C_{12}^0$  at the limit, leaving the variation of  $C_{11}$  to dominate the picture. The only other feature that merits comment is the variation of  $C_{13}$ : this very small constant makes a negative excursion in the *rG* region and then, uniquely, rises to a maximum in the middle of the transition region. The significance of this eludes me, however!

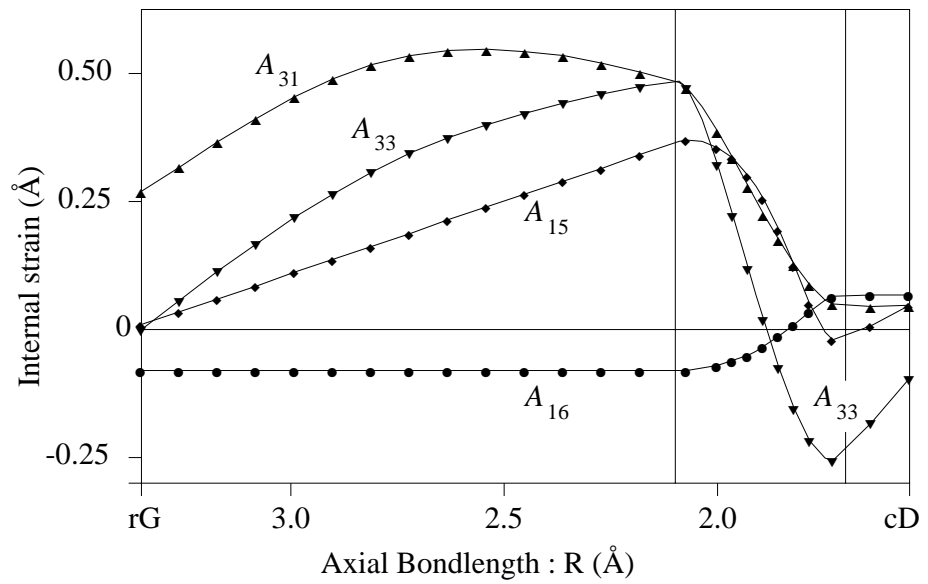


Figure 9.6: Internal strain parameters along a transformation path. Terminal values on the right are quasi- $rD$  values.

The apparent constancy of  $A_{16}(= -D_{16}/E_{11})$  is due to its net common factor of  $a$  which increases by only about 2% across the  $rG$  region. In view of the general manifestation of pseudo-symmetry in planar  $rG$  it is a little surprising that  $A_{31}(= -D_{31}/E_{33})$  does not start at zero, as do  $A_{15}$  and  $A_{33}$ .

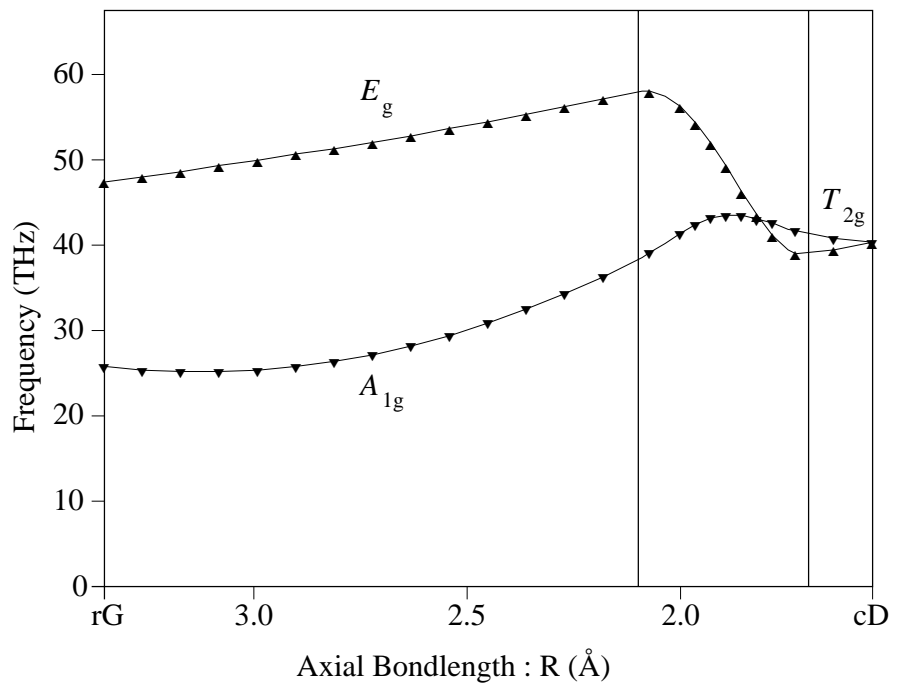


Figure 9.7: Zone-centre frequencies along a transformation path. The terminal value on the right is the quasi- $rD$  value.

The one interesting feature of the optic-mode frequencies is their (accidental?) degeneracy in the transition region at  $R = 1.8 \text{ \AA}$ . This is the very value of the onset of peaks in the electron density along the axial bond, [4], and close to the value  $1.76 \text{ \AA}$ , deducible from measurements on Fig. 3 in [10], at which a symmetry-imposed level crossing at the  $\Gamma$  point occurs. The latter is related to the change from  $sp^2 + p_z$  to  $sp^3$  bonding, essentially the same fact.

### 9.6.2 Hydrostatic compression path

Fahy, Louie and Cohen's second calculation followed a hydrostatic pressure path with results that were very different from those based on energy minimization. The path for example does not lead continuously to the  $cD$  structure but terminates when  $p = 80 \text{ GPa}$  and  $V_c = 11.0 \text{ \AA}^3$  at which point  $R = 2.1 \text{ \AA}$ ,  $r = 1.38 \text{ \AA}$  and  $\theta = 97^\circ$ . This result has been entered in row five of Table 9.7. The logic behind this calculation is not clear. The authors state that they have treated  $V_c$  as an independent variable and have varied  $r$  and  $\theta$  to minimize the enthalpy at each value of  $V_c$ . For a hexagonal cell, however, a given value of  $V_c$  does not fix the lattice parameters, only the product  $ca^2$ . A complete energy minimization should sample a range of  $(a, c)$  pairs and optimize  $R$ ,  $r$  and  $\theta$  at each (simultaneously *via*  $u$ ). There is no indication that this has been done.

Further doubt is raised by the present elasticity results. The harmonic and anharmonic axial compressibilities,  $k_c = 0.0271 \text{ GPa}^{-1}$  and  $K_c = 0.0119 \text{ GPa}^{-2}$ , imply that the effective compressibility at a pressure  $p \text{ GPa}$  is, by (5.18),  $k_c^* = k_c - 0.5(K_c - k_c^2)p = 0.0271 - 0.0056p \text{ GPa}^{-1}$ . This goes to zero at a pressure of  $4.84 \text{ GPa}$ . However, if the anharmonic part is neglected and a path is chosen that (i) changes  $a$  and  $c$  according to  $k_a$  and  $k_c$  and (ii) changes  $uc$  in the same way as  $c$ , then a modest pressure of just over  $14 \text{ GPa}$  leads to a structure very close to that of diamond. The process is illustrated in Table 9.8 below.

Table 9.8: Hydrostatic compression path.

$p/\text{GPa}$	$a/\text{\AA}$	$c/\text{\AA}$	$V_c/\text{\AA}^3$	$u$	$R/\text{\AA}$	$r/\text{\AA}$	$\theta/^\circ$
0	2.460	10.048	17.55	0.167	3.350	1.420	90.0
2	2.457	9.503	16.56	0.163	3.095	1.420	92.9
4	2.454	8.958	15.57	0.159	2.841	1.424	95.8
6	2.450	8.413	14.58	0.154	2.587	1.431	98.7
8	2.447	7.868	13.60	0.148	2.333	1.442	101.6
10	2.444	7.323	12.63	0.142	2.079	1.457	104.4
12	2.441	6.778	11.66	0.135	1.824	1.475	107.2
14	2.438	6.233	10.69	0.126	1.570	1.496	109.8
14.2	2.437	6.178	10.60	0.125	1.545	1.498	110.1

The axial bond has reached its ideal value  $1.545 \text{ \AA}$  but the other bonds are still slightly short.

Some discrepancy will always be present since  $a$  is forced to shorten in a hydrostatic compression. It is no coincidence that this pressure is close to the value at which  $hG$  undergoes a transformation to  $hD$ .

It may be that this speculative discussion is of academic interest only. In a molecular dynamics simulation of the conversion by Scandolo *et al.* [13] it was found that  $hG$  was converted into both  $cD$  and  $hD$  via an intermediate orthorhombic phase of graphite. This process resulted in different orientation relationships between the initial and final crystal structures from the one implicit in the discussions above. Although they did not explicitly study  $rG$  it seems likely that  $rG$  will behave in a similar way.

If there is a technological interest in actually achieving the  $rG$ -to- $cD$  conversion then a uniaxial stress route might be worth investigation. A compressive stress  $\sigma_3$  changes the lattice parameters according to

$$\frac{\Delta a}{a_0} = S_{13}\sigma_3 + \frac{1}{2}S_{133}\sigma_3^2 \quad (9.11)$$

and

$$\frac{\Delta c}{c_0} = S_{33}\sigma_3 + \frac{1}{2}S_{333}\sigma_3^2 \quad (9.12)$$

Since  $S_{13} < 0$  and  $S_{33} > 0$  a compressive stress (which is negative) causes  $a$  to increase and  $c$  to decrease simultaneously.

## 9.7 Summary

The Chapter began with an exploration of the precise nature of rhombohedral graphite, focusing on the initial structural studies of natural graphite and work on defects to be seen therein. It was concluded that the rhombohedral form was not a true allotrope but a mosaic distribution of microcrystalline defect regions embedded in the  $hG$  host. These regions could be sufficiently large, however, to merit their study as if they were truly allotropic. The issue of whether the equilibrium state consisted of planar or buckled layers was resolved in favour of planar layers.

The elasticity in terms of the modified Keating model was then calculated for the planar structure. The transfer of Keating parameters from  $hG$  to  $rG$  showed that the two allotropes were elastically extremely similar. The possession of a set of elastic constants for this as-yet-uncharacterized material provided an opportunity to explore the  $rG$ -to- $cD$  transformation in greater detail. There were no surprises, but there was a hint that changes in the nature of the bonding were indicated in the behaviour of the optic-mode frequencies.

## References

- [1] C. Baker, Y. T. Chou and A. Kelly, *Phil. Mag.* **6**, 1305 (1961)
- [2] J. D. Bernal, *Proc. Roy. Soc. A* **106**, 749 (1924)

- 
- [3] J.-C. Charlier, X. Gonze and J.-P. Michenaud, *Carbon* **32**, 289 (1994)
- [4] S. Fahy, S. G. Louie and M. L. Cohen, *Phys. Rev.* **B34**, 1191 (1986)
- [5] S. Fahy, S. G. Louie and M. L. Cohen, *Phys. Rev.* **B35**, 7623 (1987)
- [6] E. J. Freise and A. Kelly, *Phil. Mag.* **8**, 1519 (1963)
- [7] J. Furthmüller, J. Hafner and G. Kresse, *Phys. Rev.* **B50**, 15606 (1994)
- [8] R. R. Haering, *Can. J. Phys.* **36**, 352 (1958)
- [9] O. Hassel and H. Mark, *Z. Phys.* **25**, 317 (1924)
- [10] M. Kertesz and R. Hoffmann, *J. Solid State Chem.* **54**, 313 (1984)
- [11] H. Lipson and A. R. Stokes, *Proc. Roy. Soc. A* **181**, 101 (1942)
- [12] H. Ott, *Ann. Phys., Lpz.*, **85**, 81 (1928)
- [13] S. Scandolo, M. Bernasconi, G.L. Chiarotti, P. Focher and E. Tosatti, *Phys. Rev. Lett.* **74**, 4015 (1995)
- [14] R. Siems, S. Amelinckx and P. Delavignette, *Z. Phys.* **165**, 502 (1961)

## Chapter 10

### Bond-order potentials

The Keating model is not a potential—it is a way of storing second and third derivatives of the energy with respect to significant structural parameters, the scalar products of interatomic vectors. There are no preconceptions about the forms of interactions between atoms and crystal equilibrium is not addressed. Every elastic and inner elastic constant is a linear combination of some of the Keating parameters and if the (possibly) *many* of the former can be well reproduced by the (probably) *few* of the latter then it is likely that all significant variables have indeed been considered. This is certainly the case for *cD* and *hG* as I have shown in Chapters 6 and 7. In a manner of speaking the Keating parameters are just a distilled set of elastic constants and are not greatly illuminating.

Illumination comes from understanding the nature of the interactions in the crystal. Early work focused on the  $\phi(r) \propto 1/r^n$  potentials which could describe the Coulomb interaction ( $n = 1$ ) and the van der Waals interaction ( $n = 6$ ) rigorously, and the short-range repulsive interaction ( $n = 9$  to  $12$ ) effectively. Later work introduced exponential terms  $\phi(r) \propto \exp(-\alpha r)$  on the ground that these mimicked the spatial variation of electron wavefunctions. In reality all central potentials imply the satisfaction of Cauchy relations: equality between their contributions to different partial elastic constants at each order such as  $C_{12}^0 = C_{66}^0$  and  $C_{123}^0 = C_{144}^0 = C_{456}^0$ . As satisfaction of Cauchy relations was never found it could be concluded that interatomic distances alone could not form a complete set of significant variables and/or other contributions to the energy of the crystal had been ignored. Additional variables might be volume or angle and neglected contributions vibrational energy and electron energy.

The main factor that defeated these early attempts to define a simple analytical potential was the nature of bonding. Non-metals, with their networks of localized bonds, are the prime candidates for angular dependencies in energy. But an analytic form, as general as the Coulomb potential for ionic bonding, is unlikely to exist.

The introduction of the pseudopotential concept and the development of high-speed computing have led to ever-increasing sophistication in the treatment of the energy and bandstructure of solids. This might be thought to have made the computation of elastic constants a routine accompaniment and rendered unimportant the need for interatomic potentials. This is not the case for at least

two reasons. Firstly, the full extraction of the multitude of elastic and inner elastic constants for a crystal of relative simplicity, such as  $hG$ , still requires the computation of the energy at an enormous number of strained configurations. Thus if a few minutes suffice for one computation of energy the full elasticity may require several weeks! Secondly, large-scale molecular-dynamical simulations require computationally-rapid updating of system energies and forces. Simple algorithms based on effective short-range potentials are essential here. Such are the empirical bond-order potentials developed by Abell [1], Tersoff [16, 17, 18, 19] and Brenner [2, 3], together with a refinement due to Burgos, Halac and Bonadeo, [4]. They have the form of a short-range pair potential in which the attractive term has a factor that depends on local coordination and bond angles. Their parametrization has been carried out by considering the energies of atomic clusters, of defects, of bonds in hydrocarbon molecules, of cohesion of crystalline phases, of optical phonons etc. With relatively few parameters to fit it is not surprising that the derived potentials are only ‘good in parts’. The Tersoff/Brenner formulation involves angular dependencies that reflect only  $\sigma$  bonding and behaves poorly when applied in other situations, [11]. This drawback appears to have been overcome in the last two years through the development, by Pettifor and Oleinik, of an analytic bond-order potential that includes  $\pi$  bonding explicitly, [10, 11, 12].

As the empirical bond-order approach has similarities to the Keating approach I have shown in detail in Appendix C how they are related. Incidentally I have exposed certain general dependencies connecting the various Keating parameters at each order. In the remainder of this Chapter I report on the bond-order work with some changes in notation to prevent confusion with notation used earlier in the thesis: thus my interatomic vector  $\vec{r}^i$  and its magnitude  $r^i$ , which relate atomic site  $i$  to an implied reference site  $s$ , is used where the bond-order literature has  $\vec{r}_{ij}$  and  $r_{ij}$ . Similarly  $B_i$  replaces  $B_{ij}$  as the bond order function. Various switching functions that define cut-off distances, and which are irrelevant in a crystalline environment, have been omitted.

## 10.1 Empirical bond-order potentials

Abell’s stated motivation was the goal of developing a general description of bonding that would (i) isolate key features that determine whether a species prefers molecular or metallic bonding and (ii) would explain outstanding differences, as well as similarities, between molecular and metallic bonding, [1]. He was persuaded that such similarities existed from the observation of an apparently universal relation between binding energy and interatomic spacing discovered by Ferrante, Smith and Rose [6, 14]. His basic method was LCAO parametrization in the context of the chemical pseudopotential. His central result for the binding energy is

$$E_s = \sum_{i=1}^Z E_i \quad (10.1)$$

where  $E_s$  is the binding energy of the atom at site  $s$ ,  $Z$  is its atomic coordination and

$$E_i = \frac{1}{2}(V_R(r^i) - B_i V_A(r^i)) \quad (10.2)$$

is the pair potential relating atoms at  $s$  and  $i$ . The repulsive and attractive parts of the potential are given by

$$V_R(r^i) = A \exp(-\lambda_R r^i) = \frac{D_e}{S-1} \exp\left(-\beta\sqrt{2 \times S}(r^i - r_e)\right) \quad (10.3)$$

and

$$V_A(r^i) = B \exp(-\lambda_A r^i) = \frac{SD_e}{S-1} \exp\left(-\beta\sqrt{2/S}(r^i - r_e)\right). \quad (10.4)$$

$r^i$  is the magnitude of the vector from site  $s$  to site  $i$  and  $A$ ,  $\lambda_R$ ,  $B$  and  $\lambda_A$  are characteristic constants. The right-hand members of these equations contain alternative constants designed to expose the connection between the potential and the Morse potential that underlies the universal relationship referred to above.  $r_e$  and  $D_e$  are the bondlength and binding energy of the  $C_2$  dimer and  $S = \lambda_R/\lambda_A$ . For the original Morse potential  $S = 2$  and a critical value of the ratio,  $S_c \approx 2.7$ , appears to discriminate between close-packed structures for which  $S > S_c$ , and more open ones for which  $S < S_c$ . Eq. (10.2) is not a central potential because of  $B_i$ , the first-shell bond order in the nearest-neighbour approximation.  $B_i$  is related to the distribution of valence electrons over bonding and anti-bonding states. It is unaffected by uniform expansion but is ‘quite sensitive’ to structural changes at constant volume, thereby making Eq. (10.2) non-central.  $B_i$  is crucial to the elasticity of carbon: it is the source of the bond-bending terms in the Keating formalism. The remainder of Abell’s paper is concerned only with the energetics of metals and molecules,  $B_i$  plays no further part. Elemental carbon is referred to only once, when Abell reports Lannoo’s calculation [9] of  $S = 1.4$ .

It is in Tersoff’s work on silicon that the bond-order term  $B_i$  is given functional form. In [16] he asserts that *all* deviations from a simple pair potential are ascribed to the dependence of  $B_i$  upon the local atomic environment. Specifically  $B_i$  should be a monotonically decreasing function of the number of bonds  $r^j$  competing with  $r^i$  (i.e.  $Z - 1$  in a regular crystalline environment), the strength of the competing bonds and the cosines of the angles between the competing bonds,  $\cos\theta_{isj}$ . A trial representation of such a function is then presented which I shall not repeat here as Tersoff changes his mind in [17] in which he proposes (though with  $n$  where I write  $l$  and with  $1/2n$  where I have  $n$ )

$$B_i = \left(1 + (az_i)^l\right)^{-n} \quad (10.5)$$

where

$$z_i = \sum_{j=1}^{Z'} g(\theta_{isj}) \exp(\lambda_3^3(r^i - r^j)^3) \quad (10.6)$$

with

$$g(\theta) = 1 + c^2/d^2 - c^2/(d^2 + (\cos\theta - h)^2). \quad (10.7)$$

I have replaced his use of  $\beta$  by  $a$  to avoid possible confusion. In subsequent papers [18, 19] the factor  $\exp[\lambda_3^3(r_{ij} - r_{ik})^3]$  was omitted. Application of the potential to carbon was presented in [18]. The parameters were said to have been fitted by calculating ‘the energy and structure of numerous polytypes of carbon, and the elastic properties, phonons, defect energies and migration barriers in diamond and graphite’. ‘Graphite’ meant graphitic layers and ‘elastic properties and phonons’ referred only to diamond. In Tersoff’s opinion the elastic properties of graphite are ‘adequately described’ even though he finds  $C_{11}$  at 12.1 Mbar too large by 14% and  $(C_{11} - C_{12})/2$  at 7.0 Mbar too large by about 40%, reflecting ‘excessive bond-angle stiffness’. His arithmetic is faulty somewhere, the latter error is 59% in fact, and the figures translate to  $C_{12} = -1.9$  Mbar as opposed to the +1.8 Mbar observed—hardly ‘adequate’. The parameters deduced are shown in Table 10.1.

Table 10.1: Empirical bond-order potential parameters. Parameters in parentheses have been deduced from Eqs. 10.3 and 10.4.

Parameter	Tersoff	Brenner 1	Brenner 2	Burgos <i>et al.</i>
$A$ (eV)	1393.6	(476.45)	(518.37)	(625.67)
$\lambda_R$ ( $\text{\AA}^{-1}$ )	3.4879	(2.4094)	(2.4094)	(2.9090)
$B$ (eV)	346.74	(307.26)	(328.02)	(225.14)
$\lambda_A$ ( $\text{\AA}^{-1}$ )	2.2119	(1.8677)	(1.8677)	(1.8446)
$D_e$ (eV)	(5.1645)	6.325	6.325	6.362
$r_e$ ( $\text{\AA}$ )	(1.4472)	1.28	1.315	1.3883
$\beta$ ( $\text{\AA}^{-1}$ )	(1.964)	1.5	1.5	1.638
$S$	(1.577)	1.29	1.29	1.577
$a$	$1.5724 \times 10^{-7}$	0.0113	0.0113	$1.5724 \times 10^{-7}$
$l$	0.72751	1.0	1.0	0.891
$n$	0.687276	0.8047	0.8047	0.687276
$c$	38049.0	19.0	19.0	38049.0
$d$	4.3484	2.5	2.5	4.745
$h$	-0.57058	-1.0	-1.0	-0.7171
$m$ ( $\text{\AA}^{-1}$ )	0.0	2.25	0.0	0.0

Brenner, independently, applied the Tersoff formalism to carbon [2, 3]. His bond-order term takes the form

$$B_i = \left(1 + \sum_{j=1}^Z a z_j\right)^{-n} \quad (10.8)$$

where

$$z_j = g(\theta_{isj}) \exp(m(r^i - r^j)) \quad (10.9)$$

with

$$g(\theta) = 1 + c^2/d^2 - c^2/(d^2 + (\cos \theta - h)^2). \quad (10.10)$$

The parameter  $a$  is missing from these equations in [2] although its value is reported. It appears, however, in the later paper, [3] where it multiplies the right-hand side of  $g(\theta)$ . My placing it in  $B_i$  is equivalent, and facilitates comparison with the Tersoff form. As there are two differences between the two accounts,  $r_e$  goes from 1.28 Å to 1.315 Å and  $m$  goes from 2.25 to 0, I have listed sets 1 and 2 for Brenner.

Brenner felt that it was not obvious that the formalism was capable of describing the strong  $\pi$ -bonding that stabilizes the graphite planes whilst maintaining an almost equally energetically-stable diamond phase. To achieve these ends at the same time he used the following data: the binding energies and equilibrium bond distances of the  $C_2$  molecule, the graphite layer and the diamond phase, the binding energies of hypothetical simple cubic and face-centred cubic phases and the energy barrier calculated for the  $rG$ -to- $cD$  transition by Fahy *et al.* [5]. The parameters thereby deduced give rise to the entries for set 1 in the Table above. For set 2 the value of the dimer bondlength appears to have been relaxed.

Burgos, Halac and Bonadeo, [4], were not satisfied with the quality of fit achieved by either Tersoff or Brenner and set out to refine the computation. They focused on dynamic properties as these are particularly poorly predicted. One specific observation on the calculated ratio of the frequencies of out-of-plane modes at the  $\Gamma$  and M points of the Brillouin zone showed that the gross failure to agree with experiment was due to the form of the potential and would only be eliminated by altering Eq. (10.2). They decided to add a new term that would not disturb the static properties and chose a torsional one. Stripped of switching functions and couched in different notation this was

$$V_i^{\text{tor}} = \tau \sum_{(j,k) \neq i} T_{ijk} \quad (10.11)$$

where  $\tau = -0.208$  eV and

$$T_{ijk} = \frac{(\vec{r}^j \times \vec{r}^i) \cdot (\vec{r}^i \times \vec{r}^k)}{r^j (r^i)^2 r^k}. \quad (10.12)$$

Physically  $\vec{r}^k$  represents an interatomic vector from atom  $i$  to one of its nearest neighbours other than the reference atom, geometrically it is the negative of a vector from the reference atom to one of its nearest neighbours other than atom  $i$ . Table 2 in [4] shows the static and dynamical predictions of Tersoff, Brenner and Burgos *et al.* and compares them with experiment. Root-mean-square deviations for Tersoff and Brenner are 30.1% and 28.8% respectively. The inclusion of the torsional term and the refinement of  $D_e$ ,  $r_e$ ,  $\beta$ ,  $l$ ,  $d$  and  $h$  produced a seemingly remarkable improvement with the deviation brought down to 9.7%. This figure is heavily weighted by the predictions of various frequencies and does not reflect improvement in predicting the elastic constants: in that respect Tersoff's work is far superior, as evident in Table 10.2 below. A noteworthy outcome of this fitting was the increase in the binding energies of diamond and graphite. Care was taken to

maintain the difference between them small but their magnitudes increased to about 8.56 eV. The authors note that this is in keeping with recent *ab initio* calculations, [8, 13, 20].

There is no unique connection between bond-order potential parameters and Keating parameters. Two approaches will be described.

### 10.1.1 Matched elastic constant predictions

In this approach subsets of the spectrum of elastic and inner elastic constants obtained from the bond-order potential by the generalized homogeneous deformation program are fitted by least squares, or even exactly, to the appropriate Keating expressions. Firstly the program was run with the experimental values of lattice parameters and nearest-neighbour separations. Sizable positive values of  $C_1$  showed that the energy was not minimized at the experimental value of  $r_0$  and that the crystal was under pressure to reduce the value. Self-consistent recalculation at the implied values of  $r_0$  resulted in  $C_1$  close to zero and a marginal improvement in predicted values. The results for the first- and second-order constants are shown in Table 10.2 (columns headed BHB 1 and BHB 2 refer to calculations without and with the torsional term).

Table 10.2: SOECs of cD predicted by bond-order potentials and equivalent Keating parameters. Units: GPa for  $C$ , GPa Å<sup>-1</sup> for  $D$  and  $\alpha$  etc., and GPa Å<sup>-2</sup> for  $E$ . Also shown are the Raman frequency (in THz), the bulk modulus and the Kleinman internal strain parameter.

Parameter	Tersoff	Brenner 1	Brenner 2	BHB 1	BHB 2	This work
$C_1$	0.5	17.2	19.1	12.6	12.6	0.0
$r_0$	1.5440	1.5055	1.5406	1.5248	1.5248	1.5446
$C_1$	-0.01	-0.03	-0.01	0.02	0.02	0.00
$C_{11}$	1074.2	363.2	350.0	763.7	763.7	1072.3
$C_{12}$	101.7	199.4	197.1	140.3	140.3	130.7
$C_{44}^0$	671.2	392.2	351.9	554.8	535.6	577.8
$C_{44}$	641.6	320.0	277.2	531.0	483.2	574.0
$B$	425.9	254.0	248.1	348.1	348.1	445.0
$E_{11}$	766.7	287.7	333.5	624.8	525.2	561.9
$f_R$	47.0	27.7	30.9	41.6	38.2	40.2
$\zeta_K$	0.220	0.576	0.532	0.220	0.360	0.093
$\alpha$	1.282	0.672	0.718	1.018	1.021	0.990
$\beta$	0.851	0.147	0.134	0.552	0.552	0.824
$\sigma$	-0.019	0.018	0.082	0.117	-0.091	-0.115
$\tau$	-0.038	0.076	0.091	0.088	-0.051	0.021

The self-consistent constants are used to determine a set of equivalent Keating parameters by

inverting Eq. (6.44). There are various ways of doing this and I have chosen to take  $C_{11}$ ,  $C_{12}$ ,  $D_{14}$  and  $E_{11}$ . The results have been added to Table 10.2. Qualitatively they appear in closer agreement than do the data from which they are derived. At the third order the situation is much more chaotic and the Keating parameters vary wildly depending on the elastic constant set chosen for inversion. Parameters based on an exact fit to the first five TOECs and  $D_{114}$  are given in Table 10.3. The Tersoff  $\gamma$  is -0.064 for this fit but becomes -0.183 if just the five Keating parameters excluding  $\xi$  are fitted by least squares. If  $C_{144}^0$  is replaced by  $E_{111}$  then the least squares procedure leads to a  $\gamma$  of -2.761!

Table 10.3: TOECs of  $cD$  predicted by bond-order potentials and equivalent Keating parameters. Units: GPa for  $C$ , GPa  $\text{\AA}^{-1}$  for  $D$ , GPa  $\text{\AA}^{-2}$  for  $E$  and GPa  $\text{\AA}^{-3}$  for  $\gamma$  etc.

Parameter	Tersoff	Brenner 1	Brenner 2	BHB 1	BHB 2	This work
$C_{111}$	-6526.	-1612.	-1558.	-4059.	-4059.	-6475.
$C_{112}$	-1653.	-765.	-761.	-1170.	-1170.	-1947.
$C_{123}$	685.	-496.	-506.	189.	189.	982.
$C_{144}^0$	-1230.	-712.	-757.	-883.	-870.	91.
$C_{155}^0$	-2741.	-1264.	-1135.	-1989.	-1957.	-3079.
$C_{456}^0$	-1763.	-962.	-867.	-1261.	-1251.	-355.
$D_{114}$	-700.	-349.	-502.	-572.	-689.	-259.
$E_{111}$	-6281.	-1342.	-1487.	-3884.	-3419.	-2705.
$\gamma$	-0.064	-0.424	-0.398	-0.338	-0.445	-0.879
$\delta$	-0.018	0.031	-0.027	-0.016	-0.016	0.122
$\epsilon$	-0.671	-0.126	-0.110	-0.413	-0.413	-0.623
$\eta$	0.548	0.131	0.117	0.273	0.212	-0.152
$\theta$	-0.482	0.122	0.029	-0.169	-0.180	0.316
$\xi$	-0.018	0.043	0.024	0.014	0.009	0.000

### 10.1.2 Matched energy derivatives

In this approach an analytic link is established between derivatives of the bond-order potential and the first-, second- and third-order Keating energy expressions. Appendix C contains the derivation of these relations together with a demonstration of the arbitrariness of the Keating parameters. The results are presented in Table 10.4. Brenner 1 is not considered because of its more complex form of  $B_i$ . A single result suffices for the two BHB versions.

Table 10.4: Keating parameters of  $cD$  from derivatives of the bond-order potential. Units:  $\text{GPa \AA}$  for  $\mu$  and  $\nu$ ,  $\text{GPa \AA}^{-1}$  for  $\alpha$  etc., and  $\text{GPa \AA}^{-3}$  for  $\gamma$  etc.

Parameter	Tersoff	Brenner 2	BHB 1	This work
$\mu$	0.974	0.579	1.013	0.000
$\nu$	0.974	0.578	1.012	0.000
$\alpha$	0.887	0.527	0.644	0.990
$\beta$	0.579	0.111	0.404	0.824
$\sigma$	-0.451	-0.267	-0.439	-0.115
$\tau$	-0.163	-0.076	-0.141	0.021
$\gamma$	-0.895	-0.409	-0.603	-0.879
$\delta$	-0.363	-0.036	-0.146	0.122
$\epsilon$	-0.647	-0.100	-0.380	-0.623
$\eta$	0.214	0.121	0.190	-0.152
$\theta$	-0.103	0.050	-0.000	0.316
$\xi$	-0.057	0.029	0.050	0.000

Table 10.5: Keating parameters of graphene from derivatives of the bond-order potential. Units:  $\text{GPa \AA}$  for  $\mu$  and  $\nu$ ,  $\text{GPa \AA}^{-1}$  for  $\alpha$  etc., and  $\text{GPa \AA}^{-3}$  for  $\gamma$  etc.

Parameter	Tersoff	Brenner 2	BHB 1	This work
$\mu$	1.099	0.788	1.216	0.000
$\nu$	1.099	0.786	1.216	0.000
$\alpha$	1.924	0.892	1.283	1.662
$\beta$	2.542	0.298	1.100	1.501
$\sigma$	0.321	-0.312	-0.209	0.188
$\tau$	-0.162	-0.147	-0.184	0.334
$\gamma$	-2.173	-0.776	-1.283	-4.289
$\delta$	-4.342	-0.080	-0.458	-6.004
$\epsilon$	-5.197	-0.309	-1.253	-2.279
$\eta$	-1.115	0.105	-0.145	0.000
$\theta$	-2.886	-0.062	-0.646	0.000
$\xi$	-0.237	0.045	-0.012	0.000

## 10.2 Analytic bond-order potentials

Analytic bond-order potentials (BOPs) have been developed by Pettifor and Oleinik [10, 11] by approximating the many-atom expansion for the bond order within the two-centre, orthogonal tight-binding model. These go beyond Tersoff-Brenner in that (i) they address both  $\sigma$  and  $\pi$  bond orders and (ii) they consider self-returning hopping paths of length 4 as well as length 2 in computing their potential functions. In the context of hydrocarbon systems the BOPs handle correctly the breaking of  $\pi$  bonds on radical formation.

Unfortunately the approximation involved in deriving equation (80) in [11] for the  $\sigma$  bond order proved to lead to unphysical behaviour in molecular dynamics simulations. Properly bounded BOPs were obtained in [12] and this refined approach resulted in the quantification of single, double, triple and conjugate bonds in carbon systems to within 1% of the accurate tight-binding calculations for  $\sigma$  bonds, and to within 15% for  $\pi$  bonds. A problem has now arisen in connection with the binding energy. The data necessary for its computation are contained in Horsfield *et al.* [7]. I have confirmed all the entries for *cD* and graphene in Table V of [10] except  $U_\sigma$ , which I find is  $-24.775$  rather than  $-24.749$  eV/bond and which makes the binding energy  $-8.797$  rather than  $-8.759$  eV/atom. Thus graphene appears more stable by some 291 meV/atom although a figure near zero is expected on the grounds that the binding energy of *hG* exceeds that of *cD* by 25 meV/atom whilst the interplanar binding energy of *hG* is also about 25 meV/atom [15]. In the revised work the bond potentials are unaltered but the bond orders are different and the two binding energies become  $-7.631$  and  $-6.997$  eV/atom, respectively. These now make *cD* more stable than graphene by an enormous 634 meV/atom. In the light of this discrepancy I do not feel it worth pursuing the numerical implications. The ingredients of the formalism however remain of interest and are presented below.

Equations (9) and (12) for  $\Theta_{ij,\sigma}^{\text{BOP}}$  and  $\Theta_{ij,\pi}^{\text{BOP}}$  in [12] are the general expressions for the  $\sigma$  and  $\pi$  bond order, equivalent to two  $B$  functions. They and their associated equations are simplified in treating purely elemental carbon. The notation used below has been changed to accommodate my bookkeeping by atoms rather than bonds. The  $\sigma$  bond order is

$$B_i^\sigma = \frac{1}{\sqrt{1 + \frac{\hat{\delta}_i^2 + 2\Phi_{2\sigma}^i}{\left[1 + \sqrt{\Phi_{4\sigma}^i/\Phi_{2\sigma}^i - \Phi_{2\sigma}^i}\right]^2}}} \quad (10.13)$$

where  $\hat{\delta}_i = [2\sqrt{p_\sigma}/(1+p_\sigma)]\delta_i/V_A^\sigma(\bar{r}_0^i)$  represents a normalized  $sp$  atomic energy level separation, with  $\delta = \epsilon_p - \epsilon_s = 6.7$  eV,  $p_\sigma = 1.1$  is the ratio of two bond integrals ( $pp\sigma/|ss\sigma|$ ) and

$$\Phi_{2\sigma}^i = \sum_{j=1}^Z \left( \frac{p_\sigma}{1+p_\sigma} \right)^2 \left( \cos \theta_{isj} + \frac{1}{p_\sigma} \right)^2. \quad (10.14)$$

The 4-hop term begins in the same way as the 2-hop term, but also includes summations over cubic

and quartic factors which are not shown here:

$$\Phi_{4\sigma}^i = \sum_{j=1}^Z ' \left( \frac{p_\sigma}{1+p_\sigma} \right)^2 \left( \cos \theta_{isj} + \frac{1}{p_\sigma} \right)^2 + \sum_{j=1}^Z ' \sum_{k=1}^Z '' \dots \quad (10.15)$$

The  $\pi$  bond order is

$$B_i^\pi = \frac{1}{\sqrt{1 + \Phi_{2\pi}^i + \sqrt{\Phi_{4\pi}^i}}} + \frac{1}{\sqrt{1 + \Phi_{2\pi}^i - \sqrt{\Phi_{4\pi}^i}}}, \quad (10.16)$$

where

$$\Phi_{2\pi}^i = \sum_{j=1}^Z ' \left\{ (1 - \cos^2 \theta_{isj}) \left( \frac{p_\sigma}{1+p_\sigma} \right) \left( \frac{V_A^\sigma(\vec{r}_0^j)}{V_A^\pi(\vec{r}_0^i)} \right)^2 + (1 + \cos^2 \theta_{isj}) \right\} \quad (10.17)$$

and

$$\Phi_{4\pi}^i = \sum_{j=1}^Z ' \sum_{k=1}^Z '' (1 - \cos^2 \theta_{isj})(1 - \cos^2 \theta_{isk}) \hat{\beta}_j^2 \hat{\beta}_k^2 \cos 2(\phi_j - \phi_k), \quad (10.18)$$

where

$$\hat{\beta}_j^2 = \left( \frac{p_\sigma}{1+p_\sigma} \right) \left( \frac{V_A^\sigma(\vec{r}_0^j)}{V_A^\pi(\vec{r}_0^i)} \right)^2 - 1 \quad (10.19)$$

and the  $\phi_j$  and  $\phi_k$  are dihedral angles.

As the  $\sigma$  and  $\pi$  bond terms are additive the Keating parameters implied by the BOP can be obtained from the expressions in Appendix C by including terms for each bond type.

## References

- [1] G. C. Abell, Phys. Rev. **B31**, 6184 (1985)
- [2] D. W. Brenner, in *Atomic Scale Calculations in Materials Science*, Vol. 141 of Materials Research Society Symposia Proceedings, ed. J. Tersoff, D. Vanderbilt and V. Vitek (MRS, Pittsburgh, 1989)
- [3] D. W. Brenner, Phys. Rev. **B42**, 9458 (1990)
- [4] E. Burgos, E. Halac and H. Bonadeo, Chem. Phys. Letters **298**, 273 (1998)
- [5] S. Fahy, S. G. Louie and M. L. Cohen, Phys. Rev. **B34**, 1191 (1986)
- [6] J. Ferrante, J. R. Smith and J. H. Rose, Phys. Rev. Letters **50**, 1385 (1983)
- [7] A. P. Horsfield, P. D. Godwin, D. G. Pettifor and A. P. Sutton, Phys. Rev. **B54**, 15773 (1996)
- [8] G. Jungnickel, Th. Frauenheim, D. Porezag, P. Blandeck and U. Stephan, Phys. Rev. **B50**, 6709 (1994)

- [9] M. Lannoo, *J. Phys. (Paris)* **40**, 461 (1979)
- [10] I. I. Oleinik and D. G. Pettifor, *Phys. Rev.* **B59**, 8500 (1999)
- [11] D. G. Pettifor and I. I. Oleinik, *Phys. Rev.* **B59**, 8487 (1999)
- [12] D. G. Pettifor and I. I. Oleinik, *Phys. Rev. Letters* **84**, 4124 (2000)
- [13] D. Porezag, Th. Frauenheim, Th. Köhler, G. Seifert and R. Kaschner, *Phys. Rev.* **B51**, 12947 (1995)
- [14] J. H. Rose, J. R. Smith and J. Ferrante, *Phys. Rev.* **B28**, 1835 (1983)
- [15] M. C. Schabel and J. L. Martins, *Phys. Rev.* **B40**, 7185 (1992)
- [16] J. Tersoff, *Phys. Rev. Letters* **56**, 632 (1986)
- [17] J. Tersoff, *Phys. Rev.* **B37**, 6991 (1988)
- [18] J. Tersoff, *Phys. Rev. Letters* **61**, 2879 (1988)
- [19] J. Tersoff, *Phys. Rev.* **B39**, 632 (1989)
- [20] C. H. Xu, C. Z. Wang, C. T. Chan and K. M. Ho, *J. Phys: Condens. Matter* **4**, 6047 (1992)

## Chapter 11

### In conclusion

My twofold task has been: firstly, to display the development of inner elasticity in general terms, with a complete exposure of the underlying symmetry implications and a detailed analysis not only of how sublattice displacements contribute to the macroscopic elastic constants but also of how they determine the frequencies and eigenvectors of the optic modes at the zone centre; and secondly, to illustrate that development by detailed treatment of the elasticity and zone-centre optic modes of four carbon allotropes.

I have carried out the first task much as I did originally. I have however sharpened-up some of the argument and focused on the relation between sublattice tensors and inner elastic constants with the intention of showing the inherent, though unimportant, arbitrariness of the latter. In the connection with lattice dynamics at the zone centre it is satisfying to have derived a secular equation for the optic modes alone, a development I have not seen elsewhere.

It was part-time employment on the study of *hG* that triggered the parallel study of the other three allotropes and ultimately the writing of this thesis. The four allotropes made an interesting group: the two with two atoms in the basis have the highest and the lowest symmetries, the two with four atoms in the basis have the same intermediate macroscopic symmetry but different microscopic symmetry; a different pairing contrasts the  $sp^3$ -bonded diamonds with the  $sp^2$ -bonded-layer structures of the graphites and the remaining pairing comprises two stable materials on the one hand with a pair that consists of a crystal rarely seen outside the high-pressure cell and a crystal that has never been isolated on the other.

I felt that a common approach was the best way to handle the elasticity and that the Keating model would be a good vehicle. The main, and initially only, problem was that the model had never been applied rigorously to material in any structures other than cubic diamond or zincblende. Formal extension of the model to *hG* revealed a large number of parameters to be found and a large number of elastic constants to be fitted. Mercifully the elasticity within the graphene layers proved to require less parameters than *cD* and the weak bonding between the layers required only three bond-stretching and no bond-bending parameters to deal with the anharmonicity. The exciting reward of this fitting was the revelation of soft optic modes at the zone centre and the prediction of a pressure-induced phase-transformation at about the correct pressure.

The minor problem, that appeared only after I began applying the method to  $hD$ , was simply that Keating's original formulation of strain contained a divisor (half the lattice parameter  $a$ ) that was dependent on the choice of unit cell. By omitting this divisor, effectively absorbing it into the Keating parameters, a modified set of Keating parameters is obtained for  $cD$  which can be transferred successfully to  $hD$ . In a similar way Keating parameters derived for  $hG$  were transferred to  $rG$ .

The validity of treating the elasticity of the poorly-characterized  $hD$  by transfer of parameters was supported by good accounts of the Raman frequencies and the bulk modulus. A small problem was identified: the reported constancy of a non-ideal axial ratio to high pressures is inconsistent with the anisotropy of linear compressibility inherent in a crystal with hexagonal symmetry. Symmetry-related problems also arise with the hypothetical structure of  $rG$ : there is no mirror plane perpendicular to the axis, as there is in  $hG$ , to guarantee the planar character of the graphene layer. The lower symmetry of  $rG$  is also associated with an internal strain tensor having four independent components as opposed to  $hG$ 's one. The strong axial components are implicitly responsible for a negative anharmonic compressibility that may be the single reason for the non-existence of the pure crystalline form.

The formal part of this thesis can be considerably extended by passing from the mechanical to the thermodynamic régime and investigating the effects of electric and/or magnetic fields on sublattice displacements, generalizing the internal strain concept and anatomizing the related tensor properties in a manner analogous to that used for the elastic constants. Ferroelectricity in particular, with its phase transitions, should be rewarding.

The lattice dynamical aspects have been restricted to the zone centre, an adequate treatment for the present purpose, but could be extended usefully and with little difficulty to cover the entire Brillouin zone.

The successful use of the modified Keating model with  $hG$  suggests that the model might well be suited to studying the elasticity and the vibrational properties of nanotubes and fullerenes.

The development of the Keating model can be used in conjunction with specific interatomic potentials if that appears appropriate—to handle the Coulomb interaction in an ionic solid, for example. In such cases a first-order Keating energy has to be introduced to balance the first-order part of the additional potential and render zero the first-order elastic constants that arise.

Further possible synoptic studies of cases where a particular structural motif underlies a variety of crystal structures spring to mind:  $\text{SiO}_2$  units in quartzes, tridymites, cristobalites, coesite and stishovite;  $\text{H}_2\text{O}$  in various ices (in IceI the O atoms occupy a quasi- $hD$  configuration) and BN in its zincblende, wurtzite and graphitic versions. Rationalization of data *via* the modified Keating model can serve as a useful preliminary in the derivation of a more sophisticated transferable interatomic potential.

## Appendix A

### Generalised homogeneous deformation

The elastic constants of finite strain theory can only be computed directly when the contributions to the energy of the system are simple analytical functions of the interatomic separations or of the unit cell volume. The favoured alternative is to use infinitesimal strain theory with suitably tailored homogeneous deformations. In the traditional approach two such *ad hoc* deformations were sufficient to determine the two second-order elastic shear constants of FCC metals, such as copper [1] and aluminum [2], in which there is no inner elasticity. In the latter work the deformation was not defined in terms of a parameter that tended to zero in the unstrained state and in neither case was the volume conserved to better than first order. If the method is to be applied to higher-order elastic constants and to hexagonal and rhombohedral material, where there are at least five second-order, ten third-order and numerous inner elastic constants, a rigorous formal procedure is necessary.

#### A.1 Homogeneous deformation

Homogeneous deformations are represented by deformation gradient matrices and may operate on the crystal structure with or without sublattice displacements. They may be defined in a generalised way in terms of a uniform volume-changing part and a shape-changing part. The latter is represented by

$$J(x) = S(x)[I + xP] \quad (\text{A.1})$$

where  $P$  is a  $3 \times 3$  matrix of small integers or zeroes that determines a particular deformation of shape,  $I$  is the unit  $3 \times 3$  matrix and  $x$  is a measure of the strain.  $S(x)$  is a scaling function used to ensure that the determinant of  $J(x)$  is unity, so that the volume of the crystal is undisturbed by the shape-changing part. It is given in terms of the trace and determinant of  $P$  ( $t_p$  and  $d_p$ ) and the trace of the matrix of the cofactors of the elements of  $P$  ( $c_p$ ) by

$$[S(x)]^{-3} = 1 + t_p x + c_p x^2 + d_p x^3. \quad (\text{A.2})$$

The uniform volume-changing part is a factor  $(1 + v)^{1/3}$ , where  $v$  is the relative change of volume of the unit cell under strain, giving

$$H(x, v) = (1 + v)^{1/3} J(x) \quad (\text{A.3})$$

for the net deformation gradient matrix.

The displacement of sublattice  $\alpha$  is defined by a small vector  $\vec{u}^\alpha$  such that the position vector  $\vec{r}_0^\alpha$  of a particular atom on the sublattice in the unstrained crystal becomes  $\vec{r}^\alpha$  after strain where

$$\vec{r}^\alpha = H(x, v)\vec{r}_0^\alpha + \vec{u}^\alpha. \quad (\text{A.4})$$

An individual contribution to the free energy per unit initial volume in this approach may be written

$$\begin{aligned} \rho_0 F(u^\alpha, v, x) = & \rho_0 F(0, 0, 0) + c_v^0 v + c_x^0 x + d_i^\alpha u_i^\alpha \\ & + \frac{1}{2} c_{vv}^0 v^2 + c_{vx}^0 v x + \frac{1}{2} c_{xx}^0 x^2 + d_{iv}^\alpha u_i^\alpha v + d_{ix}^\alpha u_i^\alpha x + \frac{1}{2} e_{ij}^{\alpha\beta} u_i^\alpha u_j^\beta \\ & + \frac{1}{6} c_{vvv}^0 v^3 + \frac{1}{2} c_{vvx}^0 v^2 x + \frac{1}{2} c_{vxx}^0 v x^2 + \frac{1}{6} c_{xxx}^0 x^3 \\ & + \frac{1}{2} d_{ivv}^\alpha u_i^\alpha v^2 + d_{ivx}^\alpha u_i^\alpha v x + \frac{1}{2} d_{ixx}^\alpha u_i^\alpha x^2 \\ & + \frac{1}{2} e_{ijv}^{\alpha\beta} u_i^\alpha u_j^\beta v + \frac{1}{2} e_{ijx}^{\alpha\beta} u_i^\alpha u_j^\beta x + \frac{1}{6} f_{ijk}^{\alpha\beta\gamma} u_i^\alpha u_j^\beta u_k^\gamma, \end{aligned} \quad (\text{A.5})$$

for a specific choice of  $P$ . Summation over repeated subscripts  $i, j$  and  $k$  and over the superscripts  $\alpha, \beta$  and  $\gamma$  is implied: the former run from 1 to 3 and the latter from 1 to 2 ( $cD$  and  $rG$ ) or 1 to 4 ( $hD$  and  $hG$ ). The coefficients labelled with  $vs$  and/or  $xs$  are linear combinations, e.g.  $d_{ivx}^\alpha$  is a combination of several of the  $d_{iJK}^\alpha$ . Lower case symbols  $c, d, e$  and  $f$  have been used for the different tensors to indicate their kinship with the upper case versions used in the finite strain approach. Coefficients defined in the above way are called Fuchs constants following their introduction in [1].

The Lagrangian strain is given by

$$2\eta(x, v) + I = \tilde{H}(x, v)H(x, v) \quad (\text{A.6})$$

where the tilde denotes matrix transposition. The rotationally-invariant measures of inner displacement  $\vec{\zeta}^\lambda$  are defined from the relative displacements of atoms on two sublattices by

$$\vec{\zeta}^\lambda(x, v) = \tilde{H}(x, v)(\vec{u}^{\lambda+1} - \vec{u}^\lambda) \quad (\text{A.7})$$

or

$$\vec{\zeta}^\lambda(x, v) = \tilde{H}(x, v)\Lambda^{\lambda\alpha}\vec{u}^\alpha \quad (\text{A.8})$$

where

$$\Lambda = \begin{bmatrix} -1 & 1 & \cdot & \cdots & \cdot & \cdot \\ \cdot & -1 & 1 & \cdots & \cdot & \cdot \\ \vdots & \vdots & \vdots & \ddots & \vdots & \vdots \\ \cdot & \cdot & \cdot & \cdots & 1 & \cdot \\ \cdot & \cdot & \cdot & \cdots & -1 & 1 \end{bmatrix}. \quad (\text{A.9})$$

No generality is lost if  $P$  is taken to be symmetric and thus finally we have

$$2\eta(x, v) + I = (1 + v)^{2/3} [S(x)]^2 [I + 2xP + x^2P^2] \quad (\text{A.10})$$

and

$$\bar{\zeta}^\lambda(x, v) = (1 + v)^{1/3} S(x) (I + xP) \Lambda^{\lambda\alpha} \bar{u}^\alpha. \quad (\text{A.11})$$

The constants calculated directly from Eq. (A.5) are related to those appearing in Eq. (1.10) through chain rule differentiation with the operators

$$\begin{aligned} \frac{\partial}{\partial x} &= \left( \frac{\partial \eta_I}{\partial x} \right) \frac{\partial}{\partial \eta_I} \\ \frac{\partial}{\partial v} &= \left( \frac{\partial \eta_I}{\partial v} \right) \frac{\partial}{\partial \eta_I} \\ \frac{\partial}{\partial u_i^\alpha} &= \left( \frac{\partial \zeta_j^\lambda}{\partial u_i^\alpha} \right) \frac{\partial}{\partial \zeta_j^\lambda} = H_{ij}(x, v) \tilde{\Lambda}^{\alpha\lambda} \frac{\partial}{\partial \zeta_j^\lambda}. \end{aligned} \quad (\text{A.12})$$

Coefficients are evaluated at zero strain when differentiation is complete.

### A.1.1 Fuchs constants in terms of Brugger constants

The completely general relationships between Fuchs and Brugger constants are given by the expressions below in which summation over repeated subscripts is assumed. The convention  $\delta_I = 1$  when  $I = 1, 2$  or  $3$  and is zero otherwise, is used. The coefficients  $t_i$  are related to those in Eq. (A.2) by  $t_1 = -t_p$ ,  $t_2 = 5t_p^2 - 6c_p$  and  $t_3 = -(20t_p^3 - 45t_p c_p + 27d_p)$ .  $P$  and  $Q$  each appear in two guises: as  $3 \times 3$  matrices with elements  $P_{ij}$ ,  $Q_{ij}$ , and as  $6 \times 1$  matrices with elements  $P_I$ ,  $Q_I$ . The latter relate to the former in the same way as  $\eta_I$  relates to  $\eta_{ij}$ .

Under volume strain alone:

$$\begin{aligned} 3c_v^0 &= \delta_I C_I^0 \\ 9c_{vv}^0 &= -\delta_I C_I^0 + \delta_I \delta_J C_{IJ}^0 \\ 27c_{vvv}^0 &= 4\delta_I C_I^0 - 3\delta_I \delta_J C_{IJ}^0 + \delta_I \delta_J \delta_K C_{IJK}^0. \end{aligned} \quad (\text{A.13})$$

Under shape strain alone:

$$\begin{aligned} 3c_x^0 &= (t_1 \delta_I + 3P_I) C_I^0 \\ 9c_{xx}^0 &= (t_2 \delta_I + 12t_1 P_I + 9Q_I) C_I^0 + (t_1^2 \delta_I \delta_J + 3t_1 (\delta_I P_J + \delta_J P_I) + 9P_I P_J) C_{IJ}^0 \\ 54c_{xxx}^0 &= 4(t_3 \delta_I + 9t_2 P_I + 27t_1 Q_I) C_I^0 + 3(2t_1 t_2 \delta_I \delta_J + 3(t_2 + 4t_1^2) (\delta_I P_J + \delta_J P_I) \\ &\quad + 72t_1 P_I P_J + 9t_1 (\delta_I Q_J + \delta_J Q_I) + 27(P_I Q_J + P_J Q_I)) C_{IJ}^0 \\ &\quad + 2(t_1^3 \delta_I \delta_J \delta_K + 3t_1^2 (\delta_I \delta_J P_K + \delta_I \delta_K P_J + \delta_J \delta_K P_I) \\ &\quad + 9t_1 (\delta_I P_J P_K + \delta_J P_I P_K + \delta_K P_I P_J) + 27P_I P_J P_K) C_{IJK}^0. \end{aligned}$$

Under volume and shape strain together:

$$\begin{aligned}
18c_{vx}^0 &= 4(t_1\delta_I + 3P_I)C_I^0 + (2t_1\delta_I\delta_J + 3(\delta_IP_J + \delta_JP_I))C_{IJ}^0 \\
54c_{vxx}^0 &= -4(t_1\delta_I + 3P_I)C_I^0 + 3(2t_1\delta_I\delta_J + 3(\delta_IP_J + \delta_JP_I))C_{IJ}^0 \\
&\quad + 2(t_1\delta_I\delta_J\delta_K + (\delta_I\delta_JP_K + \delta_I\delta_KP_J + \delta_J\delta_KP_I))C_{IJK}^0 \\
54c_{vxx}^0 &= 4(t_2\delta_I + 12t_1P_I + 9Q_I)C_I^0 + (2(t_2 + 4t_1^2)\delta_I\delta_J + 36t_1(\delta_IP_J + \delta_JP_I) \\
&\quad + 72P_IP_J + 9(\delta_IQ_J + \delta_JQ_I))C_{IJ}^0 + 2(t_1^2\delta_I\delta_J\delta_K \\
&\quad + 2t_1(\delta_I\delta_JP_K + \delta_I\delta_KP_J + \delta_J\delta_KP_I) + 3(\delta_IP_JP_K + \delta_JP_IP_K + \delta_KP_IP_J))C_{IJK}^0.
\end{aligned} \tag{A.14}$$

Under sublattice displacement(s) alone:

$$\begin{aligned}
d_p^\alpha &= \tilde{\Lambda}^{\alpha\lambda} D_p^\lambda \\
e_{pq}^{\alpha\beta} &= \tilde{\Lambda}^{\alpha\lambda} \tilde{\Lambda}^{\beta\mu} E_{pq}^{\lambda\mu} \\
f_{pqr}^{\alpha\beta\gamma} &= \tilde{\Lambda}^{\alpha\lambda} \tilde{\Lambda}^{\beta\mu} \tilde{\Lambda}^{\gamma\nu} F_{pqr}^{\lambda\mu\nu}.
\end{aligned} \tag{A.15}$$

Under volume strain and sublattice displacement(s) together:

$$\begin{aligned}
3d_{pv}^\alpha &= \tilde{\Lambda}^{\alpha\lambda} (D_p^\lambda + \delta_J D_{pJ}^\lambda) \\
9d_{pvv}^\alpha &= \tilde{\Lambda}^{\alpha\lambda} (-2D_p^\lambda + \delta_J D_{pJ}^\lambda + \delta_J \delta_K D_{pJK}^\lambda) \\
3e_{pqv}^{\alpha\beta} &= \tilde{\Lambda}^{\alpha\lambda} \tilde{\Lambda}^{\beta\mu} (2E_{pq}^{\lambda\mu} + \delta_K E_{pqK}^{\lambda\mu}).
\end{aligned} \tag{A.16}$$

Under shape strain and sublattice displacement(s) together:

$$\begin{aligned}
3d_{px}^\alpha &= \tilde{\Lambda}^{\alpha\lambda} (t_1 D_p^\lambda + 3P_{ip} D_i^\lambda + (t_1\delta_J + 3P_J) D_{pJ}^\lambda) \\
9d_{pxx}^\alpha &= \tilde{\Lambda}^{\alpha\lambda} ((t_2 - t_1^2) D_p^\lambda + 6t_1 P_{ip} D_i^\lambda + ((t_2 + 2t_1^2)\delta_J + 18t_1 P_J + 9Q_J) D_{pJ}^\lambda \\
&\quad + 6P_{ip} (t_1\delta_J + 3P_J) D_{iJ}^\lambda + (t_1^2\delta_J\delta_K + 3t_1(\delta_J P_K + \delta_K P_J) + 9P_J P_K) D_{pJK}^\lambda) \\
3e_{pqx}^{\alpha\beta} &= \tilde{\Lambda}^{\alpha\lambda} \tilde{\Lambda}^{\beta\mu} ((2t_1 E_{pq}^{\lambda\mu} + 3P_{jq} E_{pj}^{\lambda\mu} + 3P_{ip} E_{iq}^{\lambda\mu}) + (t_1\delta_K + 3P_K) E_{pqK}^{\lambda\mu}).
\end{aligned} \tag{A.17}$$

Under volume and shape strain, together with sublattice displacement:

$$\begin{aligned}
18d_{vxx}^\alpha &= \tilde{\Lambda}^{\alpha\lambda} \left( 2t_1 D_p^\lambda + 6P_{ip} D_i^\lambda + 2(4t_1\delta_J + 9P_J) D_{pJ}^\lambda + 6\delta_J P_{ip} D_{ij}^\lambda \right. \\
&\quad \left. + (2t_1\delta_J\delta_K + 3(\delta_J P_K + \delta_K P_J)) D_{pJK}^\lambda \right).
\end{aligned} \tag{A.18}$$

## A.2 Computational procedures

A sufficient variety of deformations must be selected to ensure that all the independent elastic and inner elastic constants can be uniquely determined. Several dozen distinct ones are used. These involve

1. uniform volume change on its own,
2. a set of different shape-changing matrices  $P$ , detailed for the four carbon allotropes under discussion in Table A.1, each to be used both with and without volume change,
3. one of the components of sublattice displacement  $u_i^\alpha$ , or one of the pairs  $u_i^\alpha, u_j^\beta$ , or one of the triplets  $u_i^\alpha, u_j^\beta, u_k^\gamma$ , either alone or combined with the previous items.

Table A.1: Specification of the shape-changing matrices  $P$  and the corresponding scaling functions.  $P_{ij} = P_{ji}$  in each case.

Number	$P_{11}$	$P_{22}$	$P_{33}$	$P_{12}$	$P_{13}$	$P_{23}$	$S(x)^{-3}$
<i>c</i> -Diamond							
1	1	0	0	0	0	0	$1 + x$
2	0	0	0	1	1	1	$1 - 3x^2 + 2x^3$
3	0	1	-1	1	1	0	$1 - 3x^2 - x^3$
<i>h</i> -Graphite (1-5), <i>h</i> -Diamond (1-7) and <i>r</i> -Graphite (1-9)							
1	0	0	3	0	0	0	$1 + 3x$
2	0	0	3	0	0	1	$1 + 3x - x^2$
3	0	0	3	1	0	0	$1 + 3x - x^2 - 3x^3$
4	1	-1	0	0	0	0	$1 - x^2$
5	0	0	0	1	1	1	$1 - 3x^2 + 2x^3$
6	0	0	3	0	0	-1	$1 + 3x - x^2$
7	0	0	0	-1	1	1	$1 - 3x^2 + 2x^3$
8	1	1	0	1	1	0	$1 + 2x - x^2 - x^3$
9	1	1	0	-1	1	0	$1 + 2x - x^2 - x^3$

Each deformation is used with a grid of seven equally spaced values of  $x$ ,  $v$  and/or each  $u_i^\alpha$  as appropriate. The energy is determined at each point in the grid and partial energy derivatives are calculated by numerical differentiation, using least-squares fitting of a polynomial (a cubic is completely satisfactory) to seven equally spaced points.

The full set of relationships for each of the four structures featuring in this thesis are laid out in the next four subsections. The Fuchs constants are most simply expressed in terms of linear combinations of Brugger constants. Abbreviations for some of the latter are tabulated prior to the full listings. The letters indicate combinations relating solely to volume change ( $b_i$ ), solely to shape change ( $g_i$ ) or to volume and shape change ( $m_i$ ). Additional auxiliary combinations may make their appearance in various third derivatives ( $a_i$ ). The multiplier  $\tilde{\Lambda}^{\alpha\lambda}$  is defined in (A.9) above.

A.2.1 *c*-Diamond

It is useful to abbreviate certain strings of Brugger constants to prevent some of the expressions below from becoming unwieldy.

Table A.2: Linear combinations of Brugger constants for cubic crystals.

Abbreviation	Brugger combination	Abbreviation	Brugger combination
$b_1$	$C_1$ (!)	$b_3$	$\frac{1}{9}(C_{111} + 6C_{112} + 2C_{123})$
$b_2$	$\frac{1}{3}(C_{11} + 2C_{12})$	$g_3$	$-C_1 + \frac{1}{8}(C_{111} - 3C_{112} + 2C_{123})$
$g_1$	$C_1 + \frac{1}{2}(C_{11} - C_{12})$	$g_4$	$-C_1 + C_{456}$
$g_2$	$C_1 + C_{44}$	$g_5$	$C_1 + \frac{1}{2}(C_{144} - C_{155})$
		$m_1$	$-C_1 + \frac{1}{2}(C_{111} - C_{123})$
		$m_2$	$-C_1 + (C_{144} + 2C_{155})$

The expressions are further simplified because  $\lambda = \mu = \nu = 1$ , leading to  $\tilde{\Lambda}^{\alpha\lambda} = (-1)^\alpha$ , etc.

Under sublattice displacements alone

$$e_{11}^{\alpha\beta} = (-1)^{\alpha+\beta} E_{11}$$

$$f_{123}^{\alpha\beta\gamma} = (-1)^{\alpha+\beta+\gamma} F_{123}.$$

Under volume deformation

$$c_v^0 = b_1$$

$$c_{vv}^0 = -\frac{1}{3}b_1 + b_2$$

$$c_{vvv}^0 = \frac{4}{9}b_1 - b_2 + b_3$$

$$e_{11v}^{\alpha\beta} = (-1)^{\alpha+\beta} \frac{1}{3}(2E_{11} + (E_{111} + 2E_{112})).$$

Under shape deformation #1

$$c_{xx}^0 = \frac{4}{3}g_1$$

$$c_{xxx}^0 = -\frac{4}{3}g_1 + \frac{16}{9}g_3$$

$$c_{vxx}^0 = -\frac{4}{9}b_1 + \frac{4}{3}b_2 + \frac{16}{9}g_2 + \frac{4}{9}m_1$$

$$e_{11x}^{\alpha\beta} = (-1)^{\alpha+\beta} \frac{2}{3}(2E_{11} + (E_{111} - E_{112})).$$

Under shape deformation #2

$$c_{xx}^0 = 12g_2$$

$$c_{xxx}^0 = 36g_2 + 48g_4$$

$$c_{vxx}^0 = -4b_1 + 12b_2 + 16g_2 + 4m_2$$

Under shape deformation #3

$$\begin{aligned}
c_{xx}^0 &= 4g_1 + 8g_2 \\
c_{xxx}^0 &= -6g_1 - 12g_2 + 24g_5 \\
d_{1x}^\alpha &= (-1)^\alpha 2D_{14} \\
d_{2xx}^\alpha &= (-1)^\alpha 2(D_{14} + 2(D_{114} - D_{124})) \\
d_{3xx}^\alpha &= (-1)^\alpha 2(5D_{14} + 4D_{156}) \\
d_{1vx}^\alpha &= (-1)^\alpha \frac{2}{3}(3D_{14} + (D_{114} + 2D_{124})) \\
e_{13x}^{\alpha\beta} &= (-1)^{\alpha+\beta} 2(E_{11} + E_{126}) \\
e_{22x}^{\alpha\beta} &= (-1)^{\alpha+\beta} 2(2E_{11} + (E_{111} - E_{112})).
\end{aligned}$$

### A.2.2 *h*-Graphite, *h*-Diamond and *r*-Graphite

The linear combinations in the following Table are valid for all three allotropes due to their common description in terms of a hexagonal cell.

Table A.3: Linear combinations of Brugger constants for hexagonal and rhombohedral crystals. Two combinations that appear several times are further abbreviated:  $C_a \equiv C_{111} - C_{166} - 2C_{266}$  and  $C_b \equiv C_{113} - C_{366}$ .

Abbreviation	Brugger combination	Abbreviation	Brugger combination
$b_1$	$\frac{1}{3}(2C_1 + C_3)$	$b_3$	$\frac{1}{27}(8C_a + 12C_b + 6C_{133} + C_{333})$
$g_1$	$C_1 - C_3$	$g_5$	$C_1 + \frac{1}{6}(C_a - 3C_b + 3C_{133} - C_{333})$
$b_2$	$\frac{1}{9}(2C_{11} + 2C_{12} + 4C_{13} + C_{33})$	$g_6$	$C_1 + \frac{1}{2}(C_{144} + C_{244} - 2C_{344})$
$g_2$	$C_1 + \frac{1}{6}(C_{11} + C_{12} - 4C_{13} + 2C_{33})$	$g_7$	$-C_1 + \frac{1}{4}(C_{166} + C_{266} - 2C_{366})$
$g_3$	$C_1 + \frac{1}{2}(C_{11} - C_{12})$	$g_8$	$C_{166} - C_{266}$
$g_4$	$C_1 + C_{44}$	$g_9$	$C_1 + \frac{1}{2}(C_{144} - C_{244})$
$m_1$	$C_{11} + C_{12} - C_{13} - C_{33}$	$m_2$	$4C_a - 3C_{133} - C_{333}$
$a_1$	$-C_1 + (C_{11} + C_{12} + C_{13})$	$m_3$	$-C_1 + \frac{1}{3}(2C_a - 3C_b + C_{333})$
$a_2$	$C_1 + \frac{1}{2}(C_{11} + C_{12} - 2C_{13})$	$m_4$	$-C_1 + (C_{144} + C_{244} + C_{344})$
		$m_5$	$-C_1 + (C_{166} + C_{266} + C_{366})$

The relations below apply to all three allotropes. Where  $\pm$  and  $\mp$  signs occur they precede terms deriving from  $3m$  symmetry relevant to certain inner elastic constants of *h*D and to certain partial and inner elastic constants in *r*G. Additionally, in the case of *r*G, the  $\lambda$ ,  $\mu$  and  $\nu$  superscripts can all be dispensed with and the  $\tilde{\Lambda}$  factors replaced by powers of  $-1$  exactly as for *c*D.

Under sublattice displacements alone

$$\begin{aligned}
e_{11}^{\alpha\beta} &= \tilde{\Lambda}^{\alpha\lambda} \tilde{\Lambda}^{\beta\mu} E_{11}^{\lambda\mu} \\
e_{33}^{\alpha\beta} &= \tilde{\Lambda}^{\alpha\lambda} \tilde{\Lambda}^{\beta\mu} E_{33}^{\lambda\mu} \\
f_{112}^{\alpha\beta\gamma} &= \tilde{\Lambda}^{\alpha\lambda} \tilde{\Lambda}^{\beta\mu} \tilde{\Lambda}^{\gamma\nu} F_{112}^{\lambda\mu\nu} \\
f_{113}^{\alpha\beta\gamma} &= \tilde{\Lambda}^{\alpha\lambda} \tilde{\Lambda}^{\beta\mu} \tilde{\Lambda}^{\gamma\nu} F_{113}^{\lambda\mu\nu} \\
f_{333}^{\alpha\beta\gamma} &= \tilde{\Lambda}^{\alpha\lambda} \tilde{\Lambda}^{\beta\mu} \tilde{\Lambda}^{\gamma\nu} F_{333}^{\lambda\mu\nu}.
\end{aligned}$$

Under volume deformation

$$\begin{aligned}
c_v^0 &= b_1 \\
c_{vv}^0 &= -\frac{1}{3}b_1 + b_2 \\
c_{vvv}^0 &= \frac{4}{9}b_1 - b_2 + b_3 \\
e_{11v}^{\alpha\beta} &= \frac{1}{3}\tilde{\Lambda}^{\alpha\lambda} \tilde{\Lambda}^{\beta\mu} (2E_{11}^{\lambda\mu} + (E_{111}^{\lambda\mu} + E_{112}^{\lambda\mu} + E_{113}^{\lambda\mu})) \\
e_{33v}^{\alpha\beta} &= \frac{1}{3}\tilde{\Lambda}^{\alpha\lambda} \tilde{\Lambda}^{\beta\mu} (2E_{33}^{\lambda\mu} + (2E_{331}^{\lambda\mu} + E_{333}^{\lambda\mu})).
\end{aligned}$$

Under shape deformation #1

$$\begin{aligned}
c_x^0 &= -2g_1 \\
c_{xx}^0 &= -2g_1 + 12g_2 \\
c_{vx}^0 &= -\frac{4}{3}g_1 - \frac{2}{3}m_1 \\
c_{xxx}^0 &= 4g_1 + 36g_2 - 72a_2 - 48g_5 \\
c_{vxx}^0 &= -\frac{4}{3}g_1 - \frac{2}{3}m_1 + 4a_1 + 16g_2 + 4m_3 \\
c_{vux}^0 &= \frac{4}{9}g_1 - \frac{2}{3}m_1 - \frac{2}{9}m_2 \\
d_{3x}^\alpha &= 2\tilde{\Lambda}^{\alpha\lambda} (D_3^\lambda - (D_{31}^\lambda - D_{33}^\lambda)) \\
d_{3xx}^\alpha &= 2\tilde{\Lambda}^{\alpha\lambda} (-D_3^\lambda + (D_{31}^\lambda + 5D_{33}^\lambda) + (D_{311}^\lambda + D_{312}^\lambda - 4D_{313}^\lambda + 2D_{333}^\lambda)) \\
d_{3vx}^\alpha &= \frac{2}{3}\tilde{\Lambda}^{\alpha\lambda} (D_3^\lambda - (D_{31}^\lambda - 4D_{33}^\lambda) - (D_{311}^\lambda + D_{312}^\lambda - D_{313}^\lambda - D_{333}^\lambda)) \\
e_{11x}^{\alpha\beta} &= -\tilde{\Lambda}^{\alpha\lambda} \tilde{\Lambda}^{\beta\mu} (2E_{11}^{\lambda\mu} + (E_{111}^{\lambda\mu} + E_{112}^{\lambda\mu} - 2E_{113}^{\lambda\mu})) \\
e_{33x}^{\alpha\beta} &= 2\tilde{\Lambda}^{\alpha\lambda} \tilde{\Lambda}^{\beta\mu} (2E_{33}^{\lambda\mu} - (E_{331}^{\lambda\mu} - E_{333}^{\lambda\mu})).
\end{aligned}$$

Under shape deformations #2 (upper signs) and #6 (lower signs)

$$\begin{aligned}
c_{xxx}^0 &= 8g_1 + 66g_2 - 96a_2 - 12g_4 - 48g_5 - 24g_6 \mp C_{14} \pm 8C_{444} \\
d_{2xx}^\alpha &= \tilde{\Lambda}^{\alpha\lambda} (-(D_{16}^\lambda + 4D_{145}^\lambda) \mp (D_3^\lambda + 3D_{15}^\lambda + 2(D_{31}^\lambda - D_{33}^\lambda) + 2(D_{115}^\lambda + D_{125}^\lambda - 2D_{135}^\lambda))) \\
d_{3xx}^\alpha &= \frac{1}{3}\tilde{\Lambda}^{\alpha\lambda} (-4D_3^\lambda + 12D_{15}^\lambda + 13D_{31}^\lambda + 35D_{33}^\lambda + 6(D_{311}^\lambda + D_{312}^\lambda - 4D_{313}^\lambda + 2D_{333}^\lambda) + 12D_{344}^\lambda) \\
d_{2vx}^\alpha &= \pm \frac{1}{3}\tilde{\Lambda}^{\alpha\lambda} (D_3^\lambda + 6D_{15}^\lambda + (2D_{31}^\lambda + D_{33}^\lambda) + 2(D_{115}^\lambda + D_{125}^\lambda + D_{135}^\lambda)) \\
e_{11x}^{\alpha\beta} &= -\tilde{\Lambda}^{\alpha\lambda} \tilde{\Lambda}^{\beta\mu} (2E_{11}^{\lambda\mu} + (E_{111}^{\lambda\mu} + E_{112}^{\lambda\mu} - 2E_{113}^{\lambda\mu}) \mp 2E_{114}^{\lambda\mu}) \\
e_{23x}^{\alpha\beta} &= \pm \tilde{\Lambda}^{\alpha\lambda} \tilde{\Lambda}^{\beta\mu} (E_{11}^{\lambda\mu} + E_{33}^{\lambda\mu} + 2E_{135}^{\lambda\mu}) \\
e_{32x}^{\alpha\beta} &= \pm \tilde{\Lambda}^{\alpha\lambda} \tilde{\Lambda}^{\beta\mu} (E_{11}^{\lambda\mu} + E_{33}^{\lambda\mu} + 2E_{315}^{\lambda\mu}).
\end{aligned}$$

Under shape deformation #3

$$\begin{aligned}
c_{xxx}^0 &= -4g_1 + 48g_2 - 96a_2 - 48g_3 - 48g_5 - 48g_7 \\
d_{1x}^\alpha &= 2\tilde{\Lambda}^{\alpha\lambda} D_{16}^\lambda \\
d_{3x}^\alpha &= 2\tilde{\Lambda}^{\alpha\lambda} (D_3^\lambda - (D_{31}^\lambda - D_{33}^\lambda)) \\
d_{1xx}^\alpha &= -2\tilde{\Lambda}^{\alpha\lambda} (6D_{16}^\lambda + (D_{211}^\lambda - D_{222}^\lambda - 4D_{136}^\lambda)) \\
d_{2xx}^\alpha &= 2\tilde{\Lambda}^{\alpha\lambda} (2D_{16}^\lambda - (D_{211}^\lambda + D_{222}^\lambda)) \\
d_{3xx}^\alpha &= \frac{4}{3}\tilde{\Lambda}^{\alpha\lambda} (-D_3^\lambda + 4(D_{31}^\lambda + 2D_{33}^\lambda)) + 3(D_{311}^\lambda - 2D_{313}^\lambda + D_{333}^\lambda) \\
d_{1vx}^\alpha &= \frac{1}{3}\tilde{\Lambda}^{\alpha\lambda} (6D_{16}^\lambda + (D_{211}^\lambda - D_{222}^\lambda + 2D_{136}^\lambda)) \\
d_{3vx}^\alpha &= \frac{2}{3}\tilde{\Lambda}^{\alpha\lambda} (D_3^\lambda - (D_{31}^\lambda - 4D_{33}^\lambda)) - (D_{311}^\lambda + D_{312}^\lambda - D_{313}^\lambda - D_{333}^\lambda) \\
e_{12x}^{\alpha\beta} &= \tilde{\Lambda}^{\alpha\lambda} \tilde{\Lambda}^{\beta\mu} (2E_{11}^{\lambda\mu} + (E_{111}^{\lambda\mu} - E_{112}^{\lambda\mu})) \\
e_{13x}^{\alpha\beta} &= 2\tilde{\Lambda}^{\alpha\lambda} \tilde{\Lambda}^{\beta\mu} E_{136}^{\lambda\mu} \\
e_{31x}^{\alpha\beta} &= 2\tilde{\Lambda}^{\alpha\lambda} \tilde{\Lambda}^{\beta\mu} E_{316}^{\lambda\mu}.
\end{aligned}$$

Under shape deformation #4

$$\begin{aligned}
c_{xx}^0 &= -\frac{2}{3}g_1 + 4g_3 \\
c_{xxx}^0 &= -4g_8 \\
c_{vxx}^0 &= -\frac{4}{9}g_1 + \frac{16}{3}g_3 - \frac{2}{9}m_1 + \frac{4}{3}a_1 + \frac{4}{3}m_5 \\
d_{3xx}^\alpha &= \frac{2}{3}\tilde{\Lambda}^{\alpha\lambda} (D_3^\lambda + (5D_{31}^\lambda + D_{33}^\lambda) + 3(D_{311}^\lambda - D_{312}^\lambda)).
\end{aligned}$$

Under shape deformations #5 (upper signs) and #7 (lower signs)

$$\begin{aligned}
c_{xx}^0 &= -4g_1 + 4g_3 + 8g_4 \pm 8C_{14} \\
c_{xxx}^0 &= \pm(4g_1 + 12g_3 + 24g_4 - 48g_9) + 8(3C_{14} + 3C_{124} - 2C_{444}) \\
c_{vxx}^0 &= -\frac{8}{3}g_1 + \frac{16}{3}g_3 + \frac{32}{3}g_4 - \frac{4}{3}m_1 + 4a_1 + \frac{8}{3}m_4 + \frac{4}{3}m_5 \pm \frac{8}{3}(4C_{14} + (C_{114} + C_{124} + C_{134})) \\
d_{1x}^\alpha &= \tilde{\Lambda}^{\alpha\lambda} (D_3^\lambda + 2D_{15}^\lambda \pm 2D_{16}^\lambda) \\
d_{2x}^\alpha &= \tilde{\Lambda}^{\alpha\lambda} (D_3^\lambda + 2D_{15}^\lambda) \\
d_{1xx}^\alpha &= \tilde{\Lambda}^{\alpha\lambda} (2(D_{16}^\lambda + 4D_{145}^\lambda) \pm (3D_{15}^\lambda + 2(D_{115}^\lambda - D_{125}^\lambda))) \\
d_{3xx}^\alpha &= \tilde{\Lambda}^{\alpha\lambda} (\pm 4(D_{16}^\lambda + 2D_{314}^\lambda) + 2(D_3^\lambda + 4D_{15}^\lambda + 4D_{31}^\lambda + 2D_{33}^\lambda + D_{311}^\lambda - D_{312}^\lambda + 4D_{344}^\lambda)) \\
d_{1vx}^\alpha &= \frac{1}{3}\tilde{\Lambda}^{\alpha\lambda} (D_3^\lambda + 6D_{15}^\lambda + (2D_{31}^\lambda + D_{33}^\lambda) + 2(D_{115}^\lambda + D_{125}^\lambda + D_{135}^\lambda) \pm (6D_{16}^\lambda + D_{211}^\lambda - D_{222}^\lambda + 2D_{136}^\lambda)) \\
d_{2vx}^\alpha &= \frac{1}{3}\tilde{\Lambda}^{\alpha\lambda} (D_3^\lambda + 6D_{15}^\lambda + (2D_{31}^\lambda + D_{33}^\lambda) + 2(D_{115}^\lambda + D_{125}^\lambda + D_{135}^\lambda)) \\
e_{13x}^{\alpha\beta} &= \tilde{\Lambda}^{\alpha\lambda} \tilde{\Lambda}^{\beta\mu} (E_{11}^{\lambda\mu} + E_{33}^{\lambda\mu} + 2E_{135}^{\lambda\mu} \pm 2E_{136}^{\lambda\mu}).
\end{aligned}$$

Under shape deformations #8 (upper sign) and #9 (lower sign)

$$c_{xxx}^0 = \frac{554}{27}g_1 - \frac{14}{3}g_2 - 8g_3 - 20g_4 + \frac{56}{9}m_1 + \frac{16}{9}g_5 + 8g_6 + 16g_7 \pm 4(-7C_{14} + 2(C_{114} + C_{124} - 2C_{134}))$$

### A.2.3 Formal checks

There are numerous opportunities for errors to arise in a complex calculation. To test the accuracy of the calculations that are reported in this thesis the extravagance of calculating all possible components of the  $d$ ,  $e$  and  $f$  tensors was indulged. This showed explicitly that all expected crystal symmetry relations were satisfied. In this test there may be more than a million applications of the energy algorithm and several hundred applications of the least-squares fitting subroutine. Where components should have been zero small values arising from statistical noise were found though in all cases these were a million or more times smaller than the smallest non-zero components of the same tensor. The positive outcome of the test suggests that instances where two components of a tensor differ by parts in a thousand or by a factor of the order of a thousand are physically significant.

The accuracy of the subsequent conversion of the Fuchs constants into Brugger constants was tested in two ways. In the first the energy algorithm was replaced by the summation of a simple pair potential  $\phi(r) = 1/r^6$  over a cluster of more than 8000 atoms. The results of this were compared with the direct calculation of Brugger constants for this potential using the modified Ewald method described in [1]. In the second test the energy algorithm was replaced by (1.10) with the previously computed values of all the elastic constants. Self-consistency was total.

### References

- [1] K. Fuchs, Proc. Roy. Soc. A**153**, 622 (1936)
- [2] R. S. Leigh, Phil. Mag. **42**, 139 (1951)



Table B.2: Transformation matrices to convert tensor components from the standard to variant settings in monoclinic, orthorhombic and tetragonal point groups.  $a = 1/\sqrt{2}$ .

Point group	Standard setting	Variant setting	Transformation matrix									
			No.	$a_{11}$	$a_{12}$	$a_{13}$	$a_{21}$	$a_{22}$	$a_{23}$	$a_{31}$	$a_{32}$	$a_{33}$
$m$	010	100	1	0	1	0	0	0	1	1	0	0
2		001	2	0	0	1	1	0	0	0	1	0
		110	3	$a$	$a$	0	$-a$	$a$	0	0	0	1
		$1\bar{1}0$	4	$a$	$-a$	0	$a$	$a$	0	0	0	1
		101	5	$-a$	$a$	0	0	0	1	$a$	$a$	0
		$10\bar{1}$	6	$a$	$a$	0	0	0	1	$a$	$-a$	0
		011	7	0	0	1	$a$	$a$	0	$-a$	$a$	0
		$01\bar{1}$	8	0	0	1	$a$	$-a$	0	$a$	$a$	0
		$mm2$	100	010	001	$1\bar{1}0$	110	001	Matrix no. 3			
222		101	$10\bar{1}$	010	Matrix no. 6							
		011	$01\bar{1}$	100	Matrix no. 8							
		001	100	010	Matrix no. 1							
		010	001	100	Matrix no. 2							
4	001	010	Matrix no. 1									
$\bar{4}$		100	Matrix no. 2									
$4mm$	001	010	110	010	001	101	Matrix no. 1					
$\bar{4}2m$		100	010	011	Matrix no. 2							
422		001	110	010	Matrix no. 3							

## Appendix C

### Keating model parameters from bond-order potential parameters

#### C.1 The Keating model

The Keating energy expressions for cD given in (6.40) and (6.41) relate to the unit cell. If the summation over the basis is omitted the net contributions per reference atom  $s$  are

$$E_s^{(2)} = \frac{1}{2} \sum_{i=1}^Z \left( \alpha \Delta_{ii}^2 + \sum_{j=1}^{Z'} (\beta \Delta_{ij}^2 + \sigma (\Delta_{ii} + \Delta_{jj}) \Delta_{ij} + \tau \Delta_{ii} \Delta_{jj}) \right) \quad (\text{C.1})$$

and

$$E_s^{(3)} = \frac{1}{2} \sum_{i=1}^Z \left( \gamma \Delta_{ii}^3 + \sum_{j=1}^{Z'} (\delta \Delta_{ij}^3 + \epsilon (\Delta_{ii} + \Delta_{jj}) \Delta_{ij}^2 + \eta (\Delta_{ii}^2 + \Delta_{jj}^2) \Delta_{ij} + \theta \Delta_{ii} \Delta_{ij} \Delta_{jj} + \xi \Delta_{ii} \Delta_{jj} (\Delta_{ii} + \Delta_{jj})) \right) \quad (\text{C.2})$$

where the primes on the summations indicate that  $j \neq i$ , the asterisk on  $\beta$  has been dropped and the atomic coordination has been denoted by  $Z$  rather than 4 so that the derivations below have greater generality. A first-order expression, requiring two further parameters  $\mu$  and  $\nu$ , should also be considered to accommodate cases where the Keating model represents only a part of the total energy:

$$E_s^{(1)} = \frac{1}{2} \sum_{i=1}^Z \left( \mu \Delta_{ii} + \sum_{j=1}^{Z'} \nu \Delta_{ij} \right). \quad (\text{C.3})$$

##### C.1.1 Dependencies amongst the variables

When the atomic coordination is  $Z$  there are  $Z$  variables  $\Delta_{ii}$  and  $Z(Z-1)/2$  variables  $\Delta_{ij}$ . A series of relations of dependence between them may be generated from the fact that the  $Z$  vectors  $\vec{r}^i$  satisfy

$$\sum_{i=1}^Z \vec{r}^i = 0 \quad (\text{C.4})$$

whence, on squaring,

$$\sum_{i=1}^Z (\bar{r}^i \cdot \bar{r}^i + \sum_{j=1}^Z \bar{r}^i \cdot \bar{r}^j) = 0. \quad (\text{C.5})$$

This relation is true whether the structure is homogeneously deformed or not, thus it follows that

$$\sum_{i=1}^Z (\Delta_{ii} + \sum_{j=1}^Z \Delta_{ij}) = 0, \quad (\text{C.6})$$

a linear dependence of the variables. Quadratic and cubic dependencies follow from squaring and cubing this relationship. These procedures lead to nested summations over products of the variables involving distinct dummy subscripts  $i, j, k$  and  $l$  in the quadratic case and over  $i, j, k, l, m$  and  $n$  in the cubic. In the Keating model the products never involve more than two different subscripts so the following expressions have been limited to precisely that situation.

$$\sum_{i=1}^Z \left( \Delta_{ii}^2 + \sum_{j=1}^Z (2\Delta_{ij}^2 + 2\Delta_{ij}(\Delta_{ii} + \Delta_{jj}) + \Delta_{ii}\Delta_{jj}) \right) = 0 \quad (\text{C.7})$$

and

$$\begin{aligned} \sum_{i=1}^Z \left( \Delta_{ii}^3 + \sum_{j=1}^Z (4\Delta_{ij}^3 + 6\Delta_{ij}^2(\Delta_{ii} + \Delta_{jj}) \right. \\ \left. + 3\Delta_{ij}(\Delta_{ii}^2 + \Delta_{jj}^2) + 6\Delta_{ii}\Delta_{ij}\Delta_{jj} + \frac{3}{2}\Delta_{ii}(\Delta_{ii} + \Delta_{jj})\Delta_{jj}) \right) = 0. \end{aligned} \quad (\text{C.8})$$

Each of the previous three relations may be multiplied by an arbitrary factor,  $\kappa_p/2$  say, and added to the equivalent  $p$ th-order energy expression without changing its value. All the Keating parameters will change in the following way, however:

$$\begin{array}{lll} \mu \rightarrow \mu + \kappa_1 & \alpha \rightarrow \alpha + \kappa_2 & \gamma \rightarrow \gamma + \kappa_3 \\ \nu \rightarrow \nu + \kappa_1 & \beta \rightarrow \beta + 2\kappa_2 & \delta \rightarrow \delta + 4\kappa_3 \\ & \sigma \rightarrow \sigma + 2\kappa_2 & \epsilon \rightarrow \epsilon + 6\kappa_3 \\ & \tau \rightarrow \tau + \kappa_2 & \eta \rightarrow \eta + 3\kappa_3 \\ & & \theta \rightarrow \theta + 6\kappa_3 \\ & & \xi \rightarrow \xi + \frac{3}{2}\kappa_3 \end{array}$$

Clearly there will be invariant combinations, just one at the first order  $\mu - \nu$ , but numerous possibilities at the second and third order. Thus some elastic constants may be invariant, others not. For example in cD

$$C_{11} = \frac{a}{2}(\alpha + 3\beta - 2\sigma + 3\tau) \rightarrow \frac{a}{2}(\alpha + 3\beta - 2\sigma + 3\tau + 6\kappa_2) \quad (\text{C.9})$$

whereas in the planar interaction in hG

$$C_{11}^0 = \frac{2ta^2}{3d}(\alpha + \beta - 2\sigma + \tau) \quad (\text{C.10})$$

does not change.

## C.2 The bond-order potential

The bond-order potential associated with the reference atom  $s$  is

$$E_s = \frac{1}{2} \sum_{i=1}^Z \left( V_R(r^i) - V_A(r^i) B_i(c_{ij}) \right), \quad (\text{C.11})$$

where the function  $B_i$  contains a summation over the  $Z - 1$  other atoms  $j$  to which atom  $s$  is coordinated and  $c_{ij}$  is the cosine of  $\theta_{isj}$ , the angle between  $\vec{r}^i$  and  $\vec{r}^j$ . Both Tersoff and Brenner included  $r^i$  and  $r^j$  explicitly in  $B_i$  in their original treatments. Subsequently they retained only the implicit dependence *via* the  $c_{ij}$  [1, 5]. Expanded as a Taylor series the bond-order term can be written

$$\begin{aligned} B_i(c_{ij}) = & B_i^0 + \sum_{j=1}^{Z'} \left( \frac{\partial B_i}{\partial c_{ij}} \right)_0 \Delta c_{ij} + \frac{1}{2} \sum_{j=1}^{Z'} \sum_{k=1}^{Z'} \left( \frac{\partial^2 B_i}{\partial c_{ij} \partial c_{ik}} \right)_0 \Delta c_{ij} \Delta c_{ik} \\ & + \frac{1}{6} \sum_{j=1}^{Z'} \sum_{k=1}^{Z'} \sum_{l=1}^{Z'} \left( \frac{\partial^3 B_i}{\partial c_{ij} \partial c_{ik} \partial c_{il}} \right)_0 \Delta c_{ij} \Delta c_{ik} \Delta c_{il}. \end{aligned} \quad (\text{C.12})$$

This equation shows that  $B_i(c_{ij})$  may be considered as a sum of terms involving 2 bonds, 3 bonds, 4 bonds and so on. The Keating model, however, involves only 2-bond terms so it simplifies matters to extract these separately, as in

$$B_i(c_{ij}) = B_i^0 + \sum_{j=1}^{Z'} \left\{ \left( \frac{\partial B_i}{\partial c_{ij}} \right)_0 \Delta c_{ij} + \frac{1}{2} \left( \frac{\partial^2 B_i}{\partial c_{ij}^2} \right)_0 (\Delta c_{ij})^2 + \frac{1}{6} \left( \frac{\partial^3 B_i}{\partial c_{ij}^3} \right)_0 (\Delta c_{ij})^3 \right\}, \quad (\text{C.13})$$

and to ignore the 3- and 4-bond parts,

$$\begin{aligned} B_i^{(3)}(c_{ij}) = & \sum_{j=1}^{Z'} \sum_{k=1}^{Z''} \left\{ \left( \frac{\partial^2 B_i}{\partial c_{ij} \partial c_{ik}} \right)_0 \Delta c_{ij} \Delta c_{ik} \right. \\ & \left. + \frac{1}{2} \left( \frac{\partial^3 B_i}{\partial c_{ij}^2 \partial c_{ik}} \right)_0 (\Delta c_{ij})^2 \Delta c_{ik} + \frac{1}{2} \left( \frac{\partial^3 B_i}{\partial c_{ij} \partial c_{ik}^2} \right)_0 \Delta c_{ij} (\Delta c_{ik})^2 \right\} \end{aligned} \quad (\text{C.14})$$

and

$$B_i^{(4)}(c_{ij}) = \sum_{j=1}^{Z'} \sum_{k=1}^{Z''} \sum_{l=1}^{Z'''} \left( \frac{\partial^3 B_i}{\partial c_{ij} \partial c_{ik} \partial c_{il}} \right)_0 \Delta c_{ij} \Delta c_{ik} \Delta c_{il}, \quad (\text{C.15})$$

which are relevant only to more sophisticated treatments of bond order, the analytic approach in [2, 3, 4] for example. The notation  $\sum''$  means that  $k \neq i$  or  $j$ ; and  $\sum'''$  means that  $l \neq i, j$  or  $k$ .

## C.3 Equivalent Keating parameters

The relation of the Keating model to the bond-order potential is established by treating  $V_R$  and  $V_A$  as functions of the scalar products  $R_{ii} = \vec{r}^i \cdot \vec{r}^i$  or  $R_{jj} = \vec{r}^j \cdot \vec{r}^j$ , as appropriate, and  $B_i$  as a

function of  $R_{ii}$ ,  $R_{ij}$  and  $R_{jj}$  through the  $Z - 1$  cosines given by

$$c_{ij} = R_{ij} / \sqrt{R_{ii}R_{jj}}. \quad (\text{C.16})$$

Equation (C.11) can thus be written

$$E_s = \frac{1}{2} \sum_{i=1}^Z \left( V_R(R_{ii}) - V_A(R_{ii}) B_i(R_{ii}, R_{ij}, R_{jj}) \right) \quad (\text{C.17})$$

and its derivatives with respect to each of the  $R_{pq}$  identified with derivatives of the Keating expressions with respect to  $\Delta_{pq}$  since  $\partial/\partial R_{pq} \equiv (d\Delta_{pq}/dR_{pq})\partial/\partial\Delta_{pq}$  and  $d\Delta_{pq}/dR_{pq} = 1$ . Thus at the first order:

$$\mu = \left\{ \left( \frac{dV_R}{dR_{ii}} \right) - \left( \frac{dV_A}{dR_{ii}} \right) B_i - V_A(R_{ii}) \left( \frac{\partial B_i}{\partial R_{ii}} \right) - \sum_{k=1}^Z V_A(R_{kk}) \left( \frac{\partial B_k}{\partial R_{ii}} \right) \right\}_0 \quad (\text{C.18})$$

and

$$\nu = -\frac{1}{2} \left\{ V_A(R_{ii}) \left( \frac{\partial B_i}{\partial R_{ij}} \right) + V_A(R_{jj}) \left( \frac{\partial B_j}{\partial R_{ij}} \right) \right\}_0, \quad (\text{C.19})$$

where the single subscript zero indicates that all components are to be evaluated at the equilibrium configuration.

Bracketted terms in (C.1) and (C.2) indicate pairs of routes to the Keating parameters  $\sigma$ ,  $\epsilon$ ,  $\eta$  and  $\xi$  and account for the pairs of definitions embedded in the following sets of relations.

At the second order

$$\alpha = \frac{1}{2} \left\{ \left( \frac{d^2V_R}{dR_{ii}^2} \right) - \left( \frac{d^2V_A}{dR_{ii}^2} \right) B_i - 2 \left( \frac{dV_A}{dR_{ii}} \right) \left( \frac{\partial B_i}{\partial R_{ii}} \right) - V_A(R_{ii}) \left( \frac{\partial^2 B_i}{\partial R_{ii}^2} \right) - \sum_{k=1}^Z V_A(R_{kk}) \left( \frac{\partial^2 B_k}{\partial R_{ii}^2} \right) \right\}_0, \quad (\text{C.20})$$

$$\beta = -\frac{1}{4} \left\{ V_A(R_{ii}) \left( \frac{\partial^2 B_i}{\partial R_{ij}^2} \right) + V_A(R_{jj}) \left( \frac{\partial^2 B_j}{\partial R_{ij}^2} \right) \right\}_0,$$

$$\sigma = -\frac{1}{2} \left\{ \left( \frac{dV_A}{dR_{ii}} \right) \left( \frac{\partial B_i}{\partial R_{ij}} \right) + V_A(R_{ii}) \left( \frac{\partial^2 B_i}{\partial R_{ii} \partial R_{ij}} \right) + V_A(R_{jj}) \left( \frac{\partial^2 B_j}{\partial R_{ii} \partial R_{ij}} \right) \right\}_0,$$

$$\sigma = -\frac{1}{2} \left\{ \left( \frac{dV_A}{dR_{jj}} \right) \left( \frac{\partial B_j}{\partial R_{ij}} \right) + V_A(R_{ii}) \left( \frac{\partial^2 B_i}{\partial R_{ij} \partial R_{jj}} \right) + V_A(R_{jj}) \left( \frac{\partial^2 B_j}{\partial R_{ij} \partial R_{jj}} \right) \right\}_0$$

and

$$\tau = -\frac{1}{2} \left\{ \left( \frac{dV_A}{dR_{ii}} \right) \left( \frac{\partial B_i}{\partial R_{jj}} \right) + \left( \frac{dV_A}{dR_{jj}} \right) \left( \frac{\partial B_j}{\partial R_{ii}} \right) + V_A(R_{ii}) \left( \frac{\partial^2 B_i}{\partial R_{ii} \partial R_{jj}} \right) + V_A(R_{jj}) \left( \frac{\partial^2 B_j}{\partial R_{ii} \partial R_{jj}} \right) + \sum_{k=1}^Z V_A(R_{kk}) \left( \frac{\partial^2 B_k}{\partial R_{ii} \partial R_{jj}} \right) \right\}_0.$$

At the third order

$$\gamma = \frac{1}{6} \left\{ \left( \frac{d^3 V_R}{dR_{ii}^3} \right) - \left( \frac{d^3 V_A}{dR_{ii}^3} \right) B_i - 3 \left( \frac{d^2 V_A}{dR_{ii}^2} \right) \left( \frac{\partial B_i}{\partial R_{ii}} \right) - 3 \left( \frac{dV_A}{dR_{ii}} \right) \left( \frac{\partial^2 B_i}{\partial R_{ii}^2} \right) - V_A(R_{ii}) \left( \frac{\partial^3 B_i}{\partial R_{ii}^3} \right) - \sum_{k=1}^Z V_A(R_{kk}) \left( \frac{\partial^3 B_k}{\partial R_{ii}^3} \right) \right\}_0, \quad (C.21)$$

$$\delta = -\frac{1}{12} \left\{ V_A(R_{ii}) \left( \frac{\partial^3 B_i}{\partial R_{ij}^3} \right) + V_A(R_{jj}) \left( \frac{\partial^3 B_j}{\partial R_{ij}^3} \right) \right\}_0,$$

$$\epsilon = -\frac{1}{4} \left\{ \left( \frac{dV_A}{dR_{ii}} \right) \left( \frac{\partial^2 B_i}{\partial R_{ij}^2} \right) + V_A(R_{ii}) \left( \frac{\partial^3 B_i}{\partial R_{ii} \partial R_{ij}^2} \right) + V_A(R_{jj}) \left( \frac{\partial^3 B_j}{\partial R_{ii} \partial R_{ij}^2} \right) \right\}_0,$$

$$\epsilon = -\frac{1}{4} \left\{ \left( \frac{dV_A}{dR_{jj}} \right) \left( \frac{\partial^2 B_j}{\partial R_{ij}^2} \right) + V_A(R_{ii}) \left( \frac{\partial^3 B_i}{\partial R_{ij}^2 \partial R_{jj}} \right) + V_A(R_{jj}) \left( \frac{\partial^3 B_j}{\partial R_{ij}^2 \partial R_{jj}} \right) \right\}_0,$$

$$\eta = -\frac{1}{4} \left\{ \left( \frac{d^2 V_A}{dR_{ii}^2} \right) \left( \frac{\partial B_i}{\partial R_{ij}} \right) + 2 \left( \frac{dV_A}{dR_{ii}} \right) \left( \frac{\partial^2 B_i}{\partial R_{ii} \partial R_{ij}} \right) + V_A(R_{ii}) \left( \frac{\partial^3 B_i}{\partial R_{ii}^2 \partial R_{ij}} \right) + V_A(R_{jj}) \left( \frac{\partial^3 B_j}{\partial R_{ii}^2 \partial R_{ij}} \right) \right\}_0,$$

$$\eta = -\frac{1}{4} \left\{ \left( \frac{d^2 V_A}{dR_{jj}^2} \right) \left( \frac{\partial B_j}{\partial R_{ij}} \right) + 2 \left( \frac{dV_A}{dR_{jj}} \right) \left( \frac{\partial^2 B_j}{\partial R_{ij} \partial R_{jj}} \right) + V_A(R_{ii}) \left( \frac{\partial^3 B_i}{\partial R_{ij} \partial R_{jj}^2} \right) + V_A(R_{jj}) \left( \frac{\partial^3 B_j}{\partial R_{ij} \partial R_{jj}^2} \right) \right\}_0,$$

$$\theta = -\frac{1}{2} \left\{ \left( \frac{dV_A}{dR_{ii}} \right) \left( \frac{\partial^2 B_i}{\partial R_{ij} \partial R_{jj}} \right) + \left( \frac{dV_A}{dR_{jj}} \right) \left( \frac{\partial^2 B_j}{\partial R_{ii} \partial R_{ij}} \right) + V_A(R_{ii}) \left( \frac{\partial^3 B_i}{\partial R_{ii} \partial R_{ij} \partial R_{jj}} \right) + V_A(R_{jj}) \left( \frac{\partial^3 B_j}{\partial R_{ii} \partial R_{ij} \partial R_{jj}} \right) \right\}_0,$$

$$\xi = -\frac{1}{4} \left\{ \left( \frac{d^2 V_A}{dR_{ii}^2} \right) \left( \frac{\partial B_i}{\partial R_{jj}} \right) + 2 \left( \frac{dV_A}{dR_{ii}} \right) \left( \frac{\partial^2 B_i}{\partial R_{ii} \partial R_{jj}} \right) + \left( \frac{dV_A}{dR_{jj}} \right) \left( \frac{\partial^2 B_j}{\partial R_{ii}^2} \right) + V_A(R_{ii}) \left( \frac{\partial^3 B_i}{\partial R_{ii}^2 \partial R_{jj}} \right) + V_A(R_{jj}) \left( \frac{\partial^3 B_j}{\partial R_{ii}^2 \partial R_{jj}} \right) + \sum_{k=1}^Z V_A(R_{kk}) \left( \frac{\partial^3 B_k}{\partial R_{ii}^2 \partial R_{jj}} \right) \right\}_0$$

and

$$\xi = -\frac{1}{4} \left\{ \left( \frac{d^2 V_A}{dR_{jj}^2} \right) \left( \frac{\partial B_j}{\partial R_{ii}} \right) + 2 \left( \frac{dV_A}{dR_{jj}} \right) \left( \frac{\partial^2 B_j}{\partial R_{ii} \partial R_{jj}} \right) + \left( \frac{dV_A}{dR_{ii}} \right) \left( \frac{\partial^2 B_i}{\partial R_{jj}^2} \right) + V_A(R_{ii}) \left( \frac{\partial^3 B_i}{\partial R_{ii} \partial R_{jj}^2} \right) + V_A(R_{jj}) \left( \frac{\partial^3 B_j}{\partial R_{ii} \partial R_{jj}^2} \right) + \sum_{k=1}^Z V_A(R_{kk}) \left( \frac{\partial^3 B_k}{\partial R_{ii} \partial R_{jj}^2} \right) \right\}_0.$$

A sufficient condition for the pairs of relations for  $\sigma$ ,  $\epsilon$ ,  $\eta$  and  $\xi$  to be equal is that  $B_i$  and  $B_j$  each be symmetrical with respect to interchanges of  $R_{ii}$  and  $R_{jj}$ . Equation (C.16) shows this to be the case since  $B_i$  and  $B_j$  are assumed to be functions of the cosines alone.

Care is needed in evaluating the various partial derivatives in the above equations. Thus in (C.18), the expression for  $\mu$ , the partial derivative that multiplies  $V_A(R_{ii})$  involves a summation over the  $Z - 1$  values of  $j \neq i$

$$\left(\frac{\partial B_i}{\partial R_{ii}}\right) = \sum_{j=1}^Z \left(\frac{\partial c_{ij}}{\partial R_{ii}}\right) \left(\frac{\partial B_i}{\partial c_{ij}}\right) \quad (\text{C.22})$$

whereas the partial derivative that multiplies  $V_A(R_{jj})$  inside the summation (i. e. for  $k = j$ ) consists of a single term

$$\left(\frac{\partial B_j}{\partial R_{ii}}\right) = \left(\frac{\partial c_{ij}}{\partial R_{ii}}\right) \left(\frac{\partial B_j}{\partial c_{ij}}\right). \quad (\text{C.23})$$

In the expression for  $\nu$ , (C.19), both the partial derivatives are single products because specific values of  $i$  and  $j$  are implicit. Similar considerations apply to all the second- and third-order relations.

## References

- [1] D. W. Brenner, Phys. Rev. **B42**, 9458 (1990)
- [2] I. I. Oleinik and D. G. Pettifor, Phys. Rev. **B59**, 8487 (1999)
- [3] D. G. Pettifor and I. I. Oleinik, Phys. Rev. **B59**, 8500 (1999)
- [4] D. G. Pettifor and I. I. Oleinik, Phys. Rev. Letters **84**, 4124 (2000)
- [5] J. Tersoff, Phys. Rev. Letters **61**, 2879 (1988)